INFORMATION TO USERS

UNIVERSITY OF OKLAHOMA

GRADUATE COLLEGE

CHARACTERIZATION OF CEMENT-KILN-DUST

STABILIZED BASE/SUBBASE AGGREGATE

A Dissertation

SUBMITTED TO THE GRADUATE FACULTY

in partial fulfillment of the requirements for the

degree of

Doctor of Philosophy

By

JIANHUA ZHU

Norman, Oklahoma

1998

UMI Number: 9822812

UMI

300 North Zeeb Road
Ann Arbor, MI 48103

CHARACTERIZATION OF CEMENT-KILN-DUST
STABILIZED BASE/SUBBASE AGGREGATE

A Dissertation

APPROVED FOR THE
SCHOOL OF CIVIL ENGINEERING AND ENVIRONMENTAL SCIENCE

BY

Md. Musharrafuzzaman   2/18/98

Gerald A. Miller

K. K. Muraleetharan   2/16/98

Luther W. White

Alan A. Soltani

M. A. Mooney

ACKNOWLEDGEMENTS

TABLE OF CONTENTS

LIST OF TABLES

LIST OF FIGURES

ABSTRACT

In this study, a laboratory testing program was undertaken to determine the resilient modulus and other properties of a cement-kiln-dust (CKD) stabilized aggregate that are important to the design and rehabilitation of roadway pavements. Meridian limestone aggregate which is considered to be of substandard quality and unsuitable for highway base course was tested for its resilient modulus (RM) value in raw and stabilized forms. AASHTO designation T 294-92I (AASHTO T 294-92I) was followed in the RM testing process. Durability, including freezing/thawing and wetting/drying cycles, was studied in terms of RM values. Flexural strength of CKD-stabilized aggregate was studied using the one third point beam test method in accordance with standard testing procedure AASHTO T97-86.

It was observed that the raw aggregate used in this study had a range of RM values from 49 MPa to 306 MPa within tested stress levels. There was a continuous increase in resilient modulus RM with increasing amount of CKD and curing time. The 28-day cured aggregate stabilized with 15% CKD had a range of RM values from 109 MPa to 683 MPa, representing more than 120% increase over the raw aggregate.

The CKD-stabilized aggregate can develop a small amount of flexural strength. The ultimate flexural strength or modulus of rupture (MR) of 28-day cured aggregate stabilized with 15%-CKD ranges from 108 kPa to 153 kPa. This flexural strength can be deemed as an extra factor of safety for the flexible pavement design.

The RM values decrease substantially with increasing number of freezing/thawing and wetting/drying cycles. The reduction in RM value due to

freezing/thawing and wetting/drying cycles exceeds 50%.

The resilient moduli obtained in this study were found to be correlated with the deviator stress than with the bulk stress, while the combined bulk-deviator stress model gives higher correlation than single deviator stress model.

An artificial neural network (ANN) model was developed to represent relationship of RM versus various variables. A feed-forward back-propagation neural net was used to train the available data and a 9-30-1 net architecture was found to be appropriate for modeling presented data set. Excellent agreement between the experimental and ANN predicted values was observed.

The unconfined compressive strength (UCS) and elastic modulus (EM) increase with increasing CKD content and curing period. It is also observed that loading history of aggregate base influences UCS values significantly. The aggregate base having subjected to repeated traffic loading will possess a higher strength than that of new constructed aggregate base.

Microstructure analyses using scanning electron microscopy (SEM) and X-ray diffraction (XRD) techniques quantitatively identified the hydration products and changes in microstructure of the CKD-stabilized aggregate. Crystals formed during the hydration process contributed to the cementing particles as an integral body, while the filling of the intracluster voids of the fine particles minimize possible elastic deformation of the aggregate. More crystals and less voids were observed within the CKD-stabilized specimens having more amount CKD and longer curing time. The XRD analyses lead to a conclusion that the hydration of CKD was followed by crystal

formation of ettringite within the matrix observed in the micrographs. The results of the XRD analyses conform with the results of the SEM analyses and RM and UCS tests.

The layer coefficient (a_2) was determined from the bulk stress values computed using a user-friendly computer software, MICH-PAVE, for various cases consisting of different asphalt concrete (AC) layer modulus, thickness, and base course thickness. The a_2 value of the stabilized aggregates is significantly higher than those of the raw aggregate. The a_2 value of the 28-day cured aggregate stabilized with 15% CKD is more than 200% of the raw aggregate. However, the a_2 value of the stabilized aggregate base decreases significantly when the aggregate subjected to freezing/thawing and wetting/drying cycles.

CHAPTER 1

INTRODUCTION

1.1   Introduction

Surface transportation technologies offer important potential contributions to more efficient and cost-effective transportation systems for the nation. There are various signs, however, that the system is beginning to break down. Many transportation networks in the United States are overburdened, and conditions of many existing roadways are worsening due to deficiencies in design and construction. Improvements in flexible pavement design methodology were made in the mid 1980's and early 1990's with the publication of "American Association of State Highway and Transportation Officials Guide for Design of Pavement Structure" (AASHTO 1986, 1993), in which resilient modulus (RM), rather than subgrade support values, became recommended as a fundamental material parameter for the design of the pavement structure. RM is the unique property of a pavement material that mostly reflects the material response to a simulated repetitive traffic load. Many state transportation agencies have adopted the use of RM in the design of roadway pavements. This use of RM, however, is mostly focused on an untreated granular base layer, a conglomeration of particles with no flexural strength. Stabilized aggregate, on the other hand, exhibits flexural behavior. Since the mechanism of performance of a stabilized aggregate base and unstabilized or raw aggregate base may be different when subjected to traffic loading, the appropriateness of RM in the design of pavements with a stabilized aggregate needs to

be investigated.

Surface transportation quality depends, to a great extent, upon the quality of roadway construction materials. Advancement in paving materials is necessary to build roadways with high strength, durability and great ease in surfacing. As the availability of suitable natural roadway construction materials decreases, the need to utilize poor quality earthen materials for base and subbase construction increases. Instead of expensive excavation and excessive hauling of naturally high quality roadway materials, existing inferior materials can be used as pavement construction after stabilization with industrial wastes, such as fly-ash (Ingles and Metcalf, 1973; Mitchell, 1981; Hausmann, 1990; Yi, 1995; Pandey, 1996). The benefits that can be derived from stabilization of poor quality pavement materials with industrial wastes are three-fold: (1) high quality roadway pavements will be constructed that minimize maintenance cost and maximize travelers' ease; (2) poor quality natural material will be successfully utilized in construction projects that lower costs of construction material borrow from far away sources; and (3) waste materials will be safely and economically disposed of in new ways.

The general objectives of mixing chemical additives, most commonly lime, cement, and fly-ash, with poor-quality earth materials, including soils and aggregates, are to improve or control volume stability (control of swelling and shrinkage), strength and stress-strain properties, permeability, and durability. Volume stability can be improved by substitution of high hydration cations such as sodium by low hydration cations such as calcium, magnesium, aluminum or iron; by cementation and by

2

waterproofing chemicals. The development and maintenance of high strength and stiffness is achieved by elimination of large pores, by bonding particles and aggregates together, and by prevention of swelling. The permeability is altered by modification of pore size and pore size distribution of the soil/and aggregate.

Since aggregate stabilization requires calcium as the major stabilizing agent, it is possible that cement-kiln-dust (CKD), an industrial waste that results from manufacturing of portland cement, would be another useful additive in stabilizing earthen materials. Laboratory investigation has shown that both clay soil and sand can be enhanced by addition of CKD (Sayah 1993, Zaman et al. 1992, Baghdadi et al. 1995). Although there is no data or information available concerning CKD stabilization of aggregates, a high quality base/and subbase is expected to achieve through CKD stabilization in a similar way of flyash stabilization and, thus prolong service life of the pavement and reduce maintenance costs. This approach could also potentially open up a very large market for cement plants that produce nearly 5 million tons of CKD in North America every year.

1.2   Objective and Tasks

The main objective of this study is to investigate effectiveness of CKD in stabilizing a marginal Meridian aggregate that is being used in Oklahoma as a base or subbase, and to evaluate the essential properties of CKD-stabilized aggregate. More specific tasks include the following aspects:

1.   Investigate fundamental properties of a raw aggregate and CKD-aggregate mixture and perform RM and unconfined compressive strength (UCS) tests on

3

the raw aggregate.

2. Stabilize the aggregate with varying CKD amounts (5%, 10%, and 15% by weight) and cure the stabilized aggregate over a range of time (7-day, 28-day and 90-day).

3. Conduct flexural strength, RM and USC tests of the CKD-stabilized aggregate. Evaluate effects of CKD amount and curing time on the RM by comparing RM testing results with those of the raw aggregate.

4. Evaluate the effect of durability namely freezing/thawing and wetting/drying cycles on the RM and UCS of CKD-stabilized aggregates.

5. Perform SEM and XRD tests using raw and CKD-stabilized aggregates to reveal mechanism of CKD-stabilization for the marginal aggregate.

6. Conduct statistical analyses using the RM and UCS values, RM and elastic modulus (EM) values. Establish a statistical correlation between the RM values and the UCS and the EM values.

7. Evaluate existing stress-dependent models using measured RM values of both raw and stabilized aggregates. Explore a new deviator stress-based model and deviator-bulk stress model to correlate RM values.

8. Develop a framework of ANN model to simulate and predict RM values based on the available data. Backpropagation neural network is proposed for such modeling work.

9. Evaluate layer coefficients of AASHTO base/subbase to be constructed with raw and CKD-stabilized aggregates. Evaluate effects of CKD-stabilization on

4

the flexible pavement design with the help of a design example according to the AASHTO design guideline. Evaluate effects of freezing/thawing and wetting/drying cycles on the pavement design and performance.

1.3   Format of the Dissertation

Following the introduction presented in Chapter I, Chapter II provides a detailed literature review about the resilient modulus (RM) and flexural strength tests and their influential factors, state-of-the-art of stabilization using CKD, modeling techniques of RM value. In addition, a brief review of the calibrated mechanistic-empirical design methodology of flexible pavement is also presented in this chapter. Chapter III describes sources of tested materials and their fundamental properties. Specimen preparation and testing methodology for flexural strength and resilient modulus tests, and microanalysis tests are presented in Chapter IV. Chapter V presents laboratory experimental results from resilient modulus tests and flexural strength tests. Results from microanalysis tests are also shown in Chapter V. Chapter VI discusses modeling techniques for resilient modulus, including stress-dependent model and neural network model. In Chapter VII, layer coefficients of the various aggregates are evaluated and effects of stabilization and durability on the layer coefficients are discussed. An example of flexible pavement design based on resilient modulus and finite element method analysis is also presented in this chapter. Finally, in Chapter VIII summary and conclusions of this study are drawn and, recommendations for further study are discussed. All the results of RM tests conducted on the individual specimens are presented in Appendix A.

CHAPTER II

LITERATURE REVIEW

The literature review conducted in this study covers many aspects, including resilient modulus, flexural strength, cement-kiln-dust and its utilization, durability and modeling of resilient modulus. For brevity, only those pertinent points of the reviewed literature are discussed in this chapter to show a succinct background of this research.

2.1   Resilient Modulus

Resilient modulus (RM) is one of the most important parameters in the structural design of highway flexible pavements. The resilient modulus is used as an indicator to examine the behavior of the material as a support system for the pavement, when subject to vehicular loading. Since 1986, AASHTO (1986, 1993) proposed a series of new pavement design procedures that incorporated RM values to adequately describe deformation characteristics of pavement materials and subsequently published a series of interim testing procedures for the determination of RM values (AASHTO, 1986; 1991; 1992). When a heavy vehicle passes over a pavement, a dynamic stress pulse is transmitted to the base/subbase materials. This stress causes the base/subbase materials to deform, which in turn results in deflection of the pavement. Under dynamic loading conditions, the total deformations experienced by the base/subbase materials can be divided into two parts, a resilient or recoverable portion and a permanent portion, as shown in Figure 2-1. The permanent deformation of each layer is usually very small for every repeated loading and unloading sequence, and the influence of its

accumulations on the performance of pavement can be analyzed with various distress models (Monismith, 1992). The resilient modulus characterizes the elastic, recoverable deformation behavior of the base/subbase materials. It is a "measure of the elastic property of soil recognizing certain nonlinear characteristics" (AASHTO, 1993). Numerically, it is the ratio of the deviator stress σ_d to the resilient vertical strain ε_r (RM $= \sigma_d / \varepsilon_r$).

Although the concept behind the resilient modulus is quite straightforward, the determination of the RM values is not as easily achieved as in other common geotechnical tests because there exists significant variability in conducting a RM test. During the last few decades, extensive research has been performed to study the influence of various factors affecting the resilient modulus of aggregates. The following is a summary of these factors:

1.   Keeping all the other factors constant, the RM is bulk stress-dependent (Hicks and Monismith, 1971; Rada and Witczak, 1981; May and Witczak, 1981; Seim, 1989; Elliott, 1992; Chen, 1994; Zaman et al., 1995). A simple expression relating RM to the bulk stress ($\theta = \sigma_1 + \sigma_2 + \sigma_3$) is commonly written as:

$$RM = k_1 \, \theta^{k_2}$$
(2-1)

where:

k$_1$ and k$_2$ = regression constants determined experimentally.

Many experimental data show that k_1 and k_2 are inversely correlated. The range of k_1 and k_2 values is given in Figure 2-2 (Rada and Witczak, 1981).

2.   Loading conditions have measurable influences on the RM values (Mohammad

et al., 1994; Chen et al., 1995). It is found that both stress paths and stress levels influence the RM values. Figure 2-3 shows two kinds of stress paths of conditioning and first loading stage of the RM test followed in the AASHTO procedures T292-91I and T294-92I. It is known that both the conditioning and RM tests are conducted along different stress paths. Actually, the RM test starts at a relatively high stress state and ends at a low stress state in T292-91I specification, while in the T294-92I procedure, the RM test is conducted from a low stress level to a high stress level. The adoption of the latter stress paths could increase RM values by up to 55 percent with respect to those obtained from the test following the former stress paths (Chen et al., 1995). Stress level is one of the most important factors affecting the RM values of granular materials. It is obvious that the higher the stress level the greater the RM values. Although the resilient response of granular materials is significantly affected by the applied stress history, the response becomes fairly steady with increasing number of cycles. Khedr (1985) investigated the effect of loading cycles on the RM in which samples of granular base were subjected up to 10,000 load repetitions. It was reported that the RM values reached a stable value after 100 cycles of loading.

3. Location of LVDT has non-negligible effects on the RM values. Mohammad et al. (1994) used an internal LVDT system to study effects of LVDT location on the RM values. The LVDTs were placed either at the ends or the middle one-third of the specimens. Tests were performed following the stress sequences

given by either AASHTO T-292 or AASHTO T-294. Their test results showed that the RM values, irrespective of the testing procedures used, were higher for tests with LVDTs located in the middle than at the end. It was observed that a 16% higher RM values can be obtained with LVDTs located in the middle, as compared with the LVDTs located at the end.

4. Resilient modulus values vary with material type. As evidenced from the AASHTO Road Test (Elliott and Thornton, 1988), the gravel base sections experienced less deflections than the crushed stone base sections, which means the gravel possessed higher resilient modulus. Chen et al. (1995) investigated the variability of RM values due to aggregate types. Six Oklahoma aggregates including three limestones (from Comanche County, Cherokee County and Creek County), one sandstone (from Choctaw County), one granite (from Johnston County) and one rhyolite (from Murray County) were tested using a typical gradation specification by ODOT for base/subbase aggregates. These six aggregates showed very similar basic properties, e.g., the liquid limits of fine particles passing through #40 sieve between 14%-16%, optimal water content in the range of 5.2%-6.0%, and maximum dry density in the range of 23.0-23.7 kN/m^3. It was established that of the six types tested, the limestone exhibited the highest RM values, and the sandstone yielded the lowest RM values. The differences in RM values for these six aggregates were found to be within 20 to 50 percent.

5. Engineering properties, such as gradation, density and degree of saturation,

significantly affect resilient modulus values of granular materials (Kamal et al., 1993; Barkasdale and Itani, 1989). Rada and Witczak (1981) reported that the k_1 parameter had a maximum value near gradation with optimum fines content and then decreased remarkably with increasing fines content for sand-gravel materials. Hicks and Monismith (1971) found that the k_2 values decreased while the k_1 values increased with increasing fine contents for the crushed aggregates used. Generally, the RM values were found to increase with the density of the materials. Barksdale and Itani (1989) found that as the density of a granitic gneiss increased from 95 to 100 percent of the AASHTO T-180 value, the RM value increased by 50 to 160 percent at a bulk stress of 103 kPa. It was observed that the k_1 value increases gradually with the increase in density, while the k_2 remains constant (Rada and Witczak, 1981). Degree of saturation may have significant effect on the stiffness of material, thus changing the RM values of the material. It is observed that the RM values decrease rapidly above a critical degree of saturation (80% to 85%); below that point, the influence is minor (Rada and Witczak, 1981).

6. Stabilization of aggregate with fly-ash increases the RM values (Yi, 1995; Pandey, 1996). The effect of stabilization depends mainly on the amount of additives and curing time. It was observed by Pandey et al. (1997) that the RM values of some aggregate can be increased by more than 100 percent when it is stabilized with 15 % fly-ash and cured for 28-days.

Although cement-kiln-dust is an industrial waste similar to fly-ash, there are

remarkable differences between these two waste materials. First, these two wastes originate from different sources. The fly-ash is generally a result of burning of coals and various ores. It is collected from furnace facilities such as electric power plants that burn coal for energy generation, while the CKD is produced in the process of manufacturing portland cements. As can be seen later (in Section 2.3), there exists differences in chemical constituents between fly-ash and CKD. Unfortunately, the literature search reveals no references pertaining to the use of CKD-stabilized aggregate and its resilient modulus characteristics, which manifests a need of the research in this area.

2.2   Flexural Strength

As a result of stabilization, properly cured bases may develop a certain amount of flexural strength which may cause the base layer to behave like a slab or a beam (Laguros, 1964). Keshawarz (1985) studied flexural strength of stabilized aggregates using a third point loading method. Three stabilizing agents were used separately in the following proportions: 14% cement, 4.5% lime and 25% fly ash, respectively. In addition, a combination of 8% cement + 3% lime + 18% fly ash was used in the stabilization. The average ultimate flexural strength or modulus of rupture (MR) for one-month cured samples was found to be 524 kPa for cement samples, 242 kPa for lime samples, and 148 kPa for fly ash samples. Four out of six combination samples were unable to test due to cracking of the sample. The MR value from only one combination sample was found as 193 kPa. They observed that a longer curing time (6 and 12 months) did not show any tendency of increased MR values. Zenieris et al. (1988) studied flexural strength of fly ash (15% to 35% by weight) stabilized aggregates

11

that were sampled from five different sources. It was observed that the MR values ranged from 172 kPa to 1042 kPa and there were no consistent changes in MR for the three different amounts of fly ash. Sobhan (1997) studied modulus of rupture of cement-stabilized base aggregate and effect of adding waste fibers. It was observed that average MR value from two specimens of cement-stabilized aggregate was 941 kPa.

2.3   Cement-Kiln-Dust (CKD) and its Utilization

2.3.1   CKD and its Composition

Cement-kiln-dust (CKD) is a kind of waste material produced in the process of manufacturing Portland cement. In manufacturing of portland cement, materials containing different proportions of lime, silica, alumina and iron are mixed together. The prepared mixtures are fed into the upper end of a kiln and they pass through the kiln at a rate controlled by the slope of the kiln and the speed at which the kiln rotates. At lower end of the kiln fuel is burnt to reach a temperature of 1,400 to 1,650°C which changes the raw mix into a cement clinker. The clinker is cooled and then pulverized during which a small portion of the material in the form of very fine dust, known as cement kiln dust (CKD), is collected and removed as an industrial waste. Previously kiln dusts were dispersed into the atmosphere. With the advent of strict air pollution control act and measures, these waste materials are being collected by pollution control devices. It is estimated that about 5 million tons of CKD are produced annually in the United States alone (Todres et al., 1992). The geographic distribution of kiln dust throughout the United States is shown in Figure 2-4.

The physical and chemical composition of the dust vary markedly from plant to

plant, depending upon the feed raw materials, type of kiln operation, dust collection facility, and the fuel used. In general CKDs are particulate mixtures of partially calcined and unreacted raw feed, clinker dust, and fuel ash, enriched with alkali sulfates, halides, and other volatiles. Haynes and Kramer (1982) conducted laboratory analyses on the composition of CKD using 113 samples from 102 plants in the United States. Based on these tests, they had reported an approximate phase composition of CKD, as given in Table 2-1. Although there is a variability among the CKD compositions, the CKD oxide composition exhibits much affinity for three remote CKD sources, as listed in Table 2-2. For comparison purpose, Table 2-2 also gives the oxide composition of fly-ash which is widely used as a stabilizing agent for poor soil and aggregate. It can be seen from Table 2-2 that the CKD has much higher Loss on Ignition (LOI) than the fly-ash has, while the fly-ash has more Silica, Aluminum, Iron oxide and Sulphur oxide than the CKD does. A high loss on ignition (LOI) in CKDs implies that they contain a large amount of $CaCO_3$ and/or that they have been exposed to moisture. It is expected that the difference in chemical compositions between CKD and flyash may result in different stabilization effects. However, a little attention has been paid toward this issue.

2.3.2   Use of CKD

Use of industrial wastes will bring about both economic and environmental benefits. The practice of burning industrial wastes in cement kilns gained momentum in the United States during the 1980s when the cement industry tried to reduce its fuel bills to compete with the foreign cement manufacturers (Lilley, 1995). Environmental and

community groups decried this practice, claiming that cement kiln dust contains dioxins and anthropogenic radioactive elements that could cause serious health problems. Their staunch opposition to this practice discouraged many cement kiln operators from burning industrial wastes to generate alternative fuels. It also forced the government to pass new laws that will reduce the environmental impact of cement kiln dust.

The replacement of ordinary Portland cement by CKD is another potential use of this waste product. Ramakrishnan (1986) reported that the addition of CKD slightly retarded the setting time of cement but there was no apparent difference in engineering properties between the plain concrete and CKD-mixed concrete. Elwefati et al. (1990) investigated the replacement of ordinary portland cement by 10%, 20% and 30% CKD. They reported that both compressive strength and flexural strength decreased with an increase in the amount of CKD. The strength loss due to the replacement of CKD reached up to 40% of regular concrete. The expansion resulting from the water-absorbent alkali constituents, on the other hand, was found to be within acceptable limits. In addition, their results showed that the kiln dust, which normally contains higher amounts of alkalis, is likely to increase the risk of the alkali-aggregate reaction when used in concrete.

The use of CKD as a stabilizer of soils/aggregates for base/subbase applications could potentially consume a bulk of the CKD being wasted nearly 5 million tons in North American every year. The use of CKD would enhance the engineering properties of undesirable soils and aggregate, and at the same time gain benefits of reducing both solid waste and the exploitation of scarce and dwindling natural resources. The research

work related to the soil stabilization with CKD is relatively new and only a few publications could be traced. Baghdadi and Rahman (1990) and Baghdadi et al. (1995) investigated the engineering properties of CKD-stabilized dune sand which is used extensively in the construction of roadway in Saudi Arabia. It was found that the compressive strength increases with the amount of CKD and curing time. They recommended that for a light application 12-30% CKD is sufficient to upgrade dune sand; however, for an application of heavy loads the content of CKD can be as high as 50%. Zaman et al. (1992) and Sayah (1993) investigated the variation in engineering properties of an expansive soil stabilized with different amounts of CKD. It was observed that the maximum dry density of the soil decreased slightly with the addition of CKD. Specifically, the density of the raw soil decreased from 13.4 kN/m^3 to 12.3 kN/m^3 for the stabilized soil with 25% CKD, while the plasticity index (PI) was reduced from 64 to 16 and the swelling potential decreased from over 9% to an insignificant amount. The unconfined compressive strength of the stabilized soils with different amounts of CKD was about 20-30% higher than that of the raw expansive soil. Azad (1997) investigated CKD-stabilization on a highly plastic, a medium plastic and low plastic soils. He reported that the CKD significantly improved strength of all the soils, but not as effective as cement stabilization. Miller et al. (1997) investigated the effect of CKD on the collapse potential of shale compacted at three different moisture contents - dry side of, at, and wet side of optimum moisture content. It was observed that the kiln dust is a potentially useful additive for reducing wetting-induced collapse settlements and for reducing overall compressibility.

The use of CKD in stabilizing marginal aggregate primarily depends upon its pozzolanic reaction accomplished with the help of calcium, silica and aluminum ions. The calcium ions are available from CaO, $CaCO_3$, and $Ca(OH)_2$ when they react with moisture. Due to low solubility of $CaCO_3$ (Boynton, 1980), CKDs containing $CaCO_3$ will provide less calcium ions and take longer time to stabilize soils than CKDs containing CaO or $Ca(OH)_2$. In addition, as can be seen from Table 2-2, the amount of CaO contained in CKDs is about the same as that in fly-ash. CKDs, however, contain less silica and aluminum than fly-ash does. The differences in stabilization effects between fly-ash and CKD are not known at present.

2.4   Durability

The resilient modulus of base/subbase is not a single, fixed value because it changes due to a number of factors throughout the pavement's life. In addition to the factors cited before, a seasonal variation is to be expected because, in most areas of the country, roadbeds are softer in the spring than they are at other times of the year (Elliott and Thornton, 1988). The freezing/thawing and wetting/drying activities in roadways may have significant influence on the pavement performance. This is demonstrated by the seasonal variation in pavement surface deflections over a year. Figure 2-5 is a plot of deflection test data from conventional flexible pavements in the vicinity of the AASHTO Road Test site (Elliott and Thornton, 1988). From this figure one can see that the worse conditions occur around March and April while the best performance is seen in December.   The variation in pavement performance in different seasons indicates possible corresponding changes in resilient modulus of base/subbase materials,

i.e. the RM value of the aggregate will increase during freezing and drying processes and decrease during thawing and wetting stages. Therefore, design and analysis of pavement for a region where variations in temperature and moisture are appreciable would be meaningless if the seasonal effects were not taken into account

In order to evaluate the ability of chemically stabilized marginal aggregates to resist the deleterious effects of freezing/thawing and wetting/drying cycles, durability investigation on the stabilized aggregates should be conducted. There is, however, not a standard testing procedure to address measurement of resilient modulus of stabilized aggregate subjected to freezing/thawing and wetting/drying cycles. Although the ASTM testing procedures D 559-89 and D 560-89 are used to measure durability of soil-cement mixtures (ASTM, 1989), they only provide measurements of loss of specimen weight.

Laguros and Keshawarz (1987) developed a testing procedure to measure shear strength of a stabilized base material subjected to wetting and drying actions. The specimens were first placed in an oven at 140°F for 12 hours after curing periods. Then, the specimens were removed from the oven and placed in humidifiers at 70°F and 90°F temperature, and 90-100 percent relative humidity, for 24 hours. This drying for 12 hours and wetting for 24 hours constituted one cycle (Laguros and Medhani, 1984). At the end of 15 cycles, specimens were tested in a triaxial machine under wet and dry conditions. The shear parameters obtained from specimens subjected to wetting/drying cycles were found higher than those not experienced wetting/drying actions. For example, fly-ash stabilized samples not subjected to wetting/drying cycles were found

to have c value of 110 kPa and ϕ value of 21°, while for samples subjected to 15 wetting/drying cycles and tested under the wet condition, the c value is 276 kPa, and ϕ is 30°.

Sayah (1993) investigated freezing/thawing and wetting/drying-induced durability of CKD-stabilized clay samples. Freezing/thawing tests were conducted by placing the 56-day cured samples in a freezer for 12 hours and then at room temperature (70°) for 24 hours to complete one cycle. This was repeated 3 times to complete 3 cycles. The wetting/drying conditions were same as those stated earlier. The test results showed that the compressive unconfined strength decreased significantly due to the freezing/thawing and wetting/drying actions. It was observed that strength loss due to wetting/drying cycles reached 70%, while a 58% loss of strength was observed due to the freezing/thawing actions. It was also noted that some samples were unable to test because they broke during the wetting and freezing processes.

Elliott and Thornton (1988) reported variation in resilient modulus of a typical cohesive soil subjected to one cycle of freezing/thawing. They showed that the RM values could be reduced as much as 50 percent due to such effects. Neither the effect of number of freezing/thawing cycles nor testing procedure was investigated in their study.

Jin et al. (1994) investigated resilient modulus versus temperature and moisture content changes of the subgrade soils. The moisture of the specimens varied from 3.3 % to 9.8 %, and the temperature ranged from 30.1°F (-1.05°C) to 75.5°F (24.2°C). Their

results showed that the RM value decreases as the water content and temperature increase.

From the cited references, it becomes evident that there exists a need to address research on the resilient modulus versus durability for stabilized aggregates. Effects of the number of both freezing/thawing and wetting/drying cycles on the resilient behavior of an aggregate remain an important area of research.

2.5   Microanalysis

An understanding of the microstructure of stabilized aggregates is useful in revealing the mechanisms of stabilization with industrial wastes. Scanning electron microscopy (SEM) and X-ray diffraction (XRD) tests continue to be a very effective means for performing the microanalysis. The SEM utilizes a focused beam of high energy electrons that systematically scans across the surface of a specimen. The interaction of the beam with the specimen produces a large number of signals which vary with the surface structure and are eventually converted to different images shown on the scanning screen. With the pictures taken during SEM testing, one is able to identify the microstructure characteristics of the specimen. The X-ray diffraction provides a qualitative analytical tool for determining the mineral constituents of stabilized materials. The XRD and SEM investigations conducted on the CKD-stabilized clays showed the presence of hydration products and a subsequent decrease in void space, which resulted in increased strength and a reduction in the plasticity indices with curing time (Sayah, 1993). The aggregate, however, used in present study is very different than the clay soil used by Sayah (1993). The changes in microstructure of the

aggregate due to the addition of CKD is not known at present. Therefore, a study involving the microanalyses of CKD-stabilized aggregate is necessary and expected to provide useful results.

2.6   Modeling of Resilient Modulus

2.6.1   Stress-Dependent Models

Modeling of resilient behavior of base/subbase materials plays an important role in implementing a mechanistic design method for pavement and evaluation of pavement performance.   During the past few decades, several constitutive models have been developed for the resilient modulus of base/subbase materials (Hicks and Monismith, 1971; Finn et al., 1977; Uzan, 1985; Santha, 1994). The first model is the well-established one that relates the resilient modulus to the bulk stress:

$$RM = k_1 \, \theta^{k_2} \qquad\qquad (2\text{-}1)$$

where:

RM = resilient modulus of base/subbase material;

θ = bulk stress or first stress invariant $(\sigma_1 + \sigma_2 + \sigma_3)$,

k_1, k_2 = regression coefficients derived from laboratory test results.

Equation (2-1) has been implemented in various computer programs for pavement design and analysis (e.g. Finn et al., 1977; Harichandran et al., 1989) using iterative computation schemes. One of disadvantages of this model is that it does not adequately address the effect of deviator stress, or shear strain. The predicted response is not compatible with laboratory test results that show a strong dependence of the RM values on the stress level.

The second model is derived from the hyperbolic law proposed by Kondner (1963). The general form of the hyperbolic law is given by:

$$1/E = (\varepsilon_a / \sigma_d) = a + b \, \varepsilon_a \qquad (2\text{-}2)$$

where E = elastic modulus,

ε_a = axial strain,

σ_d = deviator stress, and

a, b = regression coefficients corresponding to the inverse of the initial tangent modulus of elasticity and stress at failure.

It is known that the initial modulus function resembles Equation (2-1) in which the bulk stress is replaced by the confining pressure, i.e.:

$$E_i = k_5 \, P_a \, (\sigma_3/P_a)^{k6} \qquad (2\text{-}3)$$

where E_i = initial elastic modulus,

P_a = atmospheric pressure, and

k_5, k_6 = regression coefficients.

Chou (1976) suggested that for resilient deformation of granular material the resilient modulus (RM) could be initial modulus E_i, implying that the RM value increases with the confining pressure. It is clear that the models given by Eqs. (2-1) and (2-3) have theoretical weaknesses because they would give any resilient modulus values in the case of zero deviator stress, and actually the resilient modulus should equal to zero.

The third model includes shear behavior in the bulk stress model equation (May and Witczak, 1981; Uzan, 1985), as given below:

$$RM = k_1 \, \theta^{k2} \, f(\varepsilon_a) \qquad\qquad (2\text{-}4)$$

where $f(\varepsilon_a)$ is a correlation function of axial strain. Uzan (1985) postulated that $f(\varepsilon_a)$

value decreases as ε_a increases for a granular material. Further, it has been suggested

that this function be approximated as follows:

$$RM = k_1 \, \theta^{k2} \, \varepsilon_a^{k3} \qquad\qquad (2\text{-}5)$$

or

$$RM = k_1 \, \theta^{k2} \, \sigma_d^{k4} \qquad\qquad (2\text{-}6)$$

where:

k_3 and k_4 = regression coefficients.

It seems that the model given by Equation (2-6) is more reasonable than the

other two models in that it considers both bulk and deviator stresses. A comparison of

above three models with laboratory experiment results were made by Uzan (1985) and

Equation (2-6) gave a better agreement than other models.

It should be pointed out that the data used for developing the above models were

obtained from the tests not conforming with the current AASHTO testing procedure. As

noted by Chen et al. (1995), the RM values vary greatly with different testing

procedures. Therefore, the validity of these models with respect to current test data

needs to be investigated and, new possible models need to be explored.

2.6.2 Artificial Neural Network Model

The above stress-dependent resilient modulus models are actually "local"

models in that the constant k_i (i=1,2,3,4) varies with different test results, e.g. if the degree of saturation of a sample changes, the RM value will change and the new regression coefficients will have to be re-calculated. Although multiple regression model can take into consideration such variables as density, water content, grain size, the artificial neural network (ANN) offers a more flexible and adaptive alternative for modeling resilient modulus.

An ANN is a system composed of artificial neurons and artificial synapses that simulates the activities of biological neural network, as shown in Figure 2-6 (Faghri and Hua, 1992). A biological neuron is composed of a cell body, an axon, and dendrites as shown in Figure 2-6 (a). The connections between the neurons are called synapses, and each neuron is connected to 100 to 10,000 other neurons. A neuron executes a very simple task: when presented with a stimulus, it emits an output into other neurons connected to it via the synapses (Simpson, 1990). Artificial neurons mimic the functions of biological neurons by adding the inputs presented to them and computing the total value as an output with a transfer function. Figure 2-6 (b) shows a simple example of an artificial neuron. The artificial neuron is connected by so-called weights to other artificial neurons.

ANNs have recently emerged as a very promising tool for various engineering applications. This includes pattern recognition, classification, speech recognition, manufacturing process control, and material behavior modeling (Windrowe and Lehr, 1990; Ghaboussi, 1992; Giles et al., 1994; Najjar and Basheer, 1996; Zhu and Zaman, 1996, Zhu et al., 1997b; 1997c). The neural network function is determined largely by

the connections between input and output elements. The basic one layer neural network model can be generically expressed as follows:

$$Y = F(W*X+b) \tag{2-7}$$

where X = input vector $(X_1; X_2; ...; X_i; ...; X_n)$,

Y = output vector $(Y_1; Y_2; ... ; Y_j ; ...; Y_m)$,

W, b = the weight matrix and bias vectors, respectively, and

F = an activation function.

The major objective of the neural network is to find the weights W and bias values b through a training process by minimizing an appropriate error function E. To find the proper weights and biases a number of epochs of training (or iteration calculation) are performed to the network. The goal of iteration is achieved when a sum of mean squared error between target and output values are minimized or within an acceptable range.

In many engineering nonlinear problems, a standard feed forward backpropagation neural net is considered most effective (Vogl et al. 1988; Widrow and Lehr, 1990). The architecture of a multilayer neural network with one layer of hidden units is shown in Figure 2-7. The output units (the Y units) and the hidden units (the Z units) are expressed by the following algorithm:

$$y_k = F_1 \left(w_{ok} + \sum_j z_j w_{jk} \right) \tag{2-8}$$

$$z_j = F_2 \left(v_{oj} + \sum_i x_i v_{ij} \right) \tag{2-9}$$

where, x_i = input signal from input unit i, (i=1,2,......n)

y_k = output from output unit k, (k = 1,2,......m)

24

z_j = output form hidden unit j, (j = 1,2,......p)

v_{oj}, w_{ok} = bias for hidden unit j and output unit k, respectively, and

F_1, F_2 = activation functions in output layer and hidden layer, respectively.

The training of a network by backpropagation involves three stages: (a) the feedforward of the input training pattern; (b) the calculation and backpropagation of the associated error; and (c) the adjustment of the weights. During feedforward, each input (X_i) receives an input signal and relays this signal to each of the hidden units Z_j. Each hidden unit then computes its activation and sends its output to each output unit Y_k. Each output unit computes its activation to form the response of the net for the given input pattern.

In the training process, each output unit compares its computed activation value y_k with its target value t_k to determine the associated error for that pattern with that unit. Based on this error, the factor δ_k (k=1,2,......m) is computed. δ_k is used to update the weights between the output layer and the hidden layer. In a similar manner, the factor δ_j (j = 1,2,......p) is computed for each hidden unit Z_j. δ_j is used to update the weights between the hidden layer and the input layer. The equations for calculation of network error and weight adjustment are given as follows:

$$\delta_k = (t_k - y_k) \, F_1' \left(w_{ok} + \sum_j z_j w_{jk} \right) \qquad (2\text{-}10)$$

$$\delta_j = \sum_{k=1}^{m} \delta_k \, F_2' \left(v_{oj} + \sum_i x_i v_{ij} \right) \qquad (2\text{-}11)$$

$$\Delta w_{jk} = \alpha \, \delta_k \, z_j \qquad (2\text{-}12)$$

$$\Delta w_{ok} = \alpha \, \delta_k \qquad (2\text{-}13)$$

$$\Delta v_{ij} = \alpha \, \delta_j \, x_i \qquad (2\text{-}14)$$

$$\Delta v_{oj} = \alpha \delta_j \qquad\qquad (2\text{-}15)$$

$$w_{jk}(\text{new}) = w_{jk}(\text{old}) + \Delta w_{jk} \qquad\qquad (2\text{-}16)$$

$$v_{ij}(\text{new}) = v_{ij}(\text{old}) + \Delta v_{ij} \qquad\qquad (2\text{-}17)$$

where $\qquad \alpha =$ learning rate,

Δw_{jk}, $\Delta v_{ij} =$ changes in weight w_{jk}, v_{ij}, respectively, and

Δw_{ok}, $\Delta v_{oj} =$ changes in biases w_{ok}, v_{oj}, respectively.

An activation function for a feedforward backpropagation net should have several important characteristics. It has to be continuous, differentiable and monotonically non-decreasing. Furthermore, the function is expected to saturate, i.e. approach finite maximum and minimum values asymptotically. It is desirable that the derivative of the activation function be easily calculated. One of the most typical activation functions is the binary sigmoid function, which has range of (0,1) and is given by :

$$f_1(x) = \frac{1}{1 + \exp(-x)} \qquad\qquad (2\text{-}18)$$

and its derivative can be expressed as:

$$f'_1(x) = f_1(x)[1 - f_1(x)] \qquad\qquad (2\text{-}19)$$

Another commonly used activation function is a bipolar sigmoid, which has range of (-1, 1). In a generic form, it can be expressed as follows:

$$f_2(x) = \frac{2}{1 + \exp(-x)} - 1 \qquad\qquad (2\text{-}20)$$

For this case, the derivative is given by:

$$f'_2(x) = \frac{1}{2}[1 + f_2(x)] [1 - f_2(x)].$$

(2-21)

Although the references concerning resilient modulus and ANN modeling have not been available, the possible ANN model for resilient modulus of base/subbase materials is expected to be capable of capturing variations in stress/strain-dependent material properties, environmental factors, and other factors.

2.7   Stabilization of Base and Subbase of Pavement

There are basically two types of stabilization known as pozzolanic stabilization and ion-exchange stabilization which operate in coarse-grained earth materials and fine-grained soils, respecyively.   The fine-grained soils such as clay soils having high volume instability, high plasticity and extreme sensitivity of strength to moisture content, experience stabilization via ion-exchange mechanism meditated by calcium-containing additives such as lime, hydrated lime ($Ca(OH)_2$), CKD, and portland cement. The coarse-grained materials, such as sandy-soils and aggregates, being volumetrically stable and less plastic, are strengthened by direct cementitious effects known as pozzolanic reactions. The pozzolanic materials such as fly-ash and CKD are considered to have no cementitious value of its own but in the presence of moisture and air form compounds possessing cementitious properties. Nicholson and Goeb (1982) conducted a series of investigation on CKD and fly-ash mixtures for producing subbase materials with different aggregates. The amount of CKD used for stabilizing subbase aggregate was up to 16% by weight of the mixture. It was claimed that the stabilized mixtures acquired strengths and other performance characteristics comparable to those of cement-aggregate or lime-fly ash-aggregate bases. It was found that these materials require less

27

energy to produce and cost less than the traditionally used asphalt-aggregate bases that require heating. Miller et al. (1980) studied the use of CKD and fly ash as the cementitious ingredients in developing pozzolanic bases that demonstrated comparable properties to those of a stabilized base. It was observed that the pozzolanic base samples also possessed the property of autogenous healing, by which the hairline cracks formed in the mixture are healed because of a continued chemical reactivity. Collins et al. (1983) studied substitution of CKD for lime for a number of lime-fly ash-sandy aggregate systems for subbase construction. It was observed that the majority of the CKD-treated fly ash and aggregate mixtures produced comparable strength, durability and other engineering properties to those of the conventional lime-fly ash-aggregate mixtures.

The chemical and physical compositions of the CKD were found to have an important influence on controlling the reactivity and the resulting engineering properties of the dust-fly ash-aggregate mixtures. Collins et al. (1983) reported that a combination of free lime (CaO), MgO, alkalies, and a favorable particle fineness (fraction between 70 μm, and 20 μm) always enhanced the reactivity of CKD and produced high compressive strengths, whereas CKD with higher LOI and low free lime impeded the reactivity and gave lower strengths. Napeierala (1983) examined the possibility of using CKD with different chemical constituents in stabilizing sandy soils for pavement subbase applications. It was observed that an addition of 15% CKD having 5.9% free lime and MgO, and 0.97% total alkalies (K_2O + Na_2O) ensured a compressive strength of 2.5 MPa - a standard practice in Portland - for the subgrade within 14 days of the

treatment.

2.8 Methodology of Calibrated Mechanistic Procedure for Flexible Pavement Design

The AASHTO flexible pavement design equations (AASHTO, 1986 and 1993) were empirically obtained from the AASHTO Road Test. The empirical design procedures are usually acceptable only within the range of variables under which they were developed. The research conducted at the University of Illinois has developed a calibrated mechanistic design procedure for pavements (NCHRP, 1990). The calibrated mechanistic procedure is a more specific term for the mechanistic-empirical procedure. It contains a number of mechanistic distress models which require a careful calibration and verification to ensure attainment of satisfactory agreements between the predicted and actual distress. The purpose of calibration is to establish transfer functions relating mechanistically determined responses to specific forms of physical distress (e.g. fatigue cracking, rutting). Verification involves the evaluation of the proposed models by comparing results to observations in other areas not included in the calibration process. Figure 2-8 shows the contents of the calibrated mechanistic design procedure (Huang, 1993).

There are two type of failure criteria, i.e. vertical compressive strain on the surface of subgrade and horizontal tensile strain at the bottom of asphalt layer, used in the flexible pavement design. By controlling the tensile strain at the bottom of asphalt layer, potential of fatigue cracking can be reduced; while limiting the compressive strain on the top of subgrade will minimize the possibility of rutting in flexible pavements (Lotfi et al., 1988). Significant efforts have been directed to the development of

various design procedures based on limiting strain criteria for specific pavement materials (AI, 1991; Powell, 1984; Shell, 1978; Thompson, 1987; Ullidtz, 1977). Some of these procedures are briefly summarized in Table 2-3.

Table 2-1   Approximate Composition of a Cement Kiln Dust
           (after Haynes and Kramer, 1982)

Constituent	% by weight	Constituent	% by weight
$CaCO_3$	55.5	Fe_2O_3	2.1
SiO_2	13.6	KCl	1.4
CaO	8.1	MgO	1.3
K_2SO_4	5.9	Na_2SO_4	1.3
$CaSO_4$	5.2	KF	0.4
Al_2O_3	4.5	Others	0.7

Table 2-2 Oxide Composition of CKD and Fly-ash

Chemical constituent	Composition of CKD, %			Composition of Fly-ash, %	
	(A)	(B)	(C)	(D)	(E)
Silica (SiO$_2$)	9.64	13.46	15.02	16.94	17.00
Aluminum oxide(Al$_2$O$_3$)	3.39	3.86	3.85	8.92	8.19
Iron oxide (Fe$_2$O$_3$)	1.10	2.09	1.88	9.4	8.96
SiO$_2$ + Al$_2$O$_3$ + Fe$_2$O$_3$	14.13	19.41	20.75	35.26	34.15
Calcium oxide (CaO)	44.91	40.31	41.01	41.25	43.88
Magnesium oxide (MgO)	1.29	1.76	1.4	2.66	2.04
Sulphur oxide (SO$_3$)	6.74	5.48	6.2	19.31	19.44
Sodium oxide (Na$_2$O)	0.27	4.01	0.7	---	0.35
Potassium oxide (K$_2$O)	2.40	2.15	2.5	---	0.84
Calcium Carbonate (CaCO3)	---	---	---	41	---
Free lime (CaO)	0.52	---	0.85	18.2	---
Loss on ignition (LOI)	30.24	33.04	25.7	5.34	5.59

Notes: (A) Long-dry kiln (Todres et al. 1992), (B) by Baghdadi et al. (1995), (C) Long-wet kiln (Todres et al., 1992)

(D) Brazil Creek Minerals, Inc., Arkansas, (E) Resources Materials Testing, Inc., Georgia.

Table 2-3   Examples of Analytically Based Design Procedures (Monismith 1992)

Organization	Pavement Represent-ation	Distress Modes	Pavement Materials	Design Format
Shell International Petroleum Co., Ltd. London, England	Multilayer elastic solid	Fatigue in treated layers Rutting: * subgrade strain * estimate in asphalt bound layer	Asphalt concrete, untreated aggregate, cement-stabilized aggregate	Design charts; computer program: Bisar
The Asphalt Institute, Lexington, KY (MS-1)	Multilayer elastic solid	Fatigue in asphalt treated layers Rutting: * subgrade strain	Asphalt concrete, asphalt emulsion treated bases, untreated aggregate	Design charts; computer program: DAMA
National Institute for Transport and Road Research (NITRR) South Africa	Multilayer elastic solid	Fatigue in treated layers Rutting: * subgrade strain * shear in granular layers	Gap-graded asphalt mix, asphalt concrete, cement-stabilized aggregate, untreated aggregate	Catalogue of designs; computer program
Federal Highway Administration U.S. DOT, Washington, D.C.	Multilayer elastic or viscoelastic solid	Fatigue in treated layers Rutting: * estimate at surface Serviceability (as measured by PSI)	Asphalt concrete, cement-stabilized aggregate, untreated aggregate, sulphur treated materials	Computer program: VESYS

33
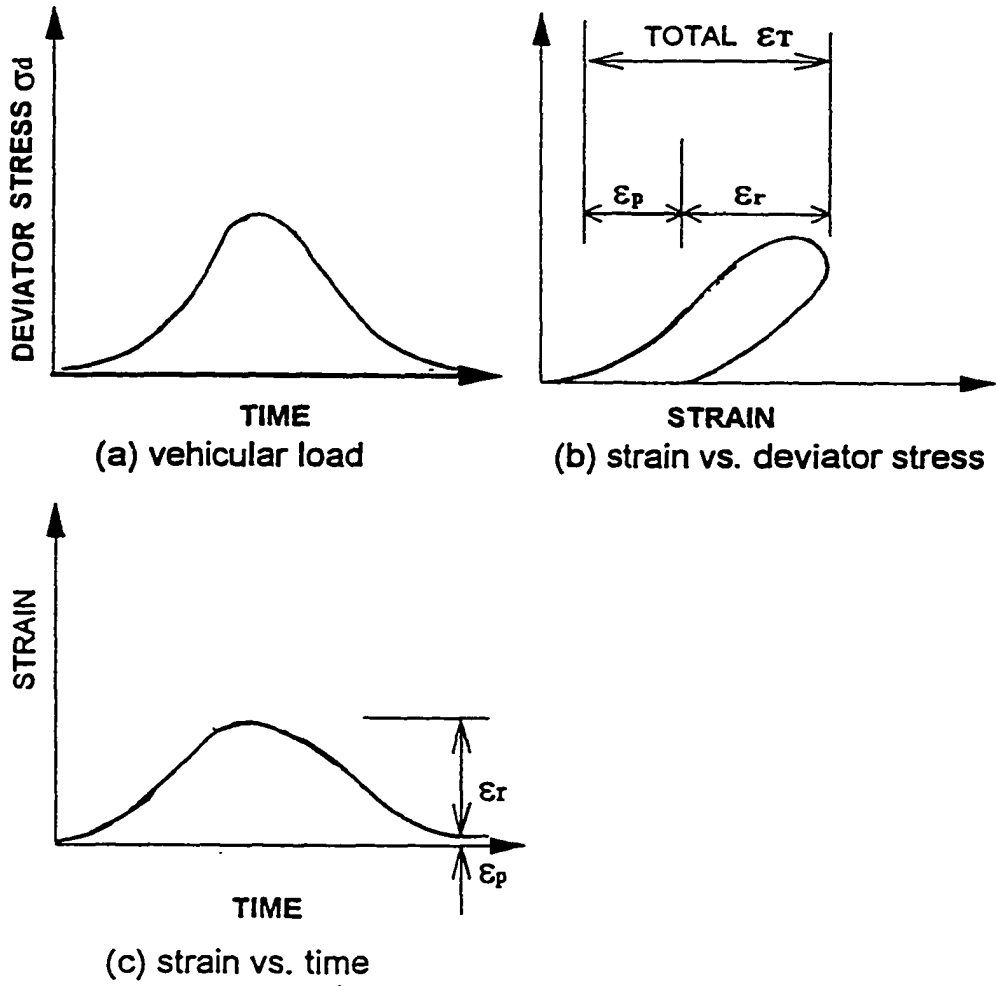
Figure 2-1   Typical Vehicular Load Response

$$\log k_1 = 4.657 - 1.807 \, k_2$$
$$M = 271$$
$$R^2 = 0.68$$
$$S.E.E. = 0.22$$
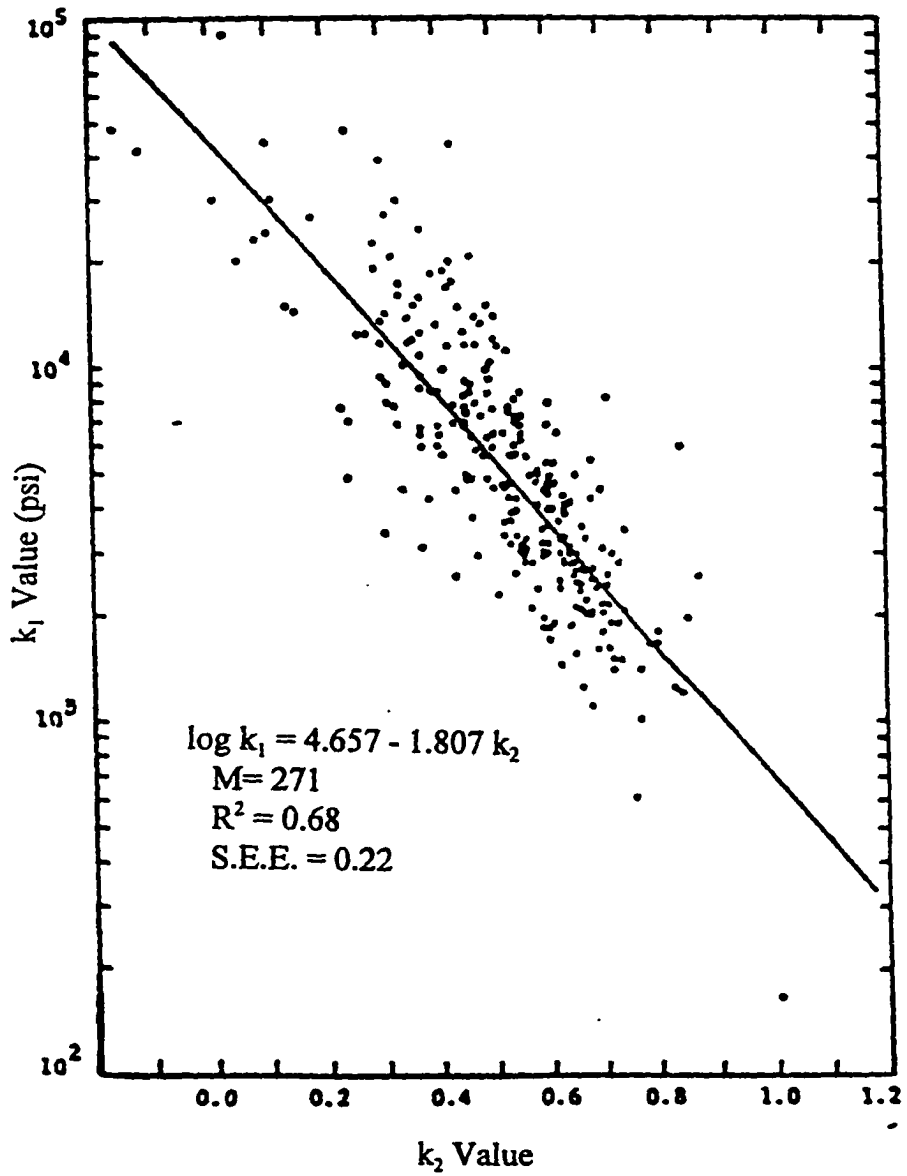
Figure 2-2 Range of k_1 and k_2 Values of Aggregates Summarized
by Rada and Witczak (1981)

35
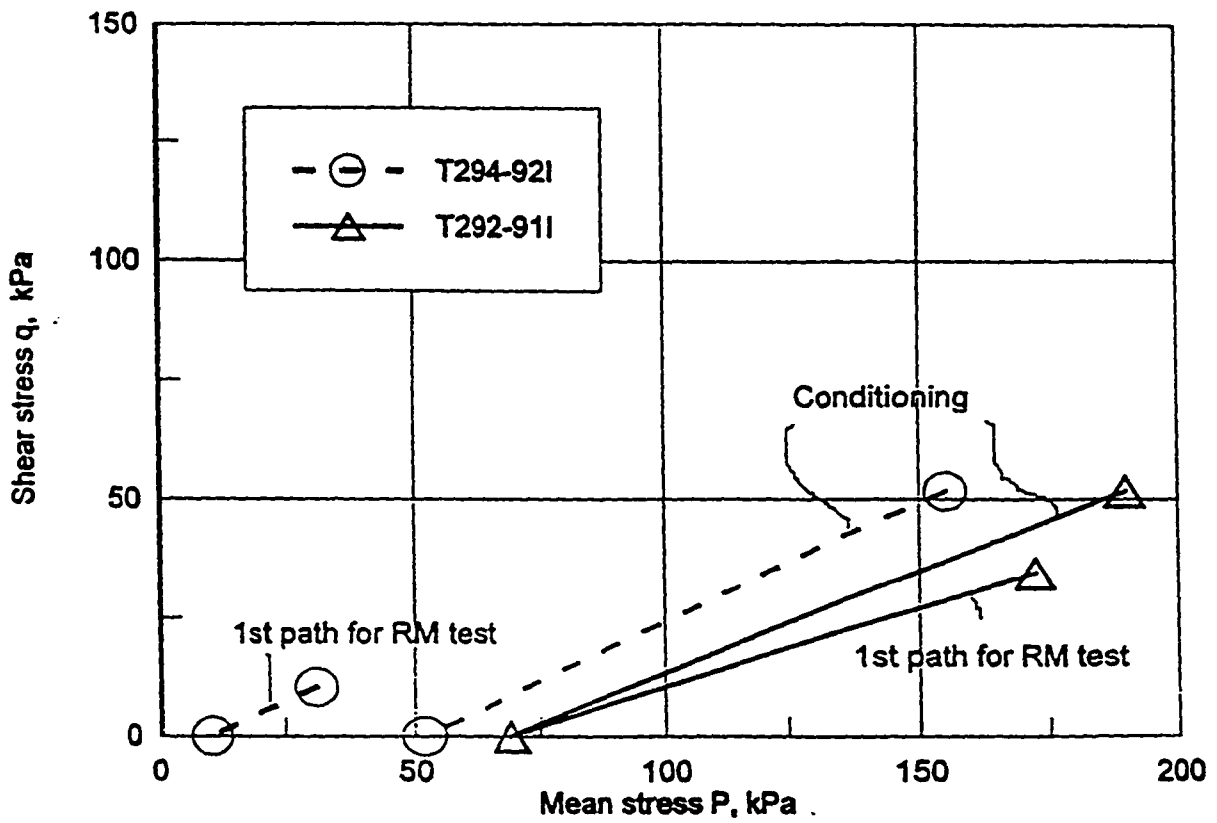
Figure 2-3   Stress Paths for Different AASHTO Testing Procedures
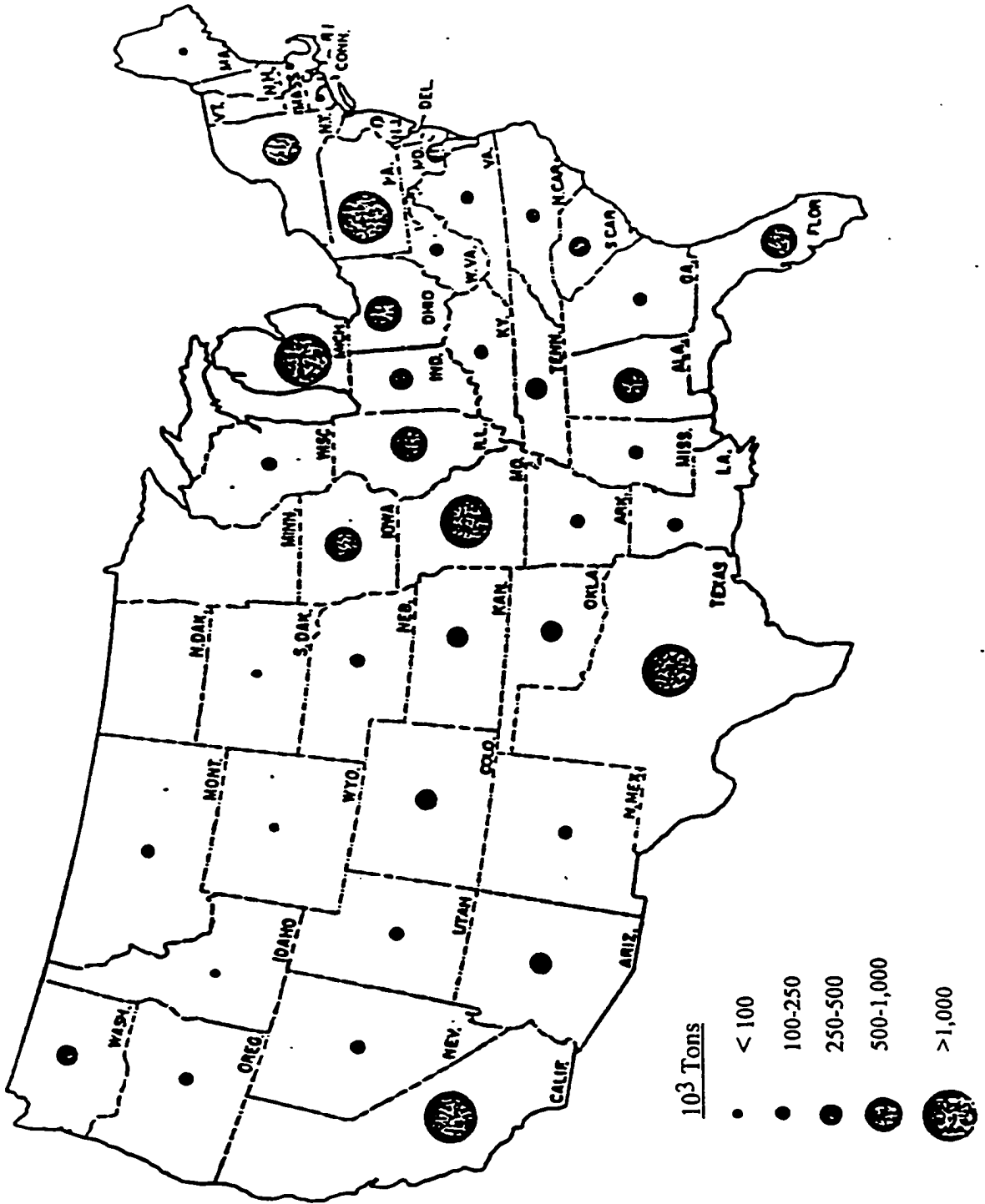
Figure 2-4   Geographic Distribution of Kiln Dust throughout the United States

(adapted from Sayah, 1993)
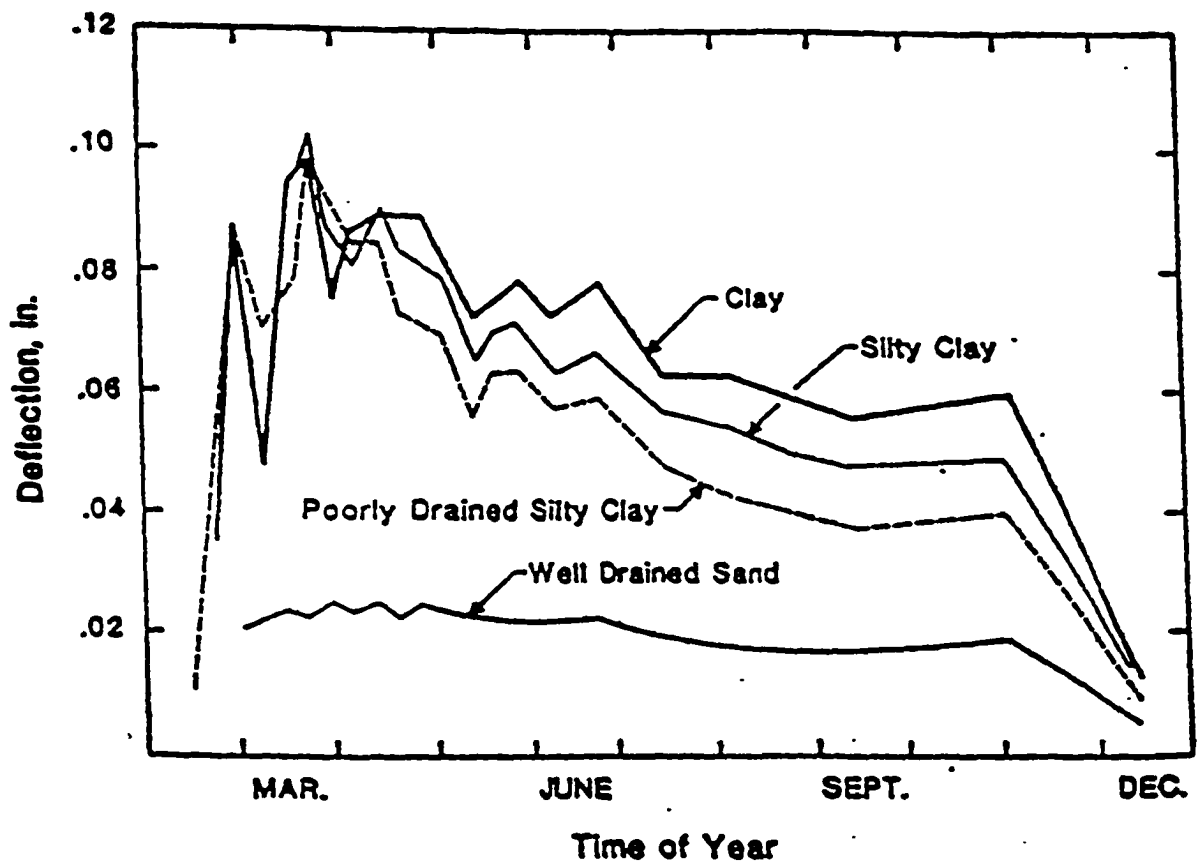
Figure 2-5   Deflection of Flexible Pavement versus Seasonanl Change
(after Elliott and Thornton, 1988)

(a) biological neuron

(b) artificial neuron
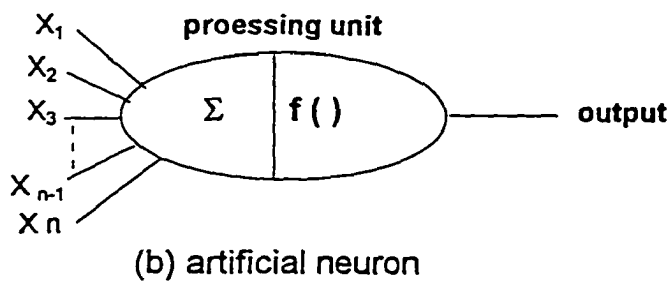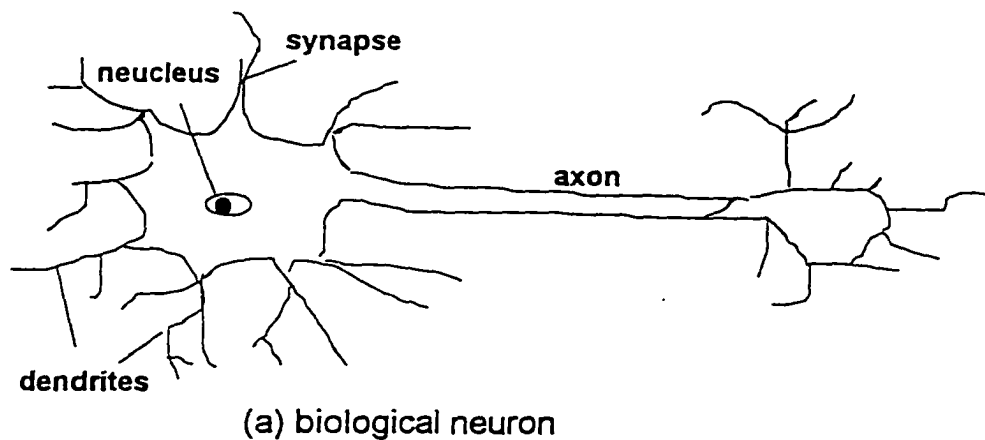
Figure 2-6   Comparison of Typical Biological Neuron and Artificial Neuron
(after Faghri and Hua, 1992) .

39
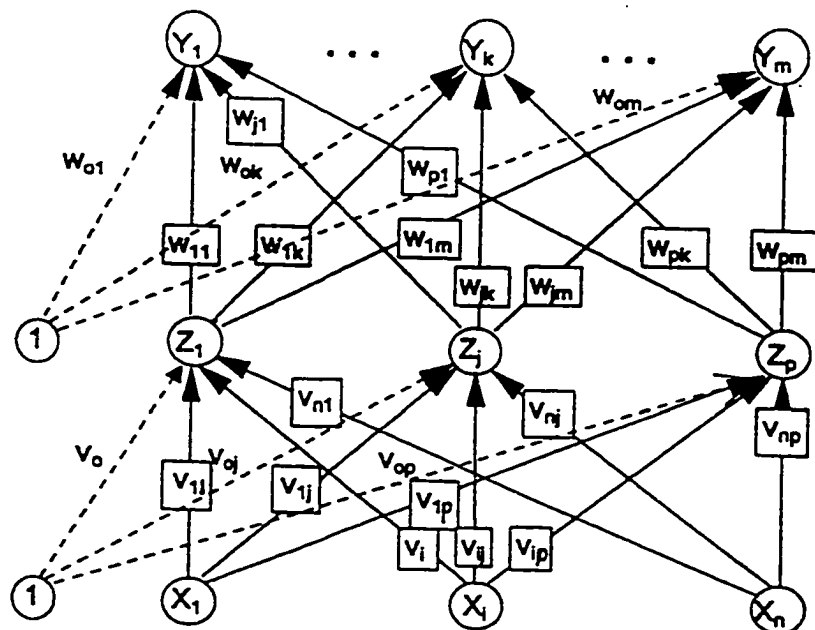
Figure 2-7   Backpropagation Neural Network with One Hidden Layer

2. INPUT
MATERIAL PROPERTIES
CLIMATE INFORMATION

1. ASSUME
PAVEMENT
CONFIGURATION

3. CLIMATE MODELS
HEAT TRANSFER
MOISTURE EQUILIBRIUM
INFILTRATION AND DRAINAGE

5. STRUCTURAL MODELS

4. INPUT TRAFFIC

6. PAVEMENT RESPONSE

Unsatisfactory

8. DISTRESS MODELS
FATIGUE CRACKING, RUTING
LOW TEMPERATURE CRACKING

7. DESIGN RELIABILITY

Satisfactory

9. FINAL DESIGN
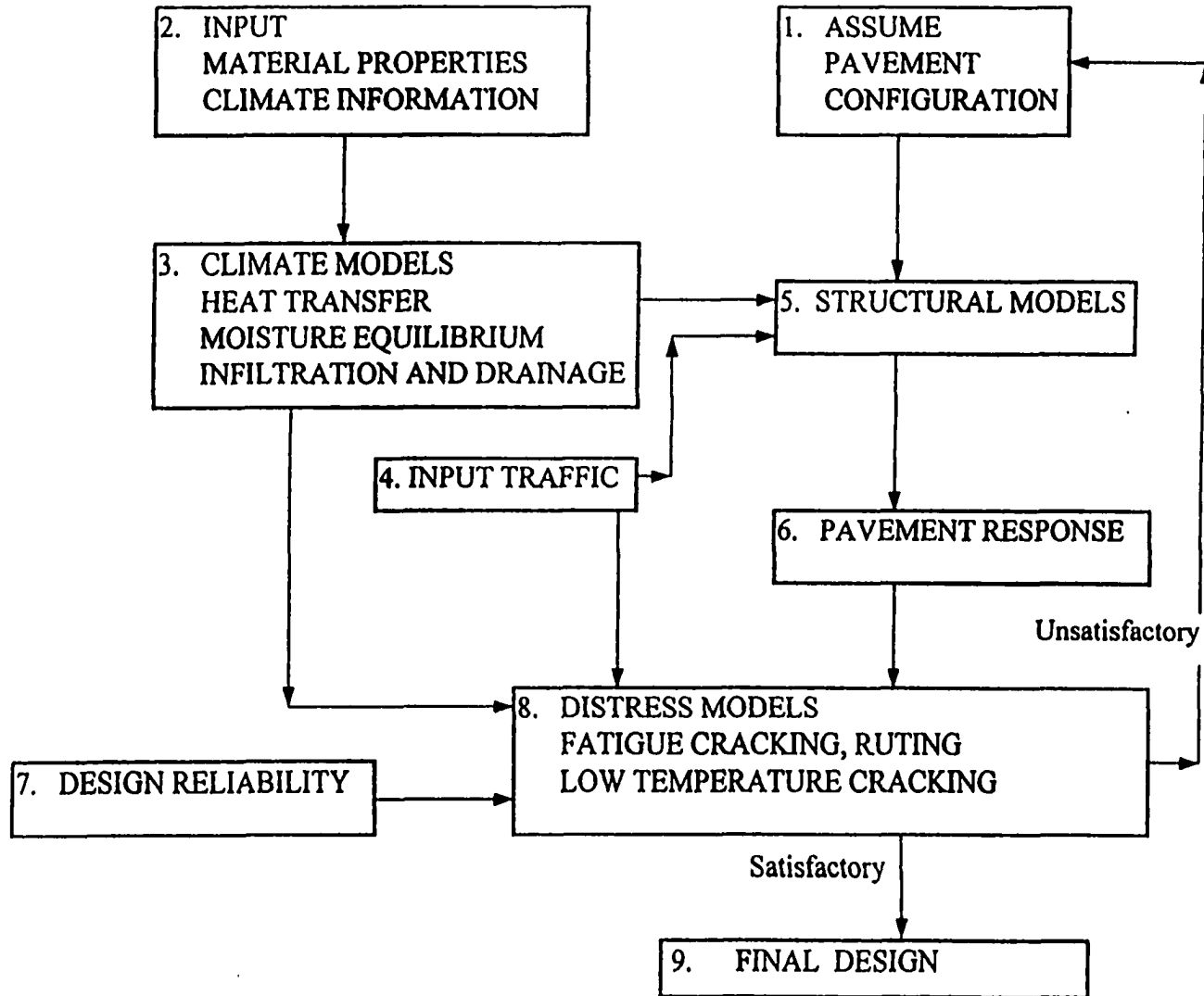
Figure 2-8   Methodology of Calibrated Mechanistic Procedure for
Flexible Pavement Design (after Huang, 1993) .

CHAPTER 3

MATERIALS USED AND THEIR
FUNDAMENTAL PROPERTIES

This chapter describes the sources of the materials used in the present study and discusses briefly their fundamental properties including grain size distribution, index properties, and chemical compositions.

3.1 Granular Base Aggregate

The aggregate used in this study is a Meridian limestone taken from Marshall County, Oklahoma where roadways are being constructed with this aggregate. Figure 3-1(a) and 3-1 (b) show the location of the site and sampling in the field. The aggregate was transported to the laboratory, dried in an oven for 24 hours, and analyzed for grain size distribution using a mechanical sieve shaker according to the standard testing procedure AASHTO T27-93. Table 3-1 and Figure 3-2 present the test results of the sieve analysis, together with the gradation curves required by Oklahoma DOT (ODOT, 1988). The test results show that the effective diameter D_{10} and the mean diameter of the aggregate D_{50} are 0.16 mm and 8.5 mm, respectively. The uniformity coefficient C_u is 75.

The aggregate fine particles, less than 4.25 μm (US No. 40 sieve), were collected after sieve analysis and, liquid limit (LL) and plastic limit (PL) tests were performed in accordance with the standard testing methods AASHTO T89-90 and T90-87, respectively. The tests showed that the LL is 22%, while the plasticity index (PI) is 9. According to the plasticity chart (Casagrande, 1948) used in the classification of

soils, the fine particles is classified as clayey soil (CL). The aggregate is classified as an A-2-4 soil according to the AASHTO M145-82 specifications.

3.2   Cement Kiln Dust (CKD)

Cement kiln dust (CKD) used in this study was provided by Blue Circle Cement Inc. located in Tulsa, Oklahoma. The Tulsa plant utilizes two giant rotary kilns of 425 feet long and 12 feet in diameter. The CKD is collected from the exhaust gases of the cement kilns using bag houses. It is an odorless gray powder with a specific gravity of 2.74 and solubility in water of 0.1 to 0.5%. The liquid limit (LL) and plasticity index (PI) of the pure CKD were determined immediately after mixing with water. The LL and PI values of the CKD were found to be 34% and 8, respectively. The chemical composition of the CKD as tested in five different periods is listed in Table 3-2. The results shown in the table indicate that chemical compositions are quite consistent for the CKD collected from the plant which has same kiln and produces the same cement type. The summation of silica (SiO_2), aluminum oxide (Al_2O_3) and iron oxide (Fe_2O_3) of the CKD ranges from 19.23 % to 20.26 % which is lower than that of fly-ash (34.15 % to 35.26 %), as shown in Table 2-2. The loss on ignition (LOI) ranges from 27.67 % to 29.38 % which is significantly higher than that of fly-ash (5.34 % to 5.59 %). The high LOI value of CKD is due to a high $CaCO_3$ (63.8% to 70.9%). As compared with other CKD composition data shown in Table 2-2, one can see that the chemical composition of the CKD used in this study is similar to that collected from the long-wet kiln, as reported by Todres et al. (1992).

43

3.3   Mixture of Aggregate and CKD

The mixture indicated here is formed by combining aggregate fines passing US No. 40 sieve (4.25 μm) with the different amount of CKD, e.g. 5%, 10% and 15% by weight. The Atterberg limits tests were conducted immediately after mixing since the mixture tended to be cementitious with time. Table 3-3 presents results of Atterberg limit tests on various mixtures. It is found that both the liquid limit (LL) and plastic limit (PL) of the mixture increases with the amount of CKD, while the plasticity index (PI) remains unchanged at 8. The fact that the PL increasing with addition of CKD would mean additional safety because the mixture will still possess strength when the field moisture reaches a value that would soften the raw aggregate.

Table 3-1   Grain Size Distribution of the Aggregates

U.S. Sieve	Sieve Opening mm	ODOT Gradation Limits %, Passing			As Tested %,passing
		Coarser	Finer	Median	
1-1/2 in.	38.1	100	100	100	98.2
1-1/4 in.	31.75	85	100	90	91.8
1.0 in.	25.4	60	100	80	81.5
0.75 in.	19	40	100	70	71.4
0.5 in.	12.7	35	85	60	58.8
0.375 in.	9.5	30	75	52.5	51.7
No.4	4.75	25	60	42.5	38.6
No.40	0.425	8	26	17	14.2
No.200	0.075	4	12	8	6.3

Table 3-2   Chemical Composition of CKD Used in the Study
(Blue Circle Cement, Inc. 1997)

Chemical Compound	Amount, %				
	A	B	C	D	E
Silica (SiO_2)	15.08	14.66	14.75	14.4	13.82
Aluminum oxide(Al_2O_3)	3.29	3.94	3.90	3.7	3.85
Iron oxide (Fe_2O_3)	1.23	1.38	1.61	1.4	1.56
$SiO_2 + Al_2O_3 + Fe_2O_3$	19.60	19.98	20.26	19.50	19.23
Calcium oxide (CaO)	41.09	41.52	41.98	42.4	44.07
Magnesium oxide (MgO)	1.41	1.40	1.46	1.4	1.46
Sulphur oxide (SO_3)	7.00	6.09	4.58	2.6	2.49
Sodium oxide (Na_2O)	0.43	0.45	0.61	0.3	0.34
Potassium oxide (K_2O)	2.37	2.44	2.65	1.7	1.54
Calcium Carbonate (CaCO3)	70.90	—	—	63.8	64.22
Loss on ignition (LOI)	27.93	28.00	27.67	28.9	29.38

Notes: A: Tested on 1/15/90; B: Tested on 10/18/90

C: Tested on 9/25/91;   D: Average of 26 samples tested in 1996.

E: Average of 32 samples tested in 1997.

Free lime is 2-3% as analyzed on July 6, 1997.

Table 3-3   List of Index Properties of Materials Used in the Study

Aggregate Type	Liquid Limit, %	Plastic Limit, %	Plasticity Index
raw aggregate	21.9	13.4	8.5
raw agg. + 5% CKD	26.3	17.8	8.5
raw agg. + 10% CKD	28.8	20.4	8.4
raw agg. + 15% CKD	31.5	23.2	8.3
raw CKD	34	25.9	8.1

Note: Aggregate particles used for Atterberg test are less than 4.25 μm.

(a) Aggregate stockpile

(b) Sampling in Progress

Figure 3-1 Meridian Aggregate Quarry Site
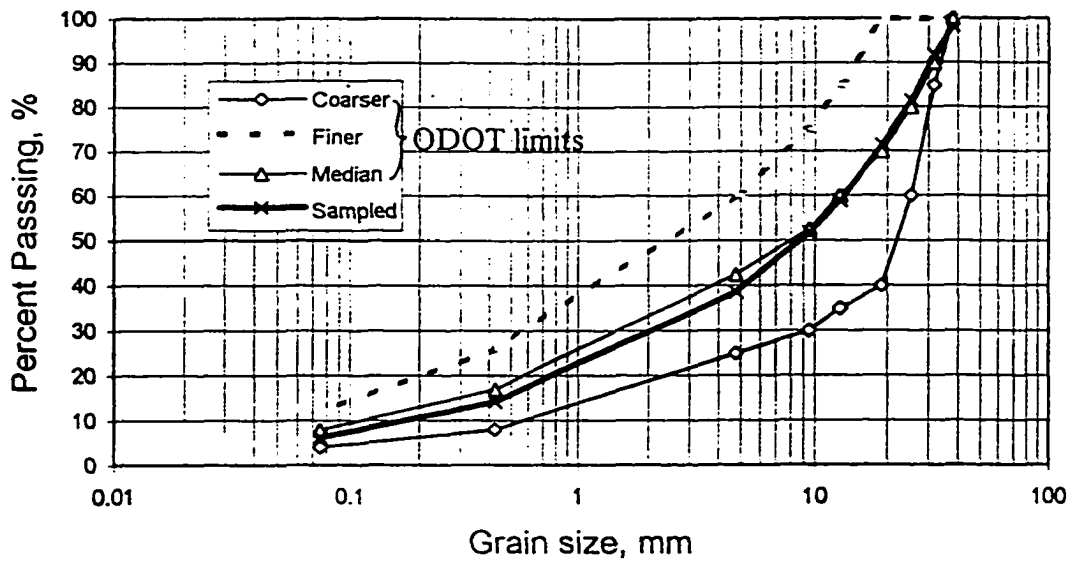
Figure 3-2   Grain Size Distribution of the Aggregate Specified by ODOT and Used in This Study

CHAPTER 4

EXPERIMENTAL METHODOLOGY AND

TESTING PROCEDURE

4.1   Introduction

To achieve the goal of this study, various laboratory experiments were conducted. These tests include Los Angles Abrasion test on raw aggregate, Moisture-Density test on both raw and CKD-stabilized aggregates, resilient modulus test on raw and stabilized aggregates, flexural strength and durability tests on stabilized aggregates, and microanalyses including XRD and SEM analyses on the raw and CKD-stabilized aggregates. A flowchart of the laboratory tests conducted are shown in Figure 4-1, including the modeling tasks undertaken. All the test methods used, except the index properties tests, namely liquid limit and plastic limit tests that have been reported in the preceding chapter, are presented in this chapter. Standard testing procedures (AASHTO) were used for tests because such procedures are available, while the durability tests were conducted using the method developed in this study.

4.2   Preliminary Tests

The preliminary tests reported here include the Los Angles (LA) abrasion and the Moisture-Density (MD) tests. The former has been widely used as an indicator of relative quality or competence of an aggregate, and the latter is mainly used for the assessment of compaction quality.

4.2.1   Los Angles Abrasion (LA) Test

The LA test is a measure of degradation of mineral aggregates of standard gradings resulting from a combination of actions including abrasion or attrition, impact, and grinding in a rotating steel drum containing steel spheres or solid balls. The tests were conducted according to the AASHTO standard test method, AASHTO Designation: T 96-94. Five replicate tests were performed and the results are presented in Table 4-1. The LA abrasion values of the aggregate range from 32.6% to 33.5% with an average of 33.26%.

4.2.2 Moisture-Density Tests

The moisture-density tests were conducted according to the AASHTO designation: T180-93 (AASHTO T180-93). The method is designed for determining a relationship between the moisture content and dry density of aggregates when compacted in a 15.24 cm diameter mold with a 44.48 N hammer dropped from a height of 45.72 cm. The raw aggregate samples were prepared according to a median gradation curve specified by ODOT for type A aggregate. The tests were also conducted on aggregates stabilized with 5%, 10% and 15% CKD by weight. The results of these tests are presented in Figure 4-2 and Table 4-2.

From Figure 4-2, one can see that the maximum dry density γ_{dmax} and optimum water content w_{opt} of the raw aggregate are 20.9 kN/m^3 and 7.5 percent, respectively. The addition of CKD in the aggregate samples actually results in an increase in fine contents of the aggregate, thus slightly reducing γ_{dmax} value, but slightly increasing the w_{opt} value. For example, the value γ_{dmax} becomes 20.3 kN/m^3, and w_{opt} gets to be 8.8%, respectively, when 15% CKD is added in the aggregate. Azad (1997) reported that the

increase in w_{opt} of compacted fine soils due to addition of CKD can be 3% more than the raw soils. The minor increase in w_{opt} in CKD-stabilized aggregate can be attributed to the existence of large portion of coarse particles which actually neither absorb water nor react with CKD.

4.3 Flexural Strength Test

As mentioned in Chapter 2 (Section 2), a stabilized aggregate may develop a certain amount of flexural strength which would be helpful in maintaining the integrality of the base. To study the effectiveness of CKD-stabilization under flexural loads, beams with 406L x 109W x 76H mm were molded in the laboratory. A pre-calculated amount of stabilized aggregate, according to a compaction criterion of 0.96 γ_{dmax}, was placed into a wooden mold using a plate for load transfer from a hydraulic jack. Three different amounts of CKD, i.e. 5%, 10% and 15%, were used in mixing materials for the beam specimens. After compaction, the beams were wrapped in plastic sheets and transferred to a curing chamber with a temperature of 70°F and a relative humidity of 90-100 percent, where they were cured for 28-days for each type of sample, and 90-days for only 15%-CKD stabilized samples.

At the end of a given curing period, the beams were unwrapped and tested in accordance with the standard testing procedure AASHTO T97-86, which relates to the flexural strength of simply supported concrete beams under third-point loading. Figure 4-3 shows loading arrangement and failure mode of the beams. The results from beam test are presented in Chapter 5 (Section 2).

52

4.4 Resilient Modulus Test

4.4.1 Test Procedure and Sample Preparation

The resilient modulus tests were conducted in accordance with the standard testing procedure AASHTO T294-94. In AASHTO T294-94, there are two types of testing methods for two different kinds of materials: Type I (unbound granular) and Type II (cohesive). The raw aggregate used in this study can be treated as an unbound granular material and therefore the procedure specified for Type I material was followed. However, presently, there is no specification for stabilized aggregates that have a tendency to behave more like an unbound granular material than a cohesive soil. So, in the present study, all the resilient modulus tests for stabilized aggregate were performed in compliance with the procedure specified for Type I material. As stated in the procedure, the cyclic stress applied is a haversine-shaped load pulse consisting of 0.1 second loading followed by 0.9 second relaxation period, as shown in Figure 4-4. Before testing a sample for the RM value, the sample is subjected to 1,000 cycles of conditioning load under 103 kPa confining pressure and 103 kPa deviator stress. This conditioning is believed to be helpful in eliminating the effect of the interval between compaction and loading and, elimination of initial loading versus reloading (Chen, 1994). It also minimizes the effect of imperfect contact between the end platens and the test specimen. Following conditioning, the deviator stress and confining pressure are both reduced to 21 kPa and 100 repetitions of cyclic deviator stress are applied and the average deformation of a specimen during the last five repetitions are used for calculating the RM value. Repeating these procedures with Sequence No. 2 through

No. 15, as listed in Table 4-3, gives the desired RM values as a function of bulk or deviator stress.

The stabilized samples were prepared in a sequence of mixing, compacting and curing. All mixes were prepared in an aluminum pan that provides enough space for mixing one cylindrical sample (D = 152.4 mm, H = 304.8 mm) at a time. First, the raw aggregates were weighed and placed in the pan where they were mixed by means of a large spoon; then, CKD was added and the whole mass was mixed to uniformity. Three different mix proportions with CKD amount being 5%, 10% and 15% weight of the raw aggregate were selected. After mixing, the measured portable water was added in small doses while the mixing was in progress. The amount of water added was determined according to an optimum water content of the samples, as determined by moisture-density tests. Mixing continued for twenty to thirty minutes after the addition of all the materials until a uniform mix was obtained.

A vibratory compaction method (Chen, 1994) was used to compact samples using a special split mould with provision to apply a desired amount of vacuum to fit the membrane tightly on the inner surface of the mold. Figure 4-5 shows a photographic view of the equipment used for the preparation of the RM samples. The internal diameter and the height of the mold are 15.24 cm and 30.48 cm, respectively. To ensure the mold would not move during vibration, the base of the mold was firmly bolted onto the vibrating table that was controlled by a controller with a maximum speed of 60 vibrations per second. The sample, with an optimum moisture content, as decided in the compaction tests, was prepared in 10 layers with approximately 1600 g

of aggregate per layer. Fifty blows with a steel rod on the surface of each layer was applied during vibration to enhance effectiveness of compaction. The vibration time was approximately 30 sec per layer for the first eight layers and 4 min per layer for the last two layers (Chen et al., 1994). This method yields more uniform specimens than those prepared by using equal vibrating times for each layer, in which case the bottom layer usually becomes denser than other layers as a result of vibrating times accumulating from bottom to top. It was found that all specimens compacted following this procedure were equal to or greater than 95% the maximum dry density at optimum moisture content. Specimens stabilized with CKD were then placed into a curing room, as shown in Figure 4-6, with a constant temperature of 70^0 F and a relative humidity of 95% or higher for the desired curing periods before testing. To ensure reliability of the results for each case, at least five replicate specimens were prepared and tested.

4.4.2   Testing Equipment

The RM testing equipment setup is shown in Figures 4-7 and 4-8. The prepared specimen was mounted on the triaxial chamber between the bottom and top platens with attached porous stones. The specimen in the chamber was subjected to a confining (air) pressure which simulates the lateral stress caused by the overburden pressure and moving vehicle loading. The material testing system (MTS) consists of a loading frame, an MTS 458.20 micro console, an MTS 458.91 micro profiler, and a hydraulic power supply. The micro profiler was programmed to apply various types of cyclic loading in a very efficient and accurate manner. The micro console was used to control the MTS load actuator.

A Gateway2000, 486 DX2 personal computer with 50 MHZ microprocessor along with a data acquisition board was used to monitor the RM test. The load cell and the LVDTs were connected with the computer for acquiring stress-strain data during the test.

4.4.3 Accuracy of Measured RM Values

Accuracy refers to the correspondence between the measured value and the actual value. In a RM test, the accuracy the recoverable axial strain ε_r is more important than the deviator stress σ_d because a very small variation in ε_r would produce a notable change in RM values. The data acquisition system used here for LVDT divides a range of vertical deformation ± 25.4 mm into 4096 segments, which means that the resolution of the measured vertical deformation is $50.8/4096 = 0.0124$ mm. The corresponding axial strain $\Delta\varepsilon$ is $4.067 * 10^{-5}$ (i.e. $0.0124/304.8$, 304.8 mm being the sample height). For a typical $\sigma_d \sim \varepsilon$ curve of RM test, as shown in Figure 4-9, the measured RM is calculated from the following equation:

$$RM = \frac{\sigma_{1d} - \sigma_{d2}}{\varepsilon_1 - \varepsilon_2} = \frac{\Delta\sigma_{d1-2}}{\Delta\varepsilon_{1-2}} \qquad (4-1)$$

Considering a possible deviation ($\Delta\varepsilon$) in the actual axial strain, the actual RM value may fall between the lower bound RM_L and the upper bound RM_U as given below:

$$RM_L = \frac{\Delta\sigma_{d1-2}}{\Delta\varepsilon_{1-2} + \Delta\varepsilon} \qquad (4-2)$$

$$RM_U = \frac{\Delta\sigma_{d1-2}}{\Delta\varepsilon_{1-2} - \Delta\varepsilon} \qquad (4-3)$$

In order to establish the level of accuracy in RM values achieved from the current experimental program, RM_L and RM_U values were evaluated from Eqs. (4-2) and (4-3) for typical RM tests. Figure 4-10 shows a typical relationship between the range of RM values and deviator stress for a 28-day cured aggregate sample stabilized with 15% CKD. In the current study, the resilient modulus (RM) mentioned subsequently refers to value obtained from experimental data using equation (4-1). However, the possible range of RM values varying between the lower bound RM_L and the upper bound RM_U should be taken into account for practical applications. In view of Figure 4-10, the possible maximum relative error is about 20%. However, for most cases this error is expected to be much smaller because of its stress dependent nature as shown in Figure 4-10.

4.5   Durability Test

To evaluate the ability of chemically stabilized aggregates to resist deleterious effects of freezing-thawing and wetting-drying cycles, the resilient modulus tests were conducted on CKD-stabilized specimens that have been subjected to different freezing/thawing or wetting/drying cycles. These specimens were prepared in the same manner as other stabilized specimens. The curing period before the commencement of freezing/thawing or wetting/drying cycles was 7 days.

One freezing and thawing cycle used here consists of placing a specimen in a freezer, as shown in Figure 4-11, not warmer than 5°F (-15°C) for 24 hours and then placing it in a cabinet having a temperature 71°F (21.6°C) and relative humidity greater than 95% for 24 hours. Three different number of cycles, i.e. 4, 8 and 12 cycles, were

used in the course of this study. At the end of specified cycles, the specimens (under thaw condition) were tested to determine their RM and UCS values.

One wetting and drying cycle used in this study consists of placing a specimen in an oven, as shown in Figure 4-12, having a temperature 160°F (71°C) for 24 hours then immersing the specimen in a portable water tank, as shown in Figure 4-13 for 24 hours. Three types of cycles, i.e. 4, 8 and 12 cycles, were pursued in the course of the testing program to determine the effect of number of wetting/drying cycles on the RM values. At the end of specified cycles, the specimens (at wet condition) were tested to determine their RM and UCS values. During the RM test, the drainage valve was kept open for all the tests except for one test, initiated by providing a database for the ANN model presented in Chapter 6, the valve was closed to see the influence of drainage on the RM value of stabilized aggregate.

4.6   Unconfined Compressive Strength Test

Since the RM test is a non-destructive test, the specimens can be used to determine some strength parameters, following the RM test. Thompson and Smith (1990) noted that the shear strength of unconditioned specimens does not represent the strength of an in-service compacted granular base material subjected to traffic loading. Therefore, most unconfined compressive strength (UCS) tests were conducted using the specimens that have been subjected to repeated triaxial loading. An effort was also made to test regular specimens that have not been subjected to RM testing. All the UCS tests were conducted in accordance with the AASHTO Designation: AASHTO T208-92. Although effect of membrane resistance is of significance for soils having low

strength (Zhu and Anderson, 1998), the strength contributed by the rubber membrane is found to be less than 1% of the UCS of the raw aggregate specimens. So, in this study the membrane resistance was not taken into account in determining UCS values for all the samples. In addition to determination of UCS, the stress-strain curves obtained in the UCS test were used to evaluate elastic modulus (EM).

4.7   X-Ray Diffraction (XRD)

The XRD analysis was employed in this study to examine the mineralogical content of the raw aggregate, raw CKD and CKD-stabilized aggregates. Portions of a broken specimen after RM and UCS tests were collected and crushed with a hammer. Every effort was made to separate the binder material from the aggregate fraction of the specimen. The material passing through U.S. standard sieve No. 1/4 was oven dried at a temperature 100°C for about two hours to remove any excess moisture. These samples were then ground with pestle and mortar to pass a U.S. standard sieve No.200. The X-ray diffraction specimen was side-loaded onto the X-ray machine to help avoid preferred orientation.

The X-ray diffraction tests were performed using a Siemen D-500 diffractometer with copper X-ray tube operated at 50 kV 27 mA. Figure 4-14 shows a photograph of the X-ray diffractometer used in this study. Two theta degrees of the diffraction range from 3° to 70.5°. For the purpose of comparison, the analysis was also performed on raw CKD samples prepared in the same manner as the aggregate.

4.8   Scanning Electron Microscopy (SEM)

To study microstructure development in the stabilized aggregate matrix and to identify the important reaction products over the various curing periods, specially prepared specimens were microscopically examined by a SEM. Following each series of RM and UCS tests, fragments about 6.0 mm sized matrix were removed and collected from the specimen for use in the SEM studies. Processing these samples are similar to that reported by Baker and Laguros (1985). The collected samples were first oven dried for about an hour, then doused with acetone to arrest hydration process. The material was again oven dried for two hours and saved in air tight bottles. After sample preparation the thinly sliced fragment was mounted on a copper stub with the help of a conductive double sided adhesive tape. A thin layer (approximately 200 Angstrom) of gold palladium was sprayed onto the specimen surface to provide surface conductivity. The coated specimen was then placed in a JEOL JSM Scanning Electron Microscope operating at 15 kV, as shown in Figure 4-15. A self-developing black and white Polaroid film was used to take the micrographs of the observation. At the same time, energy dispersive spectroscopy (EDS) was employed for a qualitative element analysis of the specimens.

Table 4-1 Los Angles (LA) Abrasion Test Results

Test No.	Sample Weight (kg)		Percent Loss (%)
	Before Test	After Test	
Test 1	5.000	3.370	32.60
Test 2	5.004	3.328	33.50
Test 3	5.000	3.326	33.40
Test 4	5.002	3.338	33.30
Test 5	5.008	3.327	33.50
Average			33.26

Table 4-2 Moisture-Density Test Results

Material Type	Maximum Dry Density γ_{dmax} kN/m^3	Optimum Water Content w_{opt}, %
Raw Aggregate	20.9	7.5
Raw Aggregate + 5% CKD	20.8	7.9
Raw Aggregate + 10% CKD	20.6	8.3
Raw Aggregate + 15% CKD	20.3	8.8

Table 4-3 Testing Sequence for Type I Soils (AASHTO T294-94)

Sequence No.	Confining Pressure σ_3 kPa	Deviator Stress σ_d kPa	Bulk Stress θ kPa	Number of Load Applications
0	103	103	412	1,000
1	21	21	83	100
2	21	41	103	100
3	21	62	124	100
4	34	34	138	100
5	34	69	172	100
6	34	103	207	100
7	69	69	276	100
8	69	138	345	100
9	69	207	414	100
10	103	69	379	100
11	103	103	414	100
12	103	207	517	100
13	138	103	517	100
14	138	138	552	100
15	138	276	690	100
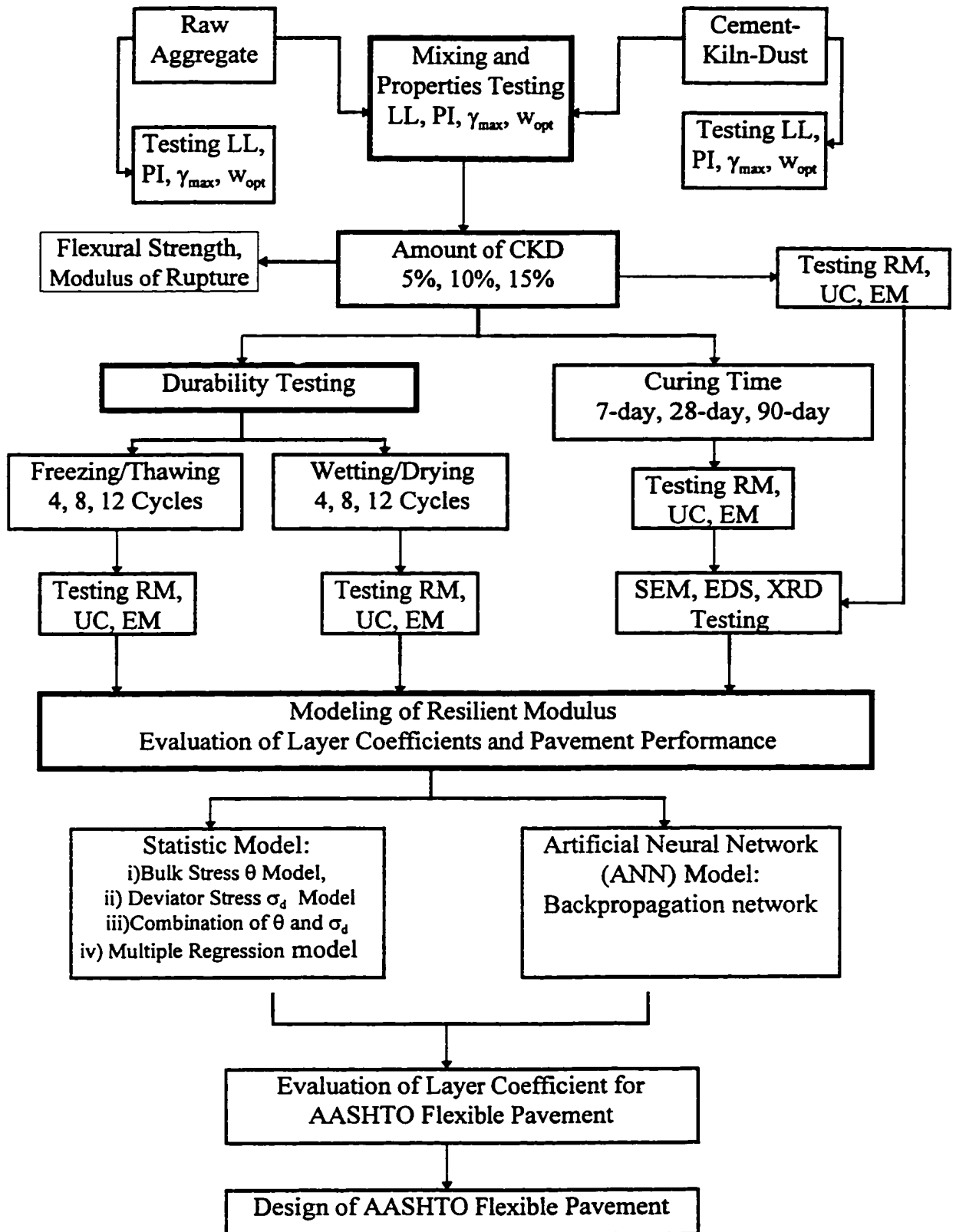
Figure 4-1   Flowchart of Experimentation and Modeling/Evaluation
of CKD-Stabilized Base/Subbase Aggregate
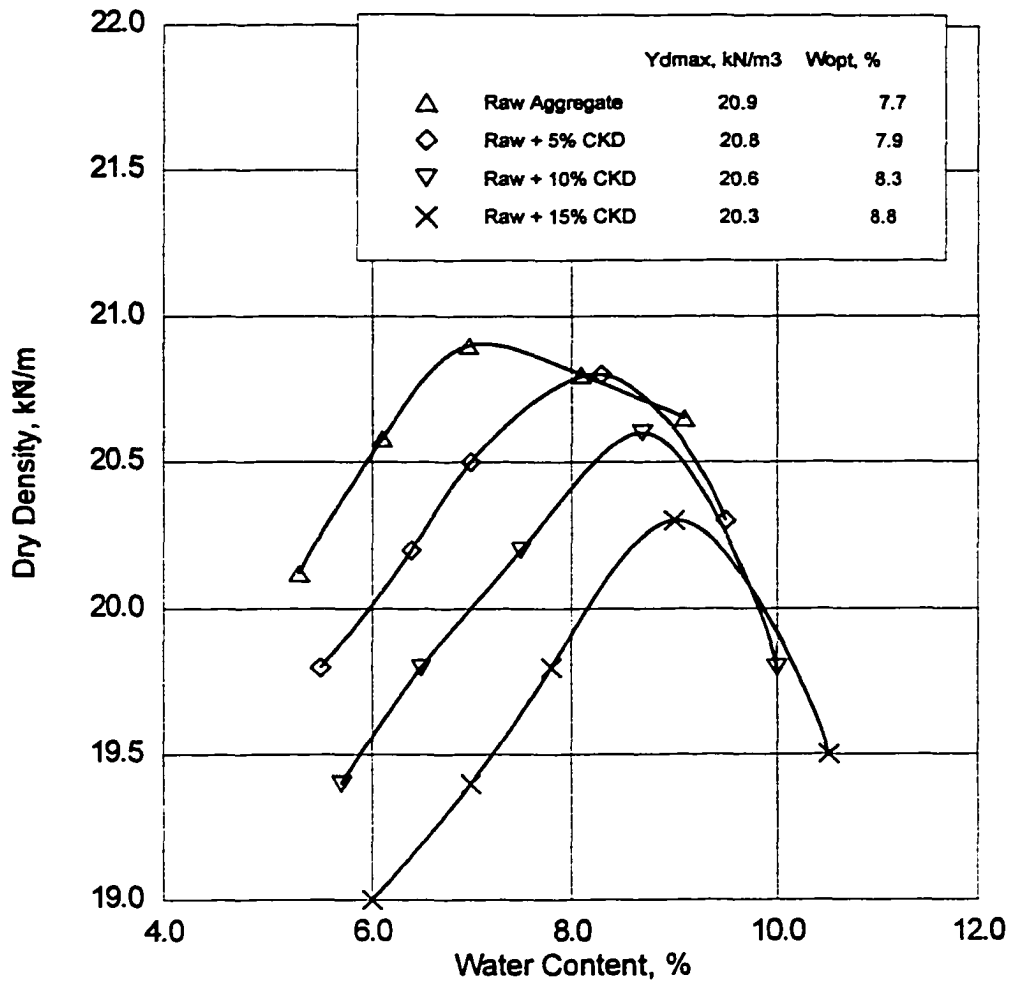
Figure 4-2 Moisture-Density Testing Results
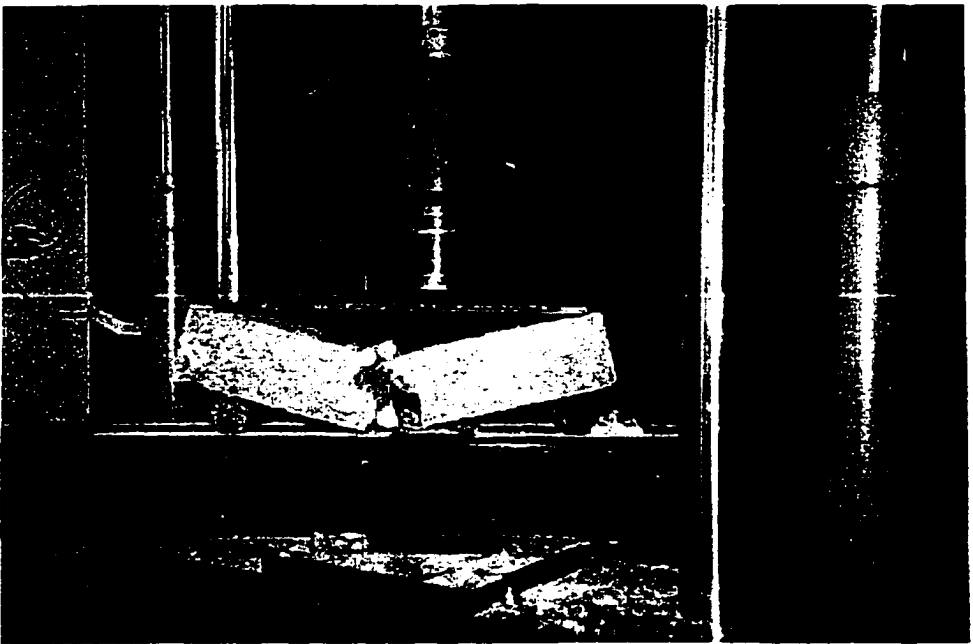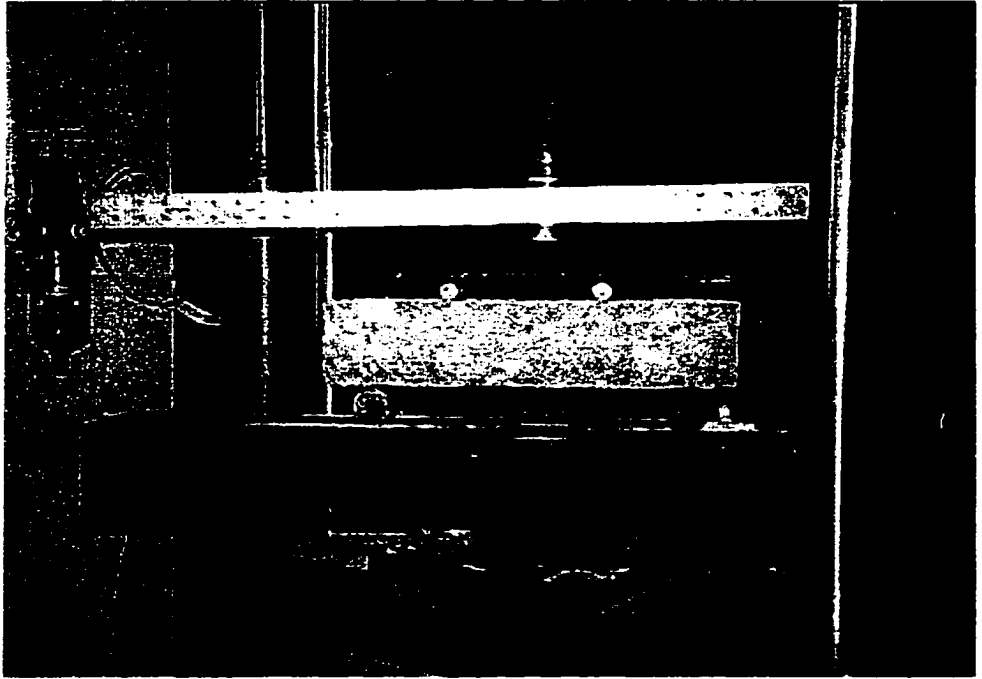
Figure 4-3   Beam Loading Arrangement and Failure Pattern
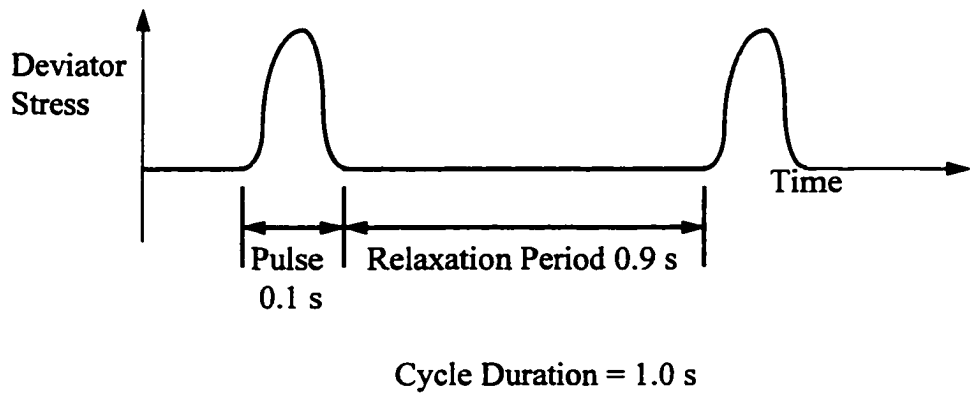
Cycle Duration = 1.0 s

Figure 4-4   Haversine Stress Pulse with 1 Second Loading Cycle Duration

Figure 4-5 Equipment for Specimen Preparation
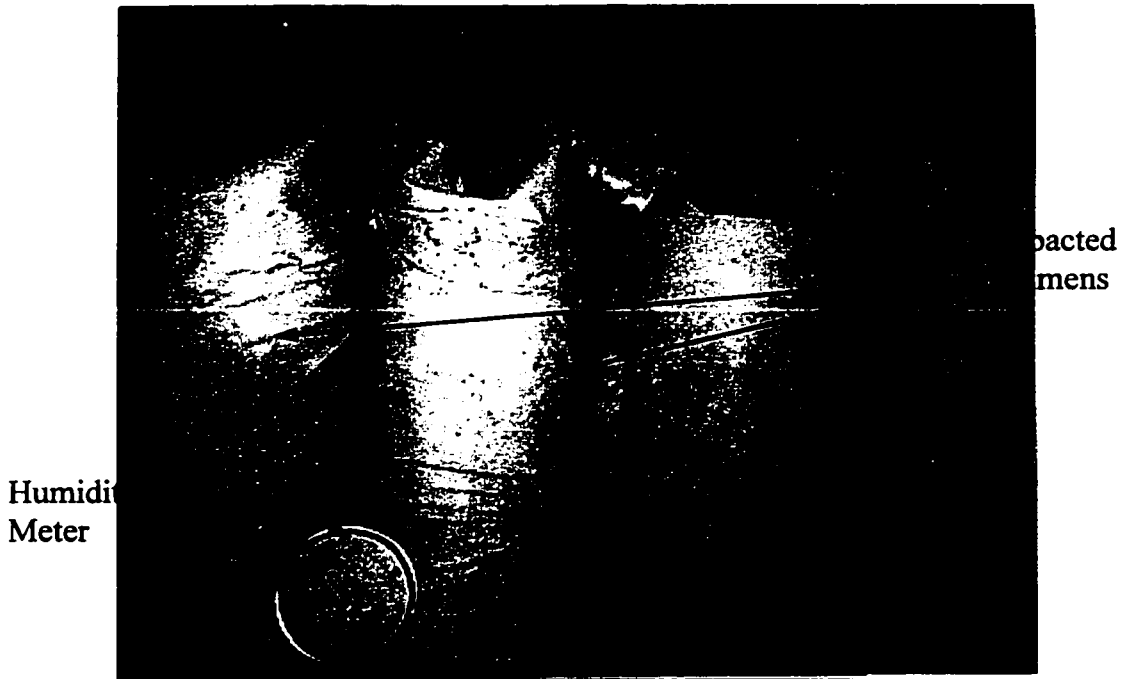
Figure 4-6   Curing of Specimens in the Humidity Chamber Having
               Temperature of 70° F and 95% or Higher Relative Humidity
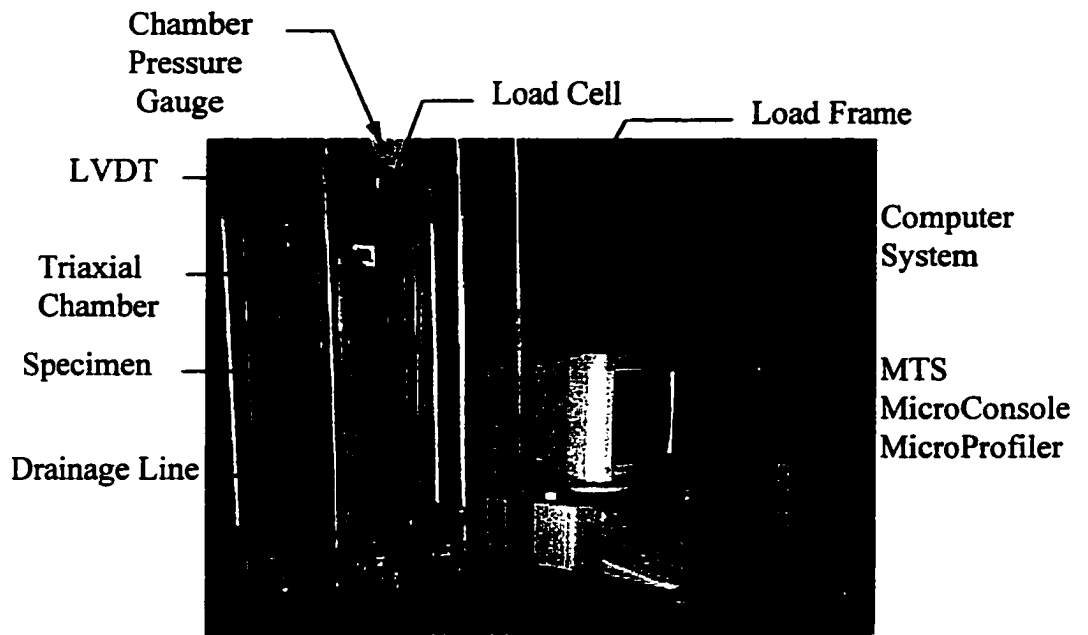
Figure 4-7   Setup of the Test Specimen in Triaxial Chamber of MTS
Machine together with the Personal Computer
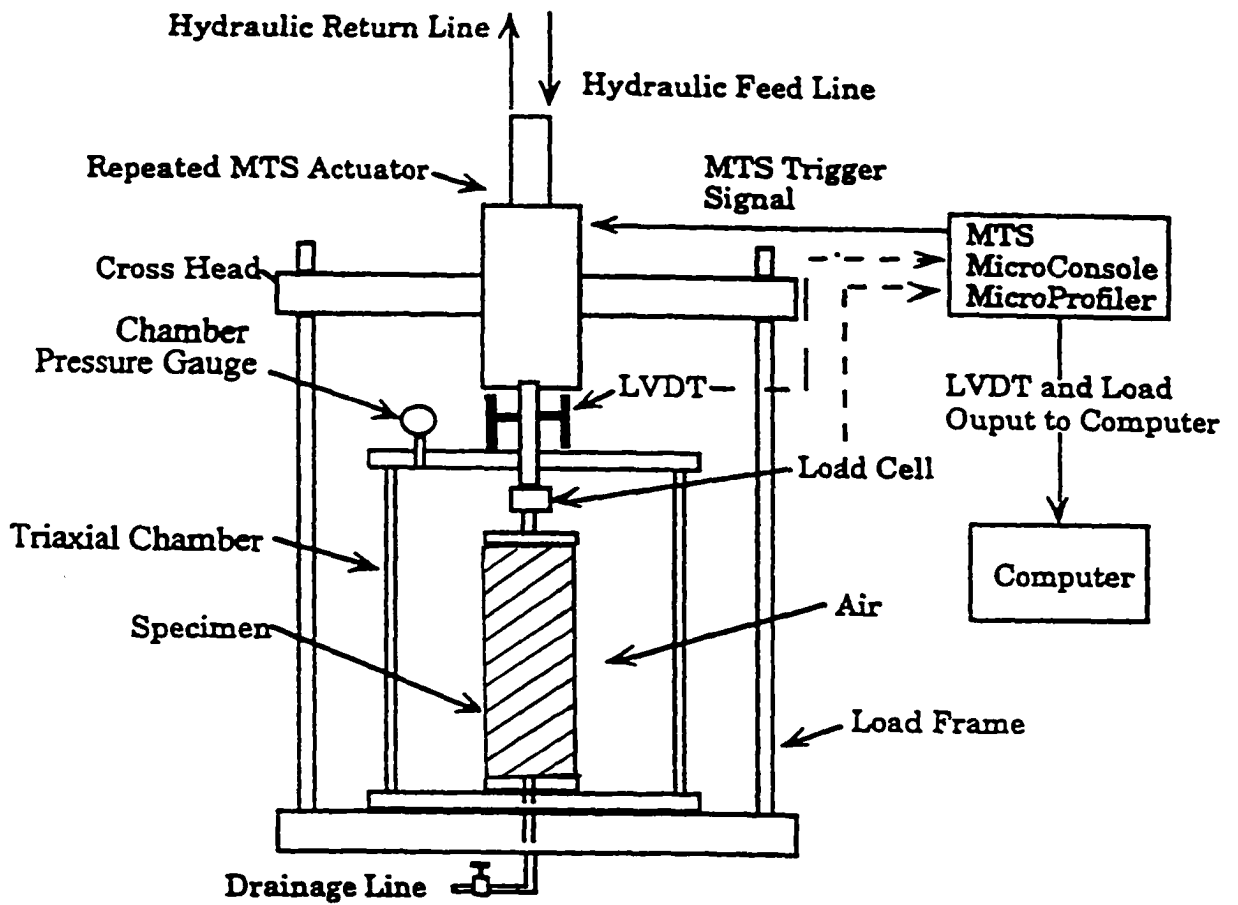
Figure 4-8 Flow Diagram of the Test Setup for Resilient Modulus Testing
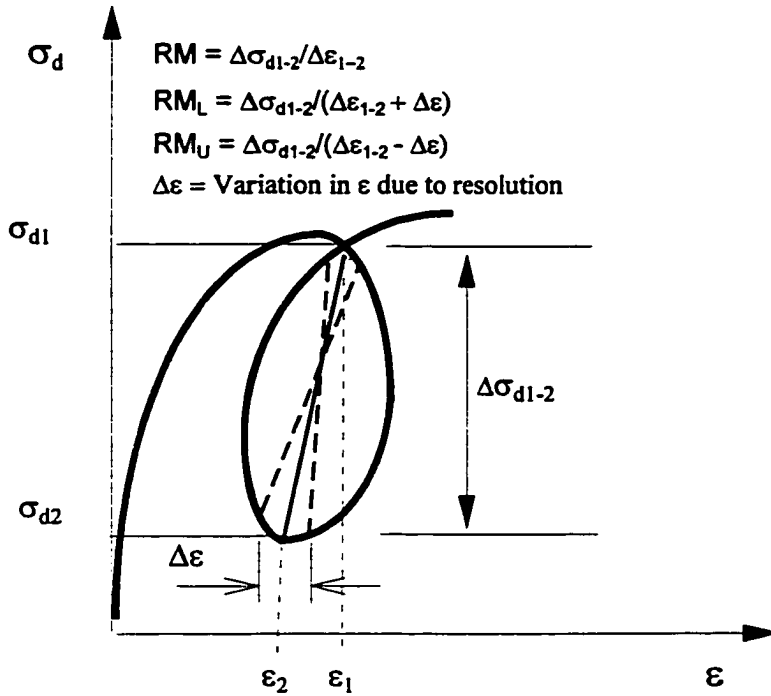
Figure 4-9   Typical σ_d - ε Curve Showing Calculation of Resilient Modulus Values

70
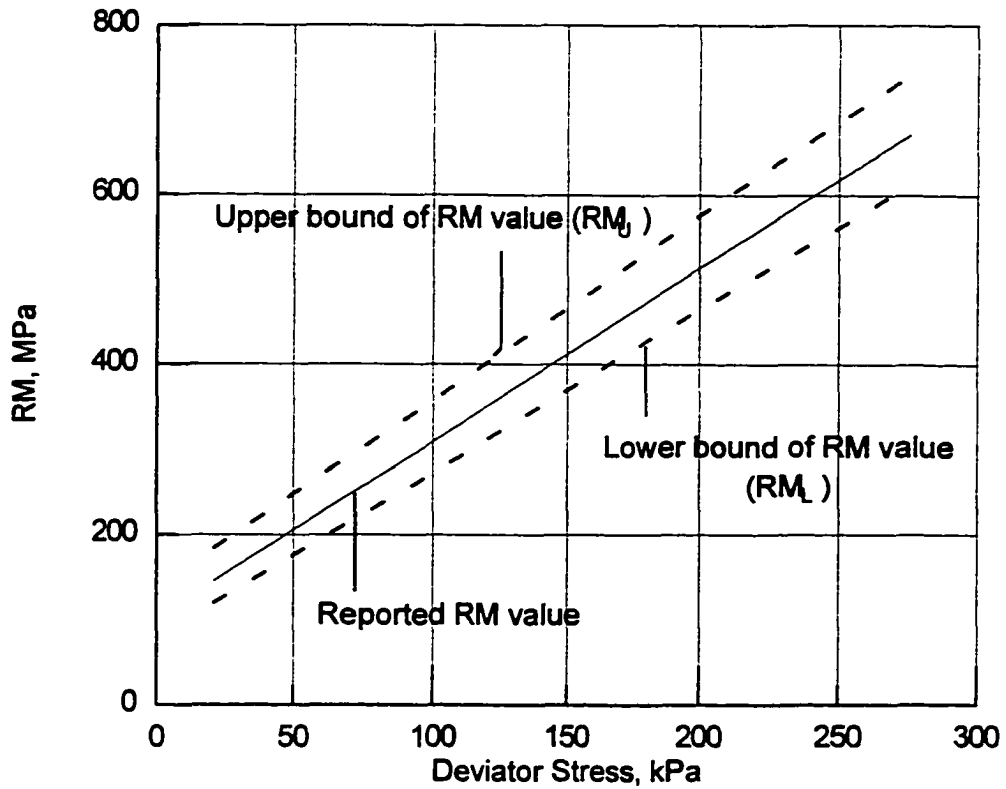
(a) Range of RM values
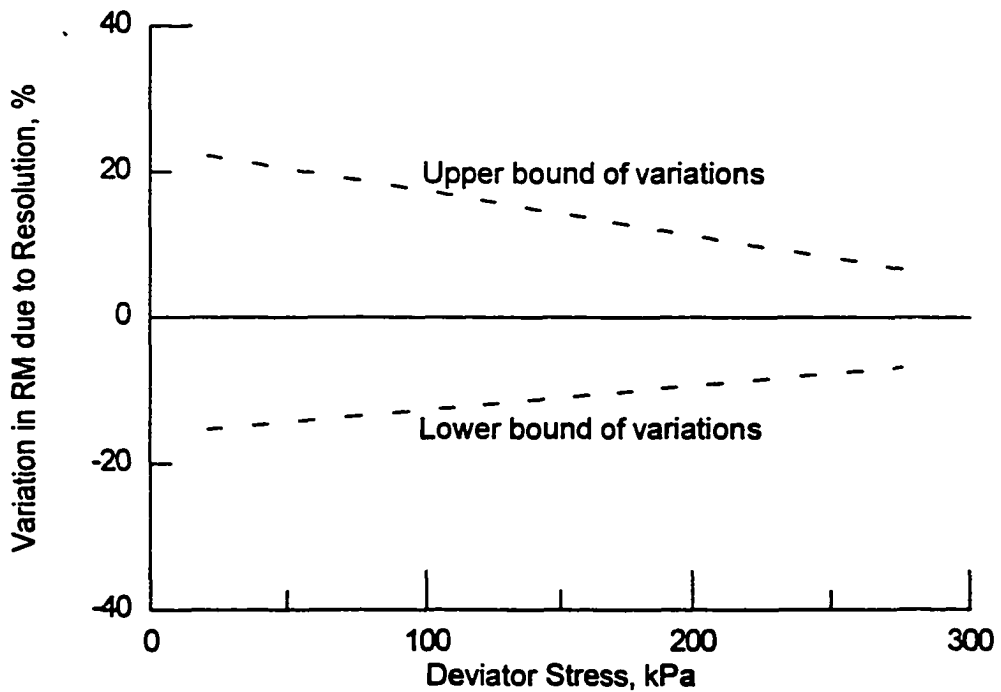
(b) Relative variations in RM

Figure 4-10   Accuracy of Measured RM Values in the Experiment
(28-day cured aggregate with 15% CKD)

71
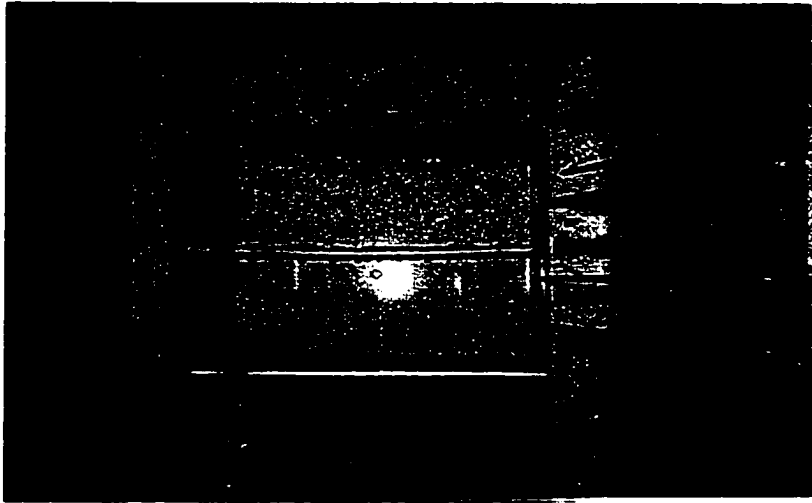
(a) A Photographic View of the Freezer
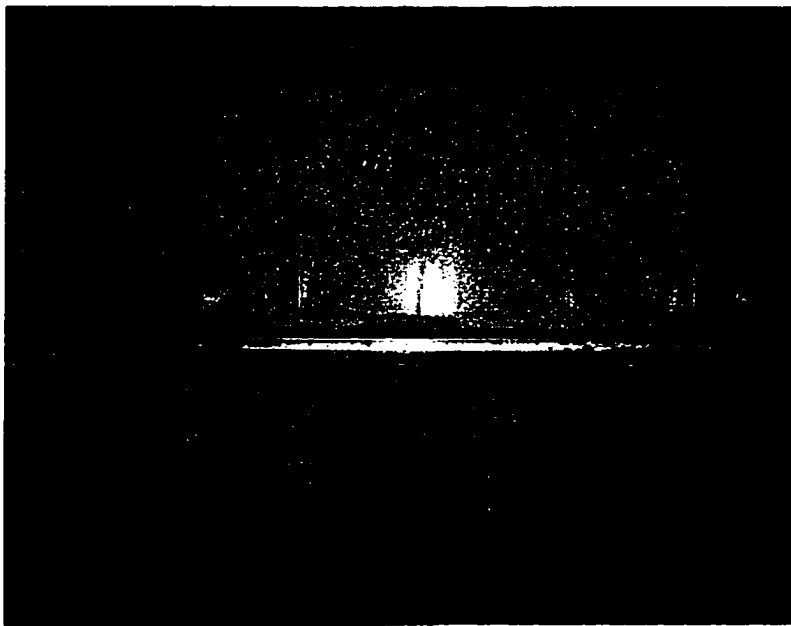
(b)   A Photographic View of Frozen Specimens

Figure 4-11   Freezing of Test Specimens in the Freezer Having a
Temperature of 5° F (-15°C)
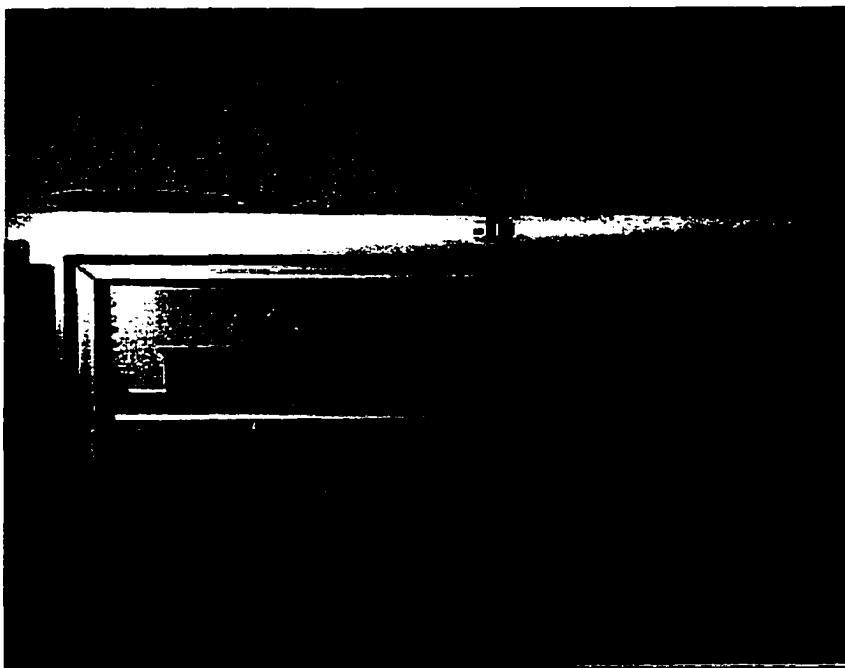
Figure 4-12   Photograph Showing Drying of Test Specimens in an
Oven Having a Temperature of 160° F (71° C)
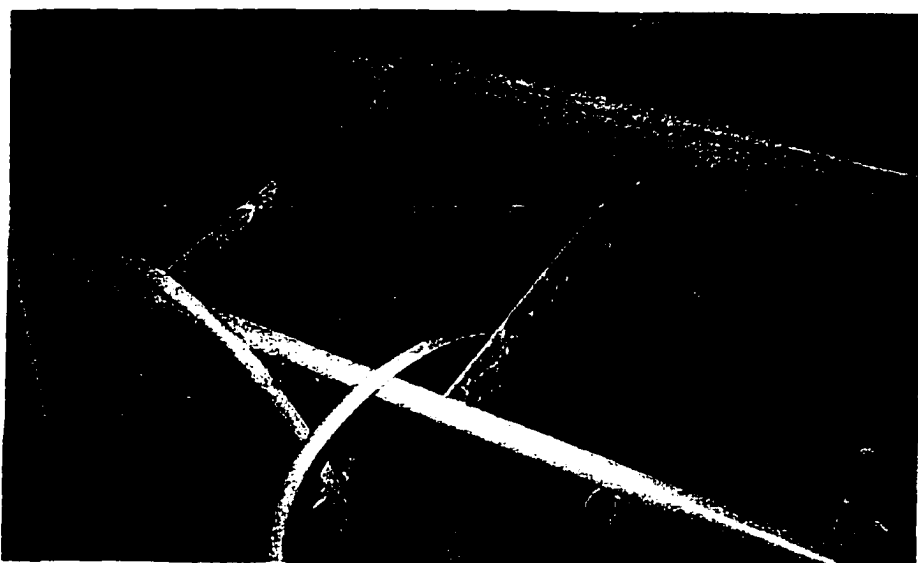
Figure 4- 13 Photograph Showing Wetting of Test Specimens in a
Water Tank

Figure 4-14 A Photographic View of the X-Ray Diffractometer
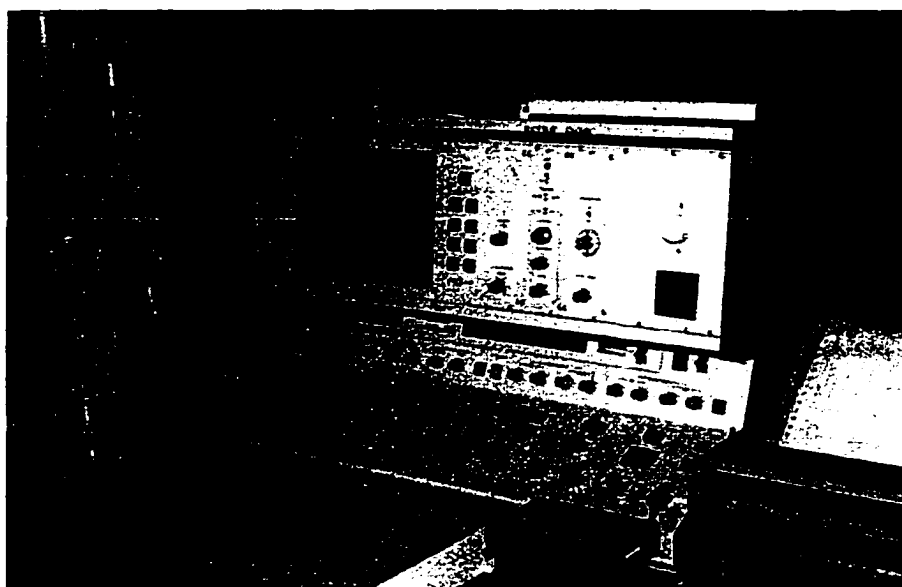
Figure 4-15 Photograph of a JEOL JSM 880 Scanning Electron
Microscope

CHAPTER 5

PRESENTATION AND DISCUSSION

OF EXPERIMENTAL RESULTS

5.1 Introduction

This chapter presents the results of the tests conducted in this study, including flexural strength test, resilient modulus and unconfined compressive strength tests, and durability tests. The effects of CKD contents and curing periods on the RM, UCS and EM values are discussed. The deleterious effects of freezing-thawing and wetting-drying cycles on the RM, UCS and EM values are evaluated. Finally, the results from XRD and SEM analyses are used to help explain and interpret the mechanisms associated with the CKD-stabilization.

5.2 Flexural Strength

Test Results

Flexural strength tests were conducted in accordance with the AASHTO Designation: T 97-86. The load deflection characteristics of the stabilized aggregates were evaluated by the third-point beam loading. Eight beam specimens were prepared with two for 28-day cured aggregate stabilized with 5%, 10% and 15% CKD, and two for 90-day cured aggregate stabilized with 15% CKD. It is noted from the beam tests that the CKD-stabilized aggregates can develop a small amount of flexural strength upon curing. However, some of the beam samples constructed with 5% and 10% CKD could

75

not be tested since they broke due to low strength as they were placed on the MTS machine.

The fracture of tested samples were all initiated in the tension surface within the middle third of the span length of the beam, as shown in Figure 4-3. The load-deflection curves of the beams tested are shown in Figure 5-1. The salient feature, as reflected by the load-deflection curves, is that the beams lost their strengths quickly upon approaching their peak strengths. The ultimate flexural strength or modulus of rupture (MR) of a beam was calculated in accordance with the AASHTO Designation: T 97-86 as follows:

$$MR = PL/bd^3 \tag{5-1}$$

where:

MR = modulus of rupture, kPa,

P = maximum applied load, N,

L = span length, mm,

b = average width of a specimen, mm, and

d = average depth of specimen, mm.

Table 5-1 shows the MR values for CKD-stabilized beams. The MR values of tested specimens ranges from 55 kPa to 154 kPa, showing significant variability of the MR values. There is no apparent tendency of the MR values varying with amount of CKD and curing time. The variability of the MR values can be deemed as the result of non-uniformity of sample preparation, because the beam samples were prepared using static method which may not produce uniform sample for the coarse aggregate mixture. As compared with cement stabilization, or lime or fly-ash stabilization (Laguros and

Keshawarz, 1987; Zenieris, 1988; Cavey et al. 1996), the CKD-stabilized aggregate develops the lowest flexural strength.

<u>Application of Flexural Strength</u>

In view of the flexural strength developed from CKD-stabilization, it may be noted that the treated aggregate base will be stronger in flexural response than an untreated aggregate base. Since the value of the flexural strength of the CKD-stabilized aggregate is relatively small, it is possible that the traffic loading may result in a flexural crackdown of the base layer. To examine the possibility of such crackdown of a base layer, an effort was made to analyze a flexible pavement behavior using a nonlinear finite element (FE) method. A computer program MICH-PAVE (Harichandran et al., 1990) was used to evaluate the deformation behavior of a layered pavement having a typical section and subjected to typical traffic loading, as shown in Figure 5-2 a. The MICH-PAVE program considers the pavement as an axisymmetric solid of revolution divided into a number of finite elements, each as a section of concentric rings, as shown in Figure 5-2 b. Chen (1994) conducted pavement analyses using several computer programs and reported that the MICH-PAVE program gave more reasonable results than other computer programs (namely, DAMA, ILLI-PAVE, ABAQUS).

The following material properties were used in the FE analysis:

1) <u>AC Layer</u>: Thickness 305 mm, Elastic Modulus 1750 MPa, Density 24 kN/m^3

2) <u>Base Layer</u>: Thickness 155 mm, Resilient Modulus 130 MPa, Friction Angle 45°, Cohesion 50 kPa, Density 22 kN/m^3.

77

3) <u>Subgrade Soil</u>: Thickness 1143 mm, Resilient Modulus 60 MPa, Cohesion 50 kPa, Density 18 kN/m^3.

The FE analysis results show that the stabilized base layer is in a state of flexure when subjected to traffic loading. The deflection of the base layer was found to decrease with an increase in depth and radial distance from 0.35 mm at the top and 0.33 mm at the bottom of the base layer. These deflection values are in the same order of magnitude as those at failure in the flexural strength test of beam, as reported earlier in this section. This observation may lead to a scenario that the stabilized base layer would crackdown and render a block structure because of excessive deflection in the base layer. Whether the stabilized base actually breaks down into blocks is beyond the scope this work.

5.3   Resilient Modulus

The RM tests were conducted on raw aggregate, and CKD-stabilized aggregate with different amounts of CKD and curing periods. As noted from AASHTO Designation: T 294-94 (Table 4-3), for a set of RM test, fifteen RM values are obtained in the range of stress levels considered in this test, i.e. confining pressure σ_3 increasing from 21 kPa to 138 kPa and deviator stress $(\sigma_1 - \sigma_3)$ varying between 21 kPa and 276 kPa. To ensure reliability of test results, at least five replicate specimens were tested for a given blend of CKD and aggregate. The mean and standard deviation of the measured RM as computed from equation (4-1) are presented in Tables 5-2 and 5-3. The RM values obtained from each test are listed in Appendix A: Tables A-1 through A-6. Again, attention should be paid that there are possible 10% to 30% deviation of these measured

RM values from the actual values due to limitation of LVDTs' resolution, as shown in Chapter 4 (Section 3).

5.3.1 Effects of CKD Amounts On Resilient Modulus

To investigate the effects of CKD amounts on the resilient modulus, three different percentages of CKD (5%, 10% and 15% by weight) were mixed with the raw aggregate. Specimens were prepared and tested after curing for a specified period. Figure 5-2 shows the effect of CKD amount on the RM values of the stabilized aggregate cured for 7 days. It is observed that with the addition of only 5% CKD, the RM value is ten to fifty percent higher than those of raw aggregate, and with 15% CKD, the RM value may exceed 1.5 times that of the raw aggregate. For example, at deviator stress of 276 kPa, the mean RM for raw aggregate is 307 MPa, while the RM increases to 499 MPa for 7-day cured aggregate stabilized with 15% CKD.

Since the resilient modulus values are directly affected by axial elastic deformations that are very sensitive to the magnitude of deviator stress, the increases in RM become dependent on the stress level. From Figure 5-3, it is evident that the increase in RM due to the addition of CKD is affected by the deviator stress level. For example, as the CKD amount increases from zero to 15%, the RM value increases from 300 MPa to 500 MPa at the 276 kPa deviator stress, and from 50 to 80 MPa at the 21 kPa deviator stress. Although there are pronounced differences in net increase in RM values at different stress levels, the differences in terms of the increased percentages are larger as the CKD amount increases. For example, when aggregate stabilized with 5% CKD, there are about 20% and 36% increases in RM values at 21 kPa and 207 kPa deviator stresses,

79

respectively; when aggregate stabilized with 15% CKD, the increase becomes 30% and 70% at 21 kPa and 207 kPa deviator stresses, respectively.

It was observed from the moisture-density tests presented in Chapter 4 that the CKD-stabilization produces lower values of dry density than the raw aggregate, because the fine contents increase with addition of CKD. The fact that the RM values increase with increasing CKD suggests that in the CKD-stabilized aggregates the cementitious action prevails over its role as a filler and it determines the strength outcome.

5.3.2   Effects of Curing Time on Resilient Modulus

Three curing periods were considered in this study, namely 7-day, 28-day and 90-day. The seven day strength is considered as early strength, and the 28-day is considered as standard strength for many cementing and stabilizing materials, while the 90-day strength can be considered to be the long term strength. Figure 5-4 shows the effect of curing time on the resilient modulus of the 15% CKD-stabilized aggregate. It is clear that the 28-day resilient modulus is much higher than that of the 7-day modulus, while there is not any significant difference in RM values between the 28-day and the 90-day curing periods. The effects of curing time can also be easily observed from Figure 5-5 which shows RM values varying with the curing time for different deviator stresses. It can be observed that there is a remarkable increase in RM value when the curing time increased from 7 days to 28 days, but there is no appreciable increase in resilient modulus between the 28-day and the 90-day curing periods. For example, when deviator stress is 276 kPa, the average RM values are 499 MPa, 683 MPa and 621 MPa, respectively, for 7-day, 28-day and 90-day curing periods. Theses values represent 60%, 123% and 102%

increase over the RM values of the raw aggregate, respectively. It is reasonable to infer that cementitious product in CKD-stabilized aggregate increases as the curing time increases from 7 days to 28 days. However, as the curing time is extended from 28 days to 90 days, further increase in cementitious product is insignificant. The fact that the RM values of some 90-day cured samples are less than the corresponding 28-day cured samples can be attributed to various factors including variability between different specimens and resolution of experimental data. Similar observation was also reported by Laguros and Zanieris (1987) who investigated strength characteristics of flyash stabilized aggregate base under static loading.

As compared with the Class C flyash (CFA) stabilization, the CKD-stabilization results in a smaller increase in RM value over the raw aggregate. Pandey (1996) reported that the increase in RM value can be as high as 300% of the raw aggregate, which is much higher than in the CKD stabilization. The possible explanation is the difference in chemical composition between the CFA and CKD materials. As seen from Tables 2-2 and 3-2, the flyash has more oxide compounds (Al_2O_3 + SiO_2 + Fe_2O_3) and lower loss on ignition (LOI) than the CKD. The different chemical composition in stabilizing agent may result in different microstructures due to chemical reactions that might lead to different strength. This aspect is discussed further in the latter part of this chapter.

5.4   Durability

To evaluate the durability of a CKD-stabilized aggregate base to resist the deleterious effects of extreme environmental conditions, RM tests were performed on specimens subjected to a certain number of freezing/thawing and wetting/drying cycles.

Since the worse situations of pavement occur mostly under the thaw/and wet conditions, all the specimens were tested at the end of either thawing and wetting process after a given number of cycles. The effects of number of cycles of both freezing/thawing and wetting/drying actions on the resilient modulus were studied and are presented hereafter.

5.4.1   Effect of Freezing and Thawing Cycles

The number of freezing/thawing cycles considered in the study is 0, 4, 8 and 12, zero cycle being the regularly stabilized specimens. The mean RM values versus stress levels for four types of specimens are listed in Table 5-4 and graphically presented in Figures 5-6 and 5-7. From Table 5-4 and Figure 5-7 one can see that RM decreases markedly when specimens underwent four cycles of freezing/thawing, and there is no significant reduction in RM after more than eight cycles. When the deviator stress is 41 kPa, the reductions in RM values with respect to the regularly cured specimens are 70 MPa, 71 MPa and 74 MPa for specimens subjected to 4, 8 and 12 freezing/thawing cycles, respectively. When the deviator stress equals 276 kPa, the corresponding reductions in RM values are 164 MPa, 258.2 MPa and 258 MPa for specimens subjected to 4, 8 and 12 freezing/thawing cycles, respectively.

Figure 5-6 illustrates a comparison of RM values between regularly cured specimens and the frozen/thawed specimens, as well as raw aggregate. The solid and dashed straight lines in the figure shows the RM values of regularly cured and raw aggregate specimens, respectively. The RM values represented by other symbols are all below the solid straight line, and the RM even lower than that of raw aggregate when subjected to more than 4 freezing/thawing cycles. It can be seen from the figure that the

absolute difference in RM values between the regularly cured specimens and frozen/thawed specimens increases with increasing RM values. However, the relative difference in RM values dose not change significantly. When the deviator stress is 41 kPa, the percentage reductions in RM values with respect to the regularly cured specimens are 46, 49 and 51 for specimens subjected to 4, 8 and 12 freeze/thaw cycles, respectively. When the deviator stress equals 276 kPa, the corresponding percentage reductions in RM values are 33, 52 and 52 for specimens subjected to 4, 8 and 12 freeze/thaw cycles, respectively, as evident from Table 5-5.

It seems reasonable to infer that the deleterious effects due to freeze/thaw cycles are remarkably dominant at the initial thawing stage, indicating that a roadway pavement would behave poorly at the onset of thaw season. Elliott and Thornton (1988) reported variation in resilient modulus of a typical cohesive soil subjected to one freeze/thaw cycle. It was shown that the RM values could be reduced by 50 percent of the regular samples, which is quite consistent with the results obtained from the present study. In view of testing protocol, it is worth mentioning that 8 or 12 cycles can be deemed as a maximum number of freezing/thawing cycles in planning to do laboratory experiments.

5.4.2   Effect of Wetting and Drying Cycles

The numbers of wetting/drying cycles considered in this study are also 0, 4, 8 and 12, as in the case of freeze/thaw cycles, with zero cycle being the regularly cured specimens. The mean RM values versus different stress level for four types of specimens are listed in Table 5-6 and graphically presented in Figures 5-8 and 5-9. From Table 5-6 and Figure 5-9 one can see that RM decreases significantly as number of wetting/drying

cycles reaches up to 8 beyond which RM decreases only slightly. For example, when the deviator stress is 41 kPa, the reductions in RM values with respect to the regularly cured specimens are 42 MPa, 59 MPa and 68 MPa for specimens subjected to 4, 8 and 12 wetting/drying cycles, respectively. When the deviator stress equals 276 kPa, the corresponding reductions in RM values are 61 MPa, 175 MPa and 183 MPa for specimens that underwent 4, 8 and 12 cycles of wetting/drying, respectively.

Figure 5-8 presents a comparison of RM values of stabilized specimens subjected to different wetting/drying cycles. The straight line in the figure shows the RM values of regularly cured specimens that did not undergo any wetting/drying action; the other symbols show degree of variation in RM values due to the cyclic wetting/drying actions. It is seen that the absolute difference in RM values between the regularly cured specimens and specimens subjected to wetting/drying cycles increases with increasing RM values. Also, the relative difference in RM values increases significantly up to 8 cycles of wetting/drying, and slightly increases thereafter (i.e. between 8 and 12 cycles). As shown in Table 5-7, when the deviator stress is 41 kPa, the percentage reduction in RM values with respect to the regularly cured specimens are 28.9, 40.7 and 47.4, respectively, for specimens subjected to 4, 8 and 12 cycles of wetting/drying. When the deviator stress equals 276 kPa, the corresponding percentage reduction in RM values are 12.1, 35.1 and 36.6. One can see that even only subjected to 4 wet/dry cycles, the RM of stabilized aggregate is lower than that of raw aggregate, indicating that the effect of wet/dry cycles is worse than that of freeze/thaw cycles.

84

It is evident that the deleterious effect resulting from wetting/drying actions remains dominant up to a certain number of cycles. In view of testing protocol, it is worth to mention that 8 to 12 cycles are needed for evaluating effect of wetting/drying actions on the resilient modulus for stabilized aggregate.

The wetting of aggregate brings water seeping into the CKD-stabilized aggregate, since the stabilized aggregate is still permeable. This portion of water will result in an excess pore water pressure development within the specimen when subjected to cyclic loading as long as drainage line is closed. An effort was made to examine the effect of drainage conditions that may have consequences on the RM values for a specimen immersed in water, and to provide a data base for modeling of RM with neural network which is discussed in Chapter 6. One exploratory test with the drainage valve closed during the entire testing process was performed on the specimens having subjected to 4 wetting/drying cycles. In Figure 5-10 the RM values are plotted against those obtained from the test under the drained condition, i.e. with the drainage line open. It is observed that the RM values obtained in an undrained condition may be as low as 73% of those obtained from a test under drained condition. The wet samples can be deemed as fully saturated because they were immersed in water for 24 hours before the test. Therefore, excess pore water pressure was expected to develop in dynamic loading when the drainage line was closed, which may be responsible for the low RM values. Because of unavailability of high resolution pore water pressure transducers, no effort was made to measure the excess pore water pressure during the dynamic loading in RM test in this study.

5.5   Unconfined Compressive Strength

Most unconfined compressive strength (UCS) tests were conducted immediately after a RM test, except one set of UCS tests was performed using regularly cured specimens that were not subjected to RM tests. Effects of amount of CKD, curing periods, number of freeze/thaw and wet/dry cycles are evaluated, as discussed in the following sub-sections.

5.5.1   Effects of CKD Amount and Curing Time

Table 5-8 lists the UCS values including the mean values and standard deviations for different specimens. Figure 5-11 shows the variation in mean value of UCS versus CKD amount for 7-day cured specimens. It is observed that the UCS increases with the increasing amount of CKD. When the aggregate is stabilized with 5% CKD, the UCS becomes 960 kPa, representing 380% increase over the raw aggregate (216 kPa). When 15% CKD is added, the corresponding gain in UCS is 1566 kPa, about 632% increase with respect to the raw aggregate.

Figure 5-12 shows the relationship between UCS and curing period for specimens with 15% CKD. A trend of UCS increasing with curing time is evident from the figure. The mean values of UCS are 1566 kPa, 2163 kPa and 2810 kPa for 7-day, 28-day and 90-day cured specimens, respectively.

5.5.2   Effect of Pre-Loading Condition

In an effort to investigate the influence of traffic loading on the strength characteristics of paving materials, a series of unconfined compressive strength tests were performed using both regular specimens and post-tested specimens. The specimens were

prepared in the same manner as other specimens, and the UCS tests were conducted immediately after a certain curing period, while for the post-tested specimens the UCS tests were performed after the specimens underwent 2,500 cycles of loading during resilient modulus testing in accordance with the AASHTO T294-94 method. Two typical stress-strain curves are plotted in Figure 5-13. A comparison of UCS values of after/and prior to RM testing is presented in Table 5-9. It is seen from this Table that, when stabilized with 15% CKD and cured for 28 days, the UCS ranges from 940 kPa to 1650 kPa for the virgin specimens, and 1800 kPa to 2450 kPa for the specimens subjected to RM tests. The reason for this is that the cyclic loading during RM testing appears to work as a pre-loading process that makes the specimens substantially stronger than their virgin counterparts (Zhu and Zaman, 1997a).

5.5.3   Effect of Freezing/Thawing and Wetting/Drying Cycles

Table 5-10 and Figure 5-14 illustrate the effect of freezing/thawing and wetting/drying cycles on the UCS values for CKD-stabilized aggregates. From Figure 5-14 one can see that the UCS decreases during first four cycles after which there is not any decreasing tendency of UCS with the increasing number of cycles. It is interesting to note that the UCS increased when specimens were subjected to 8 and 12 cycles of wetting/drying, compared with the specimens that did not undergo any wetting/drying actions. This observation may be attributed to the difference in loading rate and excess pore water pressure for the two kinds of test. In RM tests, the loading rate is much faster than that in UCS tests, thus inducing a greater excess pore water pressure in the RM test than that in the USC test. So, the dynamic loading may give a lower strength than the

static loading. Laguros and Medhani (1984) also reported that the shear strength parameters for stabilized base materials subjected to 15 cycles of wetting and drying were higher than those not subjected to wetting/drying actions. Since only one UCS result was obtained from one specimen, more definitive conclusions about UCS versus wet/dry cycles can be drawn after a comprehensive series of tests is conducted.

5.6   Elastic Modulus

Elastic modulus (EM) is computed from the initial slope of stress-strain curve of UCS tests. The individual and mean EM values of the raw and stabilized aggregates are presented in Table 5-8 (b). From this table one can see that the mean EM values of the 7-day cured aggregate stabilized with 5%, 10% and 15% CKD are 115 MPa, 164 MPa and 211 MPa, respectively. These values represent 260%, 413% and 559% increase over the mean EM values for the raw aggregate (32 MPa). The trend depicting an increase in EM values with increasing amount of CKD is graphically presented in Figures 5-15. The curing periods also have significant effect on the EM values. As seen from Figure 5-16, the EM values increase with the increasing curing time. The mean EM values for 7-day, 28-day and 90-day cured 15% CKD-stabilized aggregates are 211 MPa, 344 MPa and 439 MPa, respectively. A 63 percent increase is observed for the 28-day cured aggregate over the 7-day cured aggregate, and 28 percent increase is achieved for the 90-day cured aggregate over the 28-day cured aggregate. The EM values obtained from the durability tests are listed in Table 5-10 and graphically presented in Figure 5-17. It is noted that the aggregates subjected to freezing/thawing and wetting/drying cycles have higher EM

values than those of the regularly cured aggregates and subjected to no freezing/thawing and wetting/drying actions, due to the causes expressed in the preceding section.

5.7 RM versus UCS and EM

It is well-known that the laboratory determination of UCS and EM is much easier, and less expensive than that of RM. Lofti and Witczak (1985) attempted to correlate the RM and UCS values of five cement-treated base/subbase materials used by the Maryland State Department of Transportation. They found that a semi-logarithmic relation existed between the RM and UCS values, and the correlation coefficients were found to be from 0.842 to 0.905. In the present study, an effort was made to correlate the RM values with the UCS and EM values for the raw aggregate and regularly cured CKD-stabilized aggregates. The RM values corresponding to the bulk stresses 124 kPa and 207 kPa were used to correlate with the UCS and EM values, because most aggregate base courses are designed for the bulk stress not higher than 207 kPa (AASHTO 1993). By fitting the tested data with different models, the power model was found to be a good model to correlate the RM values with the UCS and EM values, as shown in Figures 5-18 and 5-19. The following regression equations and R^2 values are obtained for two bulk stress levels:

i. RM versus UCS:

$$RM = 19.579 \, (UCS)^{0.3207} \quad (R^2 = 0.843) \quad \text{(at 124 kPa bulk stress)} \qquad (5-1)$$

$$RM = 42.60 \, (UCS)^{0.2723} \quad (R^2 = 0.724) \quad \text{(at 207 kPa bulk stress)} \qquad (5-2)$$

ii. RM versus EM:

$$RM = 38.468 \, (EM)^{0.3098} \quad (R^2 = 0.854) \quad \text{(at 124 kPa bulk stress)} \qquad (5-3)$$

$$RM = 77.1 \, (EM)^{0.259} \quad (R^2 = 0.712) \quad (\text{at } 207 \text{ kPa bulk stress}) \qquad (5\text{-}4)$$

Since the RM values are stress-dependent, there cannot be a unique relationship between RM and UCS or EM. To develop an applicable model the stress values should be taken into consideration, which will be focused in the next chapter.

5.8   X-Ray Diffraction (XRD)

X-ray diffraction tests was performed using Siemen D-500 diffractometer with copper X-ray tube operated at 50 kV 27 mA. Two theta degrees of the diffraction range from 3° to 70.5°. For the purpose of comparison, the analysis was also performed on raw CKD samples prepared in the same manner as the aggregates. The minerals identified by XRD are presented in Table 5-11. An evaluation of XRD tests does not indicate significant differences in the mineral constituents between the raw and stabilized aggregate. However, minor ettringite was detected in the stabilized aggregate as a result of hydration, which is thought to be responsible for the strength gain of the stabilized aggregate. Also, there is a very obvious change in the intensity of peaks with the stabilized aggregate attaining average intensities. Figure 5-20 presents XRD test results performed on the raw aggregate, raw CKD and 15% CKD-stabilized aggregate. It can be seen that for all the materials the Calcium Carbonate (Calcite, $CaCO_3$) peaks are prevalent followed by Silicon Dioxide (Quartz, SiO_2) peaks. For raw CKD there appears a peak of Potassium Sulfate (Arcanite, K_2SO_4) as a result of presence of Potassium (K) which lacks in raw aggregate. The changes in minerals between the raw and stabilized aggregates are difficult to identify, except minor presence of Calcium Aluminum Sulfate Hydroxide Hydrate (Ettringite, $Ca_6Al_2 \, (SO_4)_3 \, (OH)_{12} \, 26H_2O$) in the stabilized aggregate.

The visible difference shown in the diffractograms is the intensity of the peaks which are high for raw aggregate and low for raw CKD, with the stabilized aggregate in between as a result of mixture.

5.9   Scanning Electron Microscopy (SEM)

To reveal changes in microstructure of the aggregate due to the CKD-stabilization, Scanning Electron Microscopy (SEM) analysis was performed on the raw aggregate and CKD stabilized aggregates. The investigation results are presented in the form of micrographs taken during the SEM tests, and are presented in Figures 5-21 through 5-27.

Figure 5-21 shows that the raw aggregate is essentially composed of granular materials that lack a definite form, some rounded, but the majority angular. The structure of pure CKD is seen as mostly spherical and rounded form, as shown in Figure 5-22. It is evident that, as shown in Figures 5-23 to 5-25, the crystals are formed within the stabilized aggregate structure as a result of hydration of cement-kiln-dust, and differences exist among the stabilized aggregates with different amounts of CKD and different curing periods. The hydration products like mastic and paste increase with the increase of curing time and CKD amounts, as can be seen from Figures 5-23 through 5-25. More crystals in the form of long narrow shapes are seen either spreading around or lying on the surface of aggregate particles in the 28-day cured samples, as illustrated in Figure 5-25. Voids created by angular aggregate particles can still be seen at the surface of the samples with 5% CKD, as shown in Figure 5-23, while they are filled when the CKD amount reached 15%.

Figure 5-28 shows energy dispersive spectroscopy (EDS) results obtained from samples of raw aggregate, raw CKD and stabilized aggregate with 15% CKD cured for 28 days. The EDS shows that the raw aggregate is composed of Calcium (Ca), Silicon (Si), Aluminum (Al), Iron (Fe), Palladium (Pd), and Gold (Au), with the highest peak of Calcium (Ca) followed by the Silicon (Si) peak. Figure 5-28 (b) shows the EDS of raw CKD. The elemental compositions of the raw CKD are similar to the raw aggregate, except for appearance of Potassium (K), Magnesium (Mg) and Sulfur (S) but absence of Pd and Au. Figure 5-28 (c) shows the compositions of 15% CKD-stabilized aggregate cured for 28 days. Comparing Figure 5-28 (a) and (c), one can see that the elements of the stabilized aggregate are the same as those of the raw aggregate, except that the peaks of Si and Au of the stabilized aggregate are smaller than those of the raw aggregate.

5.10   Discussion of Experimental Results

The discussion presented in this section is prepared to help clarify and rationalize some of the observations from experimental results presented earlier in this chapter. Emphasis is given to some of the issues related to flexural strength, resilient modulus, durability and unconfined strength of raw and stabilized aggregates, as appropriate.

(1) The CKD-stabilized aggregate can develop a relatively small amount of flexural strength as a result of chemical reactions within the matrix of the stabilized aggregate. Under repeated traffic loading, the tensile stresses developed in the base can exceed its tensile strength resulting in cracking of the base and developing a block-like structure. Use of resilient modulus, as a design parameter, may be justified for asphalt pavement with such aggregate bases. The small flexural strength attained as a result

of CKD-stabilization can be considered as an extra factor of safety in the design. It was noted from the experimental data on the flexural strength of the CKD-stabilized aggregate that there is no consistent changes in flexural strength when the amount CKD and curing time are increased. Evidently, the flexural strength developed due to CKD stabilization does not appear to be a stable or reliable strength parameter for the pavement design. Because many coarse particles are contained in a specimen, the method used to prepare a concrete beam sample may not be the most appropriate method for preparing aggregate samples. This sample preparation technique may be partly responsible for the significant variability observed in ultimate flexural strength or modulus of rupture of the specimens.

(2) The raw aggregate used in this study contains 14.2% of fines passing US No. 40 sieve (0.425 mm). Presence of these fine particles in an aggregate specimen makes it possible to conduct unconfined compressive strength test and determine UCS value for the raw aggregate samples. The UCS values of the raw aggregate were found to be in a range of 188 kPa to 250 kPa.

(3) The resilient modulus is a very important stress-dependent strength parameter for flexible pavement design. The addition of CKD in the aggregate produces cementitious materials within the matrix of mixture and reduces the micro-voids of the matrix. So, there is a continuous increase in RM value with the increasing amount of CKD up to a certain limit (15% in this case). Since the addition of CKD would increase the fine contents of the aggregate as well, drainage capacity of a base layer would be degraded if too much CKD is added to the aggregate. Taking both

fine content requirement and the strength gain into account, the addition of 15% CKD in the aggregate is considered to be adequate.

(4) The curing time has a significant effect on the increase in RM value for the CKD-stabilized aggregates because hydration products, namely crystals, increase with curing time, as identified by the SEM analyses. However, the RM of the CKD-stabilized aggregate cured for 90 days did not show any promising changes as compared to the 28-day cured aggregate. This observation indicates that a 28-day curing period is adequate for the CKD-stabilized aggregate from both strength gain and practical application view points.

(5) Freeze/thaw cycles have significant adverse effects on the RM values for the CKD-stabilized aggregate, partly because of the softening action resulting from the thawing process. It was found that the RM of the CKD-stabilized aggregate was even lower than that of the raw aggregate after a certain number of freeze/thaw cycles. This observation does not mean that the CKD-stabilized aggregate is poorer than the raw aggregate, since the freeze/thaw cycles are expected to have an adverse effect on the raw aggregate. Unfortunately, this issue was not addressed in this study because of the fear that collapse of the raw aggregate sample would occur when subjected to freeze/thaw cycles.

(6) The RM values of the CKD-stabilized aggregate decrease with increasing number of wet/dry cycles, but the static strength parameters such as UCS and EM show somewhat an increasing tendency after 8 wet/dry cycles. The observation showing a decrease in dynamic strength and an increase in static strength may be attributed to

the difference in loading rate and excess pore water pressure during the two testing processes. However, the results obtained in this study still need to be further confirmed by conducting UCS tests with varying loading rates. Also, an effort should be made to measure the excess pore water pressure responses during the two testing processes.

(7) Since chemical reaction within the CKD-stabilized aggregate needs moisture to produce hydration products, a water content higher than the optimum water content as achieved from the moisture-density tests seems necessary to achieve better results from CKD-stabilization. Further, it has been found that the UCS increases after 8 wet/dry cycles, implying that more available water may be beneficial for the chemical reaction within the CKD-stabilized aggregate.

Table 5-1   Flexural Strength Test Results

Test ID	Percent of CKD %	Curing Periods day	Modulus of Rupture MR, kPa
Beam 1	10	28	106
Beam 2	15	28	153
Beam 3	15	28	108
Beam 4	15	90	154
Beam 5	15	90	55

Table 5-2   Mean Resilient Modulus and Standard Deviation of 7-day Cured
CKD-stabilized Aggregates together with the Raw Aggregate

Confining Pressure kPa	Deviator Stress kPa	Bulk Stress kPa	Raw aggregate		5% CKD 7-day		10% CKD 7-day		15% CKD 7-day	
			Mean RM MPa	St. Dev. MPa	Mean RM MPa	St. Dev. MPa	Mean RM MPa	St. Dev. MPa	Mean RM MPa	St. Dev. Mpa
21	21	83	49.42	5.05	65.35	10.98	72.27	5.94	80.56	8.91
21	41	103	93.04	7.53	124.61	16.74	107.68	10.27	144.04	10.86
21	62	124	109.97	8.22	162.97	19.1	175.19	26.35	217.71	21.42
34	34	138	62.8	13.18	102.3	11.56	114.61	15.99	120.71	12.81
34	69	172	106.79	11.91	200.28	20.22	221.61	46.18	266.23	19.28
34	103	207	186.97	7.73	289.1	29.19	234.09	29.06	314.37	17.98
69	69	276	126.95	15.91	152.99	21.89	160.3	14.97	167.47	6.64
69	138	345	184.78	10.02	252.71	6.29	213.57	9.7	245.66	24.24
69	207	414	243.66	6.21	313.85	8.28	321.83	43.07	383.28	21.21
103	69	379	94.9	21.36	139.83	3.53	156.8	8.48	141.63	5.45
103	103	414	130.21	27.83	175.26	18.63	186.45	6.96	178.32	4.51
103	207	517	234.78	22.1	319.71	14.95	382.23	16.41	399.66	30.4
138	103	517	172.5	22.58	209.66	19.5	228.56	11.64	200.41	12.29
138	138	552	200.9	18.54	222.92	28.42	266.96	12.62	251.55	23.94
138	276	690	306.59	29.96	385.81	26.84	411.66	47.71	499.51	21.25

Table 5-3   Mean Resilient Modulus and Standard Deviation of 15%
CKD-stabilized Aggregates together with the Raw Aggregate

Confining Pressure kPa	Deviator Stress kPa	Bulk Stress kPa	Raw aggregate		7-day		28-day		90-day	
			Mean RM MPa	St. Dev. MPa	Mean RM MPa	St. Dev. MPa	Mean RM MPa	St. Dev. MPa	Mean RM MPa	St. Dev. Mpa
21	21	83	49.42	5.05	80.56	8.91	109.35	14.60	126.66	13.19
21	41	103	93.04	7.53	144.04	10.86	148.05	17.23	200.65	25.46
21	62	124	109.97	8.22	217.71	21.42	219.81	26.46	262.8	33.99
34	34	138	62.8	13.18	120.71	12.81	153.68	12.22	191.41	35.18
34	69	172	106.79	11.91	266.23	19.28	341.05	58.12	246.68	18.86
34	103	207	186.97	7.73	314.37	17.98	422.62	22.69	351.76	40.65
69	69	276	126.95	15.91	167.47	6.64	226.63	20.78	252.9	26.01
69	138	345	184.78	10.02	245.66	24.24	333.50	31.07	359.46	46.32
69	207	414	243.66	6.21	383.28	21.21	473.97	30.69	627.76	67.53
103	69	379	94.9	21.36	141.63	5.45	180.69	22.33	275.14	28.16
103	103	414	130.21	27.83	178.32	4.51	241.54	18.49	363.23	28.39
103	207	517	234.78	22.1	399.66	30.4	546.21	43.78	502.96	42.12
138	103	517	172.5	22.58	200.41	12.29	272.24	47.11	337.5	28.97
138	138	552	200.9	18.54	251.55	23.94	340.71	31.32	425.29	24.85
138	276	690	306.59	29.96	499.51	21.25	683.15	36.31	620.55	32.75

Table 5-4   Mean RM value of Stabilized Aggregates
Subjected to Freezing/Thawing Cycles

Confinin Pressure kPa	Deviator Stress kPa	Bulk Stress kPa	Raw Aggregate Mean RM MPa	Cycles of Freezing/Thawing *			
				0 Mean RM MPa	4 Mean RM Mpa	8 Mean RM Mpa	12 Mean RM Mpa
21	21	83	49.42	80.56	69.98	48.99	43.96
21	41	103	93.04	144.04	78.09	72.71	69.64
21	62	124	109.97	217.71	128.14	106.7	110.6
34	34	138	62.8	120.71	69.67	48.41	54.71
34	69	172	106.79	266.23	121.90	86.5	92.88
34	103	207	186.97	314.37	177.86	132.52	149.35
69	69	276	126.95	167.47	114.56	69.64	83.22
69	138	345	184.78	245.66	164.76	171.42	133.8
69	207	414	243.66	383.28	274.18	184.75	224.74
103	69	379	94.9	141.63	104.77	71.64	93.67
103	103	414	130.21	178.32	133.97	90.95	120.18
103	207	517	234.78	399.66	279.04	188.85	234.77
138	103	517	172.5	200.41	133.11	99.22	124.9
138	138	552	200.9	251.55	158.24	178.28	149.17
138	276	690	306.59	499.51	335.65	241.36	241.04

* All aggregates were stabilized with 15% CKD and cured for 7-day before freezing/thawing cycles.

Table 5-5 Absolute and Relative Difference in RM Values between the Regularly Cured Specimens and Frozen/Thawed Specimens

Deviator Stress kPa	Difference in RM Value					
	4 cycles		8 cycles		12 cycles	
	ABSΔ, MPa	RELΔ, %	ABSΔ, MPa	RELΔ, %	ABSΔ, MPa	RELΔ, %
21	10.58	13.13	31.57	39.19	36.6	45.43
41	65.95	45.79	71.33	49.52	74.4	51.65
62	89.57	41.14	111.01	50.99	107.11	49.2
34	51.04	42.28	72.3	59.9	66	54.68
69	144.33	54.21	179.73	67.51	173.35	65.11
103	136.51	43.42	181.85	57.85	165.02	52.49
69	52.91	31.59	97.83	58.42	84.25	50.31
138	80.9	32.93	74.24	30.22	111.86	45.53
207	109.1	28.46	198.53	51.8	158.54	41.36
69	36.86	26.03	69.99	49.42	47.96	33.86
103	44.35	24.87	87.37	49	58.14	32.6
207	120.62	30.18	210.81	52.75	164.89	41.26
103	67.3	33.58	101.19	50.49	75.51	37.68
138	93.31	37.09	73.27	29.13	102.38	40.7
276	163.86	32.8	258.15	51.68	258.47	51.74

Note: ABSΔ = Absolute difference, RELΔ = Relative difference

100

Table 5-6   Mean RM Values of Specimens Subjected to
Wetting/Drying Cycles

Confining Pressure	Deviator Stress	Bulk Stress	Raw Mean RM	Cycles of Wetting/Drying*			
				0 Mean RM	4 Mean RM	8 Mean RM	12 Mean RM
kPa	kPa	kPa	MPa	MPa	MPa	MPa	MPa
21	21	83	49.42	80.56	58.25	50.26	46.04
21	41	103	93.04	144.04	102.42	85.40	75.75
21	62	124	109.97	217.71	167.32	137.28	112.97
34	34	138	62.8	120.71	79.34	74.45	69.30
34	69	172	106.79	266.23	126.84	123.57	101.49
34	103	207	186.97	314.37	220.62	196.47	166.66
69	69	276	126.95	167.47	143.48	95.12	114.51
69	138	345	184.78	245.66	225.45	214.32	156.18
69	207	414	243.66	383.28	357.28	282.04	257.26
103	69	379	94.9	141.63	130.70	91.40	101.08
103	103	414	130.21	178.32	166.91	112.27	130.75
103	207	517	234.78	399.66	362.93	278.01	266.36
138	103	517	172.5	200.41	199.88	127.26	139.47
138	138	552	200.9	251.55	215.04	181.62	146.29
138	276	690	306.59	499.51	439.03	324.04	316.88

* Aggregate stabilized with 15% CKD and cured for 7-days.

101

Table 5-7 Absolute and Relative Difference in RM Values between the Regularly Cured Specimens and Wet/Dry Specimens

Deviator Stress	Difference in RM Value					
	4 cycles		8 cycles		12 cycles	
kPa	ABSΔ, MPa	RELΔ, %	ABSΔ, MPa	RELΔ, %	ABSΔ, MPa	RELΔ, %
21	22.31	27.69	30.3	37.61	34.52	42.85
41	41.62	28.89	58.64	40.71	68.29	47.41
62	50.39	23.14	80.43	36.94	104.74	48.11
34	41.37	34.27	46.26	38.33	51.41	42.59
69	139.39	52.36	142.66	53.58	164.74	61.88
103	93.75	29.82	117.9	37.5	147.71	46.99
69	23.99	14.32	72.35	43.2	52.96	31.62
138	20.21	8.23	31.34	12.76	89.48	36.42
207	26	6.78	101.24	26.41	126.02	32.88
69	10.93	7.71	50.23	35.47	40.55	28.63
103	11.41	6.4	66.05	37.04	47.57	26.68
207	36.73	9.19	121.65	30.44	133.3	33.35
103	0.53	0.27	73.15	36.5	60.94	30.41
138	36.51	14.52	69.93	27.8	105.26	41.84
276	60.48	12.11	175.47	35.13	182.63	36.56

Note: ABSΔ = Absolute difference, RELΔ = Relative difference

Table 5-8 a   Unconfined Compressive Strength of CKD-Stabilized Aggregates

Specimen Type	Unconfined Compressive Strength (kPa)						Mean Value (kPa)	Standard Deviation (kPa)	St. Dev/ Mean (%)
	Test 1	Test 2	Test 3	Test 4	Test 5	Test 6			
Raw aggregate	250	190	215	232	219	188	216	24.01	11.13
5%CKD, 7-day	900	910	1500	850	635		959	322.27	33.60
10%CKD, 7-day	1312	1105	1057	998	1243		1143	130.79	11.44
15%CKD, 7-day	1400	1205	1800	1890	1535	1408	1566	260.53	16.64
15%CKD, 28-day	1800	2350	2450	2100	2114	2212	2163	226.93	10.49
15%CKD, 90-day	2900	2750	3150	2750	2500	2300	2810	297.91	10.60

Table 5-8 b   Elastic Modulus of the CKD-stabilized Aggregate

Specimen Type	Elastic Modulus (MPa)						Mean Value (MPa)	Standard Deviation (MPa)	St. Dev/ Mean (%)
	Test 1	Test 2	Test 3	Test 4	Test 5	Test 6			
Raw aggregate	45	32	28	31	24	29	32	7.18	22.78
5%CKD, 7-day	122	102	140	98	113		115	16.85	14.65
10%CKD, 7-day	150	130	161	168	210		164	29.55	18.04
15%CKD, 7-day	210	204	190	231	221	230	211	16.03	7.59
15%CKD, 28-day	260	376	333	363	389	350	344	46.08	13.39
15%CKD, 90-day	414	350	532	450	450	420	439	59.57	13.56

Table 5-9   Comparison of UCS and EM Values for Specimens Tested Prior to and After RM Test

Test ID.	Specimen Construction	Test Condition	UCS, kPa kPa	EM MPa
un1		prior to RM test	1610	240
un2			1100	280
un3	15% CKD		940	200
unt1	28-days Curing	After RM test	1800	260
unt2			2350	376
unt3			2450	333
addu	15% CKD	prior to RM test	810	350
adbu	7-days Curing		900	300
acu		After RM test	1400	210
adu			1205	204

Table 5-10   Unconfined Compressive Strength (UCS) and Elastic Modulus (EM) of the CKD-stabilized Aggregate Subjected to Freezing/Thawing and Wetting/Drying Cycles

Specimen Type	Strength Parameters	Number of Cycles					
		4 cycles		8 cycles		12 cycles	
		Test 1	Test 2	Test 1	Test 2	Test 1	Test 2
Freezing/	UCS, kPa	980	1300	1200	1200	1320	1145
Thawing	EM, MPa	300	223	354	333	289	216
Wetting/	UCS, kPa	1100	1450	3000	2800	2450	3050
Drying	EM, MPa	325	200	386	375	333	476

Note: All the specimens are stabilized with 15% CKD and 7-day curing time.

Table 5-11   Minerals Identified by X-ray Diffraction

Name of Mineral	Chmical Formula	Symbol
Anhydrite	$CaSO_4$	A
Arcanite	K_2SO_4	Ar
Calcite	$CaCO_3$	C
Ettringite	$3CaO.Al_2O_3.3CaSO_4.32H_2O$	E
Lime	CaO	L
Phillipsite	$K_2(Ca_{0.5}Na)_4(Al_6Si_{10}O_{32})12H_2O$	Ph
Portlandite	$Ca(OH)_2$	P
Quartz	SiO_2	Q
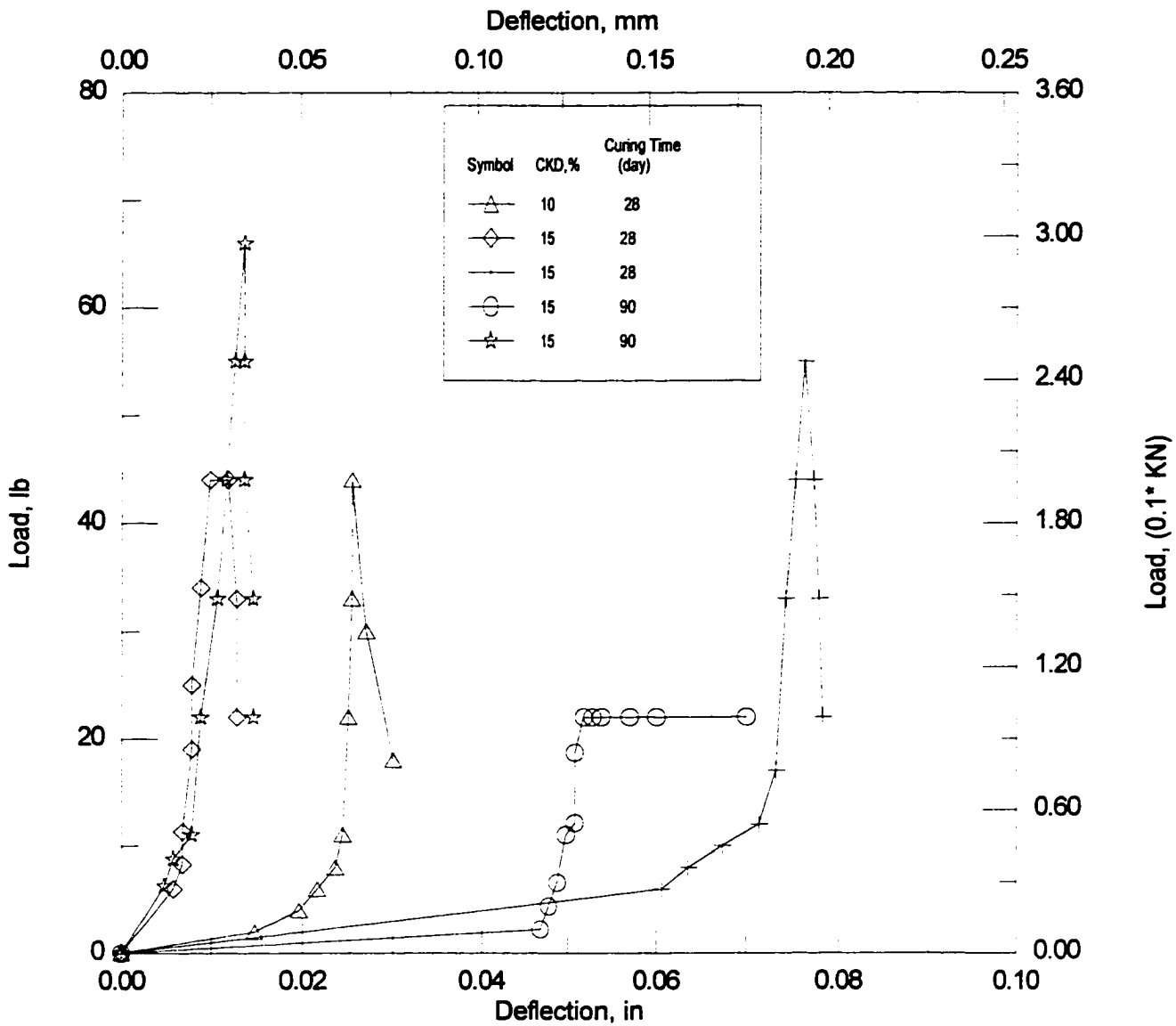
Figure 5-1   Load-defletion curves for beam test specimens

106

R = 136 mm

p = 690 kPa

AC Layer	Eac = 1,750 MPa, Dac = 305 mm γ_1 = 24 kN/m^3
Base Layer	RM = 130 MPa D$_b$ = 155 mm γ_2= 22 kN/m^3, ϕ = 45°
Subgrade Soil	RM = 60 MPa, γ_3 = 18 kN/m^3 c = 50 kPa
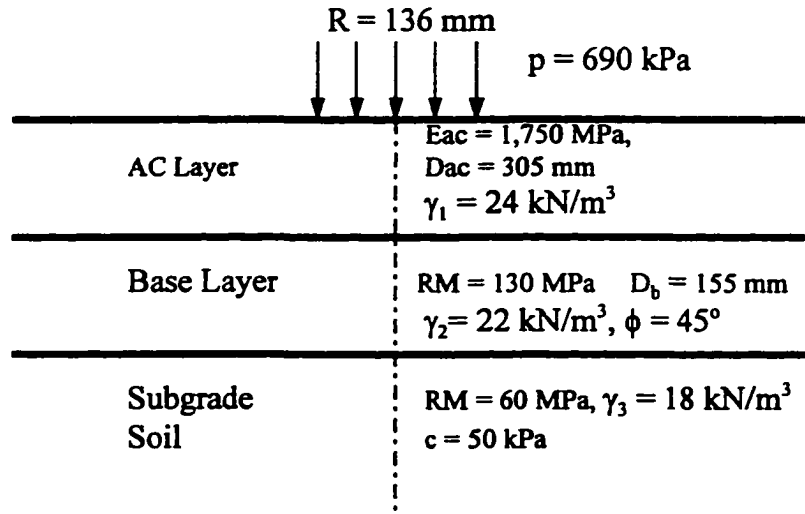
(a) Pavement Configuration Used for the Finite Element Analysis
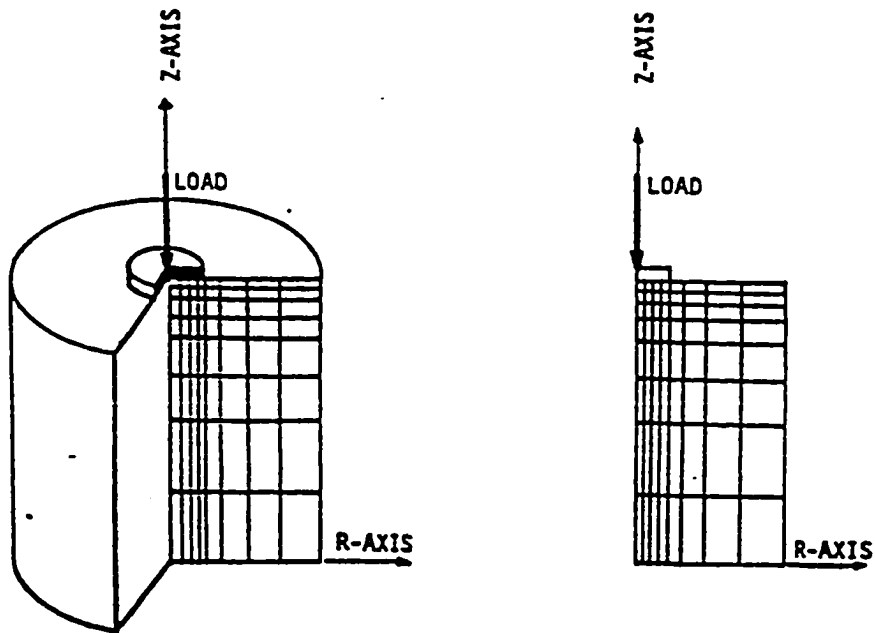
(b) Axisymmetric Idealization (after Thompson et al., 1990)

Figure 5-2   Typical Pavement Configuration and Axisymmetric Idealization

107
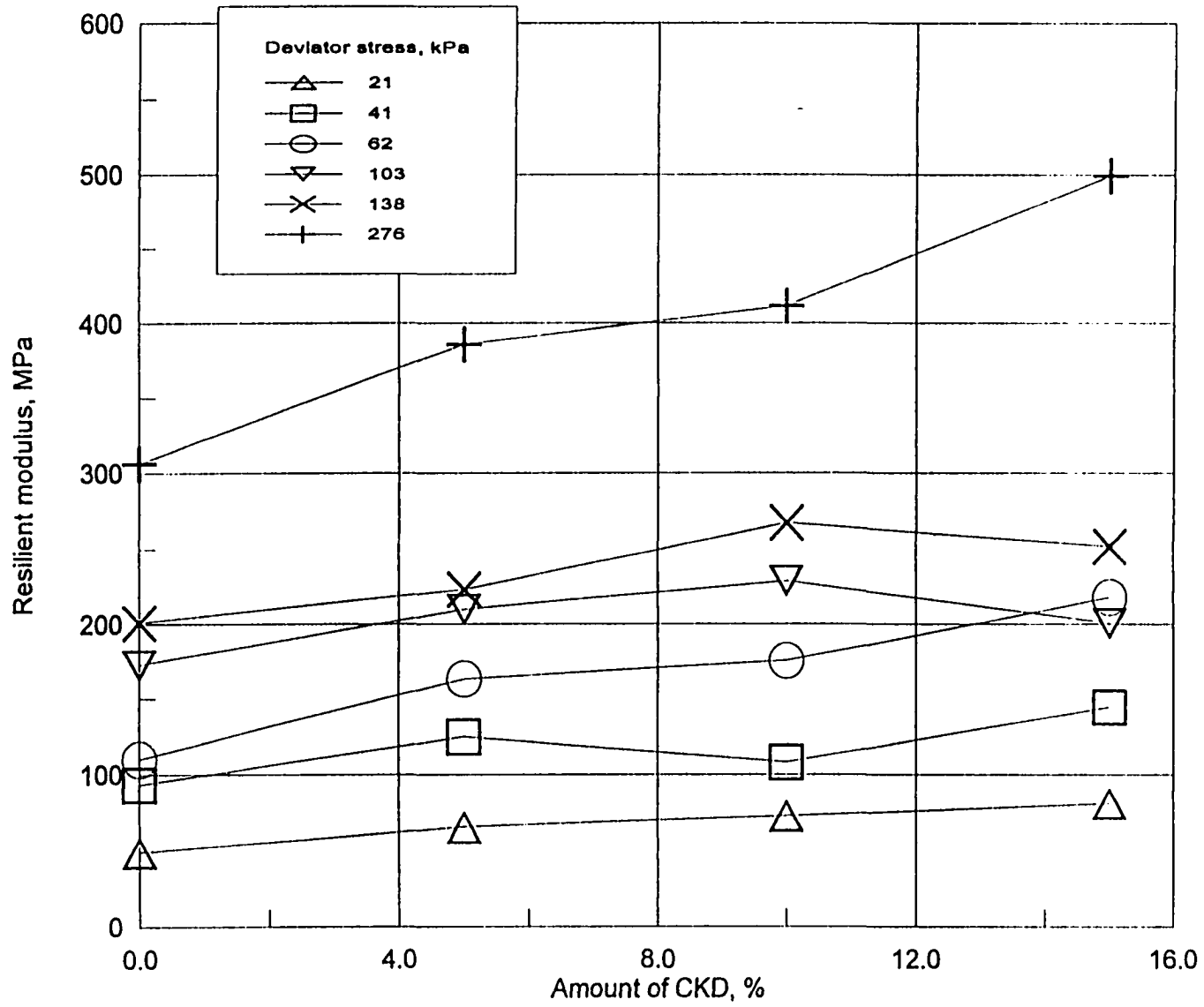
Figure 5-3   Resilient Modulus vs. Amount of CKD for Different
Deviator Stress
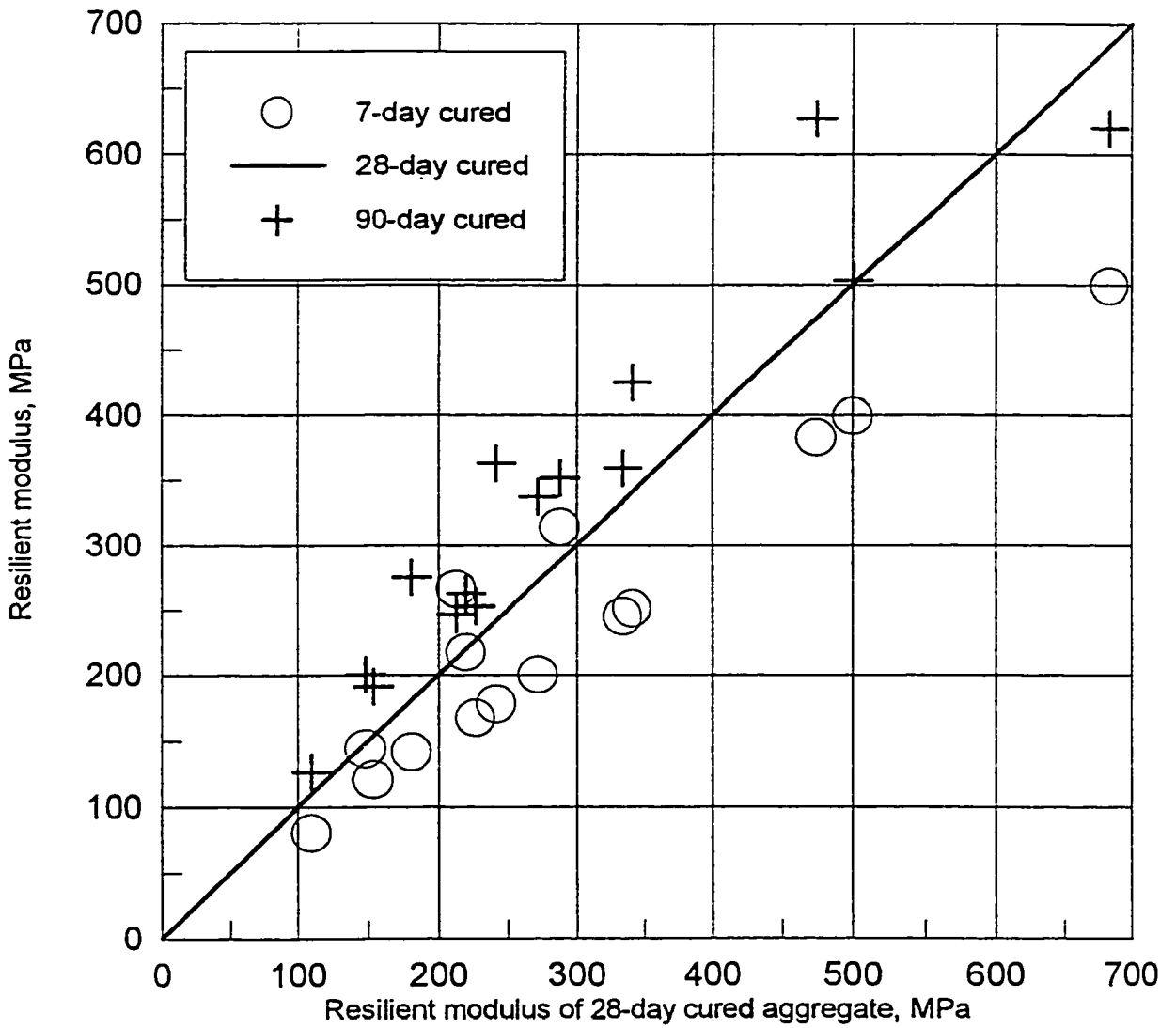
Figure 5-4   Effect of Curing Time on the Resilient Modulus of Aggregate
                  (15% CKD)
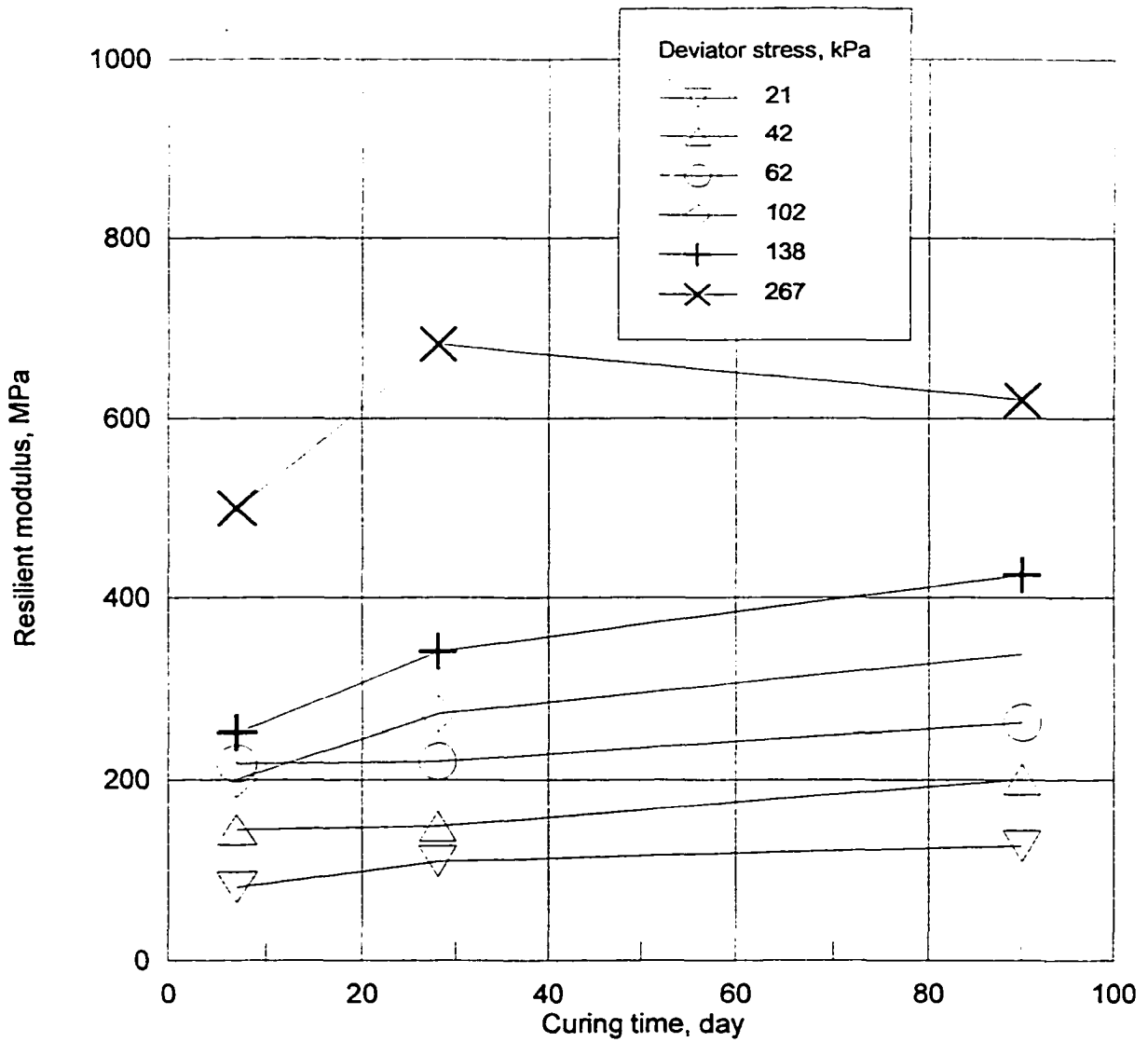
Figure 5-5 Resilient Modulus vs. Curing Time for Different Deviator Stress (15% CKD)
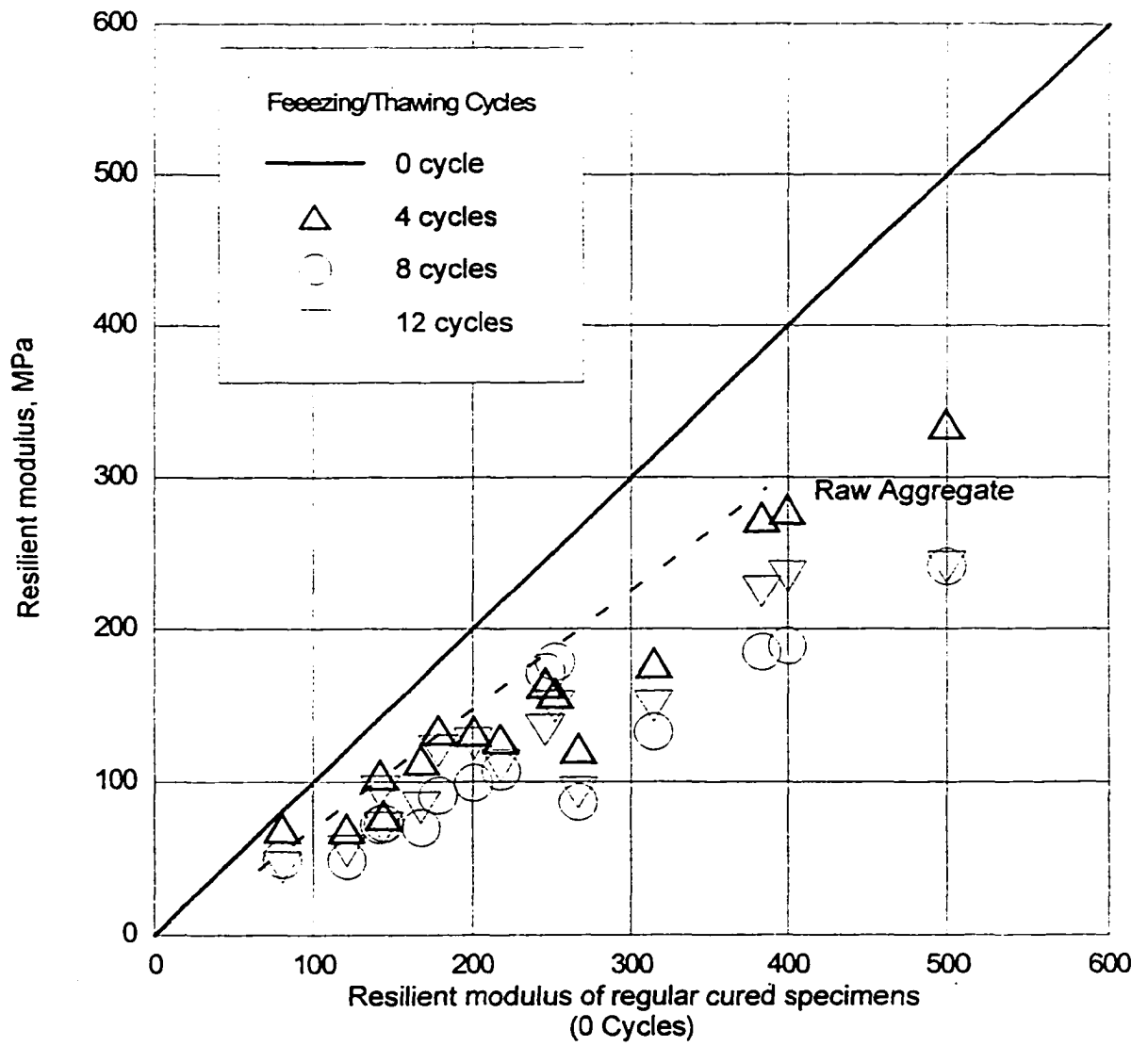
Figure 5-6   Effect of Freezing/Thawing on the Resilient Modulus of
CKD-Stabilized Aggregate (15% CKD, 7-day Curing)

111
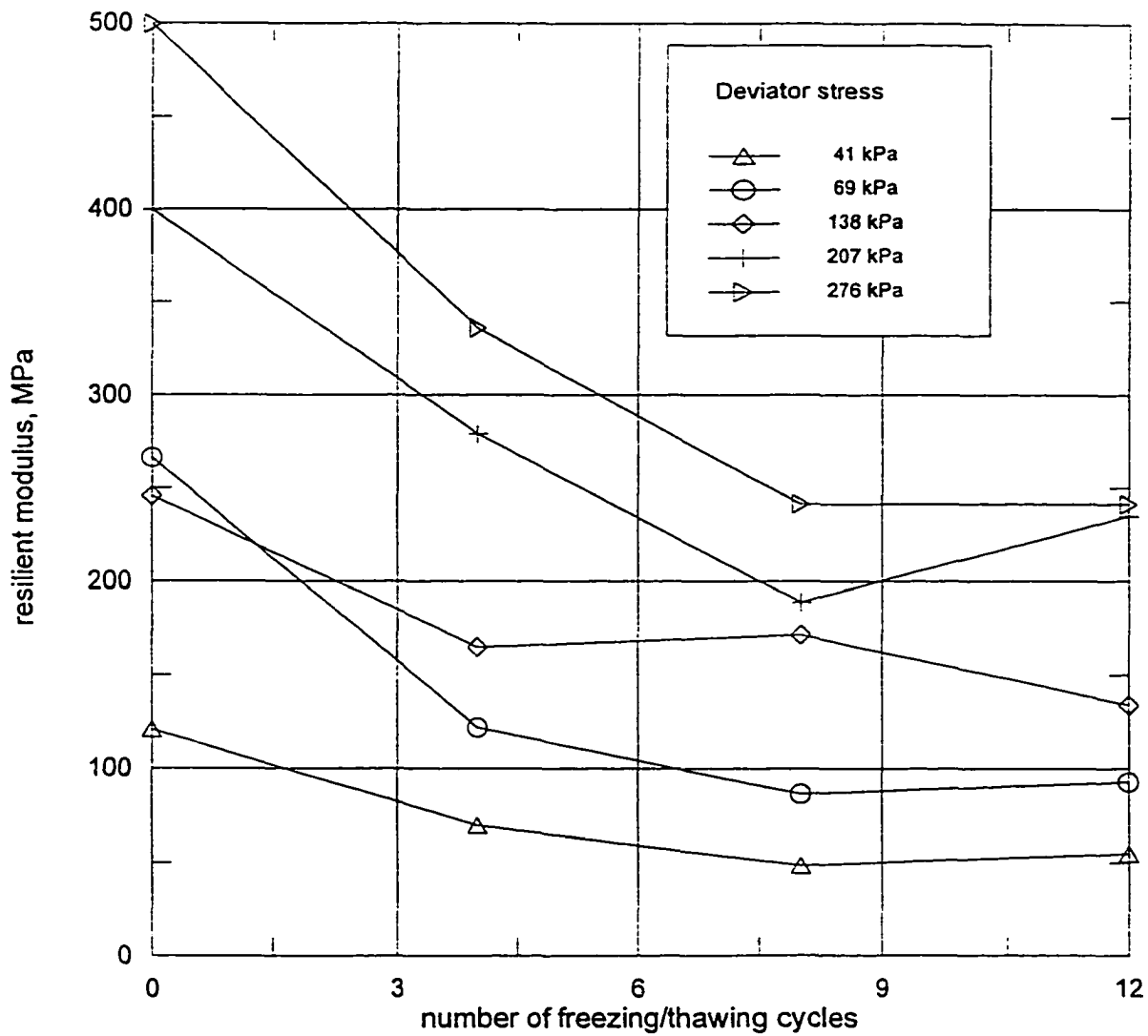
Figure 5-7   RM vs. Number of Freezing/Thawing Cycles
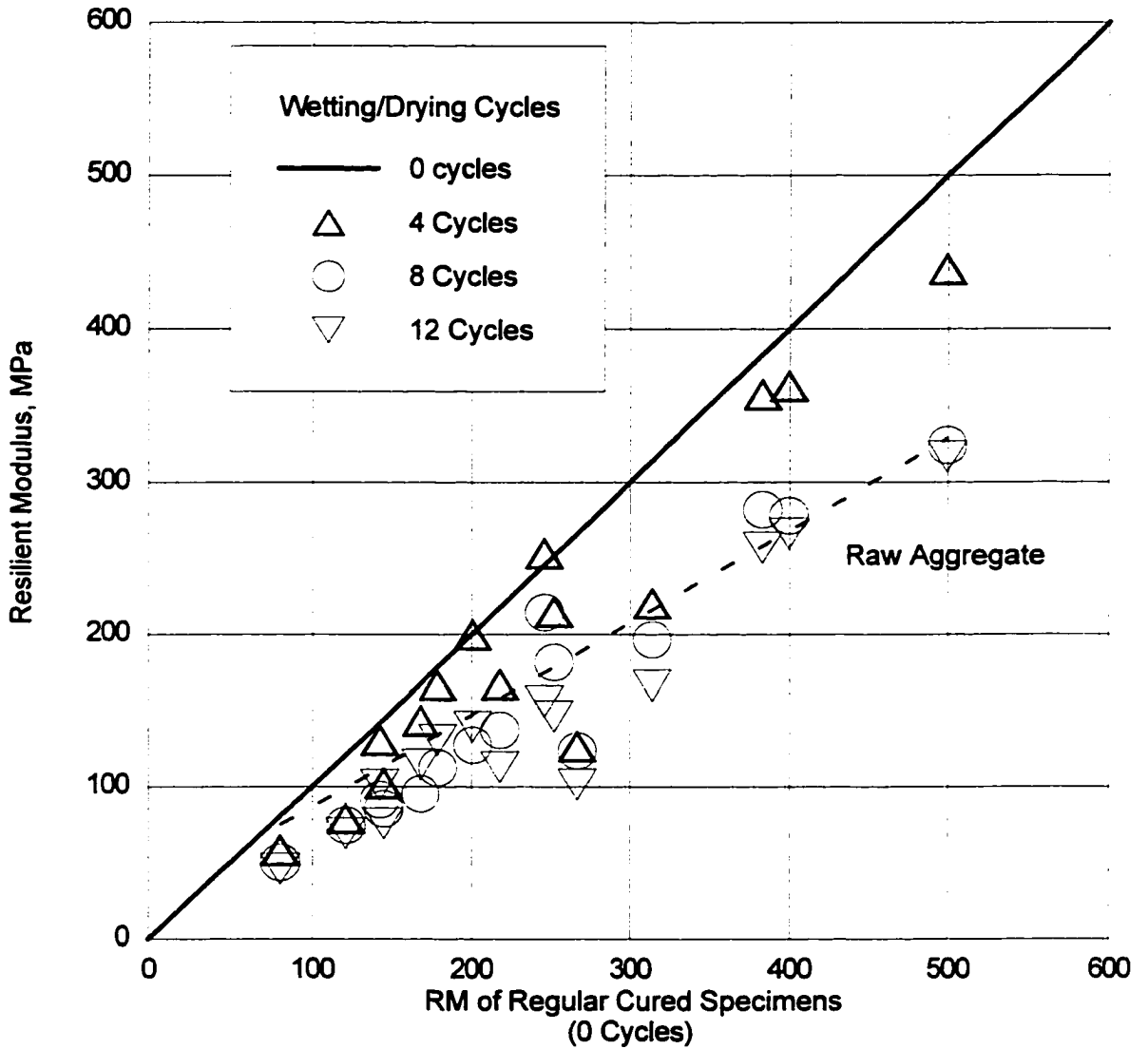
Figure 5-8   Comparison of RM of Specimens Subjected to Different
Wetting/Drying Cycles after Cured for 7-day (15% CKD)
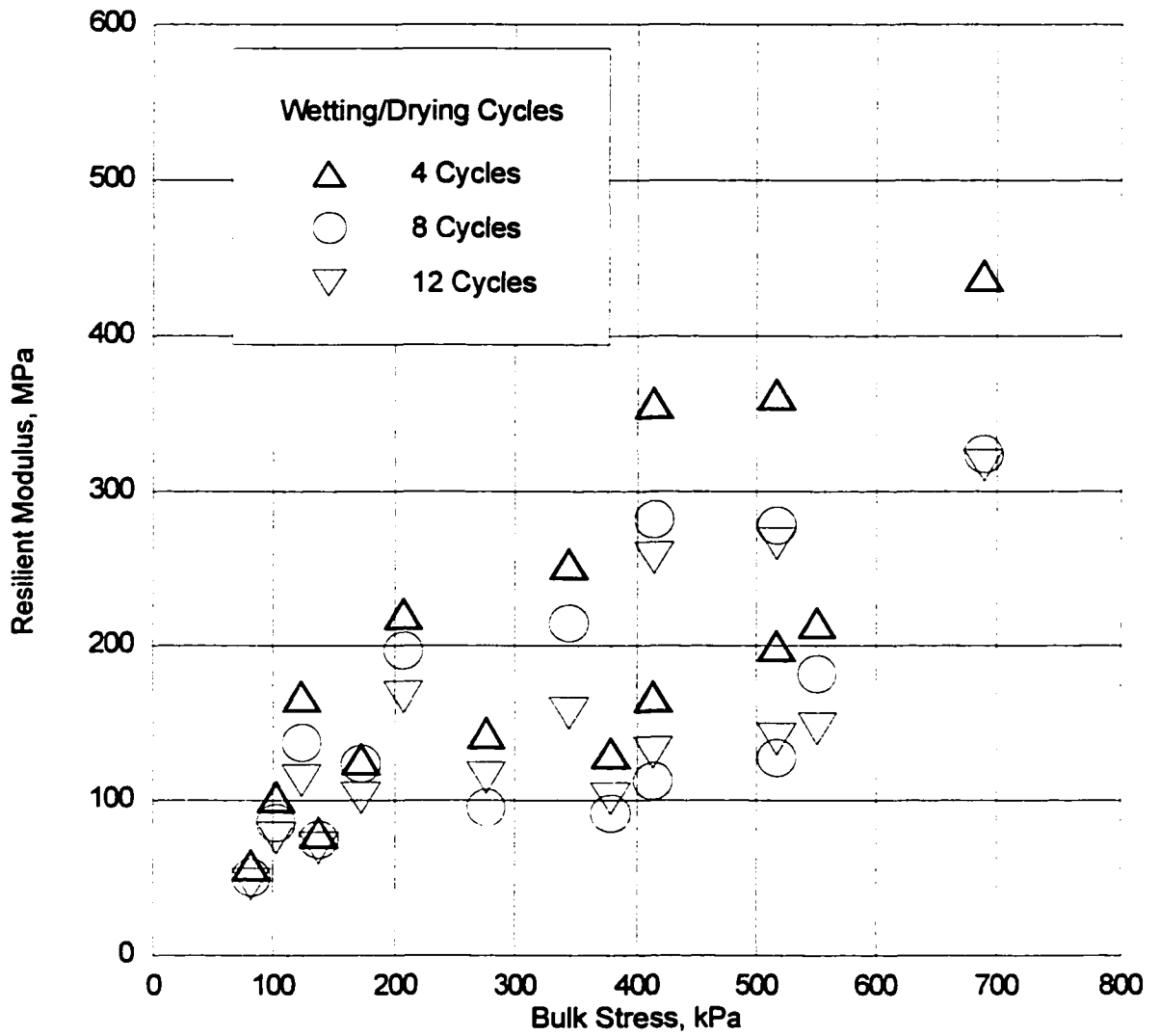
Figure 5-8 b   Relationship between RM of Specimens Subjected to Different
Wetting/Drying Cycles and Bulk Stress (7-day cured with 15% CKD)

114
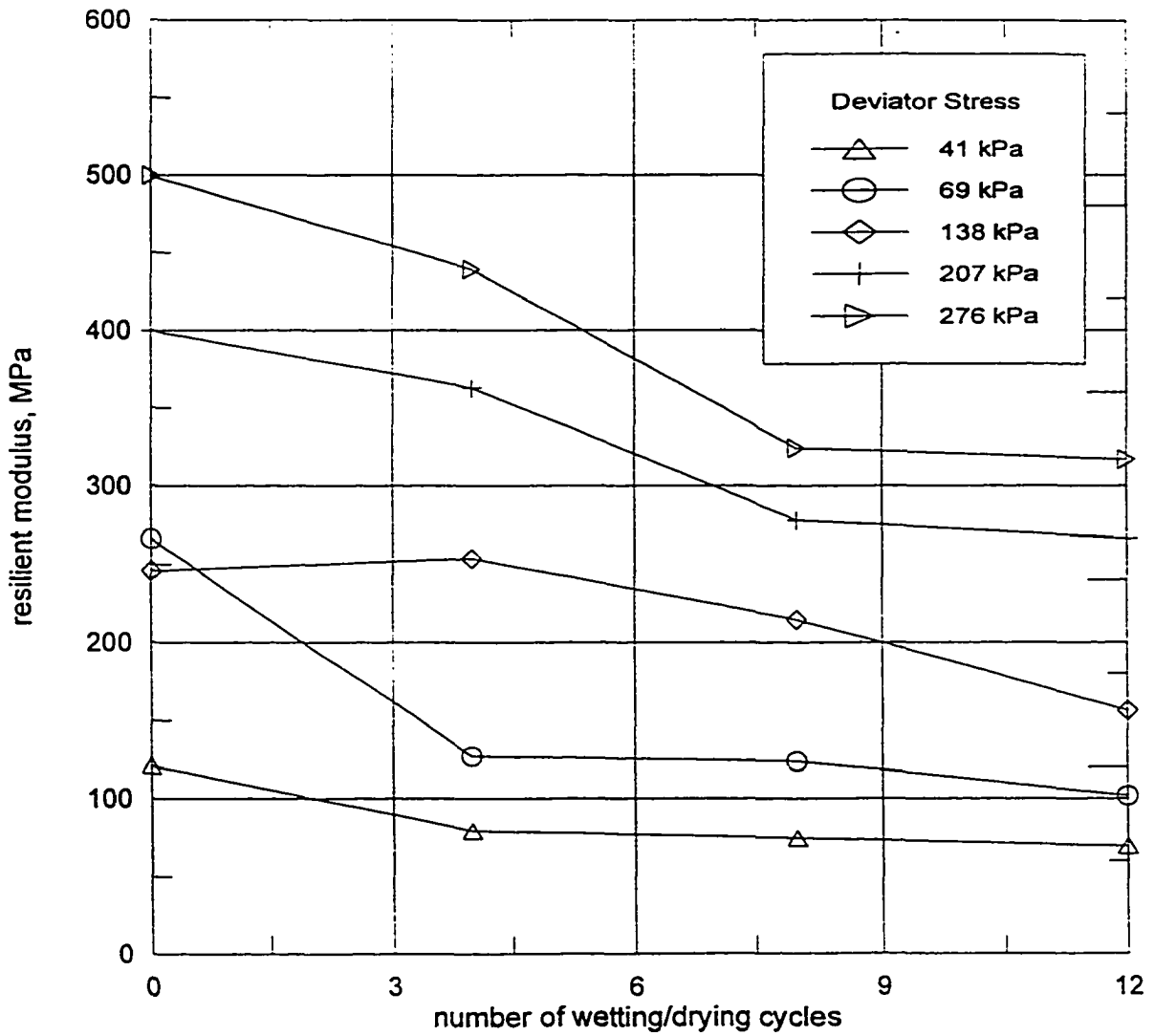
Figure 5-9   RM vs. Number of Wetting/Drying Cycles

115

fig5-10.grf
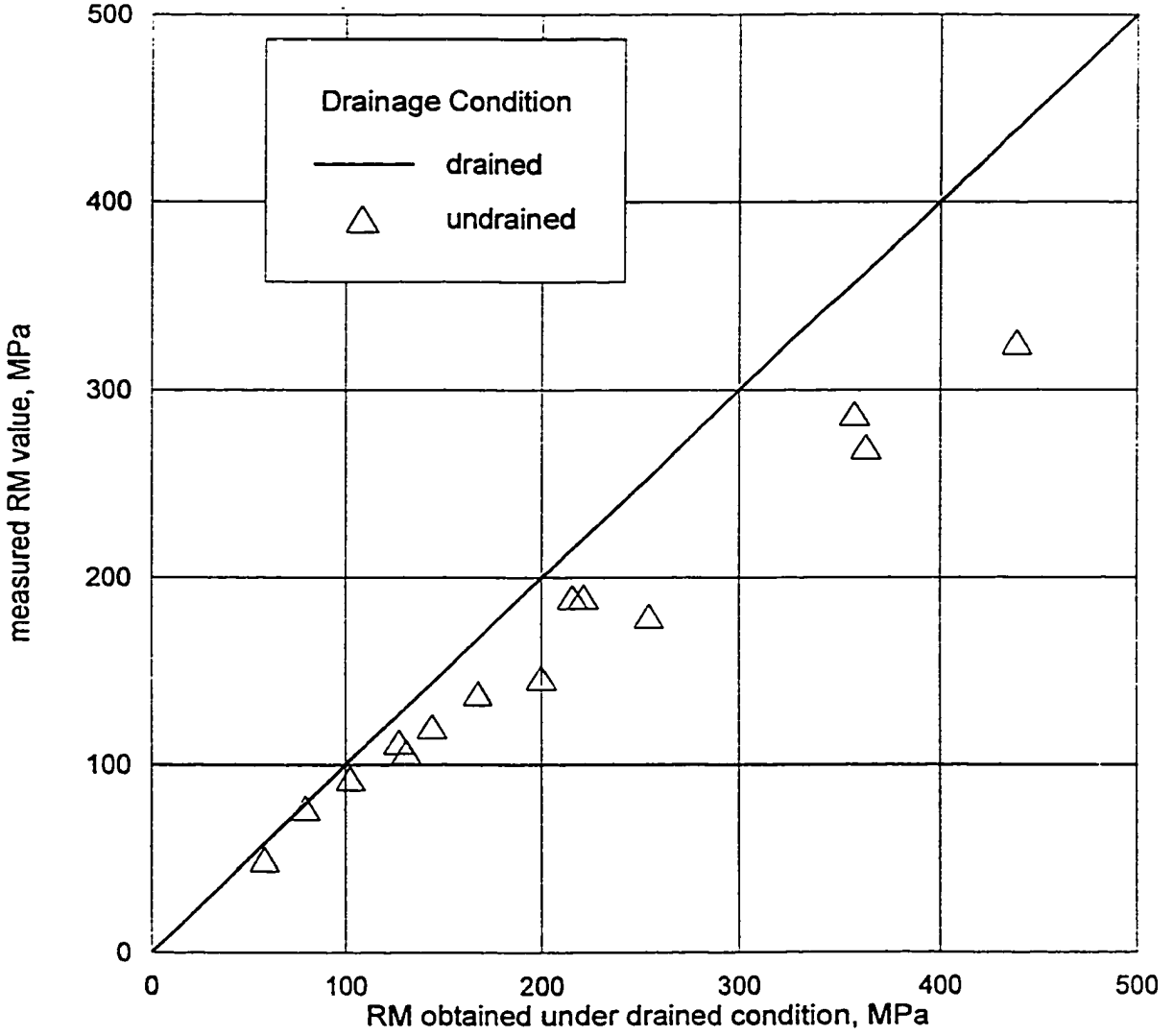
Figure 5-10   RM Value of Undrained vs. Drained Condition for Specimens
Subjected to 4 Wetting/Drying Cycles
(7-day Cured, 15% CKD)

116
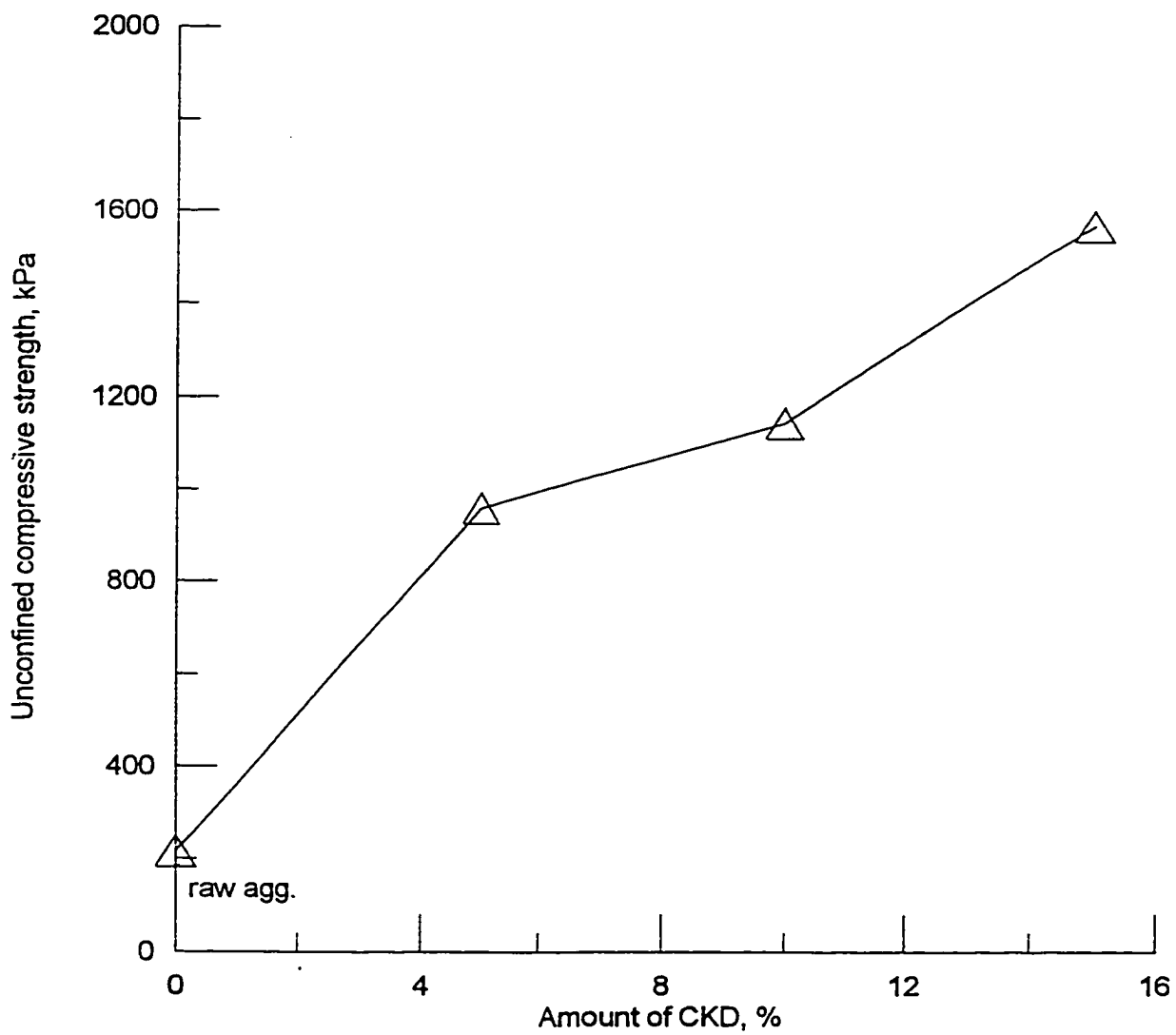
Figure 5-11   Unconfined Compressive Strength vs. Amount of CKD
(7-day Cured)
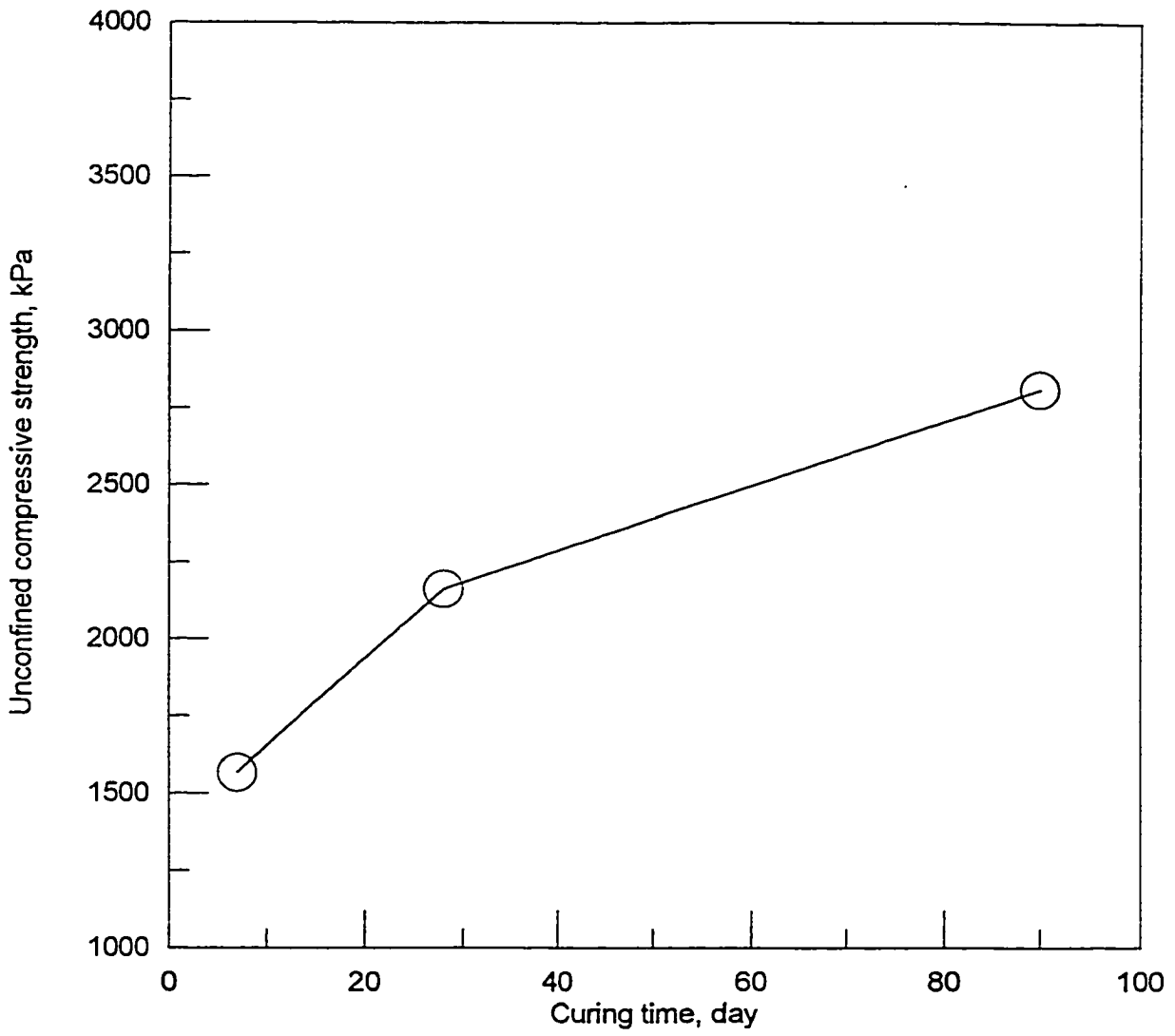
Figure 5-12   Unconfined Compressive Strength vs. Curing Time
(15% CKD)
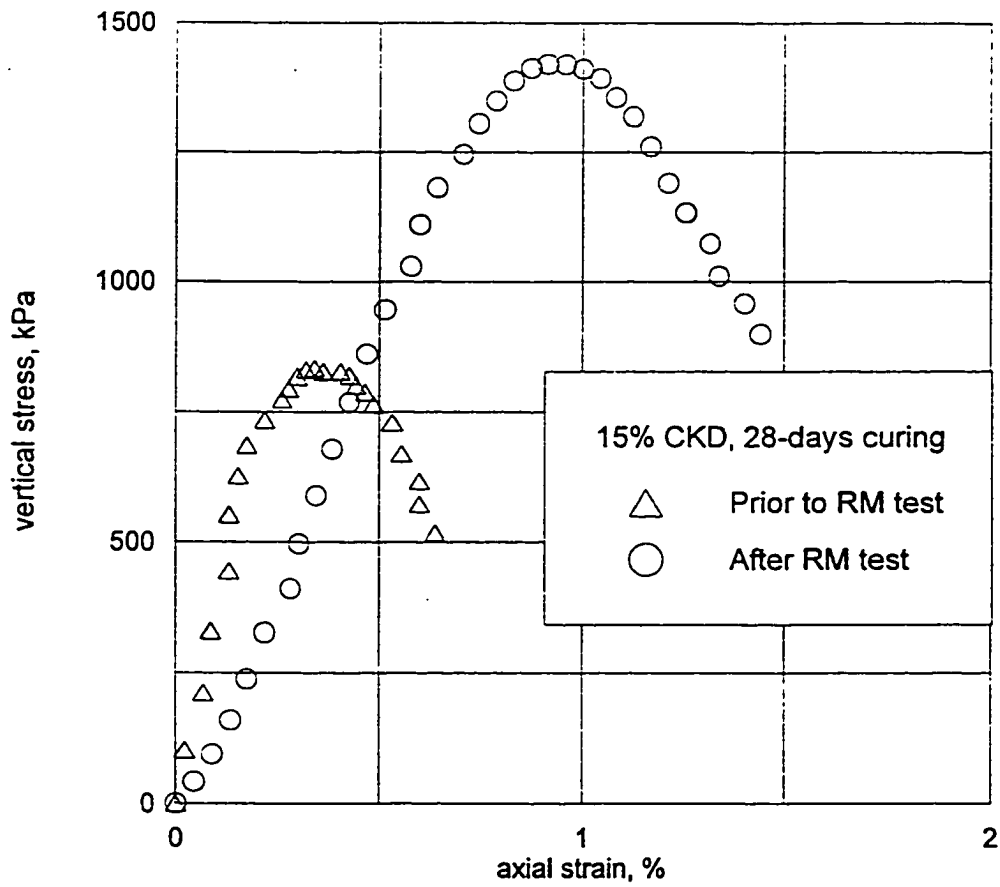
Figure 5-13   Typical Stress-strain Curves of UCS Tests Conducted After/and Prior to RM Test (15% CKD, 28-day Curing)
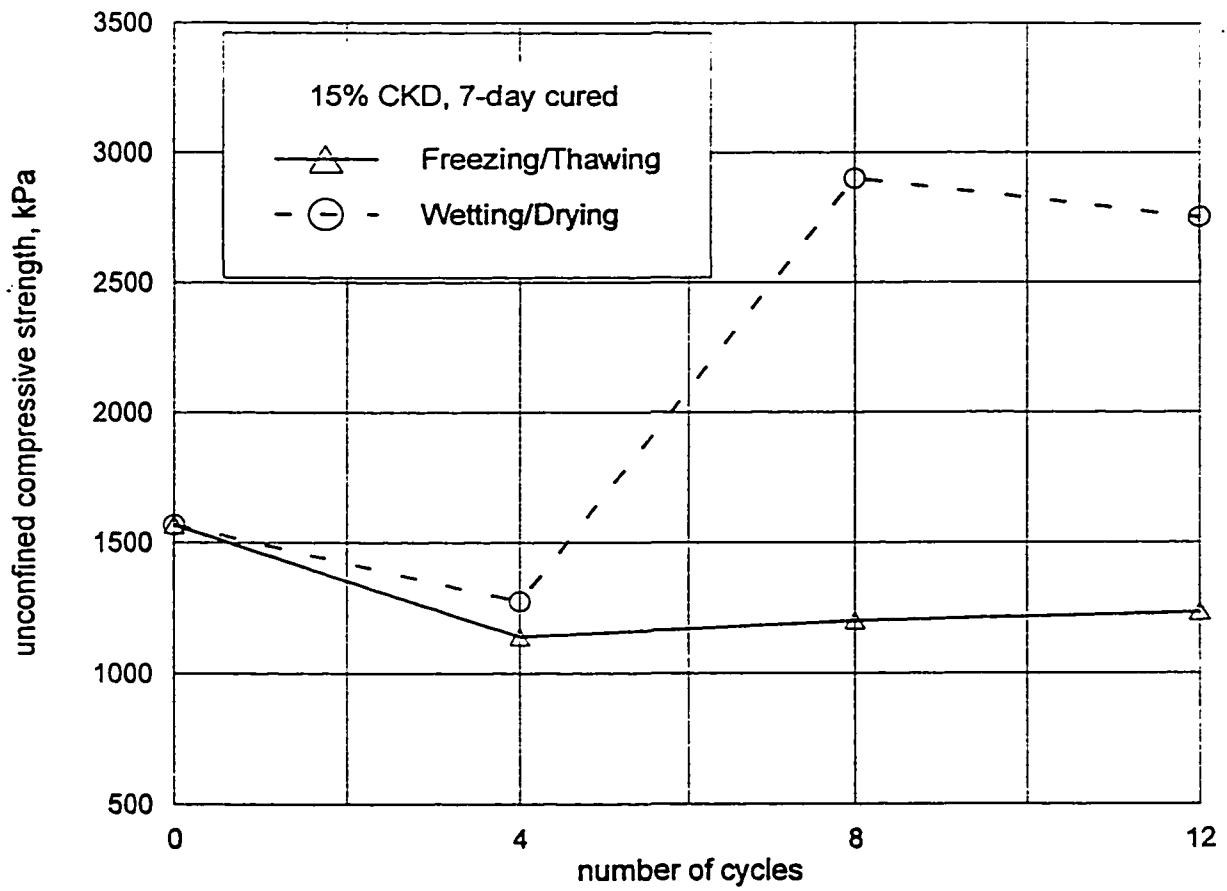
Figure 5-14   Effect of Freezing/Thawing and Wetting/Drying Cycles on the UCS
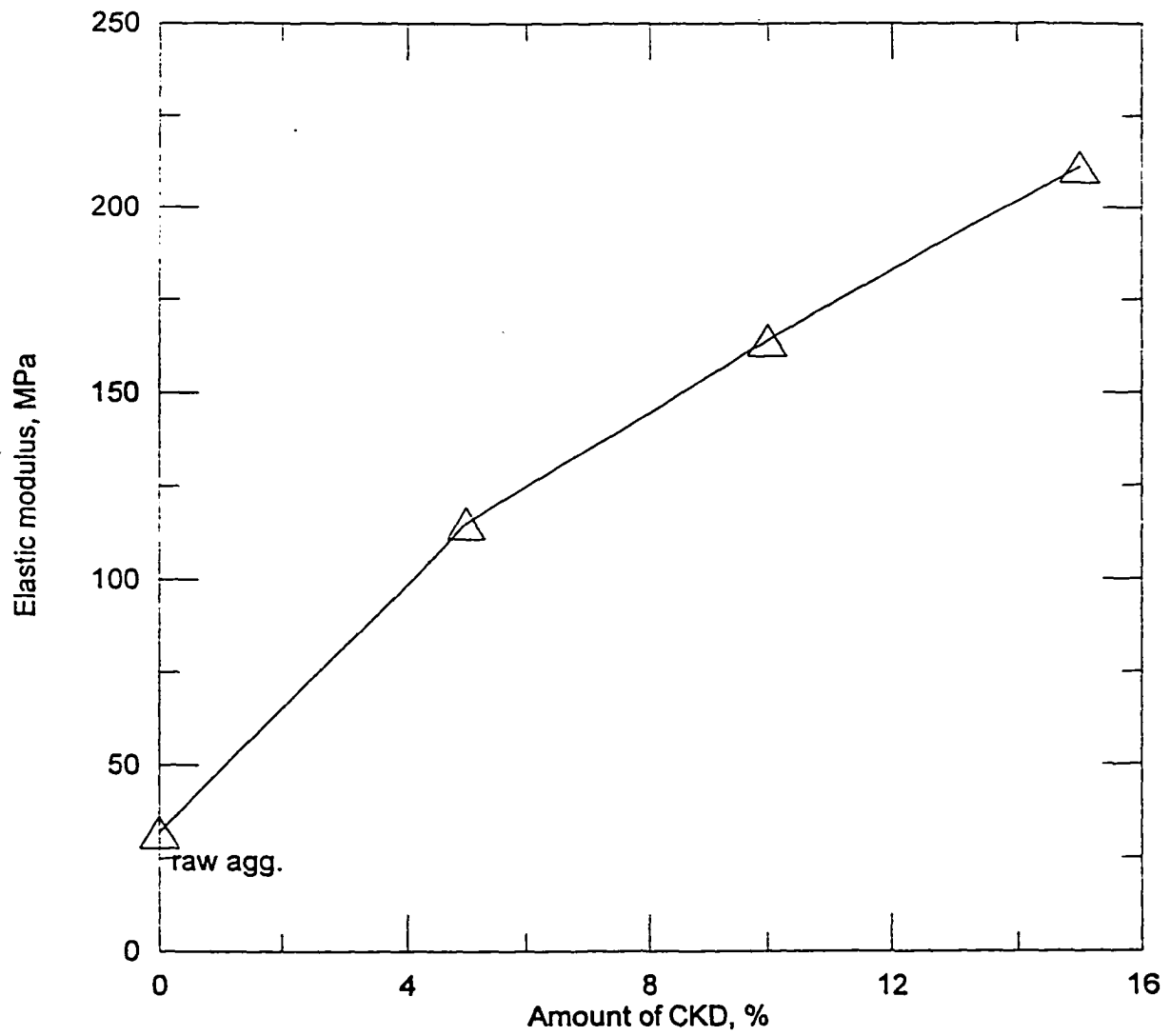
Figure 5-15   Mean Elastic Modulus vs. Amount of CKD (7-day Cured)
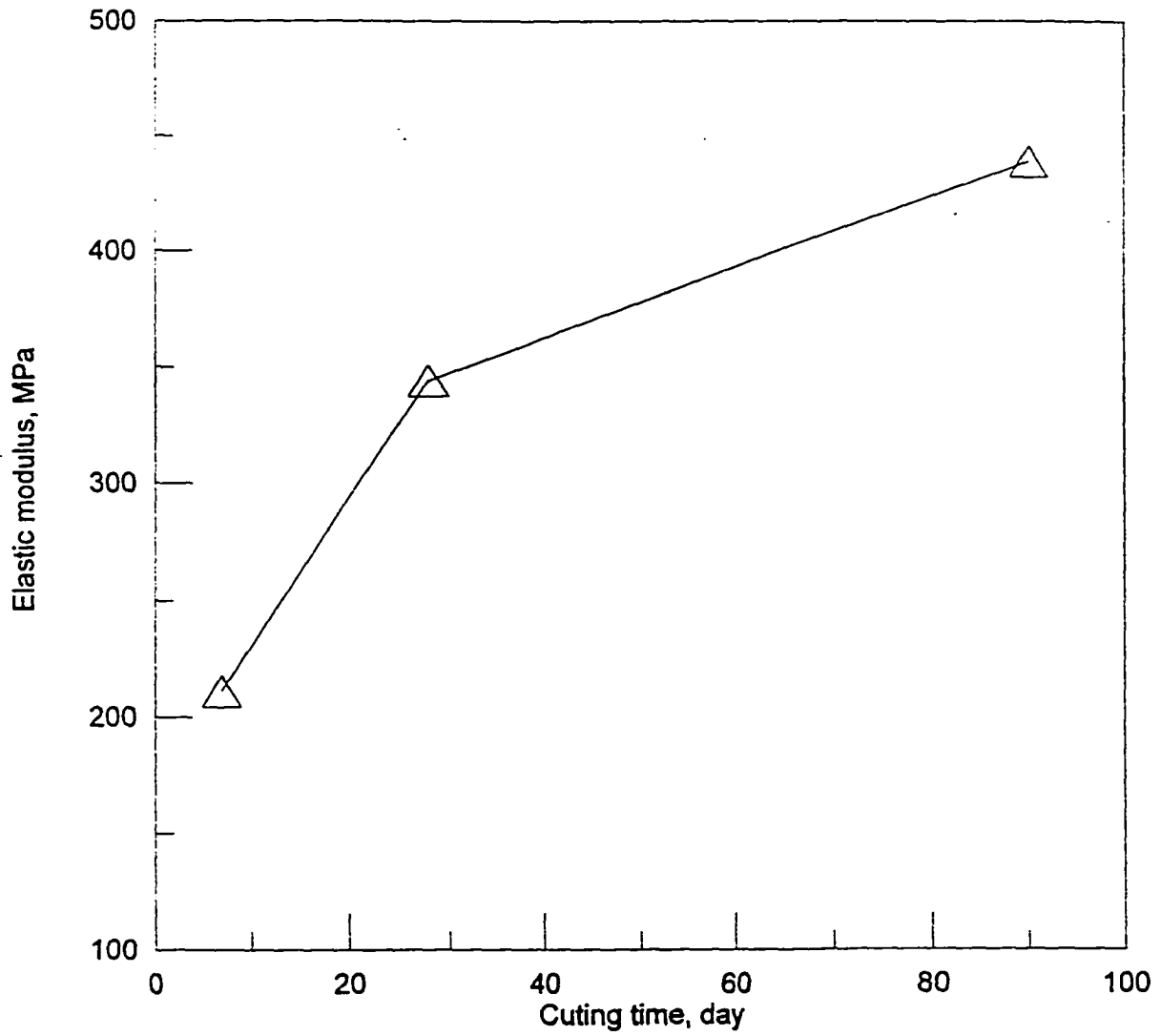
Figure 5-16   Mean Elastic Modulus of CKD-stabilized Aggregate vs.
                   Curing Time (15% CKD)
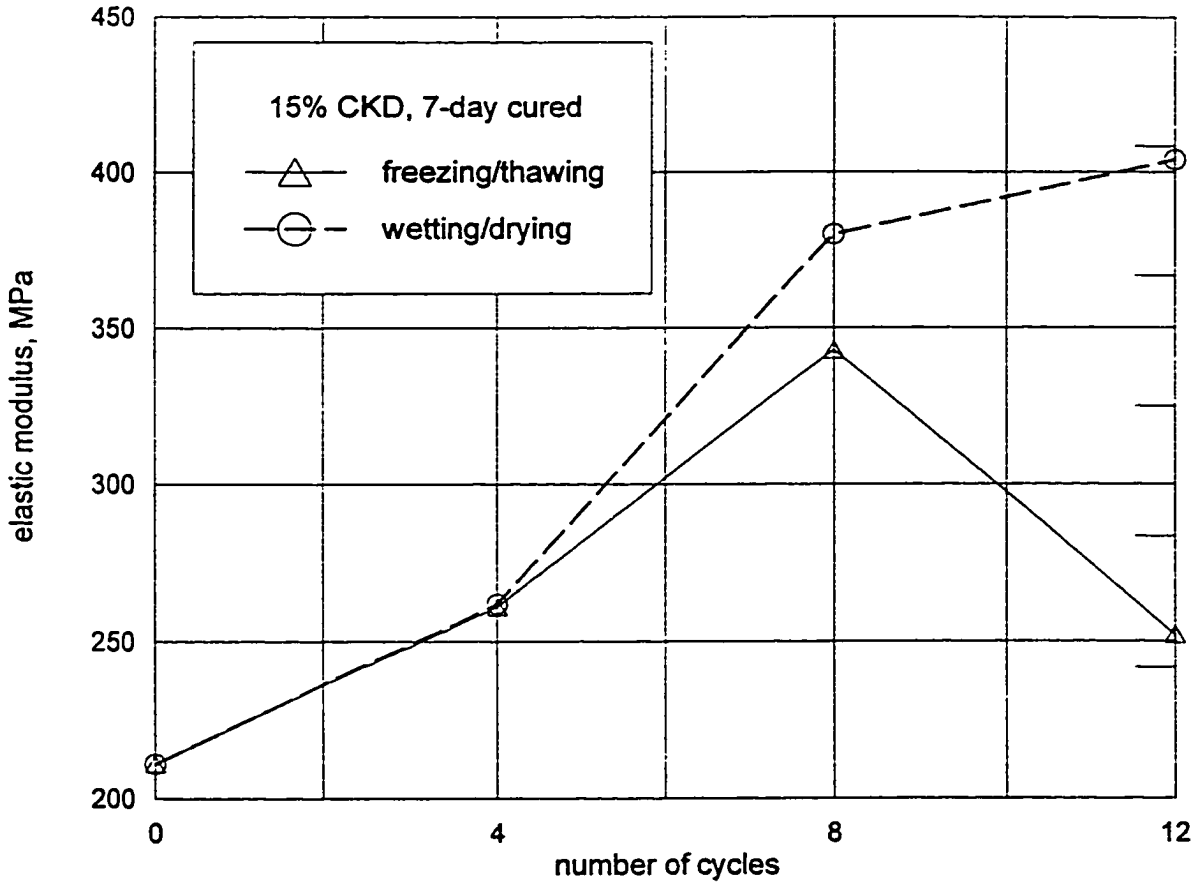
Figure 5-17. Effect of Freezing/Thawing and Wetting/Drying Cycles on the EM
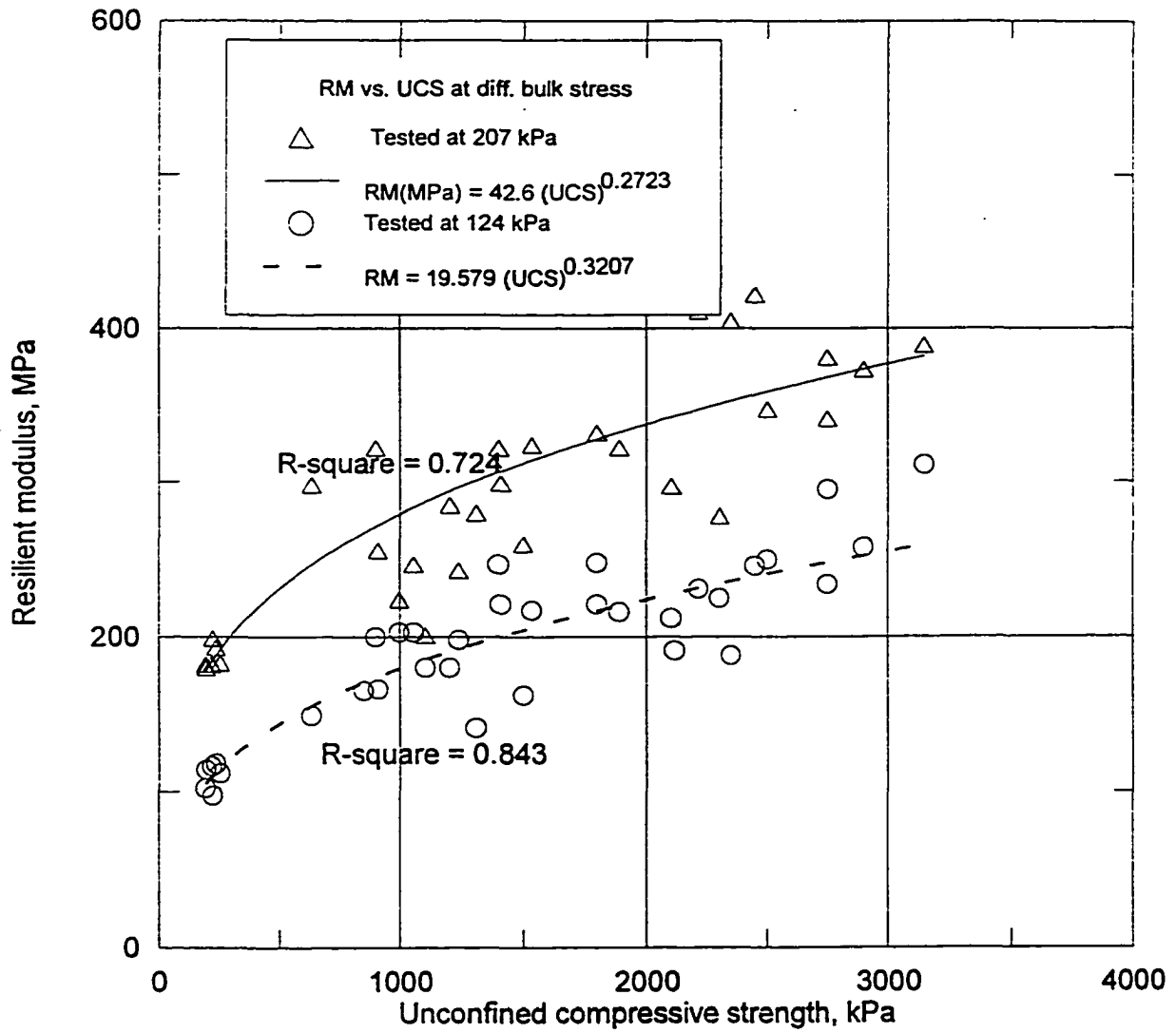
Figure 5-18   Relationship between Resilient Modulus and Unconfined Compressive Strength
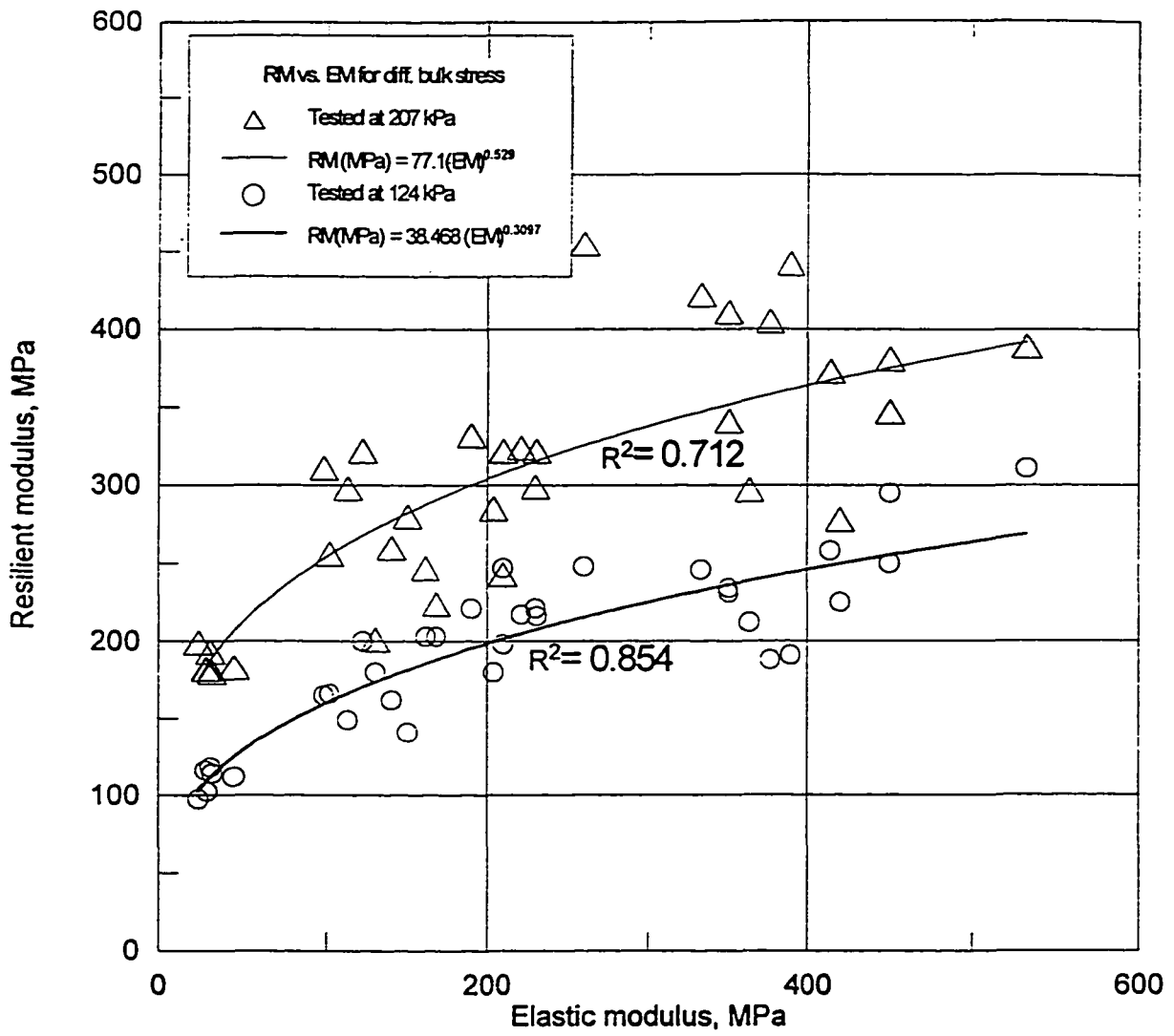
Figure 5-19   Relationship between Resilient Modulus and Elastic Modulus

125
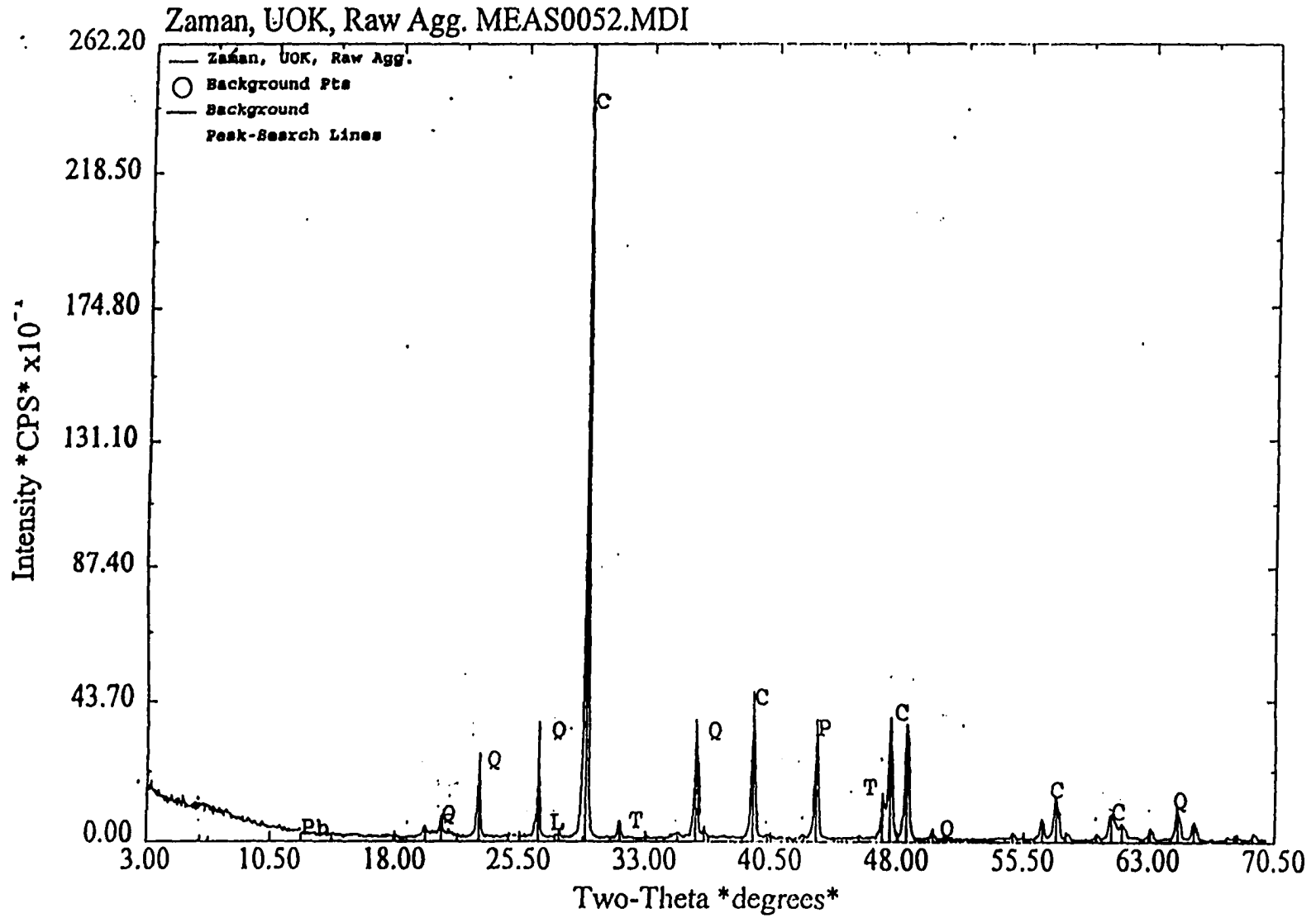
Figure 5-20 a) X-ray Diffractogrm of Raw Aggregate
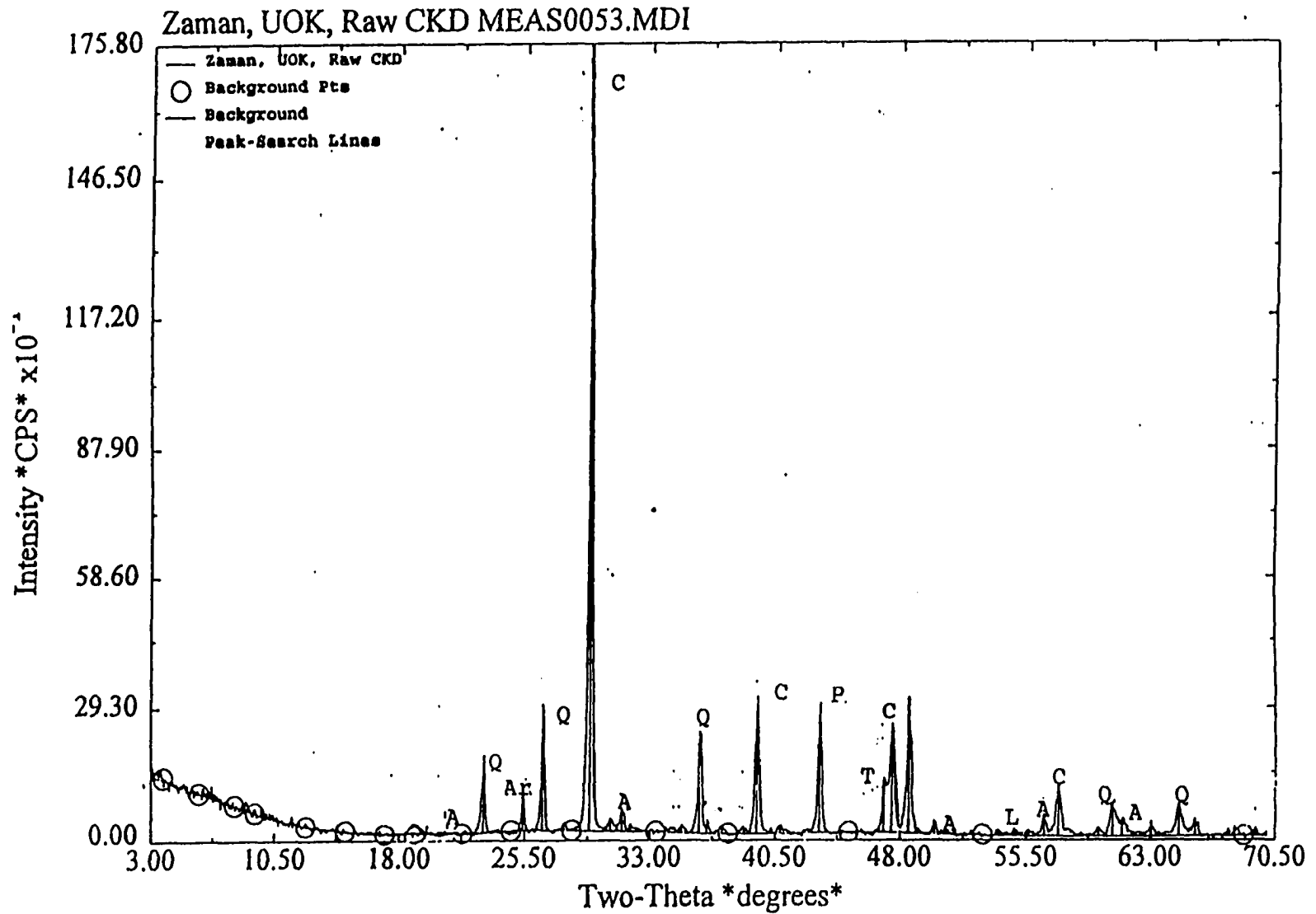
Figure 5-20 b) X-ray Diffractogrm of Raw CKD Sample
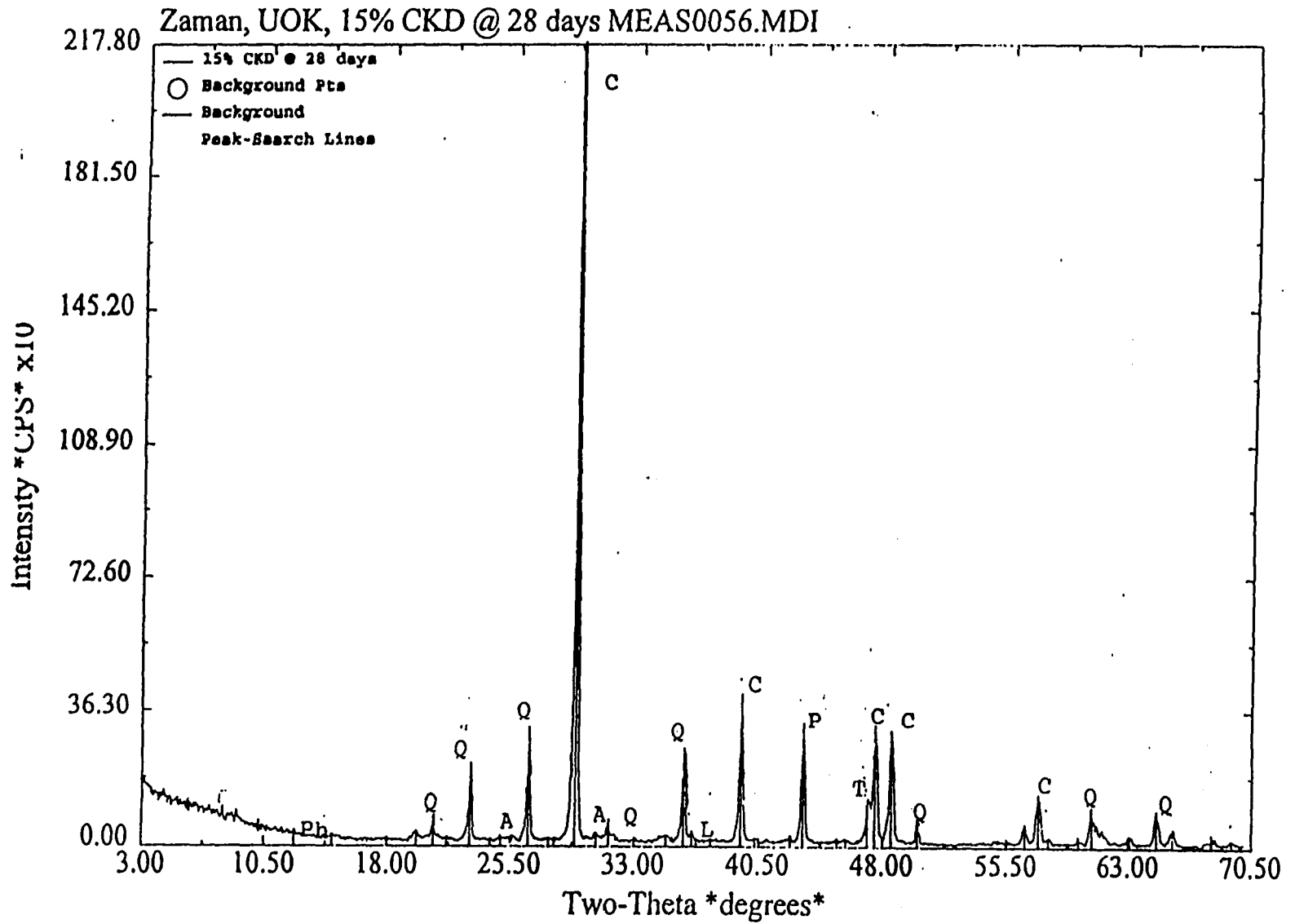
Figure 5-20 c) X-ray Diffractogrm of 28-day Cured Aggregate Stabilized
with 15% CKD
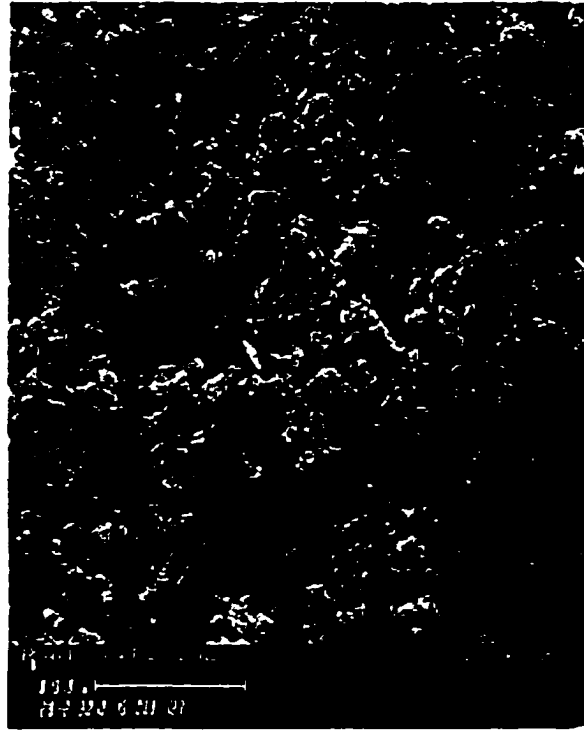
Figure 5-21   Micrograph of Raw Aggregate

Spherical or
rounded CKD
particles

IW RAW CKD
0004 15KU   X4,000   1μm
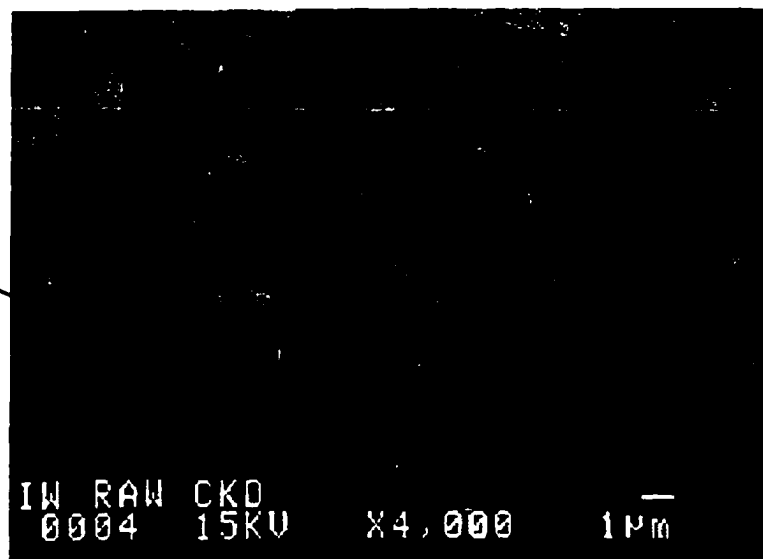
Figure 5-22 SEM Micrograph of the Raw Cement-kiln-dust

129
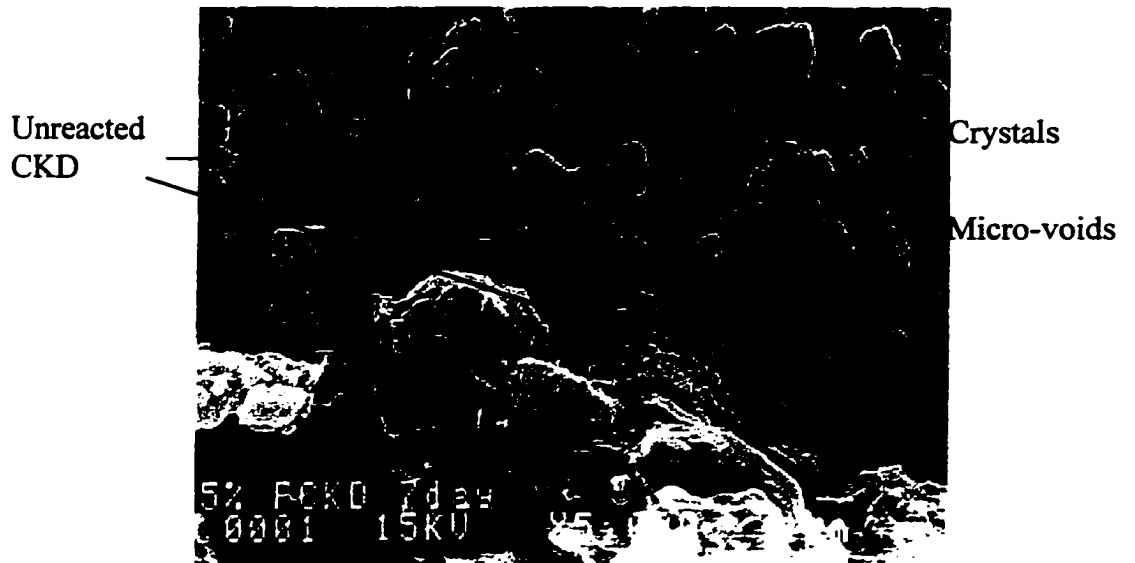
Figure 5-23 Micrograph of the 7-day Cured Aggregate Stabilized
with 5% CKD

Figure 5-24 Micrograph of the 7-day Cured Aggregate Stabilized
with 10% CKD

130

Crystals

Figure 5-25 Micrograph of the 7-day Cured Aggregate Stabilized
with 15% CKD

Crystals

Figure 5-26 Micrograph of the 28-day Cured Aggregate Stabilized
with 15% CKD

131
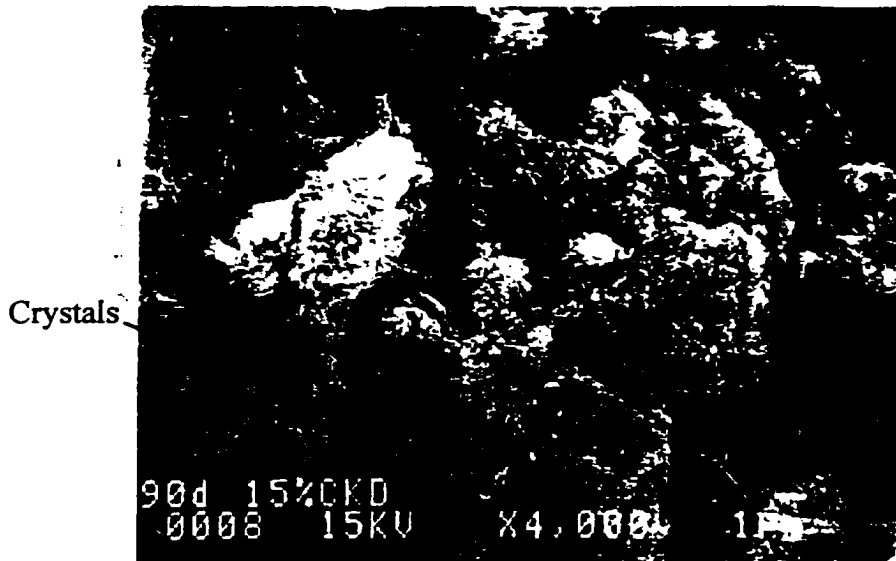
Figure 5-27 Micrograph of the 90-day Cured Aggregate Stabilized
with 15% CKD
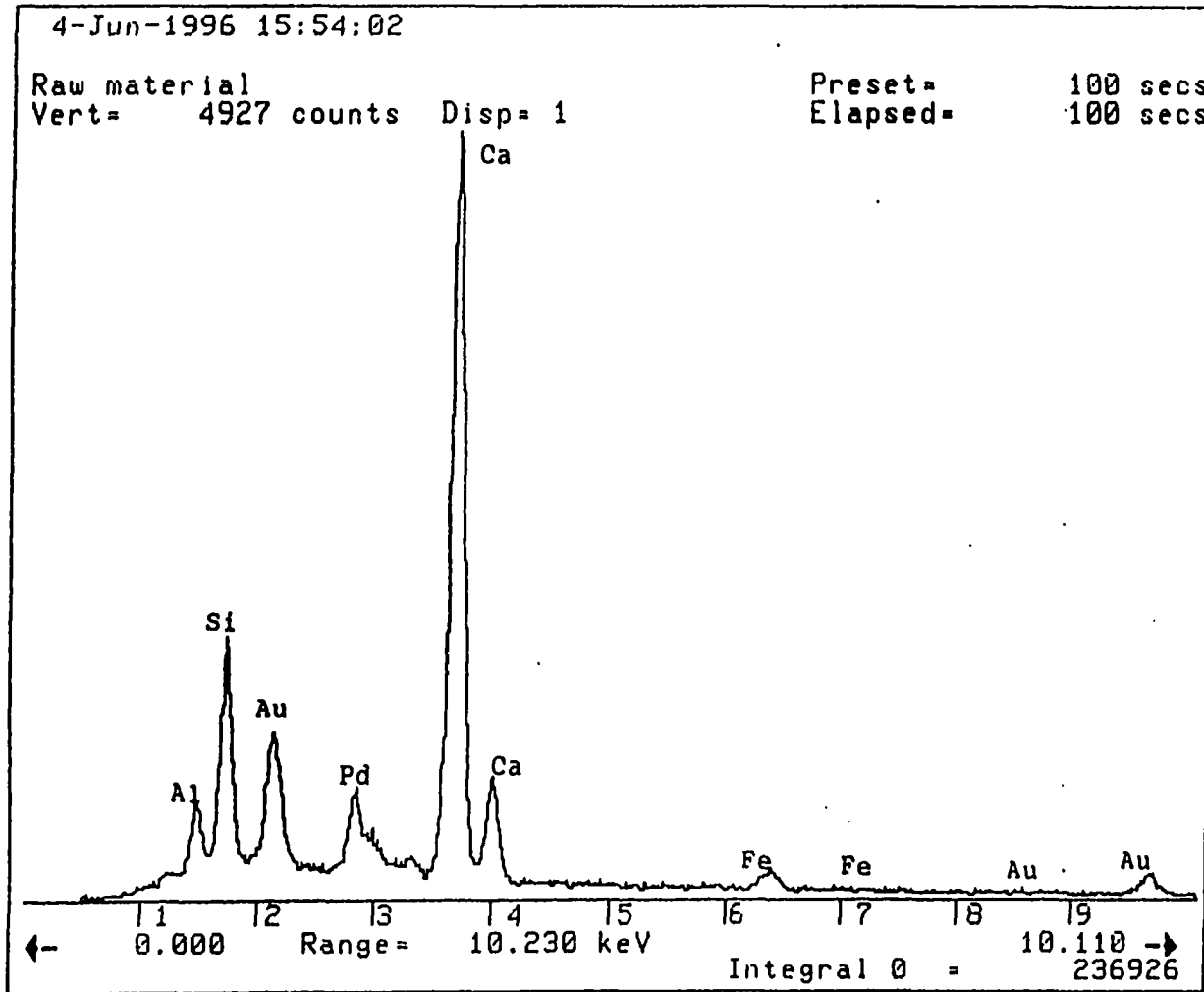
Figure 5-28 a) Energy Dispersive Spectroscopy of Raw Aggregate

133
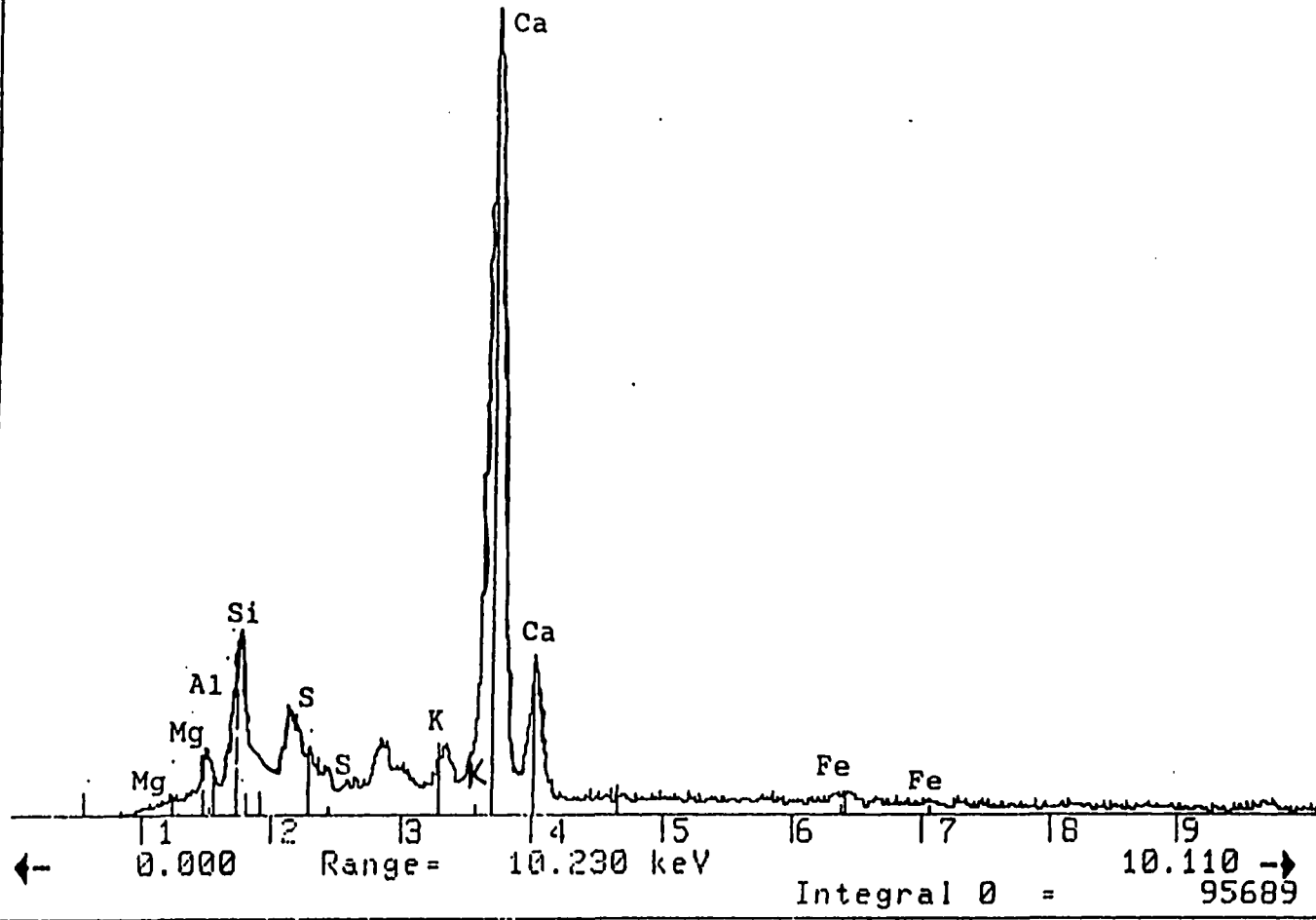
Figure 5-28 b) Energy Dispersive Spectroscopy of Raw CKD
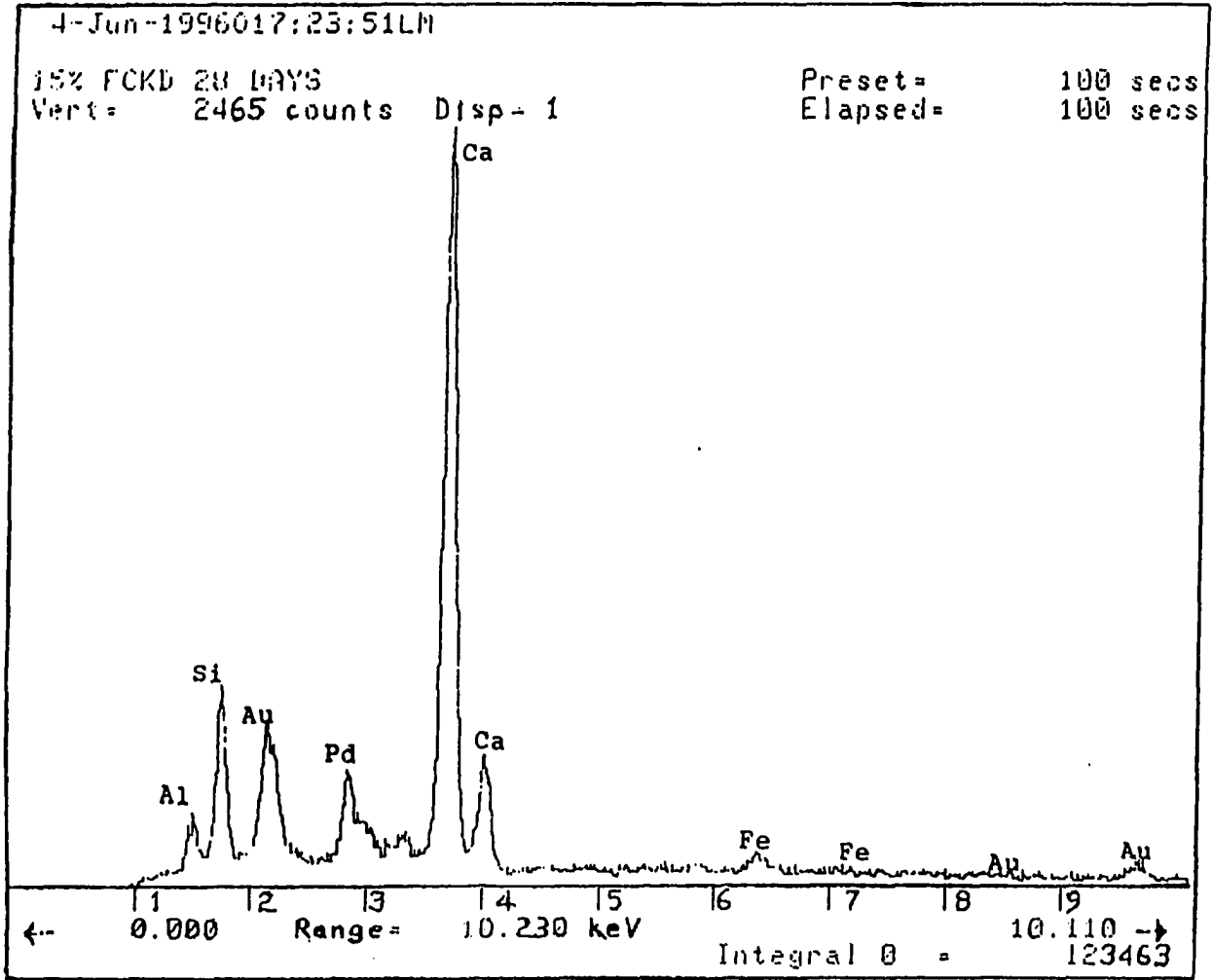
Figure 5-28 c) Energy Dispersive Spectroscopy of 28-day Cured Aggregate
Stabilized with 15% CKD

CHAPTER 6

MODELING OF RESILIENT MODULUS

6.1   Introduction

Modeling of resilient behavior of base/subbase materials plays an important role in implementing pavement design and evaluation of pavement performance. During last three decades researchers have devoted considerable effort to determine the nonlinear load-deformation characteristics of aggregates used as roadway bases. The widely discussed models for resilient modulus of such aggregates include the bulk stress model, the bulk-deviator stress model (Hicks and Monismith, 1971; Uzan, 1985; Santha, 1994). However, the data used for developing these models were all obtained from the resilient modulus tests conducted using the procedures different than the current AASHTO T-294-94 method. Therefore, the applicability of these models to estimating resilient moduli (based on AASHTO T294-94) is questionable. In this chapter, stress-dependent models including bulk stress and bulk-deviator stress models are developed based upon the laboratory data obtained in this study. Also, a deviator stress-type model is employed to correlate RM values. In addition to the stress dependent models, a neural network model is proposed based on training and testing of the available RM data.

6.2   Stress-Dependent Models

i. Bulk Stress (k - θ) Model

The widely used bulk stress model is given by:

$$RM = k_1 \, \theta^{k_2}$$ (6-1)

where:

θ = bulk stress, kPa

k_1, k_2 = regression coefficients.

Figures 6-1 through 6-4 show a relationship between mean RM values and bulk stress for different sample preparation conditions. From these figures one can see that the RM values do not change uniquely with the bulk stress. Regression analysis results indicate that the bulk stress model shows a rather poor correlation with the experimental RM values. The correlation coefficient R^2 values vary from 0.42 to 0.74, as listed in Table 6-1.

A comparison showing predicted RM values from equation (6-1) versus experimental values is presented in Figures 6-5 through 6-7. The difference between the predicted and experimental is found to be as high as 50%.

ii. Deviator Stress (σ_d) Model

The deviator stress model is given by:

$$RM = k_3 \, \sigma_d^{k_4} \tag{6-2}$$

where:

σ_d = deviator stress, kPa

k_3, k_4 = regression coefficients.

Figures 6-8 through 6-11 show a relationship between mean RM values and deviator stress for different sample preparation conditions. From these figures one can see that the RM value almost linearly changes with the deviator stress. Regression analysis results indicate that the deviator stress model provides a better correlation

137

between experimental and predicted RM values than the bulk stress model. The correlation coefficient R^2 values vary from 0.833 to 0.971, which is much higher than those obtained for the bulk stress model. The correlation results are also shown in Table 6-1 for the purpose of comparison. Again, it is evident that the deviator stress model shows a more close correlation with the RM value than the bulk stress model. This is because axial elastic strain of a specimen is mainly caused by the deviator stress rather than the bulk stress whose value can be a finite value without causing any shearing action.

The relationship between predicted RM values from equation (6-2) and experimental values is presented in Figures 6-12 through 6-14. It is observed that the predicted RM values are well complying with the corresponding experimental values. One of the weakness of the deviator stress model is that it does not take into consideration of effect of confining pressure (bulk stress) which is also an important factor affecting the resilient strain of a specimen. Fortunately, in AASHTO Designation: T294-94 each deviator stress value is given for a specific confining pressure, whose effect is automatically reflected by the designated deviator stress (Zhu et al., 1997d).

iii. <u>Combined Bulk-Deviator Stress $(\theta \sim \sigma_d)$ Model</u>

From the definition, resilient modulus is a function of both deviator stress and resilient axial strain which depends on both deviator stress and bulk stress. The RM values actually vary with both θ and σ_d values. Figures 6-15 and 6-16 present a set of contours for experimental RM values in the θ and σ_d space, that illustrates relationship between the RM values and the $\theta \sim \sigma_d$ plane for different aggregates tested in this

study. It is evident that from these figures the RM increases with increasing both θ and σ_d. The equation describing $\theta \sim \sigma_d$ model is given by:

$$RM = k_5 \, \theta^{k_6} \, \sigma_d^{k_7} \qquad (6-3)$$

where k_5, k_6 and k_7 are regression coefficients.

Table 6-2 includes a list of correlation parameters of equation (6-3) obtained from the tested aggregates. One can note that the values of k_6 range from -0.43 to -0.046, and k_7 from 0.68 to 1.01, which shows that the RM decreases slightly with increasing θ, but increases with increasing σ_d substantially. It is noted that the θ in a triaxial test can be represented as $3\sigma_3 + \sigma_d$, which implies the RM values may decrease with increasing σ_3 for the studied aggregate. This is not true because, theoretically, the elastic strain of an aggregate should decrease with increasing confining pressure σ_3, which should result in an increase in RM value ($RM = \sigma_d/\varepsilon_r$). However, for the current AASHTO testing procedure, the deviator stress increases with the increased σ_3 substantially. Therefore, the RM values are controlled predominately by the deviator stress rather than the confining stress. The goodness of the model is indicated by high correlation coefficient R^2 values ranging from 0.83 to 0.91. Figure 6-17 presents the predicted RM values from the $\theta \sim \sigma_d$ model as well as the experimental RM values, demonstrating a good agreement between the model results and the test data.

From above discussion, it becomes clear that of all the stress-dependent models, the $\theta \sim \sigma_d$ model is the best and the θ model the worst for the aggregate investigated in this study. Since the bulk stress model has been implemented previously in many pavement design programs, the use of bulk stress model still prevails in the pavement

design approach today. However, an effort should be made to include deviator stress or bulk-deviator stress type models in pavement design programs, which is beyond the scope of this study.

6.3   Artificial Neural Network Model

One of the shortcomings of above stress-dependent models is that these models are not unique, i.e. they change with such factors as aggregate types and sources, gradation, density and moisture content of the aggregate, and stabilization and sample conditioning effects. Therefore, if any one of the above-mentioned factors changes, the correlation coefficients change accordingly, which is shown in the preceding section. Although multiple regression analyses can take into consideration of the aforementioned factors, an appropriate equation through which the independent variables can best correlate with the dependent variable is difficult to speculate and establish. The artificial neural network (ANN) offers an alternative approach for modeling resilient modulus of aggregate base. There is not necessity to constitute a fixed equation to match relationship between independent variables and a dependent variable prior to application of the ANN model. Rather, an ANN can provide an approach that is closer to human perception and recognition than traditional methods. The ANN model is capable of establishing a characteristic input-output relationship without any preliminary information of the system. Specially, in situations where existing data are noisy and/or incomplete, ANN can still produce reasonable results.

In applying ANN as a computational tool to the modeling of resilient modulus, one has to consider the following aspects: (i) design of an ANN architecture, namely

selecting the number of layers and nodes in each layer, as well as the interconnection scheme like forward or backward propagation; (ii) determination of a specific optimization algorithm; (iii) initialization of training of ANN with input data upon which the relationship embedded in the data may be established and the weights between the neighboring layers are obtained; (iv) testing predictability of the trained network with testing data. These four aspects constitute a basic framework for modeling of resilient modulus presented in this study.

6.3.1   Design of the ANN Model

(1) <u>Selection of Input Variables and Output:</u>   The target output is clearly the experimental resilient modulus. The input variables are determined through preliminary modeling efforts aimed at minimizing the number of input parameters without causing a significant loss in model prediction accuracy.   In this study, more focus is directed toward stabilization parameters which show significant influence on the RM values. The selected input parameters include seven categorical variables and two discrete variables. These variables and the range for each variable are listed below.

Seven categorical variables:

     i.   STAB

             STAB = 0 for no stabilization;

             STAB = 1 for CKD stabilization; and

             STAB = 2 for fly-ash stabilization.

     ii.   DRAIN

             DRAIN = 1 if drainage line is open;

DRAIN = 0 if drainage line is close.

iii. OXIDE — amount of $SiO_2 + Al_2O_3 + Fe_2O_3 + CaO$ (%) in stabilizing

agent

OXIDE = 0 for raw aggregate;

OXIDE = 61.5 for CKD-stabilization; and

OXIDE = 76.51 for flyash-stabilization (Pandey, 1996)

iv. ASA — amount of stabilizing agent in percent, taking a value of

either 0, 5, 10 or 15;

v. CD — curing days, having a value of either 0, 7, 28 or 90;

vi. NWD — number of wetting/drying cycles, taking a value of 0, 4, 8 or

12;

vii. NFT — number of freezing/thawing cycles, taking a value of either

0, 4 or 12.

Two discrete variables:

i. σ_d — deviator stress, 21 kPa to 276 kPa;

ii. θ — bulk stress, 83 kPa to 690 kPa.

(2) Architecture of the Model: After trying different number of hidden layers, one hidden layer with connections to both input layer and output layer is used in the ANN model employed here. One hidden layer show theoretically to be able to model any nonlinear work (Giles et al., 1994; Fausett, 1994), although sometimes multiple hidden layers may efficiently deal with complex problems (Parlos et al., 1994). The number of nodes in the hidden layer is determined by a trial and error method. In the

142

preliminary study, a network with different nodes ranging from 10 to 40 in the hidden layer was trained for the same number of epochs, and the sum of squared errors (SSE) of the training sets was recorded. It was found that the value of SSE reached minimum when the number of nodes equaled to 30. So a 9-30-1 network is set up as shown in Figure 6-18.

6.3.2 Learning, Training and Testing of the ANN Model

(1) <u>Learning algorithm</u>: The mathematical equations for one hidden layer feed-forward neural network are presented in Chapter 2 section 2.6.2. The equations (2-8) through (2-17) are implemented in the ANN modeling program (The Mathworks, Inc., 1994). The learning algorithm of the network for this study is set as follows:

step 1: For each input vector s_i (i = 1, 2, 3, ..., n) perform step 2 to step 9;

step 2: set $\mathbf{x}=\mathbf{s}_i$;

step 3: if m =1, set the initial weights and biases randomly;

and go to step 5;

otherwise go to step 4;

step 4: load previously achieved weights and biases and set them as

initial weights and biases;

step 5: if stop condition is false perform step 6 to step 9;

step 6: calculate outputs from hidden layer (Z_j), and from output layer

(Y_k) using equations (2-8) and (2-9);

step 7: calculate $E=1/2* \sum_{k=1}^{n} (T_k-Y_k)^2$;

143

step 8: update weights and biases using equations (2-10) through

(2-17);

step 9: test if stopping conditions have been satisfied.

(2) Training and testing of the network: There are generally two types of training procedures involved in the ANN modeling, i.e. supervised training and unsupervised training. Perhaps most neural nets involve supervised training which is accomplished by presenting a sequence of training vectors, each with an associated target vector. The weights and biases connecting input and output vectors are adjusted by minimizing errors between the target output and the net output values. The unsupervised training is to provide a net with a sequence of input vectors, but no target vectors are specified. No guidance is presented to the network about what it is supposed to learn. The net modifies the weights according to its own built-in criteria. The unsupervised net is mainly used for clustering and self-organizing mapping (Kohonen, 1990). In this study, a supervised learning rule is employed in the proposed ANN model.

The data base used for training the net consists of nine data sets with 210 data points, which include the following:

i. one set of data from the raw aggregate;

ii. one set of data set from 7-day cured aggregate stabilized with 5% CKD;

iii. one set of data from 28-day cured aggregate stabilized with 15% CKD;

iv. one set of data from 90-day cured aggregate stabilized with 15% CKD;

v. one set of data from 28-day cured aggregate stabilized with 15% fly-ash (Pandey, 1996);

vi. one set of data from stabilized aggregate subjected to 4 cycles of freezing/thawing;

vii. one set of data from stabilized aggregate subjected to 8 cycles of freezing/thawing;

viii. one set of data from stabilized aggregate subjected to 4 cycles of wetting/drying; and

ix. one set of data from stabilized aggregate subjected to 12 cycles of freezing/thawing.

The reason for using flyash stabilized data is to leave the model more flexible, so that it can be expanded to consider various stabilization rather than only CKD-stabilization.

The feed-forward backpropagation network was used in modeling. A hyperbolic tangent function was adopted as an activation function to connect the input layer and the hidden layer; and a linear function was used to link the hidden layer and the output layer. The training was performed in a PC PS-90 computer using commercial software called MATLAB. After 50,000 epochs the network achieved its goal, which took about 20 hours. As a result of the training, the network produced 30 x 9 weights (W_1) and 30 bias values (b_1) connecting input and hidden layer, 30 x 1 weights (W_2) and 1 bias

values (b_2) connecting hidden layer and output layer. Table 6-3 presents a list of the final weights and bias values. With these weights and bias values, the network is able to simulate RM values with the trained data and to predict RM values with the untrained data by using following equations:

$$z_j = F_2 (b_{1j} + w_{1 (j \times 9)} * IN_9), \quad j = 1, 2, \ldots\ldots 30 \tag{6-4}$$

$$RM \ (MPa) = b_2 + W^T_{2(30 \times 1)} * Z_{(30 \times 1)} \tag{6-5}$$

where:

$$F_2 (x) = (e^x - e^{-x}) / (e^x + e^{-x})$$

$$IN_9 = \{STAB, DRAIN, \sigma_d, \theta, OXIDE, ASA, CD, NWD, NFT \}^T$$

6.3.3 ANN Model Results

ANN model results are presented in two aspects. One is simulation of experimental data that were used for training the network, the other is prediction of experimental data that were not used in training process. The ANN simulation generally produces a good agreement with the training experimental data since these data contributed useful information or knowledge that forms the basis of the network model. However, the excellence of ANN prediction depends, to a large degree, on the knowledge learned from training process. If the network has been trained with so called "comprehensive data", the network model is expected to predict very well with untrained data. If prediction is poor, the network should be continuously trained with new data that show poor prediction results.

ANN Simulation Results Figure 6-19 presents experimental RM and ANN modeled RM versus bulk stress for the 210 data points used in the training process. The

hollow circles represent the experimental values, and the hollow triangles symbolize the values predicted by ANN model. It can be seen that although the 210 RM values distribute everywhere in the figure, the ANN model still demonstrates excellent agreement with these values. The goodness of the fitting is further illustrated in Figure 6-20 which shows that the ANN model is almost identical to the experimental data with a correlation coefficient R^2 equaling 0.99.

An effort was simultaneously made to find a multiple regression model using the same variables as used in the ANN model. The final multiple regression model is given by:

$$RM \text{ (MPa)} = -49.6689 + 232.787 \text{ STAB} + 40.5417 \text{ DRAIN} + 1.1925 \sigma_d$$

$$+ 0.1124 \theta - 3.7166 \text{ OXIDE} + 2.5562 \text{ ASA} + 4.1239 \text{ CD}$$

$$- 6.9261 \text{ NWD} - 14.6959 \text{ NFT}$$

$$R^2 = 0.82 \tag{6-6}$$

The model results from regression equation (6-6) are also shown in Figure 6-20. It is evident from the figure that the regression model deviates from the experimental data substantially. Prediction with this model will result in a non-negligible error.

ANN Prediction Results   The predictability of the ANN model was tested using untrained experimental data, including one set of data from 7-day cured aggregate with 10% CKD and one set of data from aggregate subjected to 12 freezing/thawing cycles. Figure 6-21 shows prediction results of 30 untrained data points using the ANN model and regression equation (6-6). It is observed that the good agreement is between the ANN prediction results and the experimental RM values. This agreement demonstrates

that the ANN model trained with the data given in preceding section has stored necessary information required for prediction of RM values for the studied aggregate. In contrast with the ANN model, the multiple regression model shows rather poor prediction for the same data sets. The correlation coefficient R^2 is 0.94 for the ANN model, and 0.75 for the regression model.

It is important to note that the parameter used for the ANN model can be easily obtained without doing any special tests. The seven categorical variables can be obtained from knowledge of design and construction materials. The type, amount of stabilizing agent and chemical composition can be decided prior to construction of the base course. The number of freezing/thawing and wetting/drying cycles need to be specified before/or during design of a pavement. Deviator and bulk stresses within a base layer can be computed approximately using layered theory or finite element program like MICH-PAVE. These features make possible of application of the ANN model in practical engineering.

However, one should be cautious on the application of the ANN model to predict RM values of the aggregate having category values different than that used in the training process. Because different category values may bring about fully different behavior of the aggregate, the ANN predicted results will differ greatly from the real values. For example, if one use the developed ANN model to predict the aggregate stabilized with cement the prediction results may not be satisfied or the predictions for 12% stabilizing agent could be quite different from the measured values.

Table 6-1 Correlation Parameters of RM vs. Bulk/Deviator Stress Models*

Aggregate	$RM = k_1 \theta^{k_2}$			$RM = k_3 \sigma_d^{k_4}$		
	k_1	k_2	R^2	k_3	k_4	R^2
Raw	3760	0.6455	0.622	6636	0.6794	0.901
5% CKD 7day	12912	0.4853	0.481	13265	0.5974	0.872
10% CKD 7day	14841	0.4501	0.347	11333	0.6153	0.763
15% CKD 7 day	12780	0.5102	0.396	9852	0.6911	0.843
15% CKD 28 day	9621	0.607	0.471	10014	0.7405	0.852
15% CKD 90 day	13922	0.561	0.618	19832	0.6229	0.904
4 cycles (Freeze/thaw)	6918	0.5326	0.5676	7640	0.6492	0.917
8 cycles (Freeze/thaw)	5232	0.5370	0.5116	5305	0.6692	0.876
12 cycles (Freeze/thaw	4029	0.5972	0.6373	5069	0.6964	0.933
4 cycles (wet/dry)	3170	0.7216	0.5896	4441	0.8183	0.927
8 cycles (wet/dry)	5018	0.6022	0.4618	4347	0.7726	0.923
12 cycles (wet/dry)	2937	0.6801	0.5786	3699	0.7898	0.919

* The units used in developing model are: RM = kPa, θ and σ_d = kPa.

Table 6-2 Correlation Parameters of Bulk-Deviator Stress Model *

Aggregate Type	$RM = k_5 \theta^{k_6} \sigma_d^{k_7}$			R^2
	k_5	k_6	k_7	
Raw aggregate	7.3927	-0.0460	0.7130	0.901
5%CKD,7-day	25.2660	-0.2960	0.8230	0.912
10%CKD,7-day	28.4880	-0.4181	0.9332	0.833
15%CKD, 7-day	26.1582	-0.4315	1.0135	0.906
15%CKD, 28-day	19.2432	-0.2830	0.9462	0.878
15%CKD, 90-day	23.4211	-0.0772	0.6801	0.907
Cycles of 4	8.0515	-0.2879	0.9918	0.921
Freezing/ 8	7.0360	-0.1961	0.8536	0.919
Thawing 12	7.6330	-0.2036	0.8608	0.912
Cycles of 4	7.2955	-0.2170	0.9801	0.908
Wetting/ 8	11.5817	-0.4413	1.1066	0.914
drying 12	5.8776	-0.2048	0.9436	0.927

* The units used in developing the model are: RM = MPa, θ and σ_d
= kPa.

150

Table 6-3   List of Weights and Bias Values of the Network

$W_{1(30 \times 9)}$								
-0.8141	-2.4321	-2.5056	0.2125	0.9827	1.2862	0.1223	1.6242	-0.7359
0.6357	5.0657	-0.9610	-0.5815	-1.5413	-0.8384	1.1584	-0.4464	-0.9091
-1.1408	-7.9152	-1.2038	2.8147	-1.8213	-0.2651	0.3690	2.7426	-1.0183
-3.7811	4.3919	0.1967	1.2234	-0.0611	-0.2535	-1.2285	4.1191	-1.1720
2.4833	3.2870	-2.5856	1.6723	0.6900	2.6890	-1.4684	4.2037	-0.7340
2.5067	-0.4635	0.3812	-1.3896	1.2272	1.3729	-1.1568	-1.0808	1.0683
0.3789	4.2227	0.7373	-1.9818	-1.5936	-0.1061	0.2121	-0.4531	-1.2606
0.5428	-0.3528	0.3434	1.7003	0.3548	1.0949	-1.2263	-0.2767	-0.5827
3.5889	-3.4144	0.8472	0.3278	0.6111	0.0756	-0.3853	0.9967	1.8023
2.1870	4.0510	-1.5968	-0.1310	0.3787	-0.3882	1.9839	-1.5976	-2.5457
-1.1739	0.1628	1.2598	1.4277	-0.3050	-1.2315	-0.3792	1.5281	1.1542
1.7478	0.4822	-0.4882	-0.3832	0.3416	-0.5973	-1.4443	-0.9106	1.1962
-2.5706	2.2820	0.6426	0.4953	-1.5444	1.0189	0.6601	-1.2813	-1.5291
-1.2587	1.6164	-0.2458	-0.0471	-0.7122	-0.2863	0.2875	0.0610	-0.3191
-2.5221	1.4610	-0.2934	-0.1960	-0.8418	-1.1724	-0.9190	-1.7302	-1.3477
1.0654	0.9365	-1.9147	0.9822	0.1769	-1.3464	-1.2939	-0.0430	-1.6697
-1.0981	-0.7199	0.2178	-0.6907	-0.9514	-2.6094	0.0728	-0.7330	0.1594
0.8946	5.1444	-0.4901	-0.6188	0.0479	-1.1122	1.6134	-1.7968	0.4972
3.5038	-1.4692	0.8455	-1.5695	-0.7920	1.4171	0.0475	-0.1036	1.4440
-1.9483	-2.2305	-0.9162	-0.4996	0.0285	-0.9394	-0.3217	-0.3557	-0.4045
1.6229	0.5618	-0.6290	0.5655	-0.2018	-0.1604	-0.2086	0.8393	0.3412
-0.7302	-4.1066	-1.4242	-1.9731	1.7657	-1.8566	-0.6751	1.4869	-0.4318
0.0873	-0.9961	1.5327	-0.4751	-0.1978	-2.0555	0.1626	2.2997	1.4615
-2.2595	4.0557	-0.1853	-0.0959	1.7615	-0.3250	-0.8430	2.0854	1.0482
1.8758	3.0321	-2.5937	-0.6580	-1.7609	1.1503	1.1338	-1.2479	-1.7197
-2.0427	2.0729	-0.1023	-0.9124	0.7323	0.9003	-1.0955	1.0189	-1.3873
-3.2026	1.5917	-0.5019	0.0802	-1.2086	-1.5937	2.4622	-2.6048	-1.5061
-0.2051	-3.8254	0.7004	1.9429	-0.6260	-0.4044	0.2684	0.3961	1.0360
0.3595	0.4975	-0.1491	-0.2164	0.0464	0.8820	-0.0663	-0.4720	-1.1870
2.2477	-0.6440	-1.2236	2.2054	0.1416	-1.2810	-0.3524	0.2858	-0.2416

151

Table 6-3   List of Weights and Bias Values of the Network
(continuous)

$b_{1(30 \times 1)}$	$W_{2(30 \times 1)}$	$b_{2(1 \times 1)}$
1.6100	1.5100	-0.4350
-0.3600	0.6980	
1.2400	-0.6920	
-0.6110	-0.5020	
-0.5760	0.8970	
-0.5840	1.8300	
0.6100	2.6300	
-1.1400	1.2500	
-1.6200	-1.2900	
-2.2500	1.4200	
-1.2600	-1.8000	
-0.7110	-1.2400	
0.6830	-2.6000	
-0.6640	1.9800	
2.0600	2.1000	
1.1700	-1.8500	
3.7700	-2.2300	
-2.2500	-1.4600	
-0.1560	-1.4400	
0.6260	-1.1300	
-0.8340	2.0100	
4.2500	-0.5320	
0.8650	2.0800	
-1.7000	0.4800	
1.4100	-2.0000	
0.6020	-0.9880	
1.2800	1.1500	
-0.3350	2.8100	
1.8900	-0.1600	
1.1200	2.0100	
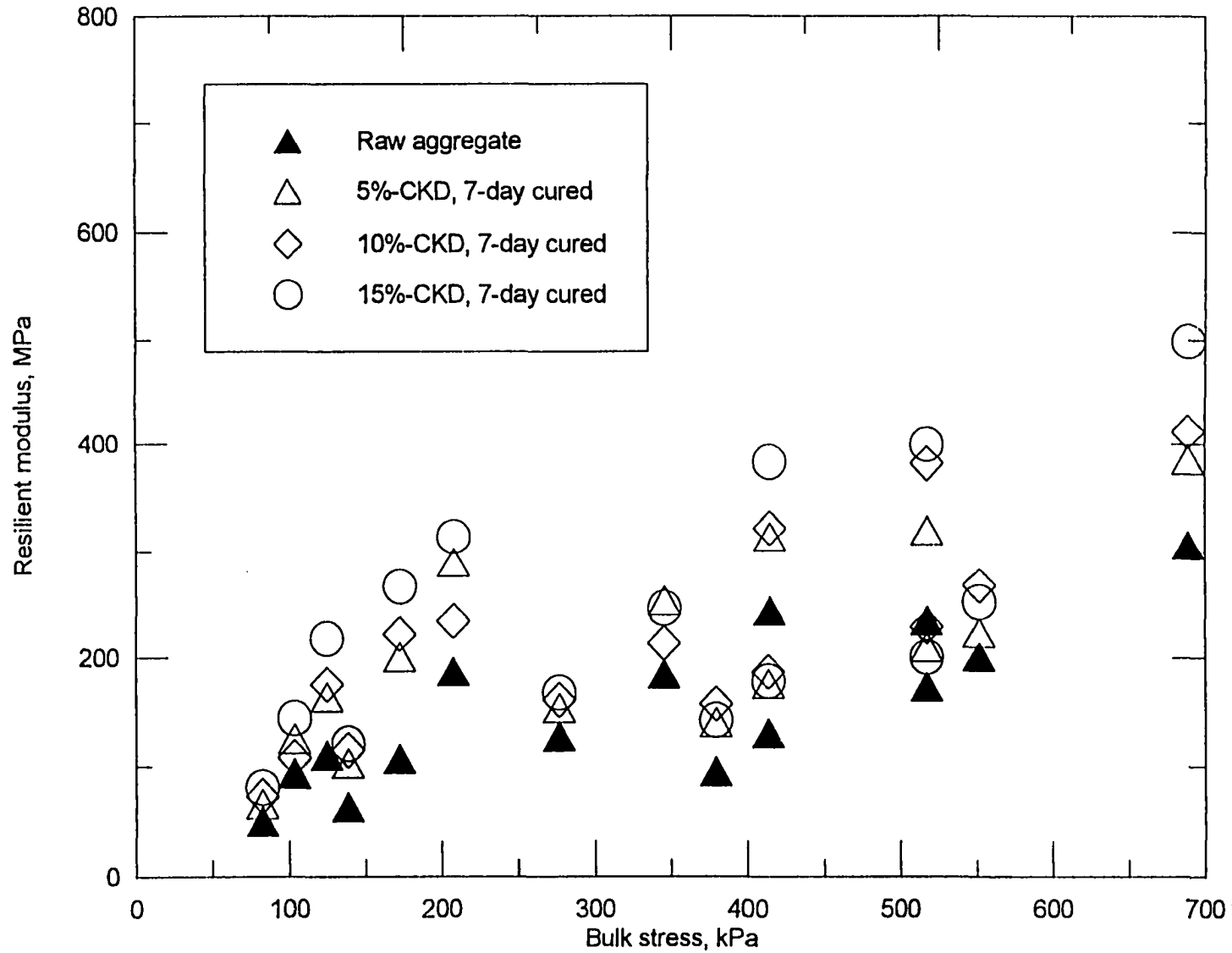
Figure 6-1   Mean RM Values vs. Bulk Stress for the 7-day Cured Aggregate
Stabilized with CKD
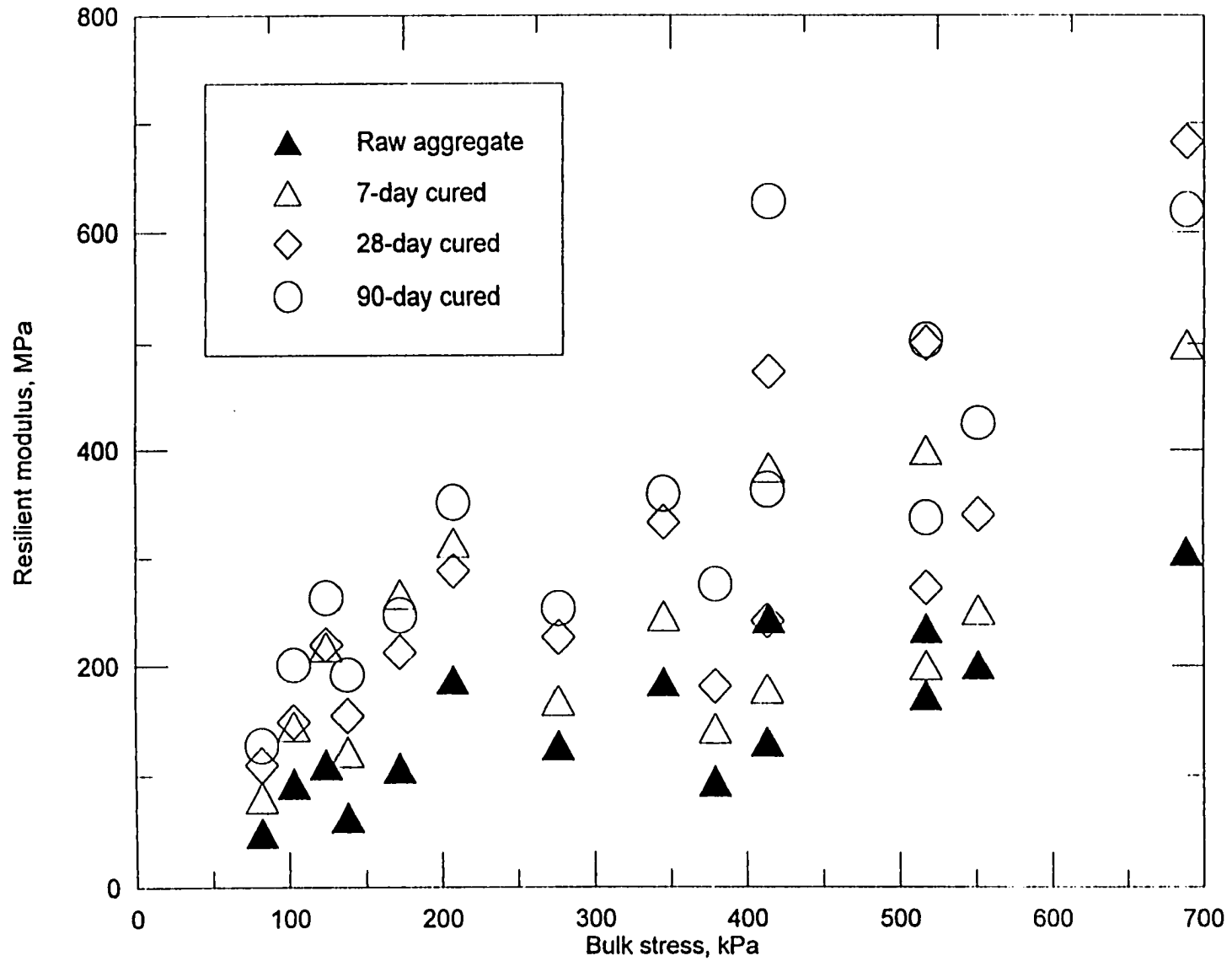
Figure 6-2   Mean RM Values vs. Bulk Stress for the Raw and 15%-CKD
Stabilized Aggregate
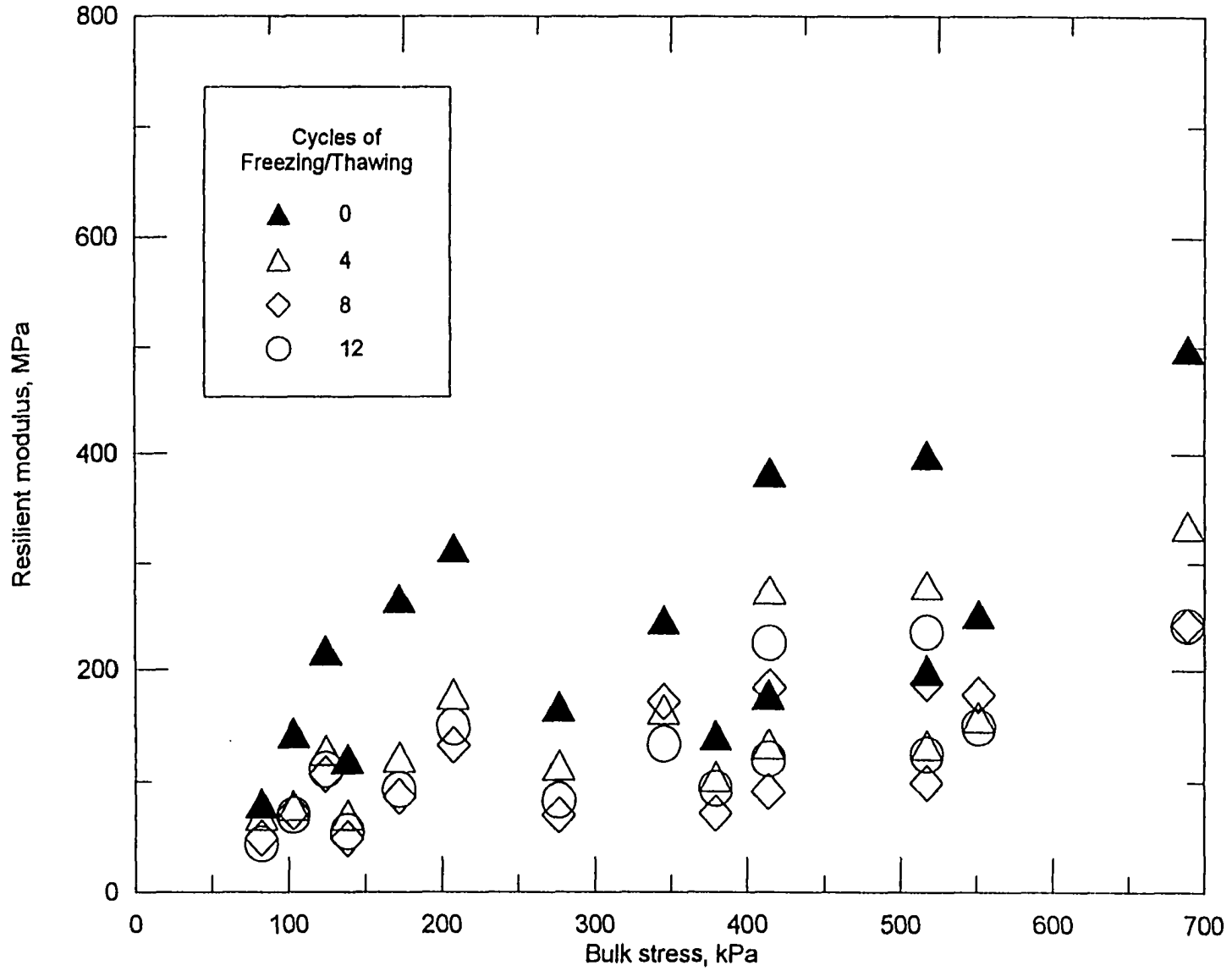
Figure 6-3   Mean RM Values vs. Bulk Stress for the Stabilized Aggregate
             Subjected to Freezing/Thawing Action
             (15% CKD, 7-day Cured)
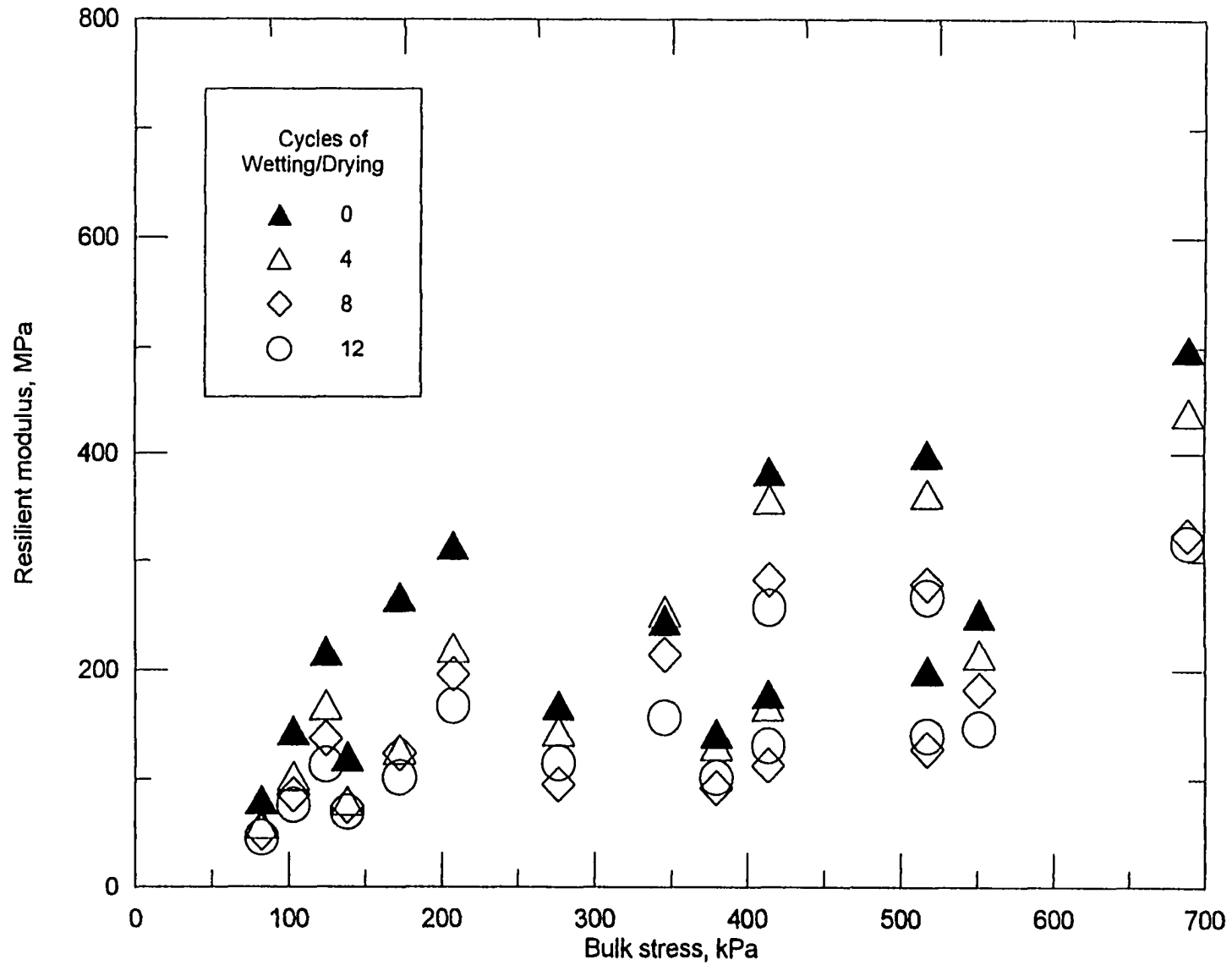
Figure 6-4   Mean RM Values vs. Bulk Stress for the Stabilized Aggregate
Subjected to Wetting/Drying Action (15% CKD, 7-day Cured)
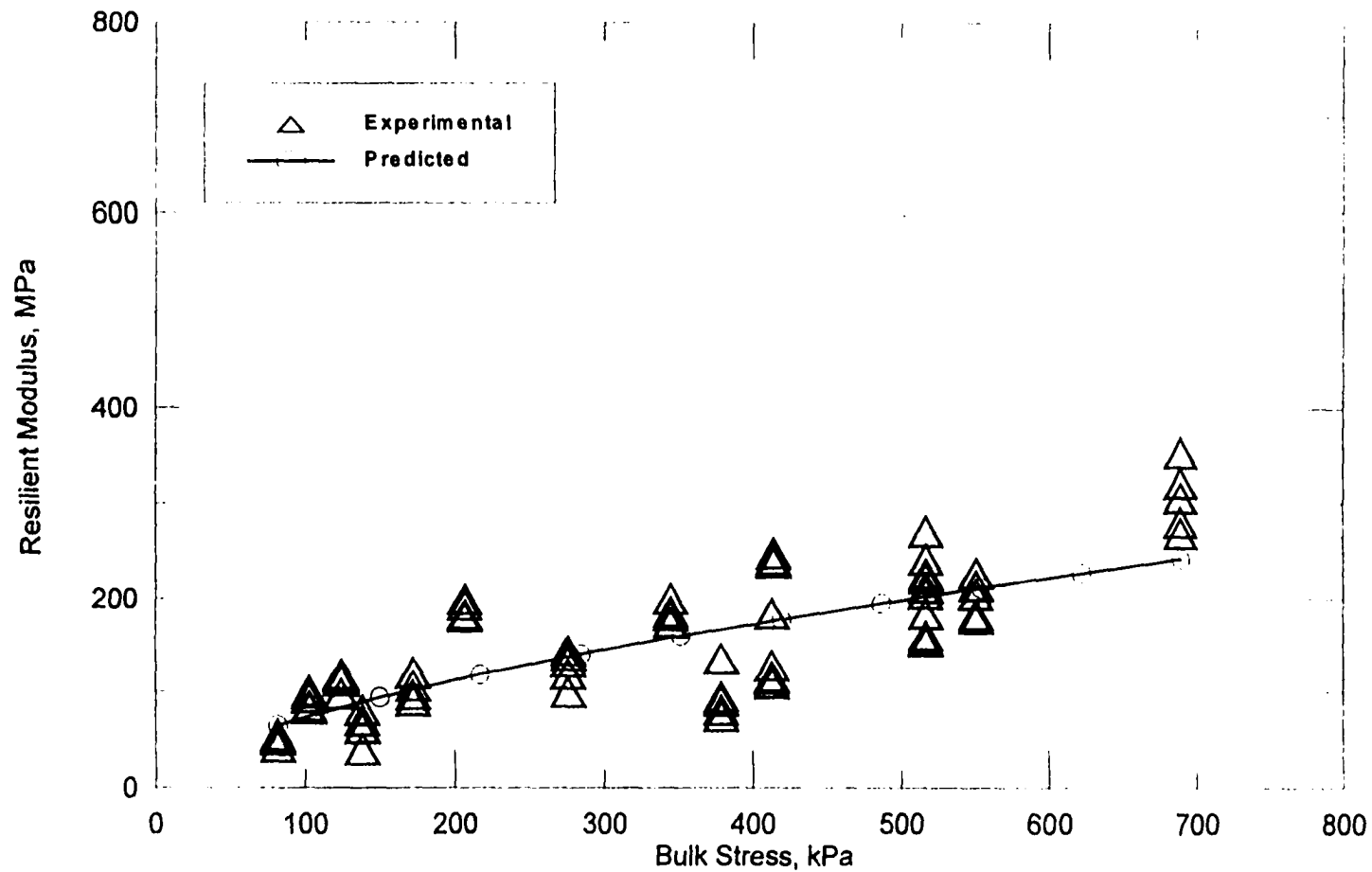
Figure 6-5 Experimental and Bulk Stress Model Predicted RM Values of the Raw Aggregate
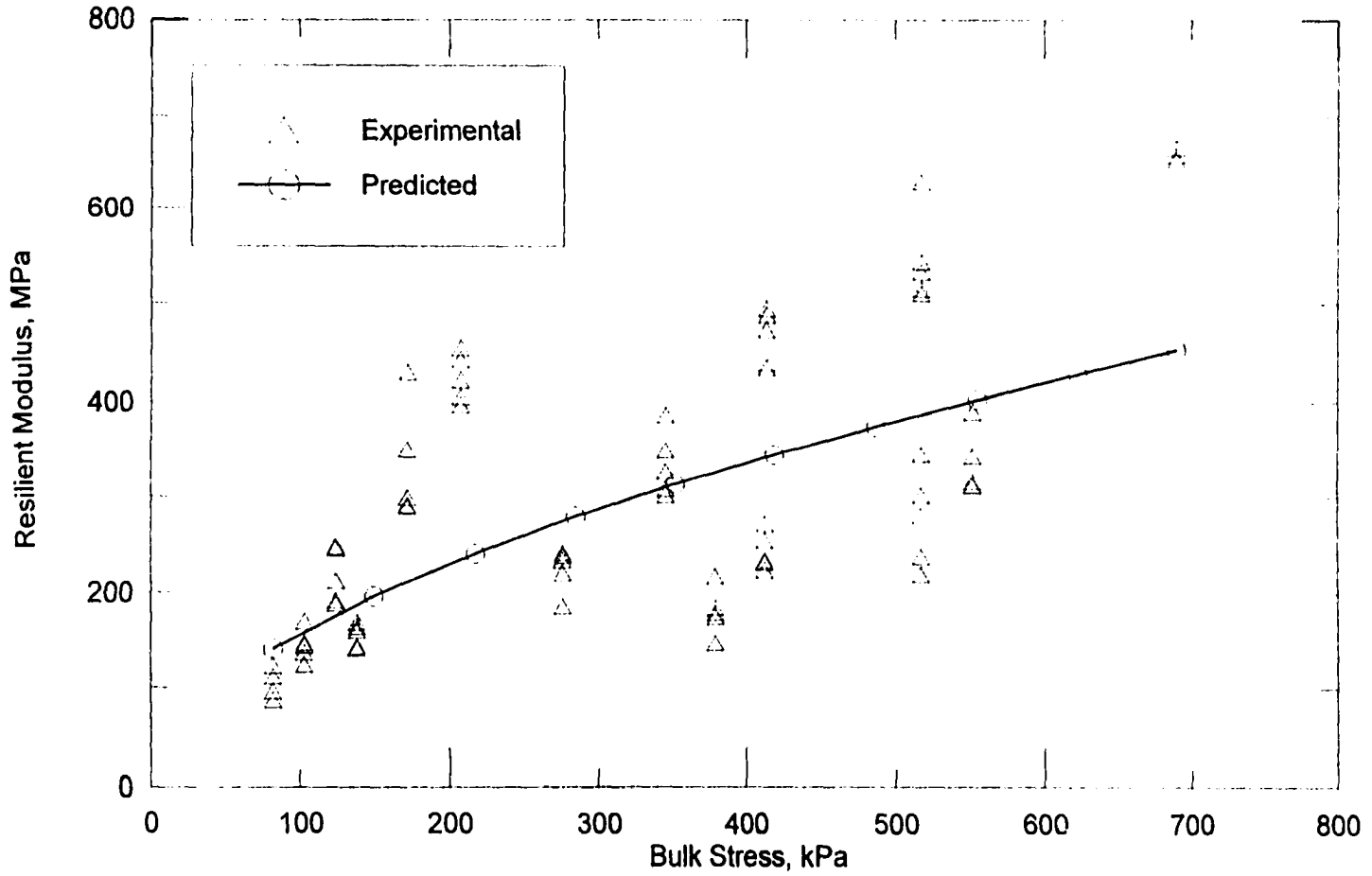
Figure 6-6 Experimental and Bulk Stress Model Predicted RM Values
of 28-day Cured Aggregate Stabilized with 15% CKD
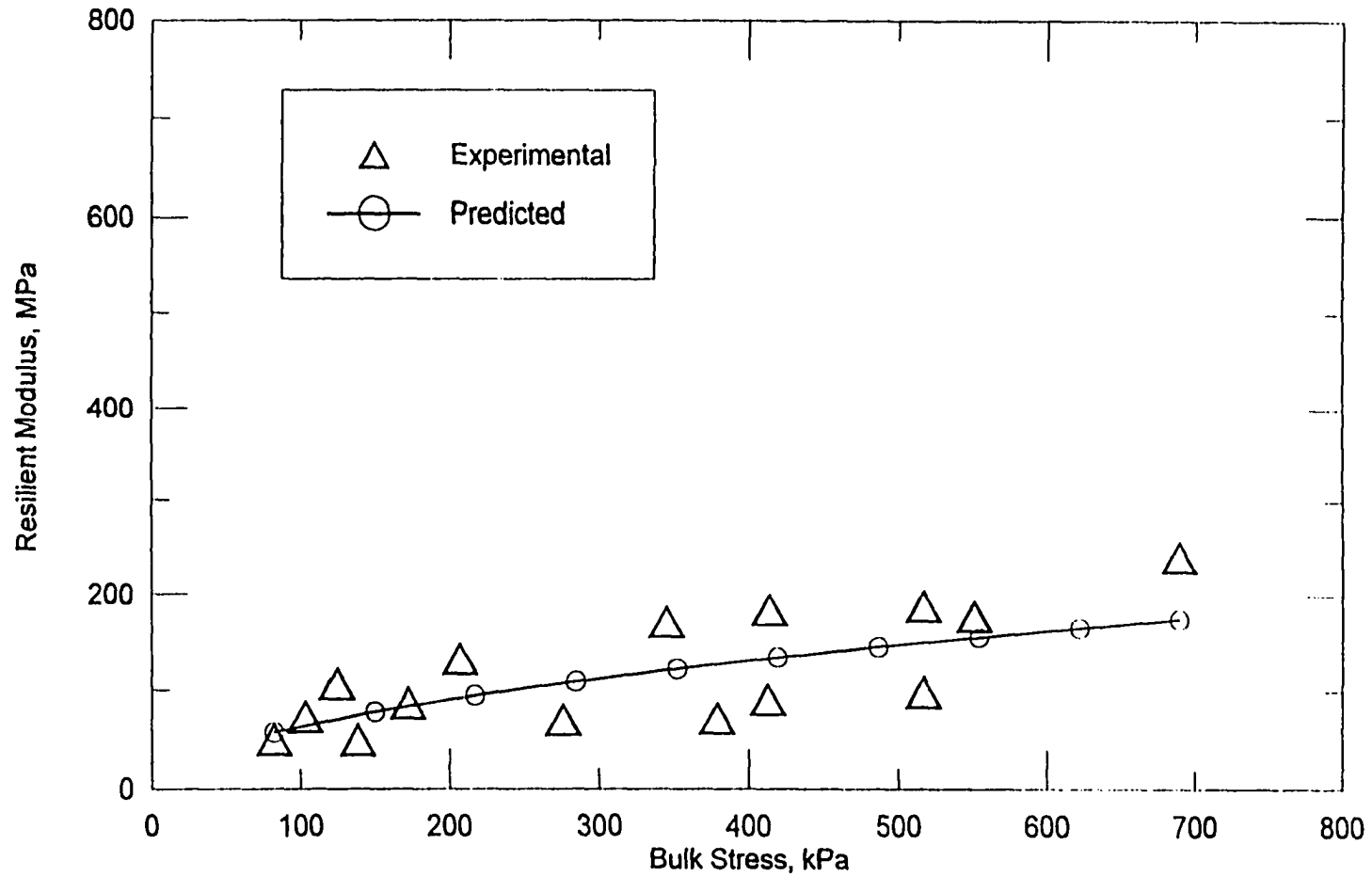
Figure 6-7   Experimental and Bulk Stress Model Predicted RM Values of the
              Stabilized Aggregate Subjected to 8-Cycles of Freezing/Thawing
              (15% CKD, Cured 7-day)
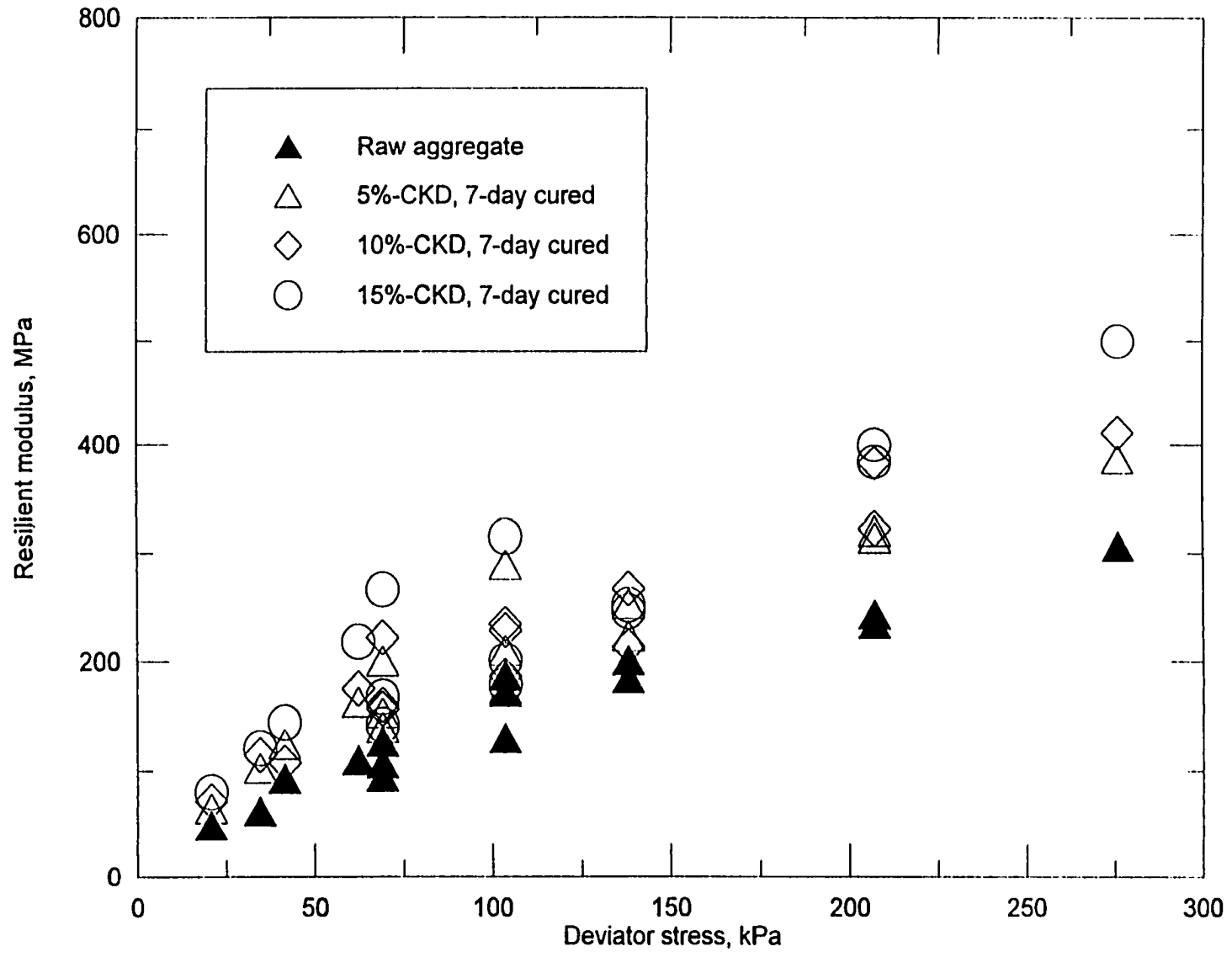
Figure 6-8   Mean RM Values vs. Deviator Stress for the Raw and 7-day Cured
Aggregate Stabilized with CKD
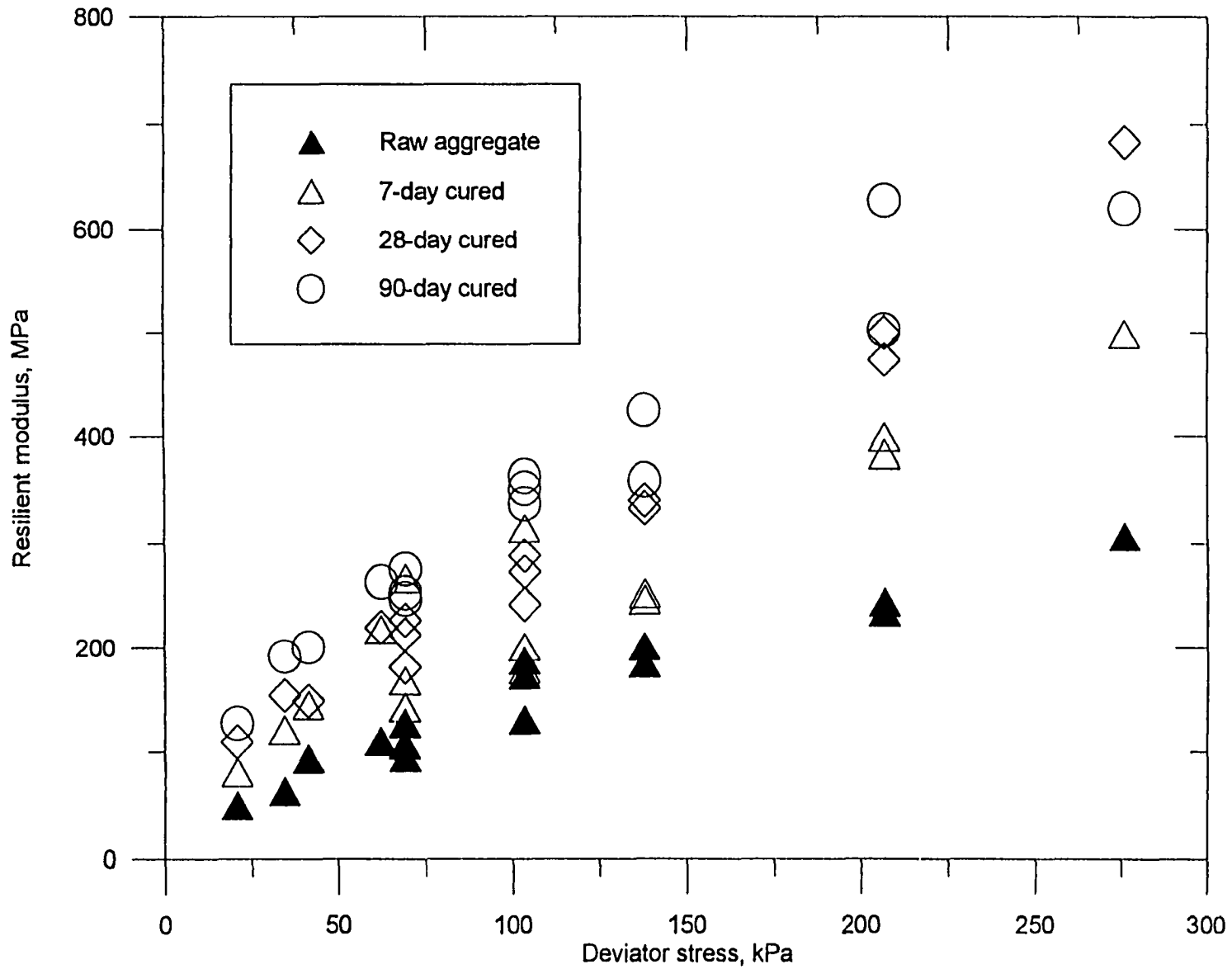
Figure 6-9   Mean RM Values vs. Deviator Stress for the Raw and Aggregate
Stabilized with 15% CKD
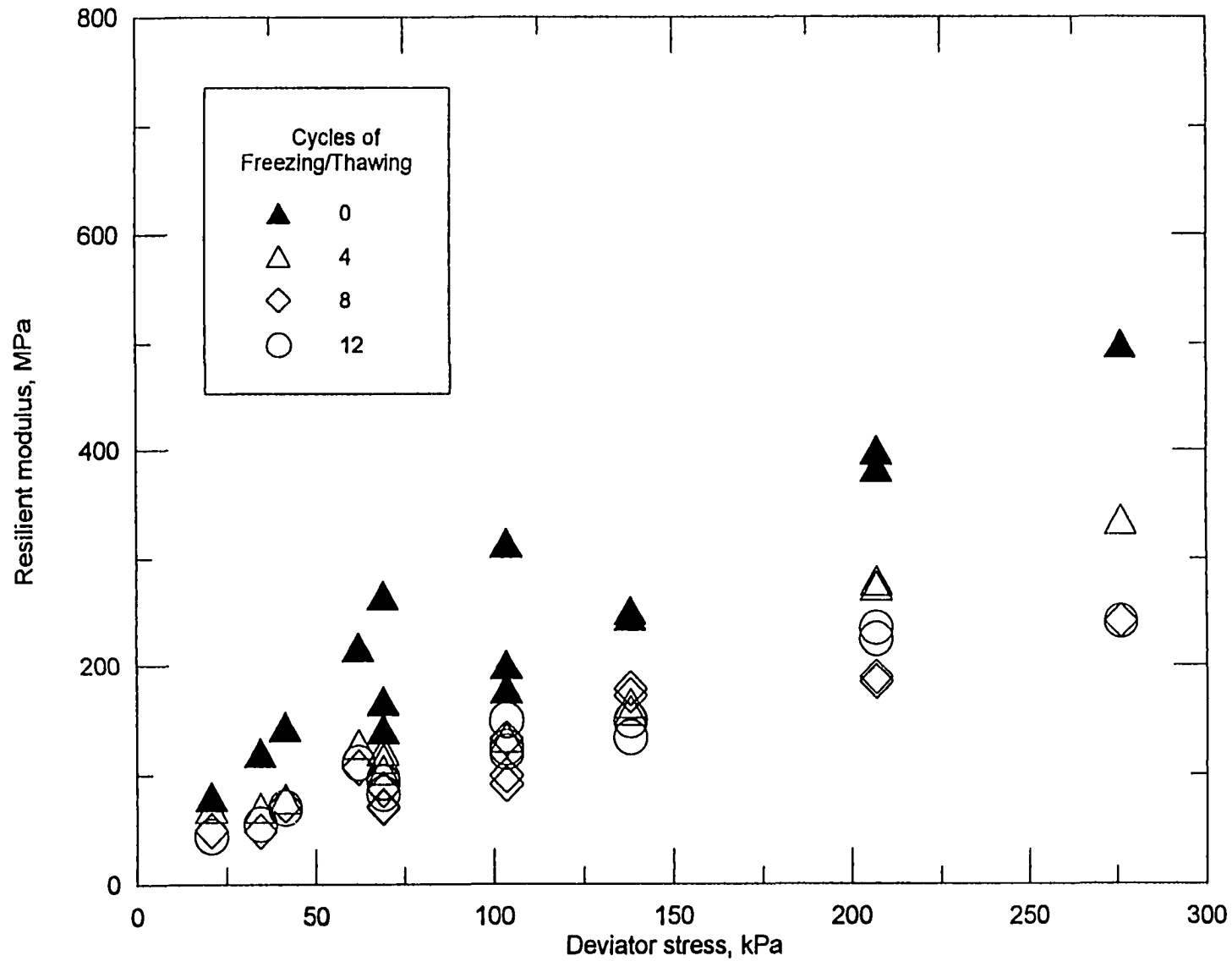
Figure 6-10   Mean RM Values vs. Deviator Stress for the Stabilized Aggregate
Subjected to Freezing/Thawing Action
(15% CKD, 7-day Cured)
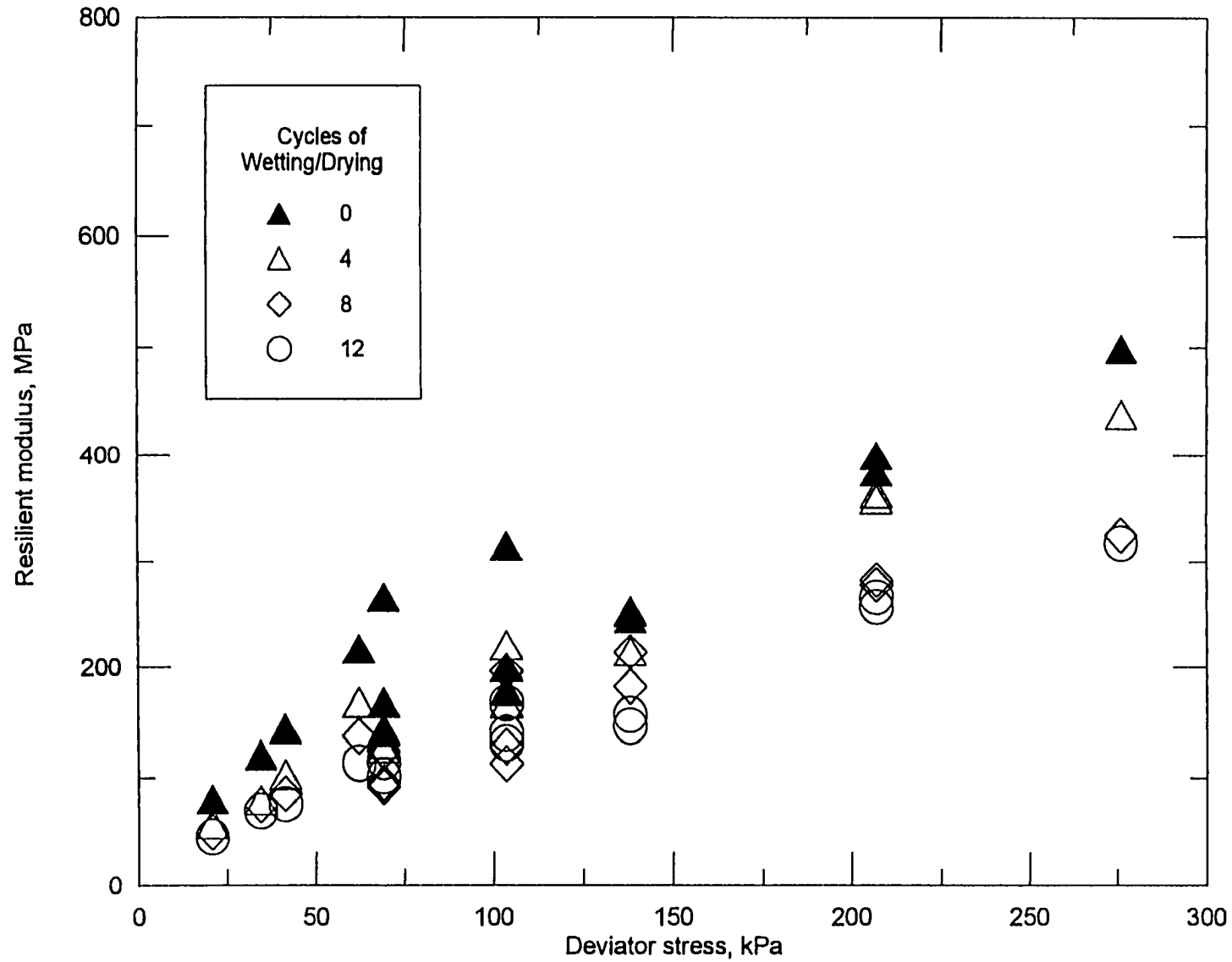
Figure 6-11   Mean RM Values vs. Deviator Stress for the Stabilized Aggregate
                 Subjected to Wetting/Drying Action
                 (15% CKD, 7-day Cured)
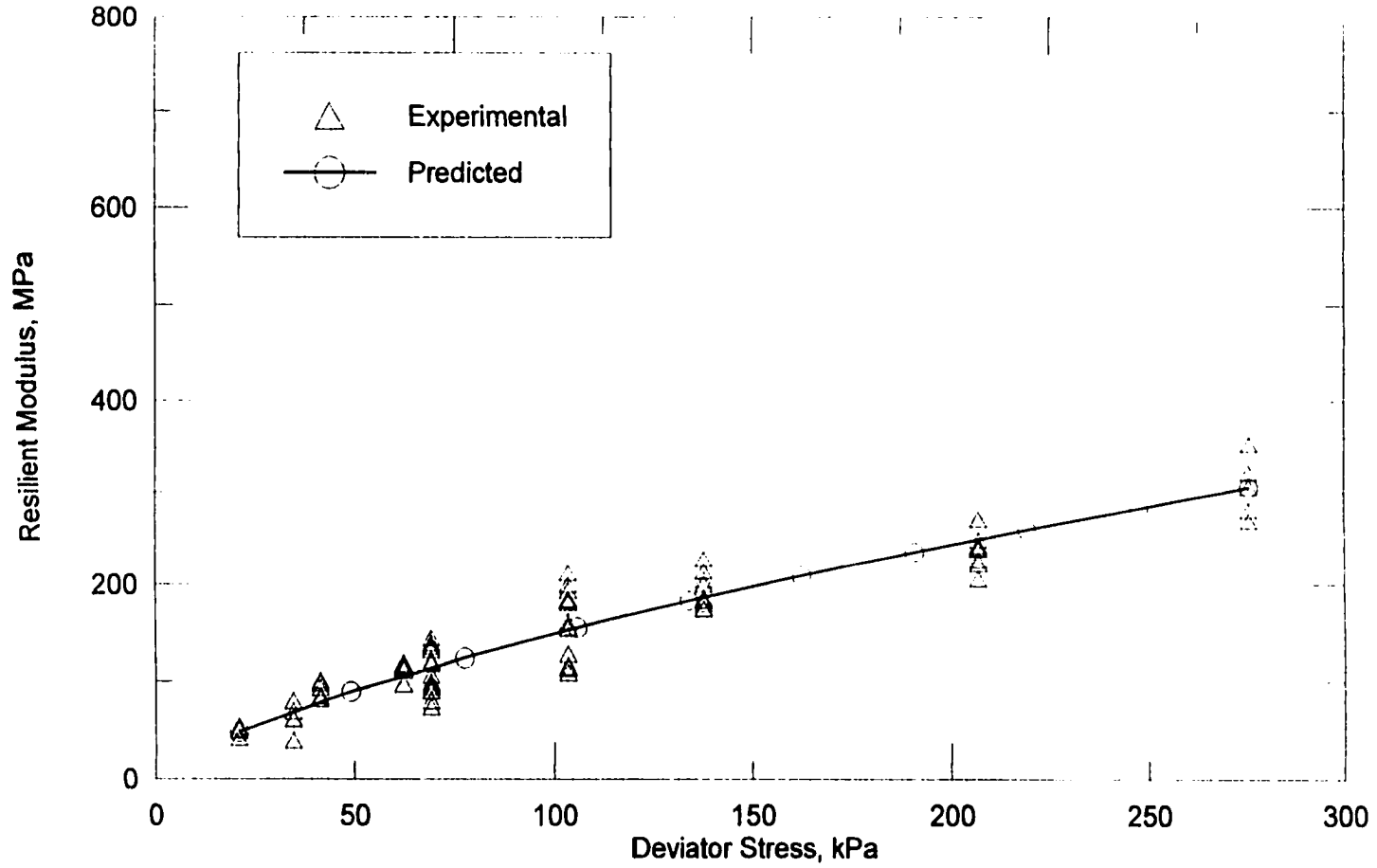
Figure 6-12 Experimental and Deviator Stress Model Predicted RM Values of the Raw Aggregate
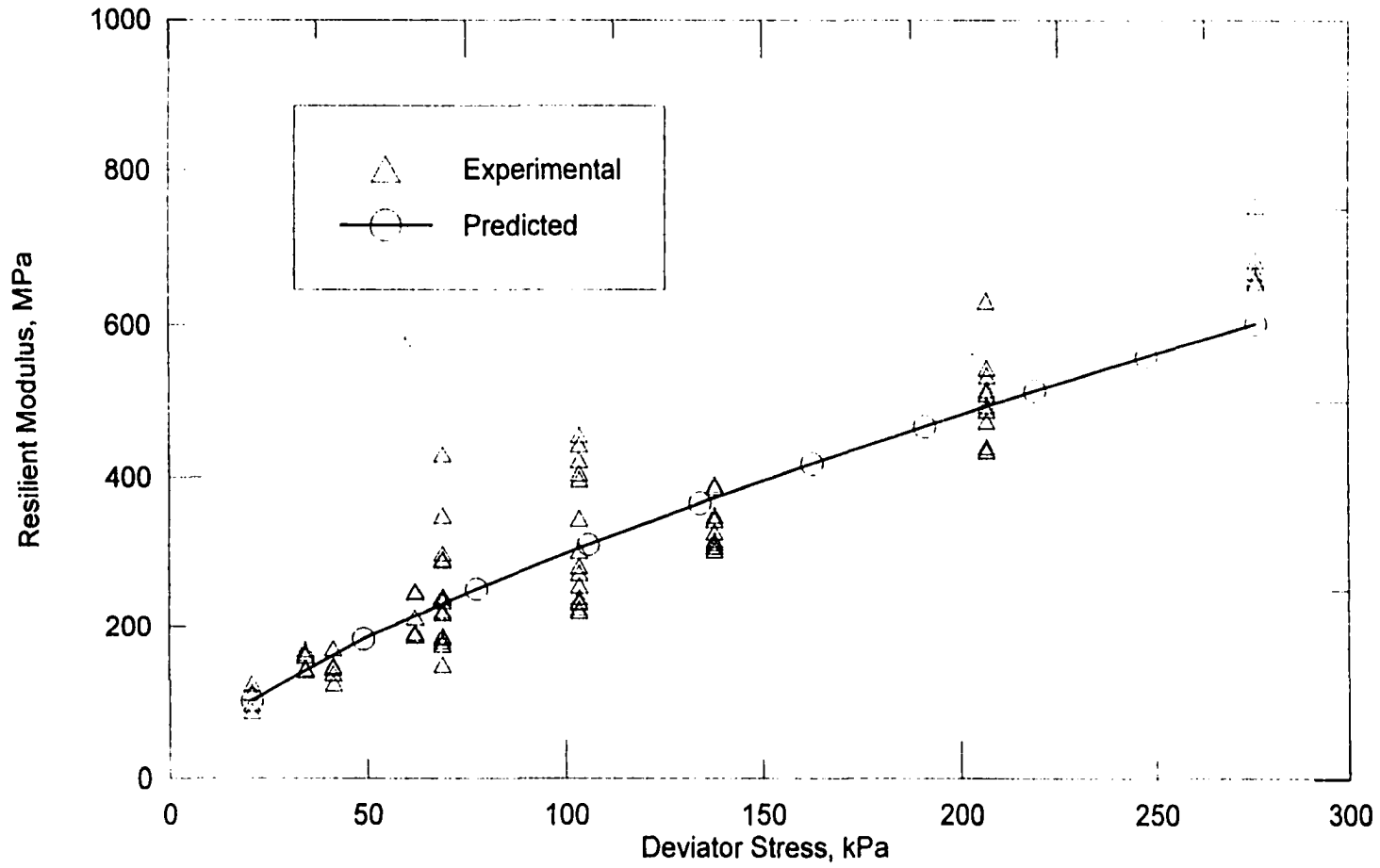
Figure 6-13 Experimental and Deviator Stress Model Predicted RM Values of 28-day Cured Aggregate with 15% CKD
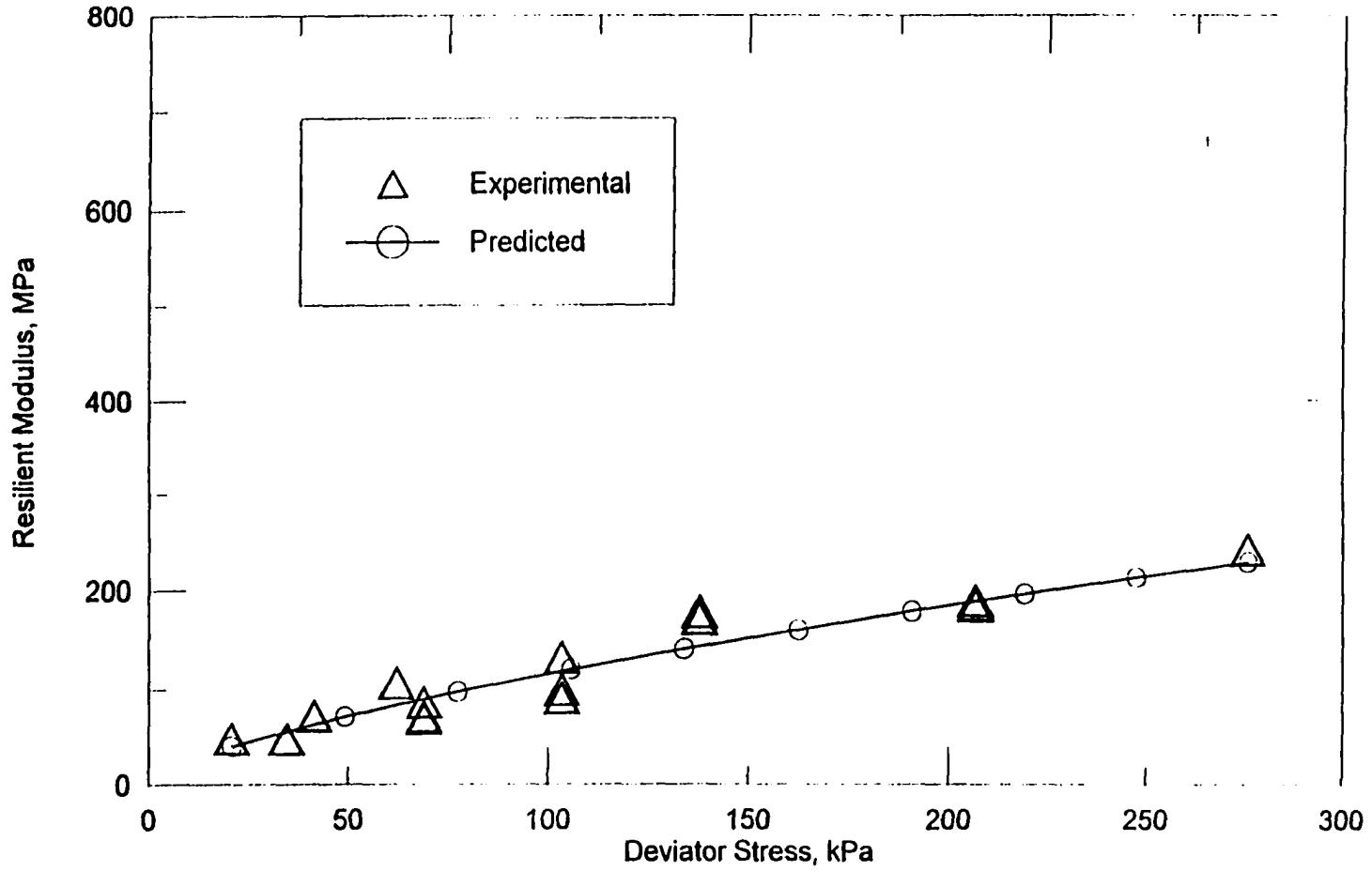
Figure 6-14 Experimental and Deviator Stress Model Predicted RM Values of
the Stabilized Aggregate Subjected to 8-Cycles of Freezing/Thawing
(15% CKD, Cured 7-day)

(a) Raw aggregate
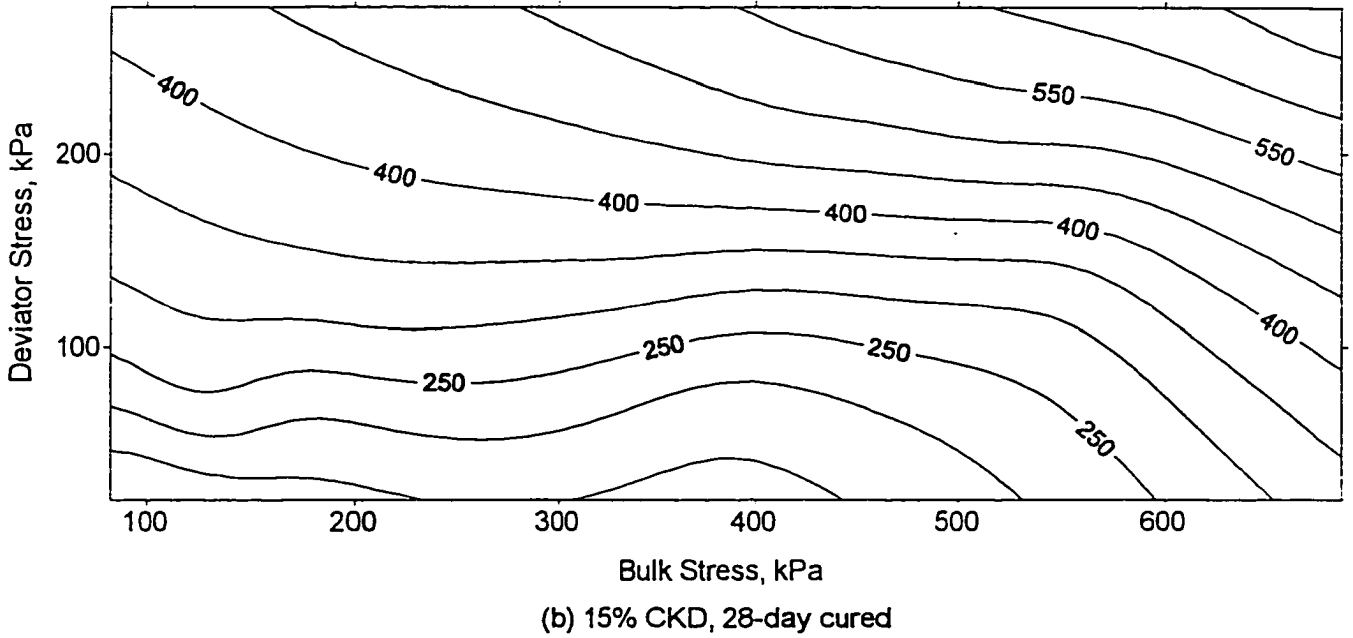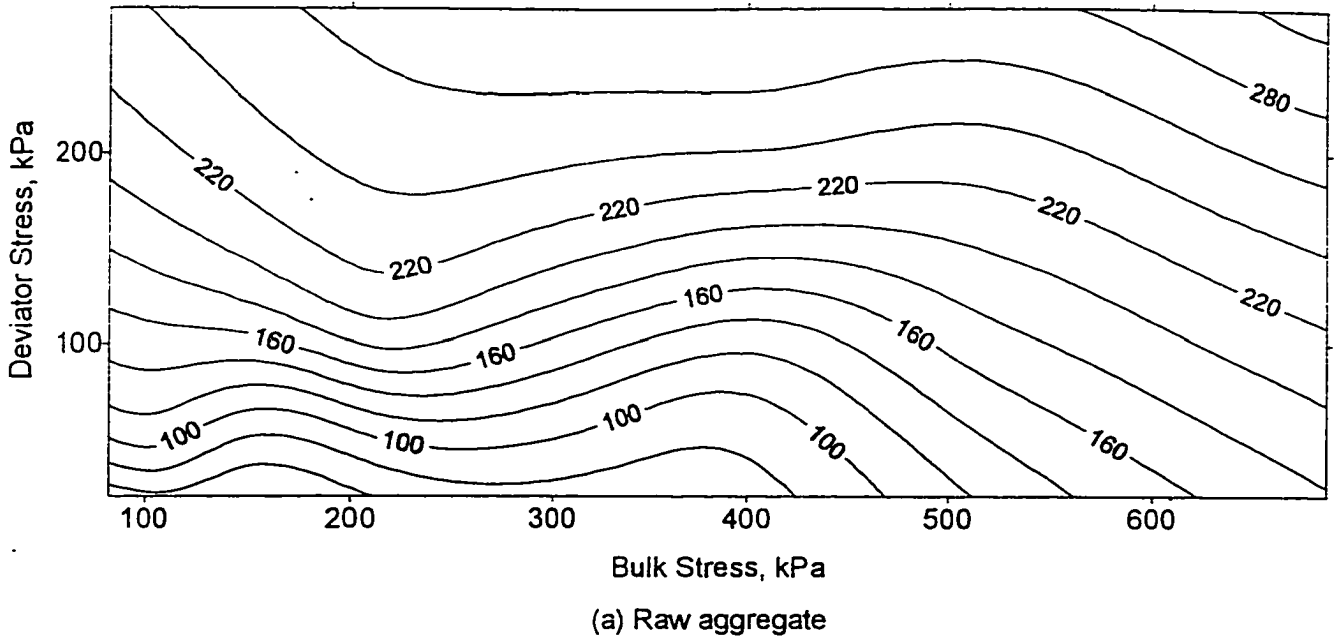
(b) 15% CKD, 28-day cured

Figure 6-15   Contours of RM vs. Bulk and Deviator Stress for Raw and 28-day Cured Aggregate Stabilized with 15% CKD

167
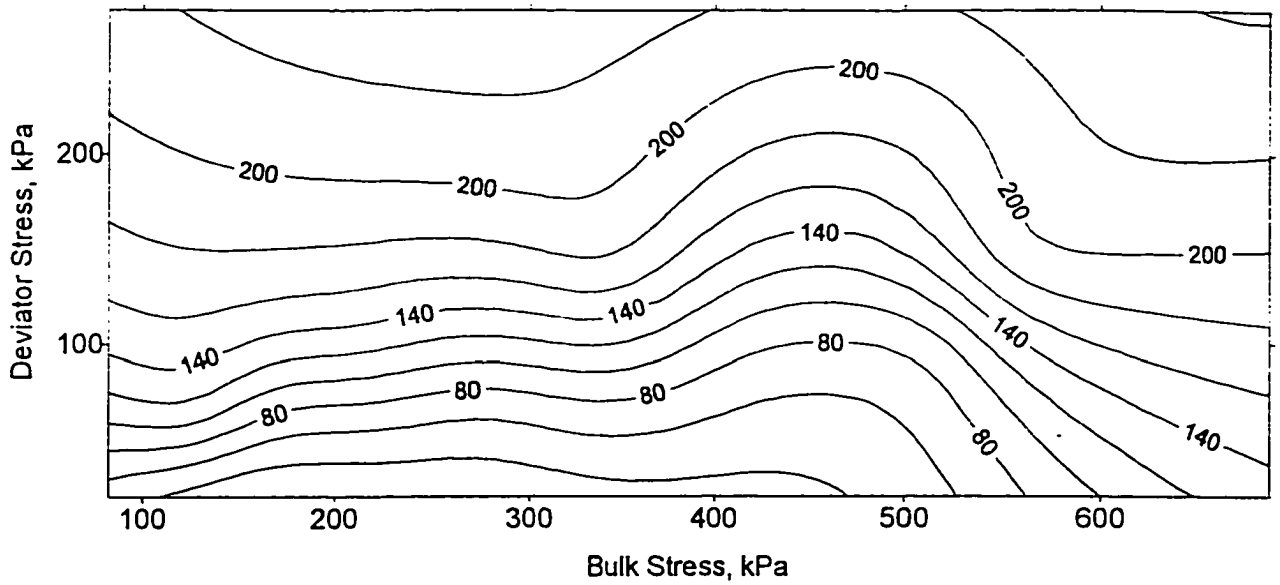
(a) 8 cycles of freezing/thawing
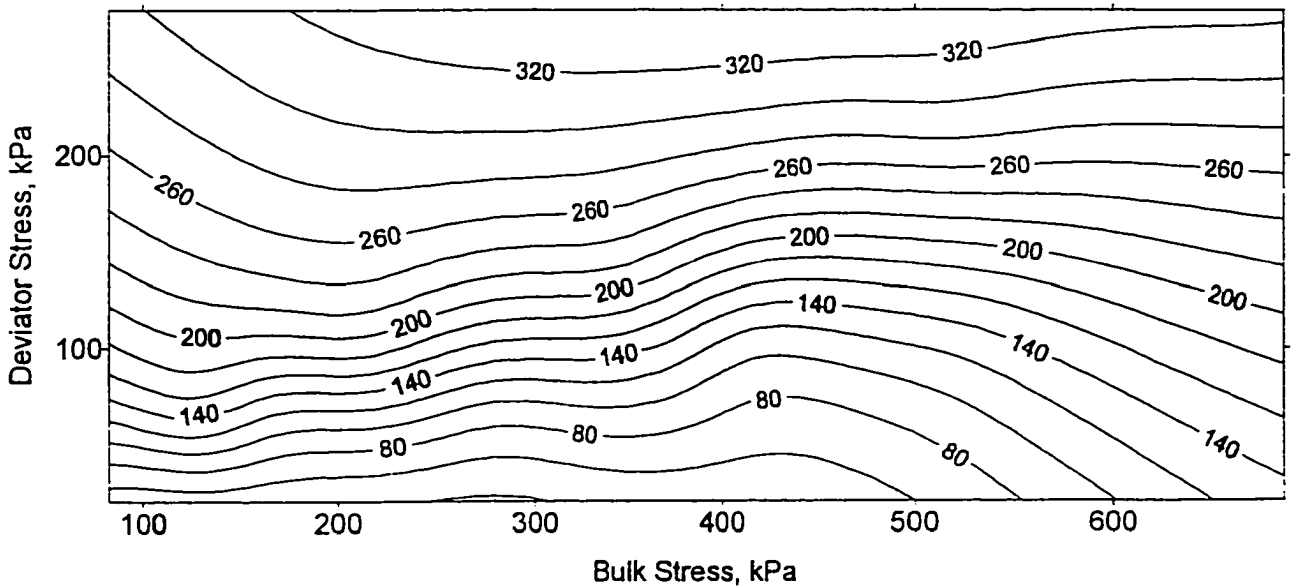
.b)   8 Cycles of Wetting/Drying

Figure 6-16   Contours of RM vs. Bulk and Deviator Stress of the Aggregates
Subjected to 8 Cycles of Freezing/Thawing and Wetting/Drying

168
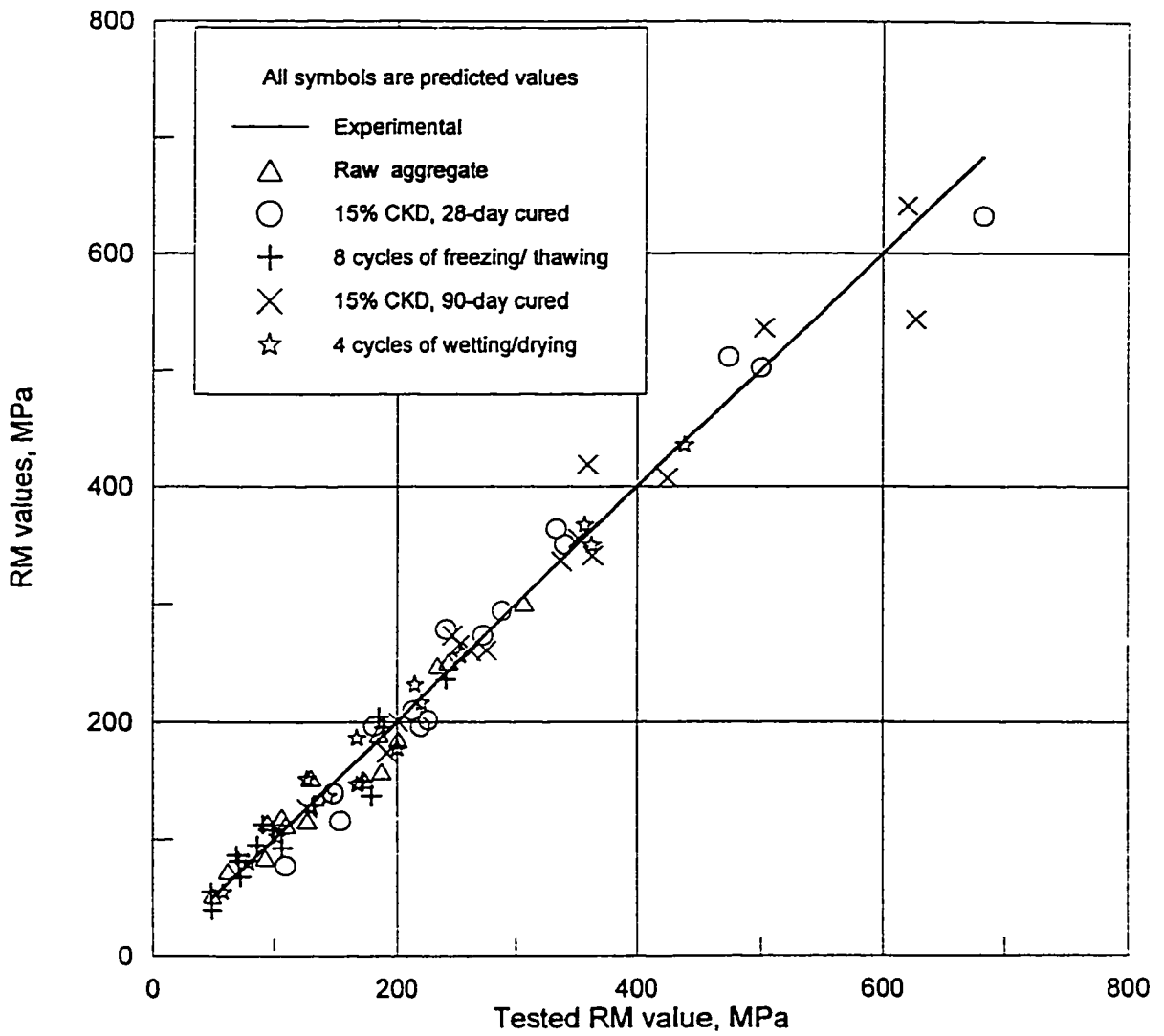
Figure 6-17 Experimental and Bulk-deviator Stress Model Predicted RM Values of Raw and Stabilized Aggregates

169

Hidden layer with 30 nodes

Input

STAB

DRAIN

σ_d

θ

OXIDE

ASA

CD

NWD

NFT

output layer

RM
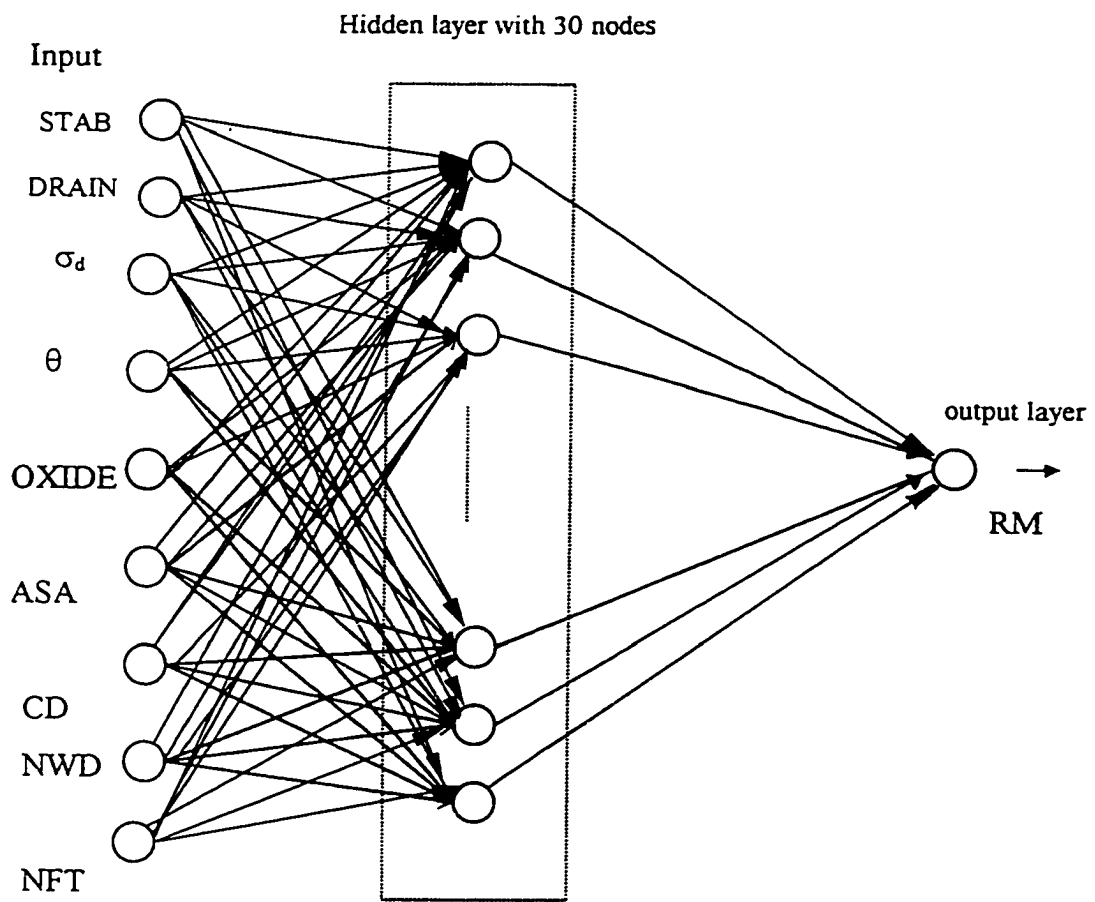
Figure 6-18   Architecture of the Artificial Neural Network for Modeling
Resilient Modulus

Net: 9-30-1
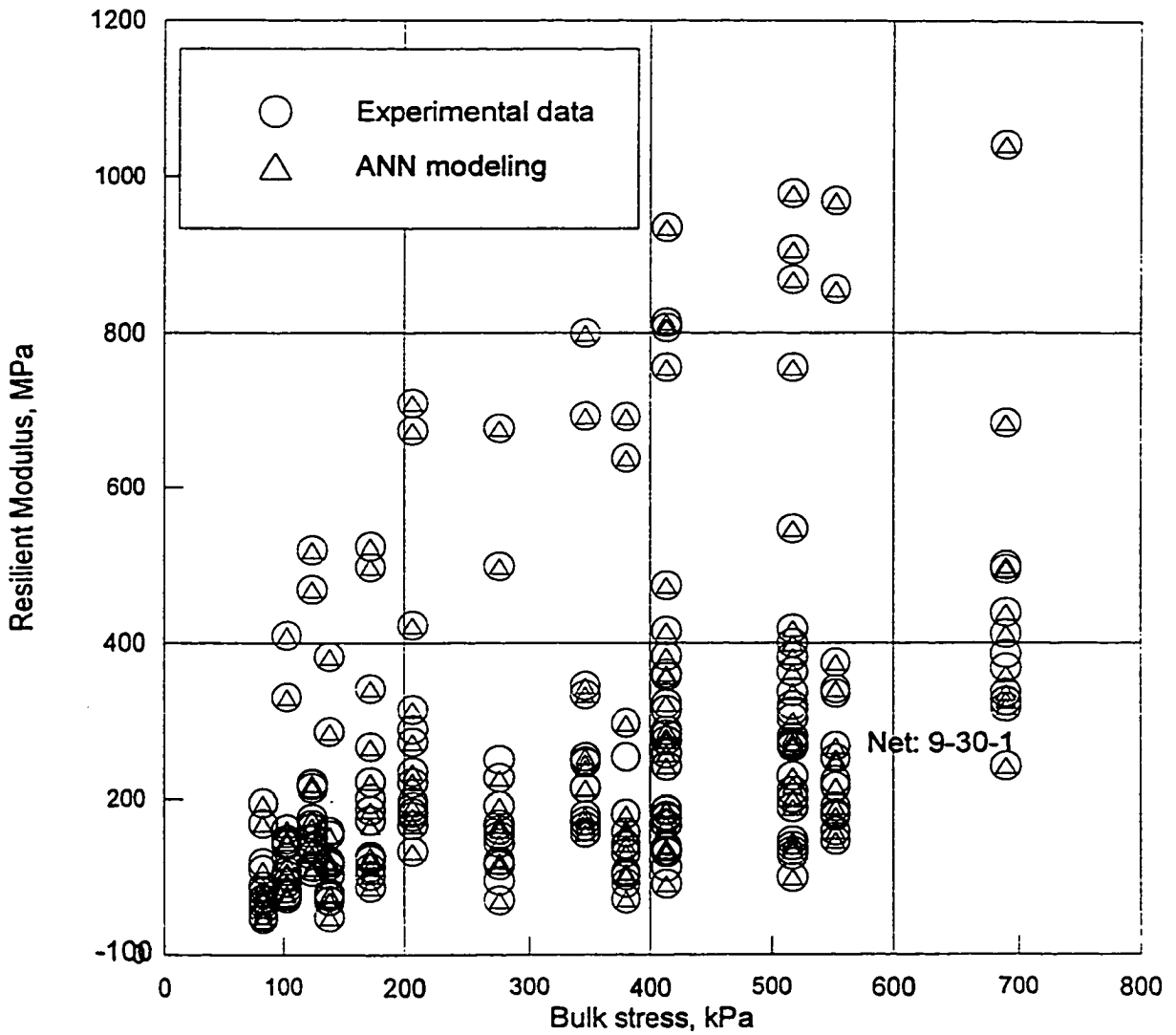
Figure 6-19   Experimental and ANN Model Predicted RM Values vs. Bulk
Stress from 210 Trained Data Points
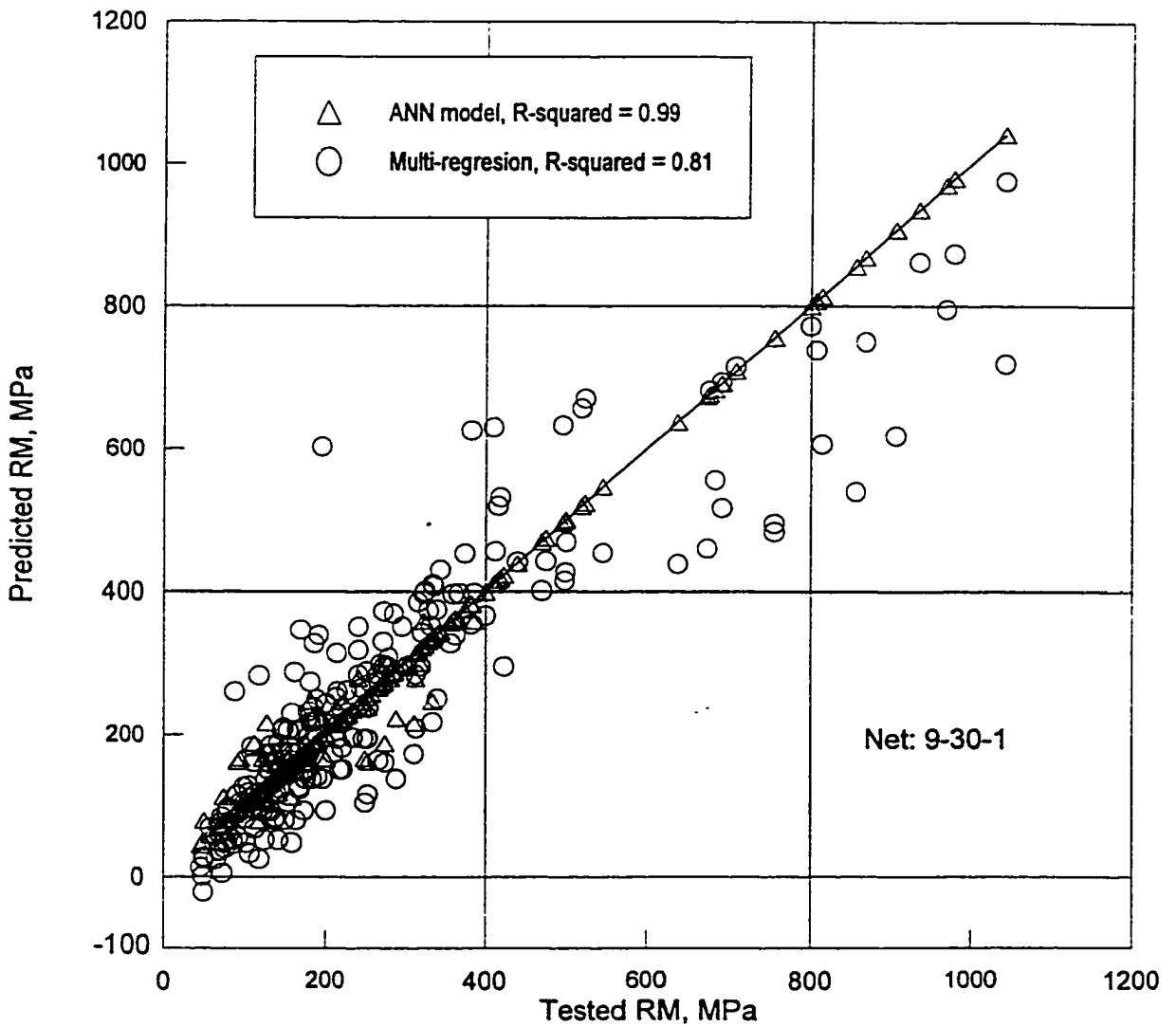
Figure 6-20   Experimental and ANN Model Predicted RM Values from
210 Trained Data Points
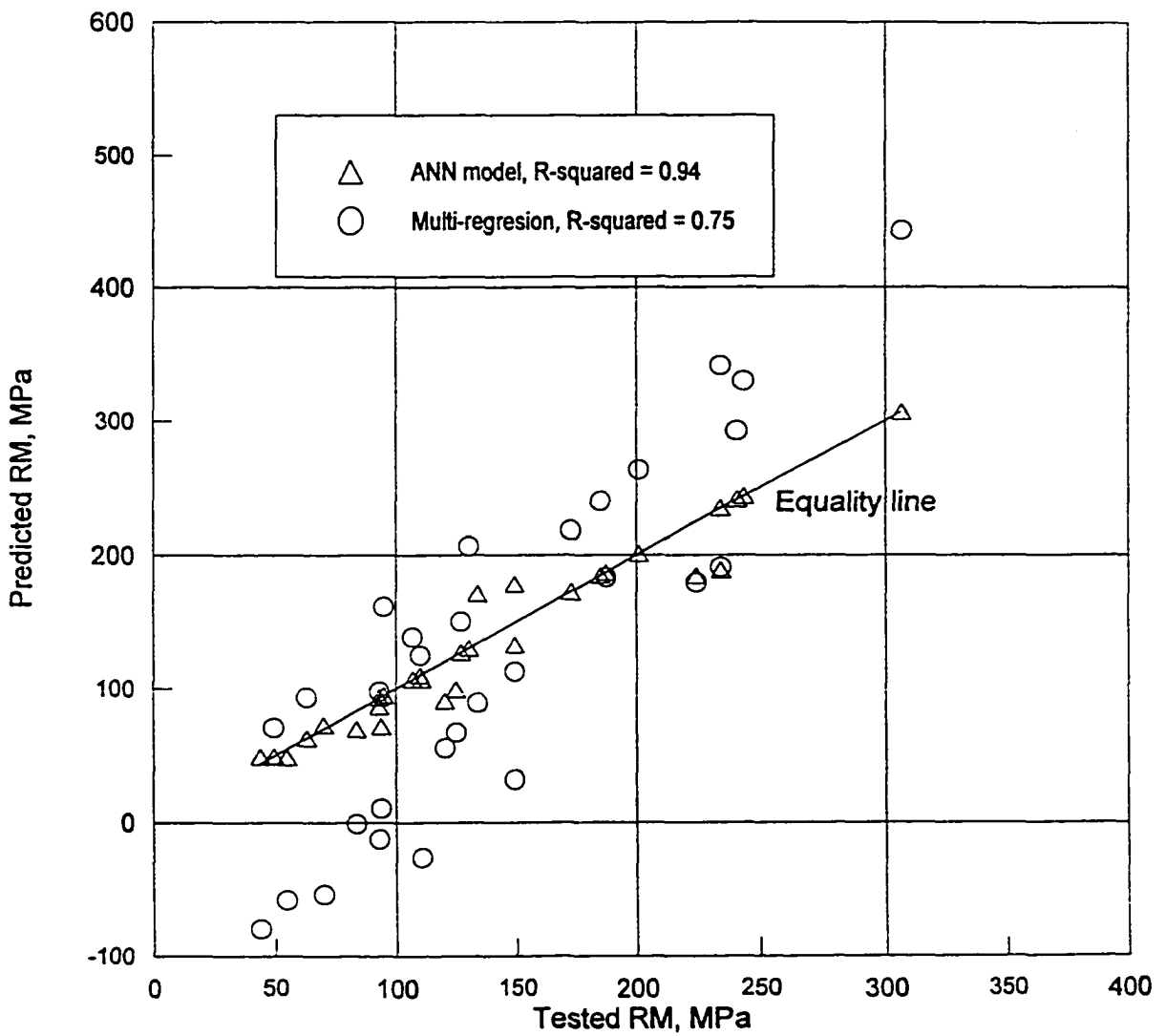
Figure 6-21   Experimental and ANN Model Predicted RM Values from
30 Untrained Data Points

173

CHAPTER 7

LAYER COEFFICIENTS AND AASHTO FLEXIBLE

PAVEMENT DESIGN

7.1   Introduction

The layer coefficient a_i is a measure of the relative ability of a given material of

a unit thickness to function as a structural component of a pavement. In the AASHTO

flexible pavement design, the layer coefficient is directly related to the structural

number (SN) and further determines thickness of base/subbase courses. In this chapter,

the methodology of computing layer coefficients from resilient modulus values is

described, and the effect of CKD-stabilization including amount of CKD and curing

periods on the layer coefficient values is evaluated. The deleterious effect due to

freezing/thawing and wetting/drying cycles on the layer coefficients is discussed based

on the test results obtained in this study. Finally, the use of the layer coefficients in the

design of AASHTO flexible pavements is demonstrated with the help of a design

example.

7.2   Layer Coefficients

In the AASHTO flexible pavement design, the layer coefficient (a_2) of a base

course is directly related to the RM value, as given by equation (7-1):

$$a_2 = 0.249(logRM) - 0.977, \quad \text{if RM takes unit of psi, or} \qquad (7\text{-}1a)$$

$$a_2 = 0.249(logRM) - 1.1858, \quad \text{if RM takes unit of kPa} \qquad (7\text{-}1b)$$

The RM of an aggregate base varies with the stress state within the base layer.

In the current pavement design program, the RM is computed by using the bulk stress

model, i.e. equation (6-1). The bulk stress, however, within the base layer varies through depth of the layer. It is desirable to compute one representative bulk stress value, termed the Equivalent Layer Bulk Stress (ELBK), for a given thickness of the base layer. Consequently, the representative RM of the base layer is computed from the ELBK value, and further determines the layer coefficient a_2.

7.2.1 Determination of ELBK

A nonlinear finite element (FE) computer program, MICH-PAVE, was used in this study to compute ELBK. The bulk stress-dependent resilient modulus and the failure criteria for granular material were incorporated in MICH-PAVE (Harichandran et al., 1989). The principal stresses in the granular and subgrade layers are modified at the end of each iteration, so that they do not exceed strength of the materials. A flexible boundary at a limited depth beneath the surface of subgrade is used in the MICH-PAVE analysis, which greatly reduces the number of finite elements and storage requirements. To simplify the problem, an axisymmetric idealization of the pavement is allowed in the program.

Figure 7-1 shows a conventional layered flexible pavement system to be used in the analysis. The layer 1 corresponds to the asphalt concrete (AC) layer, layer 2 is the aggregate base layer, and layer 3 responses the subgrade layer. Figure 7-2 shows a typical finite element mesh for MICH-PAVE. Table 7-1 gives a list of the material parameters used for calculation of ELBK in the study. The elastic modulus of AC layer considered ranges from 1725 MPa to 5175 MPa. The thickness of base layer varies from 76 mm to 304 mm, and that of AC layer falls between 76 mm and 228 mm. A

combination of these variables was selected to form 36 cases of calculation for ELBK. The calculated ELBK values for the 36 cases range from 42 kPa to 207 kPa, depending on the properties of base and AC layer materials. Table 7-2 shows a list of ELBK values, and Figure 7-3 graphically presents a relationship between the ELBK and the base layer thickness for different situations or selected cases. It can be seen from the table and figure that the ELBK generally increases with increasing thickness of base layer (D_2) until the D_2 value reaches 228 mm after which the ELBK decreases. The effect of AC layer properties on the ELBK is found to be negative, i.e. the ELBK decreases with increasing elastic modulus and thickness of AC layer. An empirical correlation of ELBK versus thickness of base and AC layer and resilient modulus of AC is given by:

$$\text{ELBK (kPa)} = 240.9774 - 0.006447 * D_2 - 0.0112038 * E_{ac} - 0.737519 * D_{ac}$$

$$R^2 = 0.85899 \hspace{4cm} (7\text{-}2)$$

where:

D_2 = thickness of base layer, mm

E_{ac} = resilient modulus of AC layer, MPa

D_{ac} = thickness of AC layer, mm

7.2.2 Determination of Layer coefficients

By plugging the ELBK value into equation (6-1) the RM values corresponding to different aggregate types are computed, and the layer coefficient a_2 of base aggregate is evaluated by using equation (7-1). The layer coefficients for the raw aggregates and CKD-stabilized aggregates are given in Tables 7-3 through 7-6, and are graphically

176

presented in Figures 7-4 through 7-6. The calculated a_2 values range from -0.091 to 0.169. The value of a_2 approaching zero or below zero means that the material is of insignificant structural support value compared to the other paving layers. It can be seen from the tables and figures that the a_2 values are greatly influenced by amount of CKD, curing time, durability and AC layer properties.

7.2.2.1 Effect of CKD-stabilization

As compared with the raw aggregate base, the CKD-stabilized aggregate base presents higher layer support capability, as expected. As shown in Table 7-3, the layer coefficients of the raw aggregate vary from -0.0412 for case 27 to 0.0748 for case 7. Of the 36 cases investigated here, there are 20 cases having negative layer coefficient values for the raw aggregate, indicating fragile supporting ability if the raw aggregate bases are used.

However, the CKD-stabilized aggregates all have positive a_2 values, except those subjected to freezing/thawing and wetting/drying cycles. The 7-day cured aggregate stabilized with 5% CKD produces a_2 values of 0.0139 to 0.1122, increasing by 50% of that raw aggregate. The a_2 values for 10% CKD-stabilized aggregate range from 0.0086 to 0.1154, indicating that there is minor increase in the a_2 values comparing with the 5%-CKD stabilization. Figure 7-5 graphically illustrates a relationship between layer coefficient a_2 and the amount of CKD for four different cases, i.e. case 1, case 7, case 8 and case 11. The case 1 represents an AC layer having thickness of 76 mm and resilient modulus of 1.725 GPa, and a base layer of 76 mm thick. Case 7 is essentially the same as case 1 except that it has a base layer of 228 mm thick. Case 8 corresponds

to a pavement having an AC layer of 152 mm thick with the E_{ac} of 1.725 GPa. Case 11 is the same as case 8 except that the base layer is 304 mm thick. It is seen that the four curves in Figure 7-5 present a similar trend of a_2 versus amount of CKD. It is observed that there is a big jump in the a_2 values when the amount of CKD increases from 0 to 5%. When the aggregate stabilized within a range of 5% to 10% CKD, the a_2 values are fairly stable and there is a remarkable increase in a_2 values when the aggregate stabilized within a range of 10% to 15% CKD. This observation confirms that the optimum CKD content for stabilization on the aggregate used in this study falls between 10% and 15%.

Similar to Figure 7-5, Figure 7-6 presents relation of a_2 values versus curing periods for 15% CKD-stabilized aggregates. The four curves shown in the figure represent four cases having different AC and base layer thickness and E_{ac} values as given in Table 7-2. It is observed from Figure 7-6 that the a_2 increases with increasing curing periods. Taking case 7 as an example, the a_2 values are 0.1285, 0.1592 and 0.1695 for 7-day, 28-day and 90-day cured aggregate, respectively. Comparing with the raw aggregate, the increase in a_2 value is 71.7%, 104.4% and 126.6% for 7-day, 28-day and 90-day cured aggregates, respectively.

It is noted that the layer coefficients vary slightly with the base thickness. For example, the layer coefficient for case 1 for the 28-day cured 15% CKD-stabilized aggregate is 0.1479 and for case 10 is 0.1448, which corresponds to base thickness of 76 mm and 304 mm, respectively. It is, therefore, concluded that one representative layer

178

coefficient value can be chosen for a range of base thicknesses that includes a given RM value of an AC layer and an AC layer thickness.

7.2.2.2 Effect of Durability

Tables 7-5 and 7-6 list a_2 values for aggregates subjected to different freezing/thawing and wetting/drying cycles. Figure 7-7 graphically demonstrates a relationship between a_2 and base thickness for the case E_{ac} =1.725 GPa and D_{ac} = 76 mm. As can be seen, the aggregates having subjected to freezing/thawing and wetting/drying actions give lower a_2 values than the regularly cured aggregates. The maximum a_2 value for the regular 7-day cured aggregate is 0.1285 for case 7, while the maximum a_2 values are 0.0499 and 0.083, respectively, for the aggregates subjected to 8 cycles of freezing/thawing and wetting/drying actions.

Figure 7-8 indicates clearly the effect of freeze/thaw cycles on the layer coefficients. The four curves of a_2 versus number of freezing/thawing cycles represent cases 7, 11, 19 and 34 as stated in preceding section. It is seen from this figure that the a_2 value decreases with increasing number of freeze/thaw cycles drastically within 8 cycles. When the number of cycles exceeds 8, the reduction in a_2 values is not noticeable. Since the four curves are seen almost parallel, the variation of a_2 versus number of freeze/thaw cycles is expected to be similar for all the cases. The decrease in percentage of a_2 values with respect to the regularly cured aggregate is 38%, 61% and 56.2% for aggregates subjected to 4, 8 and 12 freeze/thaw cycles, respectively. Among 36 cases investigated here, there are 16, 24 and 21 cases in which the a_2 values are found to be negative for specimens subjected to 4, 8 and 12 freeze/thaw cycles,

respectively. The appearance of negative a_2 means the base layer is of insignificance as a structural component in the pavement system.

Figure 7-9 depicts the effect of wetting/drying cycles on the base layer coefficient a_2. The four curves shown in the figure represent also cases 7, 11, 19 and 34. Similar to the variations due to freezing/thawing cycles, the a_2 values are found to decrease with increasing wetting/drying cycles. The four curves illustrate that a similar trend of variations in a_2 values versus number of wetting/drying cycles exists for all the cases considered here. The decrease in percentage of a_2 values with respect to the regularly cured aggregate is 20.5%, 35.4% and 45.5% for 4, 8 and 12 wetting/drying cycles, respectively. Among 36 cases investigated here, there are 16, 17 and 20 cases in which the a_2 value being negative for aggregates subjected to 4, 8 and 12 wetting/drying cycles, respectively.

7.2.2.3 Effect of AC Layer Properties

Although the purpose of this study is not related to the AC layer properties, a brief discussion on the effect of AC layer properties on the layer coefficients based on the results obtained in this study is helpful in understanding of the essence of base layer coefficients. As listed in Tables 7-3 and 7-4, the a_2 value decreases with increasing modulus and thickness of AC layer. For example, the layer coefficient of 28-day cured 15% CKD-stabilized aggregate is 0.1479 for case 1, 0.0553 for case 12 and 0.1003 for case 25, which corresponds to AC moduli of 1.725 GPa, 1.725 GPa and 5.175 GPa, and AC thickness of 76 mm, 228 mm and 76 mm, respectively. Figure 7-10 portrays the effect of AC layer properties on the layer coefficients for the 28-day cured 15% CKD-

stabilized aggregate. It is observed that the base layer coefficients a_2 have a reverse correlation with the AC layer properties. The less thickness and lower modulus of the AC layer cause a higher base layer coefficient a_2 value. This observation is reasonable because of the layer coefficients manifest the relative ability of a unit thickness of a given material in the whole pavement system. If AC layer is strong, then the base layer will be relatively week, vice versa.

It is worth mentioning that the layer coefficients listed in Tables 7-3 through 7-6 can be best utilized for paving materials having properties corresponding to a specific case number. These coefficients can also be used when a subbase layer is used below the base layer. The average subgrade soil RM of 51.75 MPa was used in the determination of these coefficients. A recommendation is that the a_2 values are useful only when the soil RM is not less than the above value, because the bulk stress in the base layer decrease with decreasing subgrade soil RM value (AASHTO, 1993).

It should be kept in mind that the layer coefficient a_2 values are computed by using bulk-stress model of the resilient modulus, the a_2 values thus obtained may not represent real capability of the base layer because low correlation coefficients were observed in the bulk-stress model. That is why a higher a_2 value was observed in the aggregate subjected to 12 freeze/thaw cycles than in the 8 freeze/thaw cycles. To obtain a reasonable value of RM and a_2, the deviator-stress and bulk-deviator stress dependent models should be implemented in the computer programs because these models show better relationship between the RM and stress variables than the single bulk-stress model.

7.3   Design Example of an AASHTO Flexible Pavement

Traffic loading is one of the most important factors in pavement design. Due to the great varieties of axle loads and traffic volumes and their intractable effects on pavement performance, most of the design methods in use today are based on the fixed vehicle concept, i.e. the thickness of pavement is governed by the number of repetitions of a standard vehicle or axle load during the design periods, called equivalent single-axle load (ESAL). On the other hand, the structural number (SN) provides a link between the structural design of a pavement and its performance. SN is given by:

$$SN = a_1\, D_1\, m_1 + a_2\, D_2\, m_2 + a_3\, D_3\, m_3 + \ldots\ldots + a_n\, D_n\, m_n \qquad (7\text{-}3)$$

where:

$a_1, a_2 \ldots\ldots a_n$ are layer coefficients for layer 1, layer 2 ...... layer n, respectively;

$D_1, D_2 \ldots\ldots D_n$ are thicknesses of layer 1, layer 2 ...... layer n, respectively;

$m_1, m_2 \ldots\ldots m_n$ are drainage coefficients for layer 1, layer 2 ...... layer n, respectively.

On the other hand, if the SN value is known, one can design thickness of base layer for a given ESAL value according to equation (7-4):

$$D_2 \geq \frac{1}{a_2 m_2} \, (\, SN - a_1\, m_1\, D_1 \,) \qquad (7\text{-}4)$$

As an example, this section presents a design of a flexible pavement according to AASHTO design method to see the effect of CKD-stabilization on the ESAL and base thickness. A computer program "AASHTO86" was employed to determine ESAL and base thickness values. The "AASHTO86" design procedure is based on the results

of the extensive AASHO Road Test conducted in Ottawa, Illinois in the 1950s and early

1960s. One of the salient features of the AASHTO design approach is that it

incorporates reliability concepts in the pavement design, which makes design more

reasonable and rational than traditional deterministic method.

Design of ESAL value   In this study, pavement conditions considered cover

case 1 through case 12. The were computed for an overall standard deviation (S_0) of

0.35, initial serviceability index (P_i) of 4.2, and terminal serviceability index (P_t) of 2.5.

The reliability of 90% was selected as an input. These values correspond to the values

observed at the AASHO Road Test (AASHTO, 1993). The computed ESAL values are

presented in Table 7-7. As can be seen from the table, the raw aggregate has small

values of ESAL with a maximum ESAL being 476,700. The CKD-stabilization

increased ESAL value greatly. When aggregate stabilized with 15% CKD and cured for

28-days, the value of ESAL increases more than 200% over that of raw aggregate and,

the maximum ESAL becomes 2, 211, 900 which is 4.6 times maximum ESAL of the

raw aggregate.

The Asphalt Institute recommends that, for urban minor arterial and light

industrial streets, the design ESAL be 1,000,000 (Huang 1993). Therefore, the raw

aggregate used in this study is considered inadequate for use as base layer, while by

addition of a small amount of CKD the aggregate becomes qualified for some special

cases, e.g. case 12. From Table 7-7, seven ESAL values are found to be greater than

1,000,000. Among the seven ESALs, two is from case 6 (7-day and 28-day cured

aggregate stabilized with 15%); two from case 9 with the same stabilized aggregates in

case 6; the other three are from case 12, which includes 7-day cured aggregate stabilized with 10% and 15% CKD, 28-day cured aggregate stabilized with 15% CKD.

<u>Design of base thickness</u>

Given an ESAL of 1,000,000 and other parameters being the same as given before, the SN was found to be 3.31. Assuming the m_1 and m_2 values to be 1.0, the base thicknesses (D_2) for different AC layer properties are calculated and listed in Table 7-8. It is seen that the base thickness decreases with the CKD amount and curing time. For AC layer modulus of 1725 MPa, the thickness of a 28-day cured aggregate base stabilized with 15% CKD is 15.69 mm for a 76 mm thick AC layer, representing a 50% decrease with respect to the raw aggregate base (33.6 mm). When the AC layer is 152 mm thick, the D_2 becomes 13.19 mm, representing an 84% decrease with respect to the raw aggregate base layer (82 mm). A reduction in base layer thickness due to CKD-stabilization indicates an economic benefit that can be gained from the CKD-stabilization.

7.4   Discussion

From the experimental results presented earlier (in chapter 5), one can see that CKD-stabilization has significant influence on the increasing base layer coefficient a_2. The properties of an aggregate base layer that does not meet the design requirements can be improved substantially by stabilization with CKD. The a_2 value of a base aggregate is calculated by using the bulk-stress RM model. So, generally, an aggregate with a higher RM value will have a higher a_2 value. However, since the bulk-stress model always shows a lower correlation between the RM and the bulk-stress values, the

184

a_2 values thus obtained sometimes show inconsistency. For example, from Figure 7-5 one cannot see an apparent increase in a_2 values between the 5% CKD-stabilized aggregate base and 10% CKD-stabilized aggregate base. The R^2 values of the bulk-stress model for the 5% and 10% CKD-stabilized aggregate were found to be only 0.48 and 0.35, respectively. It is evident that the model with such low correlation coefficients is inadequate for prediction and design-related applications. Therefore, it is important that more accurate models such as deviator stress model and combined bulk-deviator stress model be incorporated in the pavement design and analysis programs developed to produce more accurate designs.

Table 7-1 Material parameters Used for Calculation of ELBK Using MICH- PAVE

Layer Type	Poisson's Ratio	Unit Weight (pcf)	k_o	k_1	k_2	k_3	k_4	c (psi)	ϕ (deg.)
AC	0.35	150	0.7						
Base	0.38	140	0.6	5000	0.5			0	45
Soil	0.45	115	0.8	6.2	3021	1110	178	6	0

Note: 1 pcf = 0.1572 kN/m^3, 1 psi = 6.895 kPa

186

Table 7-2   A List of Values of the Equivalent Layer Bulk Stress (ELBK)
of the Aggregate Base Layer

Eac	Base	Dac, mm (in)								
MPa	Thickness	76 (3)			152 (6)			228 (9)		
[ksi]	D2		ELBK			ELBK			ELBK	
	mm [in]	Case No.	psi	kPa	Case No.	psi	kPa	Case No.	psi	kPa
1725	76 [3]	Case 1	27.62	190.59	Case 2	12.2	86.92	Case 3	7.83	54.03
[250]	152 [6]	Case 4	28.92	199.52	Case 5	12.6	86.94	Case 6	7.59	52.37
	228 [9]	Case 7	30.08	207.40	Case 8	13	89.7	Case 9	7	48.30
	304 [12]	Case 10	26.27	181.26	Case 11	11.98	82.66	Case 12	7.2	49.68
3450	76 [3]	Case 13	21.7	149.73	Case 14	9.17	63.27	Case 15	5.88	40.57
[500]	152 [6]	Case 16	21.73	149.94	Case 17	9.26	63.89	Case 18	5.93	40.92
	228 [9]	Case 19	22.53	155.46	Case 20	8.86	61.13	Case 21	6.19	42.71
	304 [12]	Case 22	20.42	140.90	Case 23	8.22	56.72	Case 24	6.44	44.44
5175	76 [3]	Case 25	17.35	119.72	Case 26	7.52	51.89	Case 27	5.37	37.05
[750]	152 [6]	Case 28	18.33	126.48	Case 29	7.33	50.58	Case 30	5.64	38.92
	228 [9]	Case 31	19.31	133.24	Case 32	7.27	50.16	Case 33	5.89	40.64
	304 [12]	Case 34	17.93	123.72	Case 35	7.43	51.27	Case 36	6.11	42.16

Table 7-3   Layer Coefficient (a₂) of the Raw and CKD-stabilized Aggregate Base

Eac MPa [ksi]	Base Thickness D2 mm [in]	Raw Aggregate Dac, (mm)			5% CKD, 7-day Dac, (mm)			10% CKD, 7-day Dac, (mm)		
		76 a2	152 a2	228 a2	76 a2	152 a2	228 a2	76 a2	152 a2	228 a2
1725	76 [3]	0.0691	0.0162	-0.0158	0.1074	0.0626	0.0354	0.1101	0.0615	0.0320
[250]	152 [6]	0.0722	0.0163	-0.0179	0.1100	0.0626	0.0337	0.1130	0.0615	0.0300
	228 [9]	0.0748	0.0184	-0.0233	0.1122	0.0644	0.0291	0.1154	0.0634	0.0250
	304 [12]	0.0658	0.0129	-0.0214	0.1045	0.0597	0.0307	0.1070	0.0583	0.0268
3450	76 [3]	0.0529	-0.0051	-0.0351	0.0936	0.0445	0.0191	0.0952	0.0418	0.0142
[500]	152 [6]	0.0530	-0.0045	-0.0345	0.0937	0.0450	0.0196	0.0953	0.0424	0.0147
	228 [9]	0.0554	-0.0075	-0.0316	0.0958	0.0425	0.0220	0.0975	0.0396	0.0174
	304 [12]	0.0488	-0.0125	-0.0290	0.0902	0.0382	0.0243	0.0914	0.0350	0.0199
5175	76 [3]	0.0378	-0.0185	-0.0412	0.0809	0.0331	0.0139	0.0813	0.0295	0.0086
[750]	152 [6]	0.0415	-0.0202	-0.0379	0.0840	0.0317	0.0167	0.0847	0.0279	0.0116
	228 [9]	0.0450	-0.0208	-0.0350	0.0870	0.0312	0.0192	0.0879	0.0274	0.0143
	304 [12]	0.0400	-0.0193	-0.0325	0.0827	0.0325	0.0213	0.0833	0.0287	0.0166

Table 7-4   Layer Coefficient (a₂) of the 15% CKD-stabilized Aggregate Base Cured for Different Periods

Eac	Base	15% CKD, 7-day			15% CKD, 28-day			15% CKD, 90-day		
MPa	Thickness	Dac, (mm)			Dac, (mm)			Dac, (mm)		
[ksi]	D2	76	152	228	76	152	228	76	152	228
	mm [in]	a2	a2	a2	a2	a2	a2	a2	a2	a2
1725	76 [3]	0.1241	0.0840	0.0596	0.1479	0.1008	0.0723	0.1644	0.1168	0.0879
[250]	152 [6]	0.1265	0.0840	0.0580	0.1506	0.1008	0.0704	0.1672	0.1168	0.0860
	228 [9]	0.1285	0.0856	0.0539	0.1529	0.1027	0.0655	0.1695	0.1187	0.0811
	304 [12]	0.1216	0.0814	0.0553	0.1448	0.0978	0.0672	0.1614	0.1137	0.0828
3450	76 [3]	0.1118	0.0677	0.0450	0.1334	0.0817	0.0551	0.1498	0.0975	0.0706
[500]	152 [6]	0.1119	0.0682	0.0454	0.1335	0.0823	0.0556	0.1499	0.0981	0.0711
	228 [9]	0.1137	0.0660	0.0476	0.1356	0.0797	0.0582	0.1521	0.0954	0.0737
	304 [12]	0.1087	0.0621	0.0496	0.1297	0.0752	0.0605	0.1461	0.0909	0.0761
5175	76 [3]	0.1003	0.0576	0.0403	0.1200	0.0698	0.0496	0.1362	0.0855	0.0651
[750]	152 [6]	0.1032	0.0563	0.0428	0.1233	0.0683	0.0526	0.1395	0.0839	0.0680
	228 [9]	0.1058	0.0558	0.0451	0.1264	0.0678	0.0552	0.1427	0.0834	0.0707
	304 [12]	0.1020	0.0569	0.0469	0.1219	0.0691	0.0574	0.1382	0.0848	0.0729

Table 7-5   Effect of Freezing/Thawing Cycles on the Layer Coefficient (a_2)

Eac MPa [ksi]	Base Thickness D2 mm [in]	4 cycles Dac, (mm)			8 cycles Dac, (mm)			12 cycles Dac, (mm)		
		76 a2	152 a2	228 a2	76 a2	152 a2	228 a2	76 a2	152 a2	228 a2
1725	76 [3]	0.0747	0.0292	0.0016	0.0450	-0.0006	-0.0283	0.0509	0.0002	-0.0305
[250]	152 [6]	0.0774	0.0292	-0.0002	0.0476	-0.0006	-0.0301	0.0538	0.0002	-0.0325
	228 [9]	0.0796	0.0310	-0.0049	0.0499	0.0012	-0.0348	0.0563	0.0022	-0.0378
	304 [12]	0.0718	0.0263	-0.0033	0.0420	-0.0036	-0.0331	0.0476	-0.0031	-0.0360
3450	76 [3]	0.0607	0.0108	-0.0150	0.0309	-0.0191	-0.0449	0.0353	-0.0203	-0.0490
[500]	152 [6]	0.0608	0.0113	-0.0145	0.0310	-0.0185	-0.0444	0.0354	-0.0197	-0.0485
	228 [9]	0.0629	0.0088	-0.0120	0.0331	-0.0211	-0.0419	0.0377	-0.0226	-0.0457
	304 [12]	0.0572	0.0044	-0.0097	0.0274	-0.0254	-0.0396	0.0314	-0.0274	-0.0432
5175	76 [3]	0.0477	-0.0007	-0.0203	0.0180	-0.0306	-0.0502	0.0208	-0.0331	-0.0549
[750]	152 [6]	0.0509	-0.0022	-0.0174	0.0211	-0.0321	-0.0473	0.0244	-0.0348	-0.0517
	228 [9]	0.0539	-0.0027	-0.0149	0.0242	-0.0326	-0.0448	0.0278	-0.0353	-0.0489
	304 [12]	0.0496	-0.0014	-0.0128	0.0199	-0.0313	-0.0427	0.0230	-0.0339	-0.0466

Table 7-6   Effect of Wetting/Drying Cycles on the Layer Coefficient (a_2)

Eac	Base	4 cycles			8 cycles			12 cycles		
MPa	Thickness	Dac, (mm)			Dac, (mm)			Dac, (mm)		
[ksi]	D2	76	152	228	76	152	228	76	152	228
	mm [in]	a2	a2	a2	a2	a2	a2	a2	a2	a2
1725	76 [3]	0.0956	-0.0379	-0.0673	0.0775	0.0263	-0.0046	0.0638	0.0060	-0.0290
[250]	152 [6]	0.0991	-0.0379	-0.0693	0.0804	0.0263	-0.0067	0.0671	0.0060	-0.0312
	228 [9]	0.1022	-0.0360	-0.0743	0.0830	0.0284	-0.0119	0.0700	0.0083	-0.0372
	304 [12]	0.0917	-0.0410	-0.0725	0.0742	0.0231	-0.0101	0.0601	0.0023	-0.0351
3450	76 [3]	0.0767	-0.0576	-0.0851	0.0617	0.0056	-0.0233	0.0460	-0.0173	-0.0500
[500]	152 [6]	0.0769	-0.0570	-0.0845	0.0618	0.0063	-0.0227	0.0461	-0.0166	-0.0494
	228 [9]	0.0797	-0.0597	-0.0819	0.0642	0.0034	-0.0199	0.0488	-0.0199	-0.0462
	304 [12]	0.0720	-0.0643	-0.0794	0.0578	-0.0015	-0.0174	0.0415	-0.0254	-0.0433
5175	76 [3]	0.0593	-0.0698	-0.0907	0.0472	-0.0073	-0.0292	0.0296	-0.0319	-0.0567
[750]	152 [6]	0.0636	-0.0714	-0.0876	0.0508	-0.0089	-0.0260	0.0336	-0.0338	-0.0531
	228 [9]	0.0676	-0.0719	-0.0849	0.0541	-0.0095	-0.0232	0.0374	-0.0344	-0.0499
	304 [12]	0.0619	-0.0706	-0.0827	0.0493	-0.0081	-0.0208	0.0320	-0.0328	-0.0472

Table 7-7 Structural Number (SN) and EASL of the Aggregate Base

Case No.	Raw aggregate		5% CKD, 7-day		10% CKD, 7-day		15% CKD, 7-day		15% CKD, 28-day	
	SN	EASL	SN	EASL	SN	EASL	SN	EASL	SN	EASL
Case 1	1.2	2,900	1.29	4,200	1.29	4,200	1.36	5,600	1.43	7,300
Case 2	2.03	52,900	2.14	72,300	2.16	76,500	2.23	92,500	2.28	105,600
Case 3	2.93	476,700	3.05	607,200	3.08	644,200	3.15	737,800	3.19	796,300
Case 4	1.43	7,300	1.59	13,000	1.61	13,900	1.75	22,300	1.89	34,800
Case 5	2.08	61,100	2.3	111,200	2.35	126,500	2.48	174,800	2.58	221,700
Case 6	2.87	420,900	3.12	696,400	3.18	781,300	3.32	1,014,200	3.39	1,151,300
Case 7	1.67	17,100	1.91	37,000	1.94	40,600	2.15	74,400	2.36	133,100
Case 8	2.15	74,400	2.48	174,800	2.55	206,600	2.75	325,400	2.9	448,100
Case 9	2.78	339,900	3.15	737,800	3.25	891,300	3.45	1,281,200	3.56	1,552,400
Case 10	1.79	25,400	2.13	70,400	2.18	80,800	2.45	162,400	2.73	311,400
Case 11	2.15	74,400	2.59	226,900	2.67	272,400	2.96	506,900	3.15	742,100
Case 12	2.73	311,400	3.23	858,600	3.36	1,090,700	3.63	1,749,900	3.77	2,211,900

Table 7-8 Thickness of Aggregate Base Layer for 1,000,000 ESAL

Aggregate Base Type	Eac = 1725 MPa (250 ksi)		Eac = 3450 MPa (500 ksi)	
	Dac , mm		Dac , mm	
	76	152	76	152
Raw Aggregate	33.57	82.10	36.20	*
5%-CKD, 7-day	21.60	21.25	20.44	11.69
10% CKD, 7-day	21.07	21.63	20.09	12.44
15% CKD, 7-day	18.69	15.83	17.13	7.68
15% CKD, 28-day	15.69	13.19	14.36	6.36
15% CKD, 90-day	14.11	11.39	12.78	5.33

* The value approaches infinite because of too small layer coefficient of the base
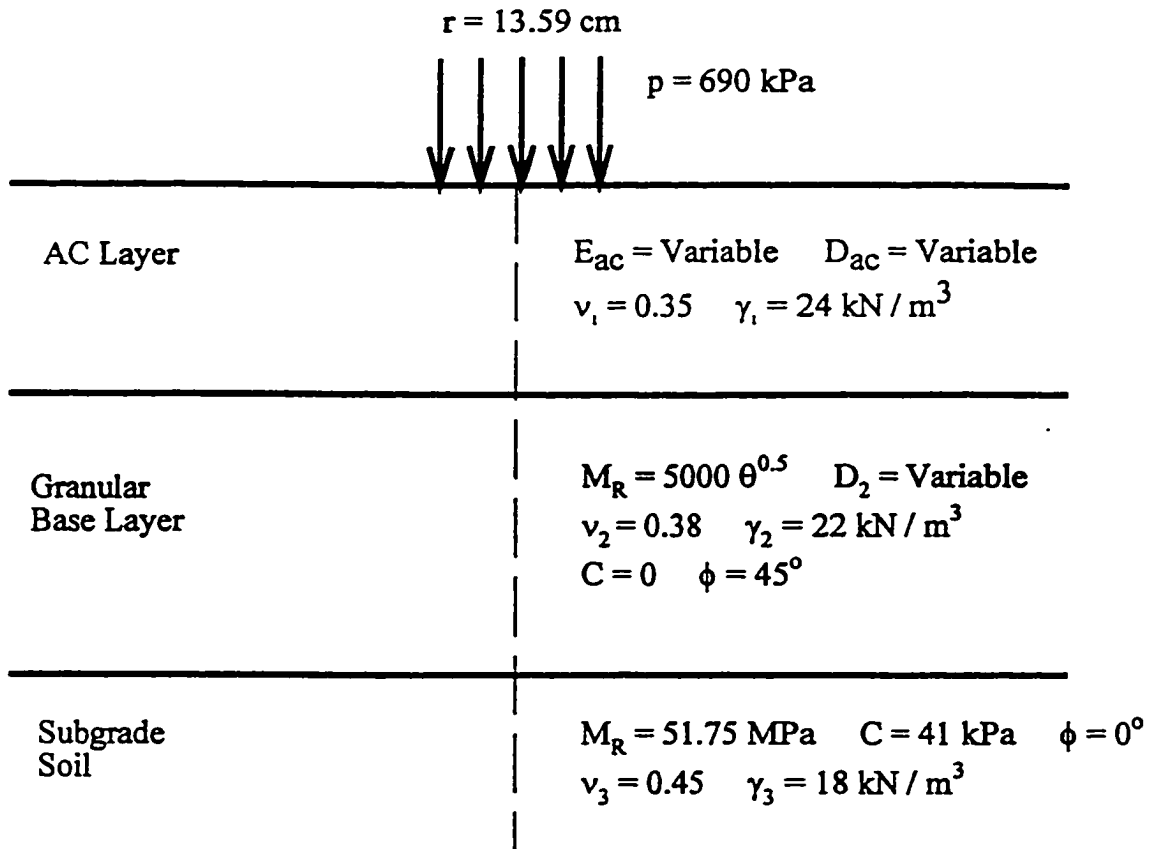
Figure 7-1   Pavement Configuration Used for the ELBK Calculation
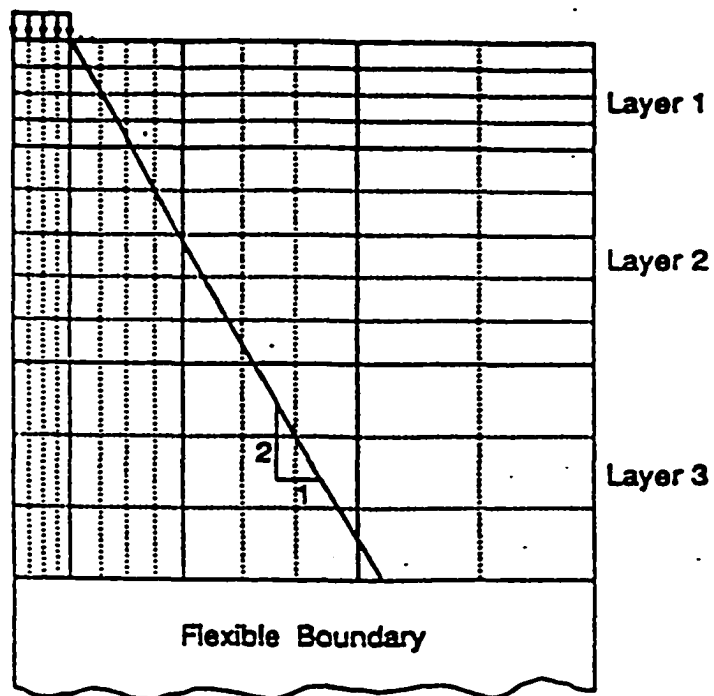
Figure 7-2   Typical Finite Element Mesh for MICH-PAVE
              (after Harichandran et al., 1990)

195
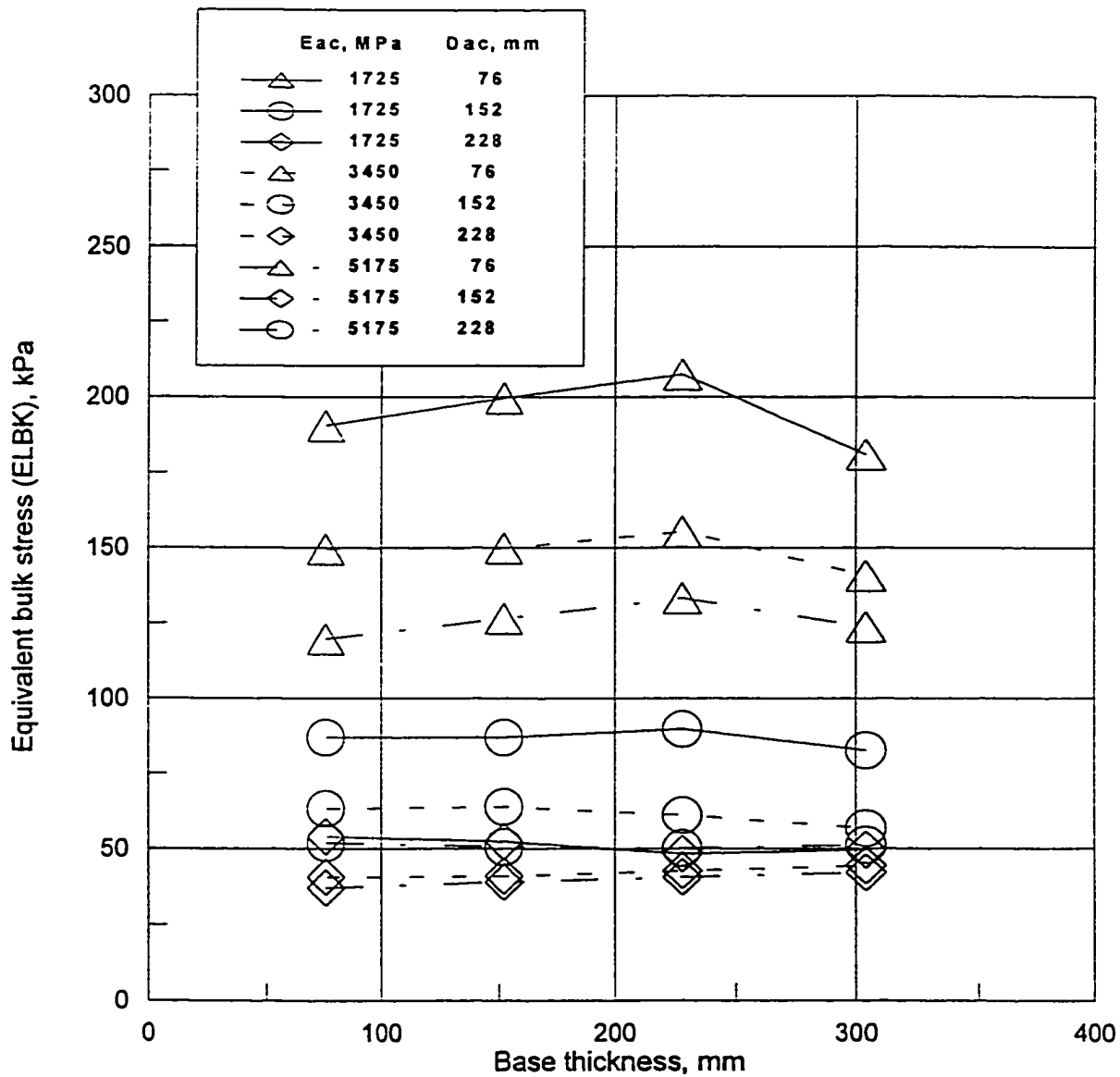
Figure 7-3   Calculated Equivalent Bulk Stress (ELBK) Values
              vs. Base Thickness
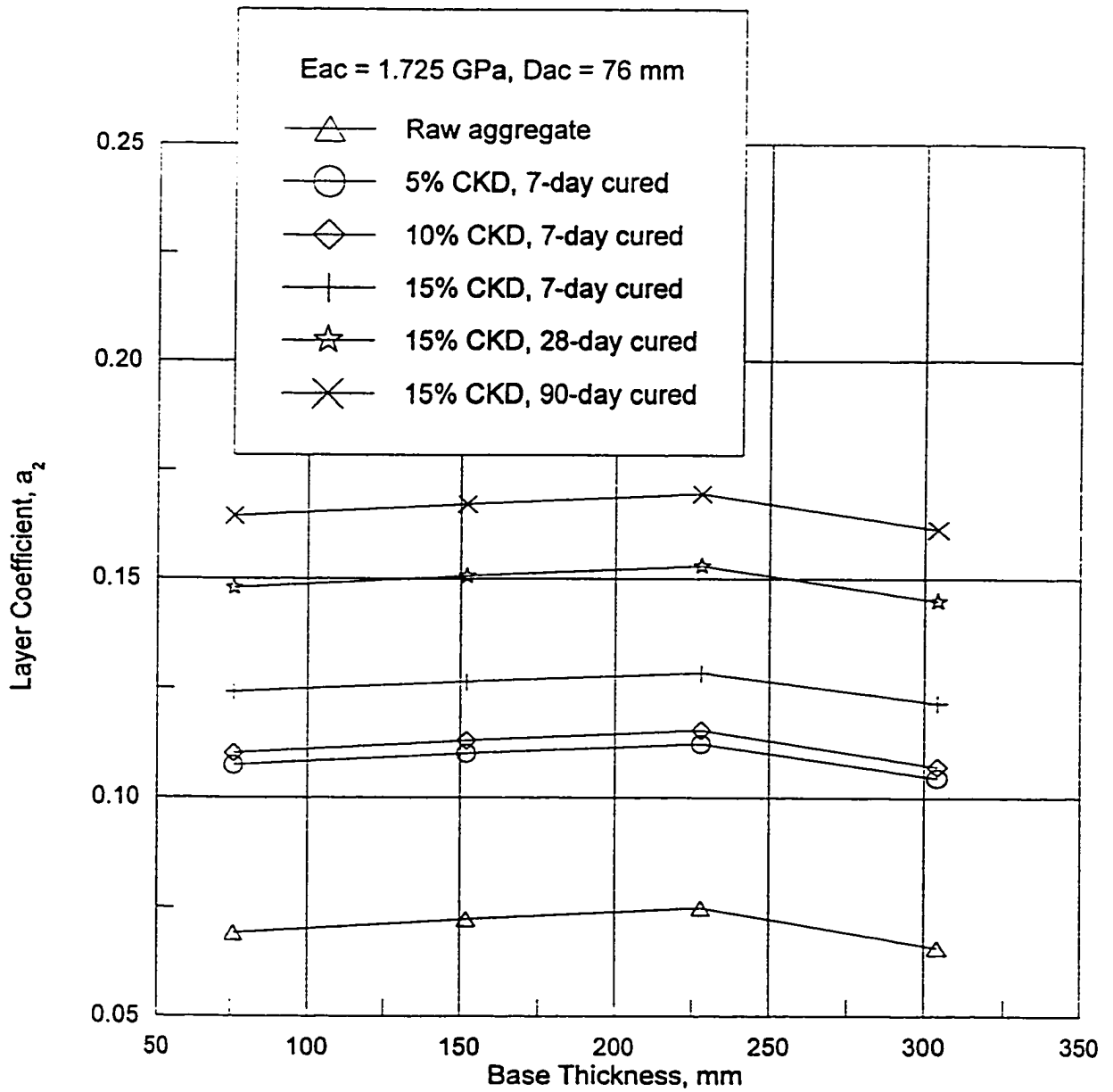
Figure 7-4   Effect of CKD-stabilization on the Base Layer Coefficient

197
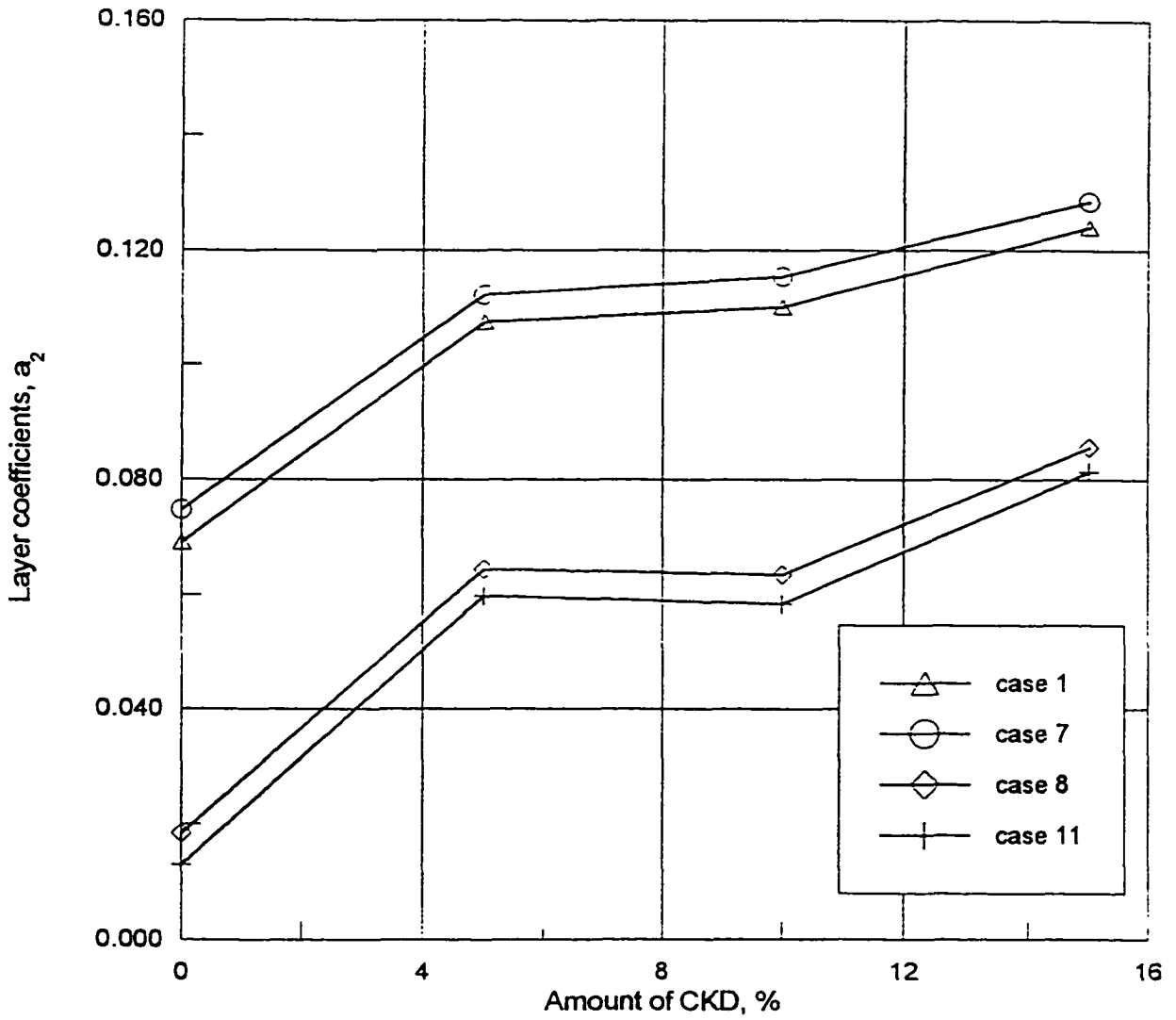
Figure 7-5   Effect of CKD Amount on the Base Layer Coefficient
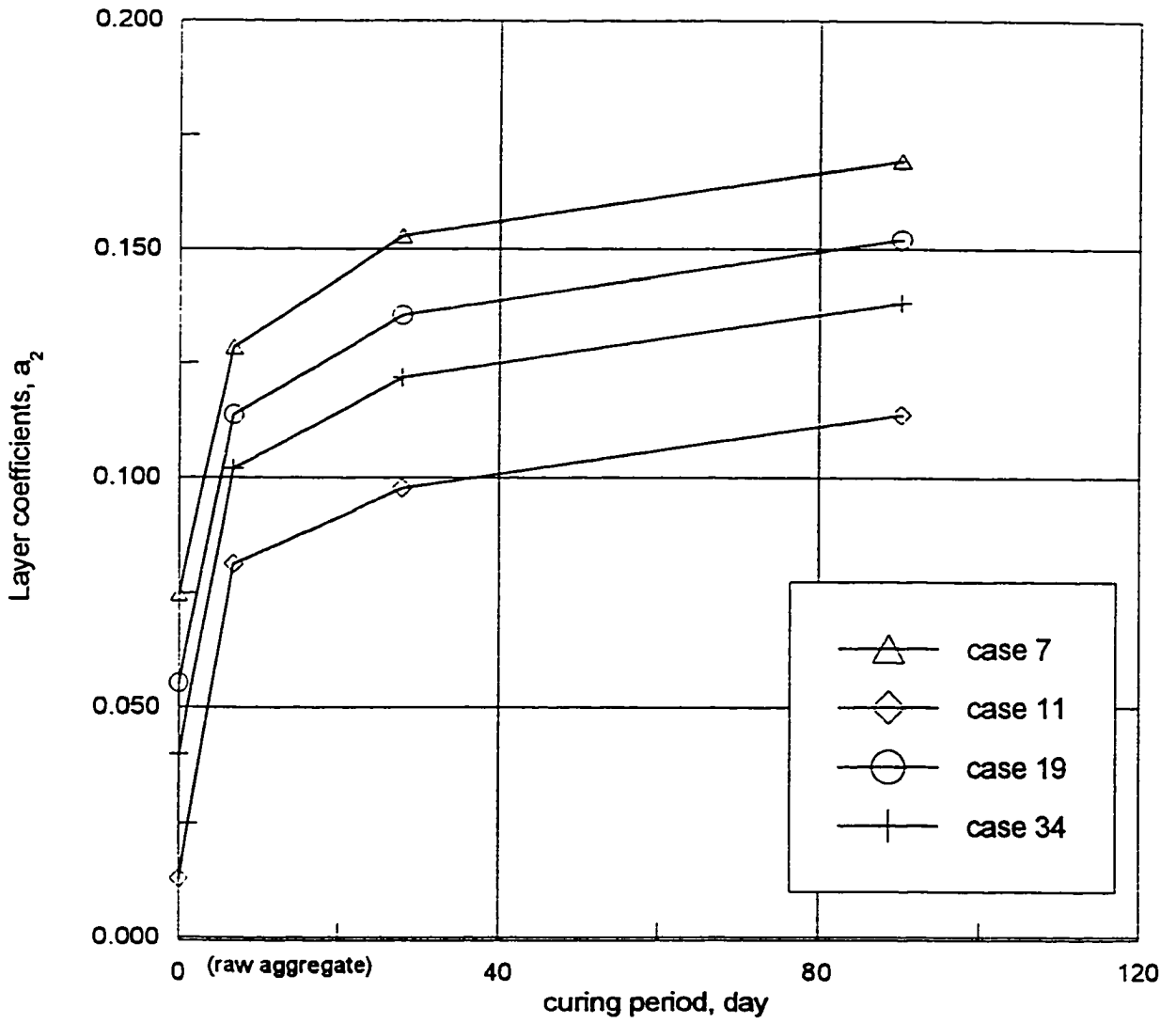
Figure 7-6   Effect of Curing Time on the Base Layer Coefficient

199
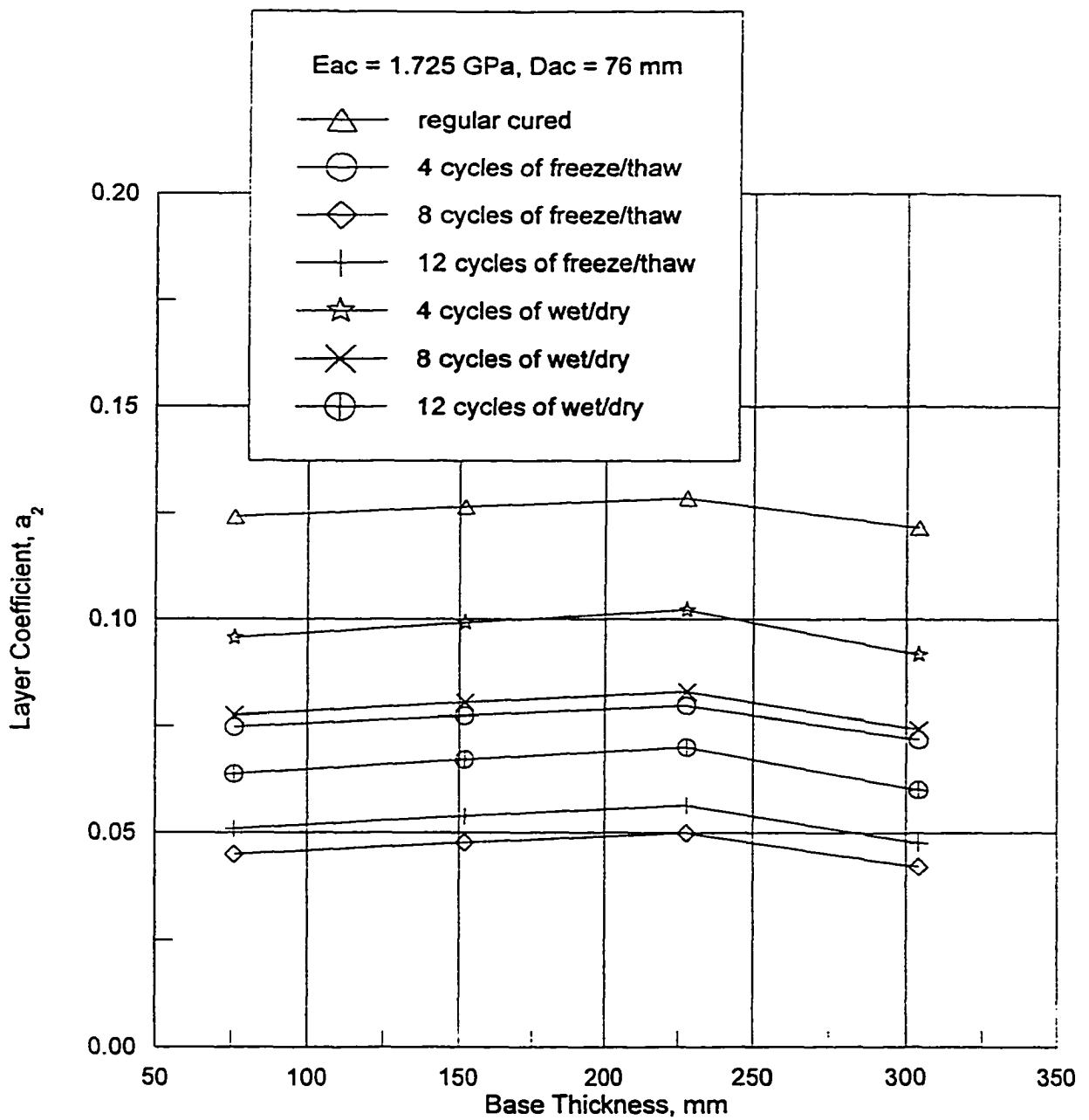
Figure 7-7   Effect of Durability on the Base Layer Coefficient
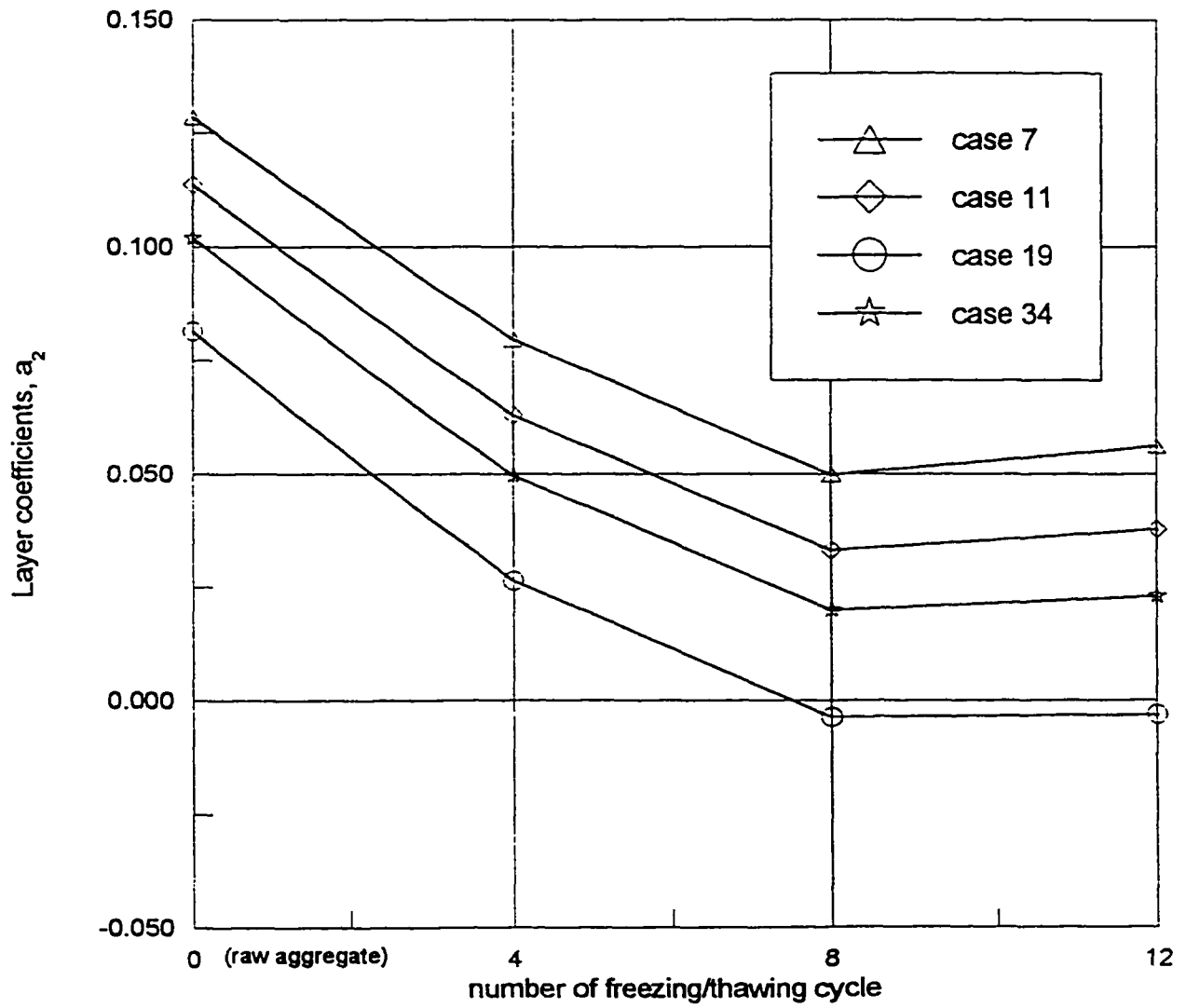
Figure 7-8   Effect of Freezing/Thawing Cycles on the Layer Coefficient
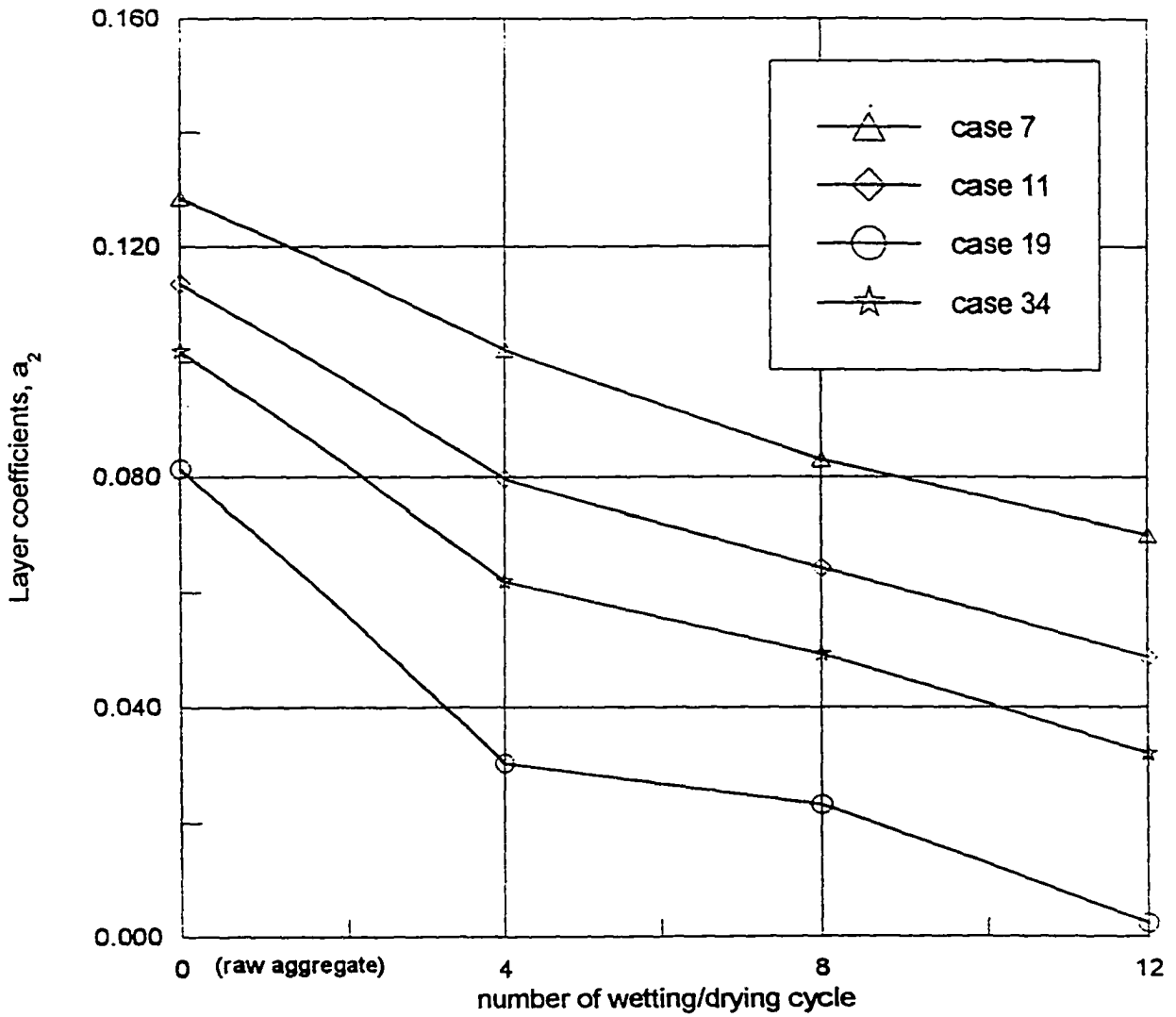
Figure 7-9   Effect of Wetting/Drying Cycles on the Layer Coefficient
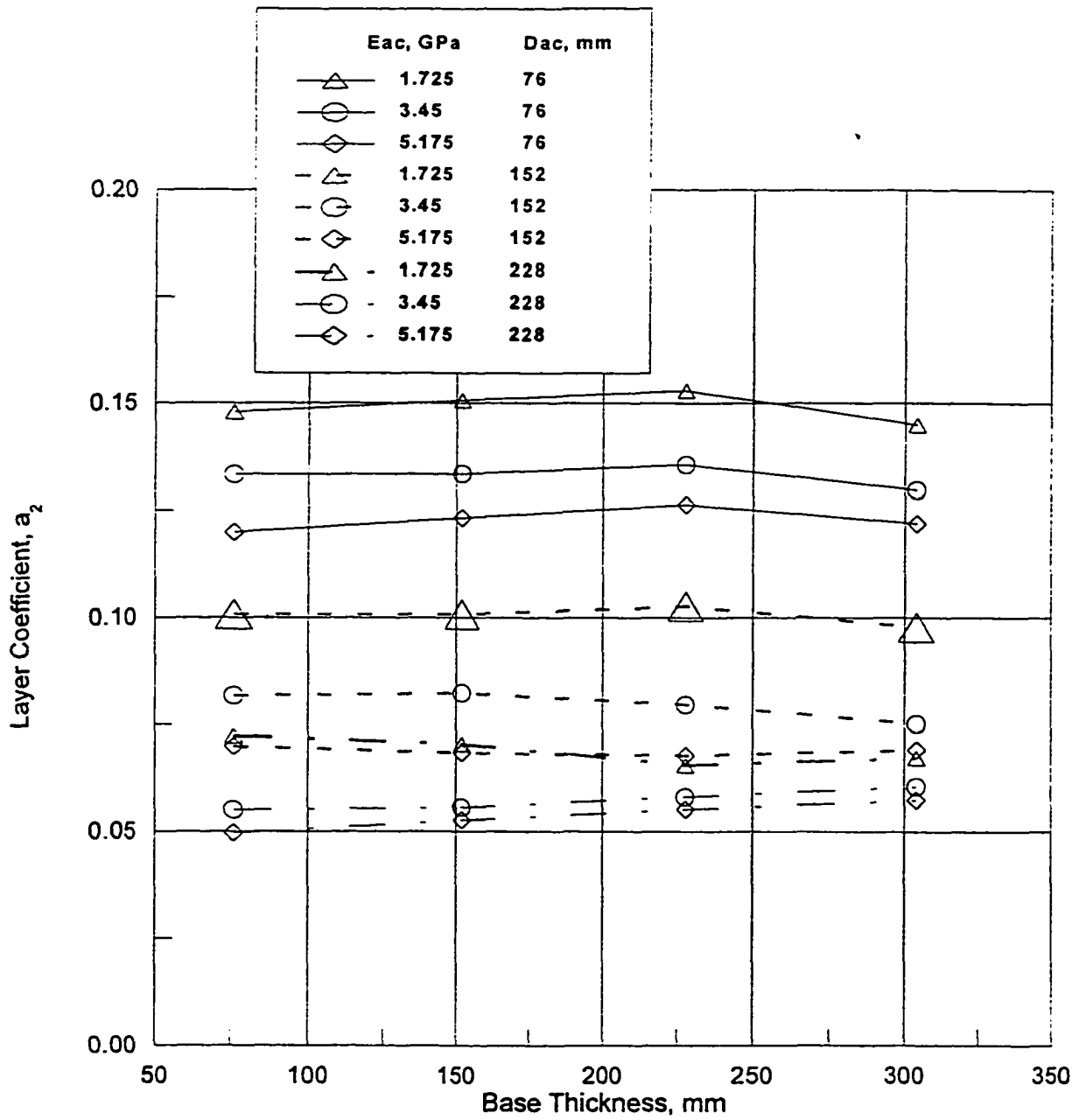
Figure 7-10 Effect of Layer Properties on the Layer Coefficient
(15% CKD, 28-day Cured)

CHAPTER 8

SUMMARY, CONCLUSIONS, AND RECOMMENDATIONS

8.1   Introduction

This chapter provides a summary of the study and presents conclusions drawn from the data obtained in laboratory experiments and the calculations performed. Finally, recommendations for further research are suggested.

8.2   Summary

A comprehensive study on characterization of CKD-stabilized aggregate base was conducted. Meridian limestone aggregate which is considered to be of substandard quality and unsuitable for highway base course was tested for its RM value in raw and stabilized forms. The aggregate was first tested for its Los Angeles (LA) abrasion value. Moisture-density tests were conducted according to AASHTO designation T 180-93 (AASHTO T 180-93) at gradation specified by the median line of the ODOT specified gradation band for Type A aggregate (ODOT, 1988). RM test specimens of 152 mm diameter and 304 mm height were prepared according to the AASHTO designation T 294-92I (AASHTO T 294-92I). The test specimens were compacted at an optimum moisture content (w_{opt}) and above 95% of the maximum dry density (γ_{dmax}) value obtained from the moisture-density tests. The specimens were then tested for their RM values.

The Meridian aggregate was stabilized with 5%, 10%, and 15% of CKD based on the dry weight of the aggregate. Flexural strength of CKD-stabilized aggregate was studied using one third point beam test method in accordance with standard testing

204

procedure AASHTO T97-86. At least five replicate specimens of stabilized aggregate were prepared for RM test for each case. The specimens were cured for 7-days, 28-days, and 90-days in a chamber at a controlled relative humidity of above 95% and a constant room temperature of 70 °F. RM tests were conducted on the specimens at the end of their respective curing period. UCS tests were conducted following the RM tests on the specimens, except for one set of UCS test which was conducted prior to RM test. The results of the UCS test were used to compute EM values of the specimens.

Exploratory investigation on the durability including freezing/thawing and wetting/drying cycles on the RM values were conducted using 7-day cured CKD stabilized aggregate. One freezing/thawing cycle consists of placing specimens in the freezer for 24 hours and then in room temperature for 24 hours. One wetting/drying cycle consists of placing specimens in the oven for 24 hours and then in portable water tank for 24 hours. The number of cycles exercised on specimens are 4, 8 and 12. The RM values of specimens were tested under the thaw/or wet condition which is the worst situation may exist in practice.

SEM and XRD analyses were conducted on the raw and stabilized aggregate to qualitatively identify the hydration product and change in the microstructure of the matrix of the stabilized aggregate and to help interpret the results of the RM and UCS tests.

The stress-dependent models including $k - \theta$ model, $k - \sigma_d$ and $k - f(\theta, \sigma_d)$ models were evaluated using tested results. The material parameters k_i ($i = 1, 2, 3, 4, 5, 6$) and R^2 values were calculated to evaluate goodness of the various stress-dependent models. The $\theta - \sigma_d$ combination model is found to be more suitable in representing stress-

dependent resilient characteristics of the various stabilized aggregates.

Artificial neural network (ANN) model was developed to represent relationship of RM versus various variables. A feedforward backpropagation neural net was used to train the available data and, a 9-30-1 net architecture was found to be appropriate for modeling presented data set. The developed ANN model shows unquestionable advantages over the stress-dependent model and statistical model.

The AASHTO flexible pavement design methodology uses layer coefficients to relate the structural design of the pavement with its performance (AASHTO 1993). Layer coefficient (a_2) values corresponding to the base course layer were determined for each combination of the three different AC layer RM values, three different AC layer thickness, and four different base course layer thickness. The layer coefficients were determined from the bulk stress values computed using a user friendly computer software, MICH-PAVE for each of the AC layer RM, thickness, and base course thickness combination. The effect of CKD-stabilization and durability on the layer coefficient was evaluated. A flexible pavement design example was presented based on the results achieved in this study.

8.3   Conclusions

Based on the study presented in previous chapters the following conclusions have been drawn:

1. The raw Meridian aggregate used in this study has a range of RM values from 49.42 MPa to 306.59 MPa within tested stress level. The raw aggregate thus produces low base layer support values with layer coefficients below 0.0748 for a

206

wide range of flexible pavement designs.

2. Cement-kiln-dust, an industrial waste, is an effective stabilizing agent for strengthening base/and subbase aggregate. There is a continuous increase in resilient modulus RM within the range of addition of CKD. For 7-day curing time, the increased RM values can be up to 33%, 60% and 73% for the aggregate stabilized with 5%, 10% and 15% CKD, respectively. Considering strength gain and compaction preference, 15% CKD-stabilized aggregate is considered to be most appropriate.

3. Curing time has a substantial influence on the increases in resilient modulus of CKD-stabilized aggregate. The 28-day curing period provides sufficient time for major completion of hydration and other chemical reactions helpful for the strength gain. Therefore, a remarkable increase in resilient modulus is observed in the 28-day specimens. Compared to raw aggregate, the RM values of 15% CKD-stabilized aggregate increase up to 128% for specimens cured for 28 days.

4. The resolution of the data acquisition system used may have appreciable influence on the measured resilient modulus. The possible maximum difference between the measured and actual RM values is found to be in a range of 10% to 20%, depending on the stress level. This difference may be responsible for some of the inconsistent observations associated with the test results.

5. The CKD-stabilized aggregate can develop a certain amount of flexural strength. The ultimate flexural strength or modulus of rupture (MR) of 28-day cured aggregate stabilized with 15%-CKD ranges from 108 kPa to 153 kPa. However,

the MR values obtained from 90-day cured specimens showed inconsistency with the 28-day's values. The remarkable variability in MR values manifests that the method used for testing concrete beams may not be appropriate for testing the coarse aggregate samples. Since the base layer is actually in a compressive stress state when subjected to traffic loading, one can not expect the tensile crack will happen in the CKD-stabilized aggregate base simply because of the low flexural strength of the aggregate. Rather, the flexural strength developed due to CKD-stabilization can be deemed as an extra strength gain which will make a flexible pavement safer and more reliable.

6. Durability including freezing/thawing and wetting/drying cycles has remarkable adverse effect on the resilient modulus of CKD-stabilized aggregate. Within a range of 8 cycles, the RM values decrease substantially with increasing number of freezing/thawing and wetting/drying cycles. The highest reduction in RM value due to freezing/thawing is 54.21%, 67.51% and 65.11% for 4, 8, and 12 cycles, respectively. For wetting/drying actions, the highest reduction in RM value is 34.27%, 53.58% and 61.88% for 4, 8, and 12 cycles, respectively.

7. Drainage condition has significant effect on resilient behavior of stabilized aggregate base when it is at wet state. The RM value determined under undrained condition shows 25% lower than drained RM. This fact indicates importance of keeping drainage facility in an effective condition.

8. For the studied raw and CKD-stabilized aggregate, the resilient moduli obtained using AASHTO current testing procedure are correlated better with the deviator

208

stress than with the bulk stress, while the combined bulk-deviator stress model gives higher correlation than single deviator stress model. Within the specified stress range, the value of resilient modulus increases more evidently with the deviator stress than with the bulk stress.

9. An artificial neural network (ANN) model was developed to represent relationship of RM versus various variables. A feedforward backpropagation neural net was used to train the available data and, a 9-30-1 net architecture was found to be appropriate for modeling presented data set. The nine variables used in the ANN model include two stress variables and seven category variables depicting stabilization situations. The excellent agreement between the experimental and ANN simulated values is observed. However, the user should be cautioned that ANN prediction by using the data with different category values may give rather poor results.

10. The UCS values increased with increasing CKD content and curing period. The aggregate stabilized with 15% CKD produced UCS values of 2163 kPa and 2810 kPa when cured for 28-days and 90-days, respectively. These values represent more than 900 percentage higher than the UCS value (216 kPa) of the raw aggregate.

11. Loading history of aggregate base influences UCS values significantly. For 28-day cured aggregate stabilized with 15% CKD, the UCS value ranges from 1800 kPa to 2450 kPa for specimens tested after RM test, while 940 kPa to 1610 kPa for specimens tested prior to RM test. This finding indicates that the base having

subjected to repeated traffic loading will possess a higher strength than that of new constructed aggregate base.

12. The EM values of the aggregate also increase significantly as a result of stabilization. The EM values increased with the increase in CKD content and curing period. The 28-day and 90-day cured aggregate stabilized with 15% CKD yielded EM values of 344 MPa and 439 MPa, respectively.

13. It is found that there exists a nonlinear relationship between RM and UCS/ and EM values. Because of high stress-dependence of the RM value, however, the relationship of RM versus UCS or EM is stress-dependent and, it is useful only for the specific stress level upon which the relation is developed. It is advisable to note variation in the correlation between RM and USC/or EM, which indicates some uncertainty of the regression formula.

14. Microstructure analysis using SEM technique reveals the mechanism of increase in resilient modulus of CKD-stabilized aggregate. Crystals formed during the hydration process contribute to the cementing particles as an integral body, while the filling of the intracluster voids of the fine particles minimize possible elastic deformation of the aggregate. More crystals and less voids are observed with the CKD-stabilized specimens having more amount of CKD and longer curing time.

15. The XRD analyses show chemical activity within the aggregate matrix as a result of stabilization. The analyses lead to a conclusion that the hydration of CKD was followed by crystal formation of ettringite within the matrix observed in the micrographs. The results of the XRD analyses conform with the results of the

SEM analyses and RM and UCS tests.

16. The layer coefficients of the stabilized aggregates are significantly higher than those of the raw aggregates. The layer coefficients of the 28-day cured aggregate stabilized with 15% CKD are more than double those of the raw aggregate. However, the layer coefficient of the stabilized aggregate base drops significantly when the aggregate experienced freezing/thawing and wetting/drying cycles. When subjected to about eight cycles of freezing/thawing or wetting/drying, the layer coefficients of CKD-stabilized aggregate base close to or lower than those of the raw aggregate base.

8.4   Recommendations

Based on the conclusions formulated above and considering the positive aspects of this study, the following recommendations are made for further studies.

1.   Pavement design and performance depend to a great extent on the properties of base layer. When subjected to traffic loading, the stabilized base layer may suffer a certain amount of deformation which may or may not break down the base layer. Since the flexural strength of the stabilized base aggregate is rather small, the use of flexural strength in the design for pavement base may not be realistic approach. Consequently, the resilient modulus value, which is essentially proposed for the design of an untreated aggregate base, may be an appropriate strength parameter for the design of stabilized aggregate base. However, since the stabilized aggregate is not a loose particulate material rather a cementitious material, the mechanisms that governs behavior of the stabilized aggregate base

may differ from those for granular aggregate bases. Further study to illustrate these issues is necessary to shed light on the design of stabilized aggregate base.

2. The RM values have been found to be sensitive to variations in gradation of the aggregate. The present study was conducted with aggregate having ODOT median gradation. However, in the field, the gradation of base aggregate may vary significantly. This variation in gradation will result in variation in RM values and, even stabilization effects. It is, therefore, evident that there is a need to investigate the effect of ODOT coarse and fine gradation limits on the RM and on the CKD stabilization. Also, further study should be directed to CKD-stabilization on aggregates from different sources. Through these further studies, design and/ or construction guidelines for CKD-stabilized aggregate base could be developed.

3. At the present time, there is little experience in the application of CKD in base aggregate stabilization and pavement construction. To get first-hand knowledge, field investigation on CKD stabilization of base aggregate is needed. The field implementation may yield observations that deviate from laboratory behavior. The study of these deviations, if present, is essential to develop design procedures and specifications.

4. Because of the variability of CKD product from one source to another, a frequent testing of this material is required to evaluate its performance and quality. Therefore, it is recommended that parallel experiments be conducted by using different CKD with different chemical compositions. These further studies should be performed to allow establishment of general guidelines and specifications for

the use of CKD in aggregate stabilization.

5. To evaluate drainage capability of a CKD-stabilized aggregate base, permeability tests should be performed on CKD-stabilized aggregate specimens. Such tests may include flexible wall triaxial permeability tests, which can also take into consideration the effect of vehicle load-induced stresses on the hydraulic conductivity.

6. The ultimate goal for investigating resilient behavior of an aggregate is to implement the resilient modulus value in the pavement design. So far, most pavement design programs adopt only bulk stress model to input RM values of the aggregate base. Since the bulk stress model shows poorer correlation with RM value than the deviator stress and combined bulk-deviator stress models, an effort to modify or develop a new flexible pavement design program that can implement the above-mentioned stress-dependent model in the pavement design is needed. Further, an attempt should be towards to include ANN model in finite element analysis for pavement design and evaluation.

7. In evaluating effect of freezing/thawing and wetting/drying cycles on the RM, the specimens were tested at either thaw or wet state to mimic the worst environmental conditions. It seems necessary to test specimens at freeze or dry state to get systematic data that would provide valuable information about the performance of aggregate base during its whole life. Also, there is a need to test raw aggregate specimens to evaluate the difference in durability effect between the raw and the stabilized aggregate bases. Special attention should be paid to

avoid damaging samples during the freeze/thaw and wet/dry processes.

8. The 15% CKD content yields the highest RM values in this study. A study using CKD contents higher than 15% should be pursued to find an optimum CKD content that yields the highest RM values and beyond which the RM values decrease. However, a decision to use higher CKD contents than the one used in this study should be viewed from the standpoint of the field application and economic consideration.

9. Further cost analysis of the application of different stabilizing agents (e.g. fly ash, lime, cement and CKD) should be conducted to determine the most cost-effective method of chemical stabilization of base/and subbase aggregates.

REFERENCES

AASHTO (1986A), *AASHTO Guide for Design of Pavement Structures*. Washington, D.C.

AASHTO (1986B), Standard Method of Test for Resilient Modulus of Subgrade Soils, Washington, D.C.

AASHTO (1991), *Interim Method of Test for Resilient Modulus of Subgrade Soils and Untreated Base/Subbase Materials*. Washington, D.C.

AASHTO (1992), *Interim Method of Test for Resilient Modulus of Unbound Granular Base/Subbase Materials Subgrade Soils*. Washington, D.C.

AASHTO (1993), *AASHTO Guide for Design of Pavement Structures*. Washington, DC.

AI (1991), Asphalt Institute, Computer Program DAMA (CP-1/1991 Revision) - Pavement Structural Analysis Using Multi-Layered Elastic Theory. Asphalt Institute, Lexington, KY.

ASTM (1989), *Standard Test Methods for Wetting and Drying Tests of Compacted Soil-Cement Mixtures, Designation: D 559-89*, Philadelphia, PA.

ASTM (1989), *Standard Test Methods for Freezing and Thawing Tests of Compacted Soil-Cement Mixtures, Designation: D 560-89*, Philadelphia, PA.

Azad, S. (1997), "Soil stabilization of three different soils using cement kiln dust." *Master Thesis*, School of Civil Engineering and Environmental Science, University of Oklahoma.

Baghdadi, Z. A. and Rahman, A. (1990). "The potential of cement kiln dust for the stabilization of dune sand in highway construction." *J. Build. And Envir.* , Oxford, England, 25(4), pp.285-289.

Baker, M. D. and Laguros J. G. (1985), "Reaction products in fly ash concrete." *Proceedings, Symposium on Fly Ash and Coal Conversion By-Products: Characterization, Utilization and Disposal I,* Materials Research Society, Vol. 43, Pittsburgh, Pennsylvania, pp. 49-58.

Boynton, R. S. (1980), *Chemistry and Technology of Lime and Limestone*, 2nd. Edn., John Wiley & Sons, Inc., New York, N.Y.

Burczyk, J. M., Ksaibati, K., Richard, A. S. and Farrar, M. J. (1995), "Factors Influencing

Determination of a Subgrade Resilient Modulus Value." *Transportation Research Record 1462*, TRB, National Research Council, Washington, DC. , pp. 72-78.

Casagrande, A. (1948), "Classification and identification of soils." Trans. ASCE, Vol. 113, pp. 901-930.

Chen , D. H. (1994), "Resilient modulus of aggregate bases and a mechanistic-empirical methodology for flexible pavements," Ph.D. dissertation, University of Oklahoma, Norman.

Chen, D. H., Zaman, M. M. and Laguros, J. G. (1994), " Characterization of base/subbase materials under repetive loading," *Journal of Testing and Evaluation*, Vol. 23, No. 3, May 1995, ASTM, Philadelphia, Pennsylvania, pp. 180-188.

Chen, D. H., Zaman, M. M. and Laguros, J.G. (1995), "Resilient Moduli of Aggregate Materials: Variability Due to Testing Procedure and Aggregate Type." *Transportation Research Record 1462*, TRB, National Research Council, Washington, D.C. , pp. 57-64.

Collins, R. J. and Emery, J. J. (1983), "kiln Dust-Fly Ash Systems for Highway Bases and Subbases, Report No. FHWA/RD-82/167, USDOE and USDOT, Washington D. C..

Diamond, S. (1981), "The characterization of fly ashes." *Proc., Effects of Fly Ash Incorporation in Cement and Concrete, Symposium N*, Material Research Society, Pittsburgh, Pennsylvania, pp. 12-23.

Elliott, R. P. and Thornton, S. I. (1988). "Resilient Modulus and AASHTO Pavement Design." *Transportation Research Record 1196*, TRB, National Research Council, Washington, D.C. , pp. 116-124.

Elwefati, A. M., Albaden, A. S. and Abushwereb, M. A. (1990), "Cement kiln dust as a partial replacement for Portland cement in concrete." *Proc., 15th Conf. On Our World in Concrete and Struct.*, pp. 119-125.

Finn, F., Saraf, C., Kalkarni, R., Nari, K., Smith, W. and Abdullah (1977), "The use of distress prediction subsystems for design of pavement structures." *Proc. 4th Int. Conf. On the Structural Design of Asphalt Pavements*, Ann Arbor, Mich., Vol. 1 pp.1-38.

Faruque, M. O. (1987), "A Third Invariant Dependent Cap Model for Geological Materails,." *J. Soils and Foundations*, ASCE, Vol. 27, pp. 12-20.

Ghaboussi, J. (1992), "Potential application of neural -biological computational models in

geotechnical engineering." *Proc. 4th Int. Sym. On Neumerical Models in Geomechnics*, Swansea, U.K.

Giles, C. L., Kuhn, G. M. and Williams, R. J. (1994) " Dynamic Recurrent Neural Networks: Theory and Applications." *IEEE Transactions on Neural Network*, Vol. 5, No. 2, pp. 153-160.

Hausmann, M. R. (1990), *Engineering principles of ground modification*. McGraw-Hill Book Co., Inc., New York, N. Y.

Hicks, R. G. and Monismith, C. L. (1971), "Factors Influencing the Resilient Respond of Granular Materials," in Highway Research Record 345, HRB, National Research Council, Washington, DC..

Harichandran, R. S., Baladi, G. Y. and Yeh, M. (1989), *Development of a Computer Program for Design of pavement Systems Consisting of Bound and Unbound Materials*, Department of Civil and Environmental Engineering, Michigan State University.

Harichandran, R. S., Yeh, M. and Baladi, G. Y. (1990). "MICH-PAVE: A nonlinear finite element program for analysis of flexible pavements." *Transportation Research Record 1286*, TRB, National Research Council, Washington, DC. , pp. 123-131.

Huang, Y. H. (1993), *Pavement Analysis and Design*. Prentice Hall, Englewood Cliffs, New Jersey.

Ingles, O. G. and Metcalf, J. B. (1973), "Soil stabilization - principles and practice." *Halsted Press*, New York, N.Y.

Keshawarz, M. S. (1985). "Field Stabilization of Ponca City Shale." Ph.D. dissertation, University of Oklahoma, Norman.

Khedr, S. (1985). "Deformation characteristics of granular base course in flexible pavements." *Transportation Research Record 1043*, TRB, National Research Council, Washington, DC. , pp. 131-138.

Kohonen, T. (1990). "The Self-Organizing Mapping." *Proc. of the IEEE*, Vol. 78, No.9, pp. 1464-1480.

Kondner, R. L. (1963), "Hyperbolic Stress-Strain Response : Cohesive Soils." Proc. ASCE. Vol. 89, No. SM1, pp.115-143.

Laguros, J. G. (1964). "Lime Stabilized Soil Properties and the Beam Action Hypothesis," *Highway Research Board*, No. 92, pp. 12-20.

Laguros, J. G. and Keshawarz, M. S. (1987), Construction and Performance of the Stabilized base Course on U.S. 77 Ponca City, Kay County. *Final Report ODOT Study No. 83-07-2, ORA 155-487,* The University of Oklahoma.

Laguros, J. G. and Medhani, R. (1984), "Fly Ash in Soil stabilization." *Ashtech '84,* 2nd Int. Conf. On Ash Technology and Marketing, Barbican Center, London.

Laguros, J. G. and Zenieris, P. (1987), "Feasibility of using flyash as a binder in coarse and fine aggregates for base." *Technical report ODOT 83-03-2, ORA 155-404,* The University of Oklahoma.

Lilley, Roger (1995), "Burning waste in the United States." *The Ecologist,* Vol. 25, No. 6, pp. 235-236.

Lotfi, H. A., Schwartz, C. W. and Witczak, M. W. (1988), "Compaction specification for the control of pavement subgrade rutting." *Transportation Research Record 1196,* TRB, National Research Council, Washington, DC. , pp. 108-115.

Lofti, H. A. and Witcark, M. W. (1985), "Dynamic characterization of cement-treated base and subbase materials." *Transportation Research Record 1031,* TRB, National Research Council, Washington, DC. , pp. 41-48.

May, R. W. and Witczak, M. W. (1981), "Effective Granular Modulus to Model Pavement Responses." *Transportation Research Record 810,* TRB, National Research Council, Washington, DC. , pp. 1-9.

McManis, K. L. and Arman, A. (1989). "Class C fly ash as a full or partial replacement for Portland cement or lime." *Transportation Research Record 1219,* TRB, National Research Council, Washington, DC. , pp. 68-81.

Miller, C. T., Bensch, D. G. and Colony, D. C. (1980), *Use of Cement-Kiln Dust and Fly ash in Pozzolanic Concrete Base Courses,* in Emulsion Mix Design, Stabilization and Compaction, TRB, Transportation Research Record 754, National Academy of Sciences, Washington, D. C., pp. 36-41.

Miller, G. A., Azad, S. and Dhar, B., (1997), "The Effect of Kin Dust on the Collapse Potential of Compacted Shale." *Testing Soil Mixed with waste or Recycled Materials, ASTM STP 1275.* Mark A. Wasemiller, Keith B. Hoddinott, Eds., American Society for Testing and Materials.

Mitchell, J. K. (1981), " Soil improvement - state of the art report." *Proc., 11th ICSMFE,* Vol. 4, 509-565.

Mohammad, L. N., Puppala, A. J. and Alavili, P. (1994), "Influence of Testing Procedure and LVDT Location on Resilient Modulus of Soils." *Transportation Research Record 1462*, TRB, National Research Council, Washington, DC. , pp. 91-101.

Monismith, C. L. (1992), "Analytically Based Asphalt Pavement Design and Rehabilitation: Theory and Practice, 1962-1992," *Transportation Research Record 1354*, TRB, National Research Council, Washington, DC. , pp. 5-26.

Najjar, Y. M. and Basheer, I. A. (1996), "Discussion of Stress-Strain Modeling of Sands Using Artificial Neural Networks, " *J. Geotech. Engrg.*, Vol. 122, No. 11, ASCE, pp. 949-950.

Napeierala, R. (1983), "Stabilization of the Subsoil with the Dust from the Kilns for Portland Cement Clinker Burning." Cement-Wapno-Gips, Vol. XXXVI/L, No.4, pp,. 127-138.

Nicholson, J. P. and Goeb, E. O. (1982), " 1980's: The Pozzolanic Pavement Era in American Construction, in the Challenge of Change." *Proc. of Sixth Int. Ash Utilization Symp.*, Morgantown Energy Technology Center, USDOE, and National Ash Association, DOE/METC/82-52, Vol. 1, pp. 358-368

Oklahoma Department of Transportation (1988), *Standard Specifications for Highway Construction.*

Pandey, K. K. (1996), "Evaluation of resilient moduli and layer coefficients of a coal ash stabilized marginal aggregate base for AASHTO flexible pavement design." Ph.D. dissertation, the University of Oklahoma, Norman.

Pandey, K. K., Zaman, M. M. and Laguros, J. G. (1998), "Resilient Moduli of Raw and Stabilized Aggregate Bases and Evaluation of Layer Coefficients for AASHTO Flexible Pavement Design." Final Report ODOT Study, Volume III, ORA 125-4262, the University of Oklahoma, Norman.

Parlos, A. G., Chong, K. T. and Atiya, A. F.(1994), "Application of the Recurrent Multilayer Perceptron in Modeling Complex Process Dynamics." *IEEE Transactions on Neural Network*, Vol. 5, No. 2, pp. 255-285.

Powell, W. D. et al. (1984), "The Structural Design of Bituminous Pavements." *TRRL Laboratory Report 1132*, Transportation and Road Research Laboratory, U.K.

Rada, G. and Witczak, M. (1981). "Comprehensive evaluation of laboratory moduli results for granular material." *Transportation Research Record 810*, TRB, National Research Council, Washington, DC. , pp. 23-33.

Ramakrishnan, V. (1986), " Evaluation of kiln dust in concrete." *ACI SP91-39 Fly Ash,*

Silica Fume, Slag and Natural Pozzolans in Concrete. Proc., 2ⁿᵈ Int. Conf. On Concrete, Vol. 1, Am. Concrete Inst. (ACI), Detroit, Mich., pp. 821-839.

Santha, B. L. (1994), "Resilient Modulus of Subgrade Soils: Comparison of Two Constitutive Equations." *Transportation Research Record 1462,* TRB, National Research Council, Washington, DC. , pp. 79-90.

Sayah, A. I. (1993), "Stabilization of Expansive Clay Using Cement Dust," M.Sc. Thesis, Graduate College, University of Oklahoma, Norman.

Shell (1978), International Petroleum, Co. Ltd., Shell Pavement Design Manual.

Simpson, P. K. (1990), *Artificial Neural System.* Pergamon Press, Inc., New York, N.Y.

Sobhan, K. (1997), "Stabilized fiber-reinforced pavement base course with recycled aggregate." Ph.D. dissertation, Civil Engineering, Northwestern University.

The Mathworks, Inc. (1994), *TOOLBOXES* in Matlab, Version 4.2c.1.

Thompson, M. R. (1987), "ILLI-PAVE Based Full-Depth Asphalt Concrete Pavement Design Procedure." *Proc. 6ᵗʰ Int. Conf. On Struct. Design of Asphalt Pavements,* Ann Arbor,MI.

Thompson, M. R. and Smith, K. L. (1990), "Repeated Triaxial Characterization of Granular Bases." *Transportation Research Record 1278,* TRB, National Research Council, Washington, DC. , pp.7-17.

Tian, P., Zaman, M. and Joakim, G. L. (1997), "Influence of testing procedure on resilient modulus of aggregate materials." *Proc. of the 9ᵗʰ Int. Conf. On Computer Methods and Advances in Geomech.,* Wuhan, China, Vol. 2, pp. 795-800.

Todres, H. A., Mishulovich, A. and Ahmad, J. (1992), "Cement kiln dust management permeability." *Res. And Devel., Bull. RD 103 T.* Portland Cement Assoc., Skokie, Ill.

Ullidtz, P. (1977), "Overlay and Stage by Stage Design." *Proc. 4ᵗʰ Int. Conf. On Struct. Design of Asphalt Pavements,* Ann, Arbor, MI.

Uzan, J. (1985), "Characterization of Granular material." *Transportation Research Record 1022,* TRB, National Research Council, Washington, DC. , pp. 52-59.

Vogl, T. P., Mangis, J.K., Rigler, A. K., Zink, W.T. and Alkon, D. L. (1988), "Accelerating the convergence of the back propagation method," *Biological Cybernetics,* Vol. 59, pp. 257-263.

Widrow, B. and Lehr, M. A. (1990), "30 Years of Adaptive Neural Networks: Perceptron Madaline and Backpropagation," *Proc. IEEE.*, 78.(9), pp. 1415-1442.

Yi L. (1995), "Resilient moduli of fly ash stabilized aggregates." Master's thesis, University of Oklahoma, Norman.

Zeniris, P. E. (1988). "Fly Ash - Aggregate Mixes For Roadway Bases." Master's thesis, University of Oklahoma, Norman.

Zaman, M., Laguros, J. G. and Sayah, A. (1992), " Soil Stabilization Using Cement Kiln Dust," *Proc. 7th Int. Conf. On Expansive Soils*, Dallas, Texas, pp. 1-5.

Zhu, J. H. and Zaman, M. (1996), "Prediction of stress-strain behavior of soil with neural networks. " *Intelligent Engineering Systems Through Artificial Neural Networks*, Vol. 6, ASME Press, New York, pp.809-814.

Zhu, J. H. and Zaman, M. (1997a), "Discussion of 'Resilient Modulus of Cohesive Soils'." Manuscript accepted for publication in the *J. of Geotech. And GeoEnviro. Eng.*, ASCE. (in press)

Zhu, J. H., Zaman, M. and Anderson, S. A. (1997b), "Modeling of Shearing Behavior of a Residual Soil with Recurrent Neural Network." Manuscript accepted for publication in the *International Journal for Numerical and Analytical Methods in Geomechanics.* (in press)

Zhu, J. H., Zaman, M. and Anderson, S. A. (1997c), "Modeling of Soil Behavior with Recurrent Neural Network." Manuscript accepted for publication in *Canadian Geotechnical Journal.*

Zhu, J. H., Zaman, M. and Laguros, J. G. (1997d), "Resilient modulus and microstructure of cement-kiln-dust stabilized aggregate." Manuscript accepted for publication in Journal *Soils and Foundations*, Japanese geotechnical Society.

Zhu, J. H. and Anderson, S. A. (1998), "Corrections for Triaxial Tests on Undisturbed Soils." *Journal of Testing and Evaluation*, ASTM, (May issue of 1998). (in press)

APPENDIX A   Laboratory Experimental Resilient Modulus Data

Table A-1 Resilient Modulus Values of Raw Aggregate

Confining Pressure kPa	Deviator Stress kPa	Bulk Stress kPa	Tested Resilient Modulus, MPa						Mean RM MPa	Standard Deviation SD	SD/Mean %
			No.1	No.2	No.3	No.4	No.5	No.6			
21	21	83	54.40	43.01	52.13	43.16	50.75	53.06	49.42	5.05	10.22
21	41	103	100.94	84.95	93.77	98.60	82.74	97.25	93.04	7.53	8.09
21	62	124	111.86	114.05	116.11	118.04	97.50	102.27	109.97	8.22	7.48
34	34	138	80.57	61.70	40.40	69.83	62.17	62.16	62.80	13.18	20.99
34	69	172	120.36	106.35	90.68	119.70	96.86	106.79	106.79	11.91	11.15
34	103	207	183.67	180.59	182.25	193.72	199.46	182.14	186.97	7.73	4.13
69	69	276	138.23	131.50	143.75	118.48	99.51	130.24	126.95	15.91	12.53
69	138	345	173.98	174.75	186.22	182.25	200.01	191.47	184.78	10.02	5.43
69	207	414	241.93	239.50	248.02	239.50	238.76	254.26	243.66	6.21	2.55
103	69	379	135.21	90.19	94.39	74.26	80.46	94.90	94.90	21.36	22.51
103	103	414	184.51	109.29	113.56	127.70	115.97	130.21	130.21	27.83	21.37
103	207	517	271.37	206.37	222.57	226.50	242.08	239.81	234.78	22.10	9.41
138	103	517	212.57	160.18	153.98	155.90	184.72	167.66	172.50	22.58	13.09
138	138	552	214.30	183.03	179.36	205.36	227.54	195.81	200.90	18.54	9.23
138	276	690	353.85	280.91	269.73	322.00	306.48	306.59	306.59	29.96	9.77

Table A-2   Resilient Modulus of 5% CKD-stabilized Aggregate

Confining Pressure kPa	Deviator Stress kPa	Bulk Stress kPa	Tested Resilient Modulus, MPa					Mean RM MPa	Standard Deviation SD	SD/Mean %
			No.1	No.2	No.3	No.4	No.5			
21	21	83	73.72	72.06	70.04	64.10	46.83	65.35	10.98	16.80
21	41	103	135.56	132.51	128.78	131.20	94.99	124.61	16.74	13.43
21	62	124	200.92	166.94	162.24	165.30	149.59	162.97	19.10	11.72
34	34	138	121.63	101.06	98.21	100.06	90.55	102.30	11.56	11.30
34	69	172	223.26	177.92	180.28	213.13	206.80	200.28	20.22	10.10
34	103	207	322.27	256.82	260.23	311.65	298.51	289.10	29.19	10.10
69	69	276	150.38	140.99	142.86	191.41	139.29	152.99	21.89	14.31
69	138	345	261.15	256.01	248.09	253.00	245.30	252.71	6.29	2.49
69	207	414	322.57	321.42	306.44	314.23	304.58	313.85	8.28	2.64
103	69	379	145.93	136.82	138.64	139.31	138.47	139.83	3.53	2.53
103	103	414	193.40	163.48	183.73	187.05	148.64	175.26	18.63	10.63
103	207	517	323.48	344.17	307.30	312.85	310.75	319.71	14.95	4.68
138	103	517	225.05	175.60	213.80	217.66	216.20	209.66	19.50	9.30
138	138	552	249.46	194.64	189.59	241.27	239.65	222.92	28.42	12.75
138	276	690	383.37	373.90	432.71	370.77	368.28	385.81	26.84	6.96

Table A-3   Resilient Modulus of 10% CKD-stabilized Aggregate

Confining Pressure kPa	Deviator Stress kPa	Bulk Stress kPa	Tested Resilient Modulus, MPa					Mean RM MPa	Standard Deviation SD	SD/Mean %
			No.1	No.2	No.3	No.4	No.5			
21	21	83	71.38	69.70	78.08	64.13	78.08	72.27	5.94	8.22
21	41	103	112.56	123.57	96.52	107.33	102.70	107.68	10.27	9.54
21	62	124	141.22	180.90	203.29	203.13	198.48	175.19	26.35	15.04
34	34	138	130.13	124.04	101.41	94.59	99.57	114.61	15.99	13.95
34	69	172	276.51	286.67	203.83	190.14	200.15	221.61	46.18	20.84
34	103	207	280.03	201.62	247.86	224.79	243.38	234.09	29.06	12.42
69	69	276	123.21	161.18	141.42	128.26	131.95	160.30	14.97	9.34
69	138	345	199.15	189.16	193.09	175.12	180.17	213.57	9.70	4.54
69	207	414	371.78	257.22	312.78	283.67	291.84	321.83	43.07	13.38
103	69	379	124.48	114.94	113.43	102.87	105.83	156.80	8.48	5.41
103	103	414	148.25	144.02	145.34	131.81	135.61	186.45	6.96	3.74
103	207	517	379.85	338.77	357.35	358.66	341.66	382.23	16.41	4.29
138	103	517	161.43	161.50	182.35	184.65	164.31	228.56	11.64	5.09
138	138	552	199.81	205.28	231.03	212.04	201.99	266.96	12.62	4.73
138	276	690	404.42	405.52	310.11	309.32	351.11	411.66	47.71	11.59

225

Table A-4 Resilient Modulus of 15% CKD-stabilized Aggregate
(Curing 7-day)

Confining Pressure kPa	Deviator Stress kPa	Bulk Stress kPa	Tested Resilient Modulus, MPa						Mean RM MPa	Standard Deviation SD	SD/Mean %
			No.1	No.2	No.3	No.4	No.5	No.6			
21	21	83	80.26	70.12	96.05	73.93	82.57	80.46	80.56	8.91	11.06
21	41	103	144.22	133.16	140.65	136.62	145.51	164.09	144.04	10.86	7.54
21	62	124	247.89	180.92	221.86	216.80	217.57	221.21	217.71	21.42	9.84
34	34	138	137.35	110.87	137.02	112.00	112.69	114.36	120.71	12.81	10.61
34	69	172	258.46	230.42	281.26	273.32	274.88	279.03	266.23	19.28	7.24
34	103	207	322.27	285.31	332.12	322.61	324.51	299.43	314.37	17.98	5.72
69	69	276	164.16	155.84	174.81	169.59	170.67	169.77	167.47	6.64	3.96
69	138	345	272.79	199.95	254.72	248.44	249.50	248.57	245.66	24.24	9.87
69	207	414	397.73	346.04	369.25	394.69	396.95	395.04	383.28	21.21	5.53
103	69	379	131.56	146.85	145.99	141.41	142.40	141.58	141.63	5.45	3.85
103	103	414	181.27	170.03	183.20	178.09	179.08	178.25	178.32	4.51	2.53
103	207	517	460.37	378.05	397.83	386.35	388.66	386.72	399.66	30.40	7.61
138	103	517	216.64	178.81	205.39	200.20	201.10	200.31	200.41	12.29	6.13
138	138	552	242.98	235.95	300.04	242.89	244.31	243.12	251.55	23.94	9.52
138	276	690	506.53	498.37	487.84	518.50	521.40	464.40	499.51	21.25	4.26

Table A-5 Resilient Modulus of 15% CKD-stabilized Aggregate
(Curing 28-day)

Confining Pressure kPa	Deviator Stress kPa	Bulk Stress kPa	Tested Resilient Modulus, MPa						Mean RM MPa	Standard Deviation SD	SD/Mean %
			No.1	No.2	No.3	No.4	No.5	No.6			
21	21	83	123.02	96.36	123.17	111.53	87.30	114.73	109.35	14.60	13.36
21	41	103	170.44	144.63	147.28	137.13	124.11	164.71	148.05	17.23	11.64
21	62	124	248.47	188.33	246.25	212.37	191.71	231.77	219.81	26.46	12.04
34	34	138	160.30	143.52	164.24	169.04	141.46	143.52	153.68	12.22	7.95
34	69	172	291.36	350.98	299.12	430.43	289.51	384.88	341.05	58.12	17.04
34	103	207	455.51	405.21	422.64	397.37	443.38	411.60	422.62	22.69	5.37
69	69	276	238.97	186.80	241.57	221.04	234.66	236.73	226.63	20.78	9.17
69	138	345	387.02	308.34	350.20	327.65	302.76	325.03	333.50	31.07	9.32
69	207	414	494.33	435.13	473.91	440.16	488.43	511.83	473.97	30.69	6.47
103	69	379	218.16	148.59	184.92	175.41	179.68	177.39	180.69	22.33	12.36
103	103	414	272.28	232.64	224.43	255.80	234.09	230.02	241.54	18.49	7.65
103	207	517	533.26	630.75	510.23	543.74	515.19	544.08	546.21	43.78	8.01
138	103	517	302.48	220.30	281.11	239.33	346.47	243.74	272.24	47.11	17.31
138	138	552	344.75	312.62	316.83	316.83	390.37	362.88	340.71	31.32	9.19
138	276	690	682.61	753.67	655.03	659.09	667.51	680.99	683.15	36.31	5.32

Table A-6   Resilient Modulus of 15% CKD-stabilized Aggregate (Curing 90-day)

Confining Pressure kPa	Deviator Stress kPa	Bulk Stress kPa	Tested Resilient Modulus, MPa						Mean RM MPa	Standard Deviation SD	SD/Mean %
			No.1	No.2	No.3	No.4	No.5	No.6			
21	21	83	113.11	122.50	119.54	136.70	119.77	148.35	126.66	13.19	10.42
21	41	103	173.83	186.83	227.87	221.91	220.25	173.20	200.65	25.46	12.69
21	62	124	258.97	234.58	311.57	295.35	250.74	225.60	262.80	33.99	12.93
34	34	138	192.83	181.77	241.47	221.96	151.05	159.36	191.41	35.18	18.38
34	69	172	254.97	250.74	269.07	256.56	231.41	217.33	246.68	18.86	7.65
34	103	207	373.41	341.29	389.00	381.09	347.64	278.14	351.76	40.65	11.56
69	69	276	253.24	247.18	288.48	277.29	225.23	225.99	252.90	26.01	10.29
69	138	345	325.78	313.33	423.53	391.96	318.17	384.00	359.46	46.32	12.89
69	207	414	615.56	731.42	662.96	641.71	574.66	540.28	627.76	67.53	10.76
103	69	379	254.66	303.32	277.51	313.80	245.18	256.36	275.14	28.16	10.23
103	103	414	339.23	379.83	391.90	391.65	325.85	350.93	363.23	28.39	7.82
103	207	517	467.82	567.49	539.88	500.16	464.81	477.58	502.96	42.12	8.37
138	103	517	343.26	351.60	368.16	357.75	309.51	294.72	337.50	28.97	8.58
138	138	552	438.34	462.65	437.72	405.39	408.73	398.89	425.29	24.85	5.84
138	276	690	567.53	663.35	619.81	641.79	625.77	605.05	620.55	32.75	5.28

Table A-7   Resilient Modulus of CKD-stabilized Aggregate
Subjected to Freezing /Thawing Cycles.

			Cycles of Freezing/Thawing					
Confining	Deviator	Bulk	4		8		12	
Pressure	Stress	Stress	Test 1	Test 2	Test 1	Test 2	Test 1	Test 2
kPa	kPa	kPa	MPa	MPa	MPa	MPa	MPa	MPa
21	21	83	60.06	79.91	47.23	55.3	32.61	25.37
21	41	103	84.26	92.39	79.15	71.91	46.89	55.23
21	62	124	149.69	148.59	113.70	106.6	72.6	83.08
34	34	138	72.88	86.12	55.78	66.47	33.31	34.2
34	69	172	142.45	141.49	97.77	101.36	74.27	75.22
34	103	207	212.16	215.54	134.87	143.55	128.15	130.18
69	69	276	133.14	125.63	88.34	95.98	73.82	70.95
69	138	345	195.89	201.95	127.88	133.63	115.64	105.96
69	207	414	312.07	325.93	172.58	236.29	183.56	196.92
103	69	379	114.32	135.69	81.44	95.22	51.64	81.84
103	103	414	152.17	184.44	114.61	115.77	55.92	97.29
103	207	517	319.93	349.71	164.65	238.15	119.84	123.06
138	103	517	145.76	179.55	112.81	120.46	70.26	105.63
138	138	552	186.3	222.43	155.85	160.18	115.91	169.55
138	276	690	383.43	323.08	216.37	287.87	159	266.35

Table A-8   Resilient Modulus of CKD-stabilized Aggregate
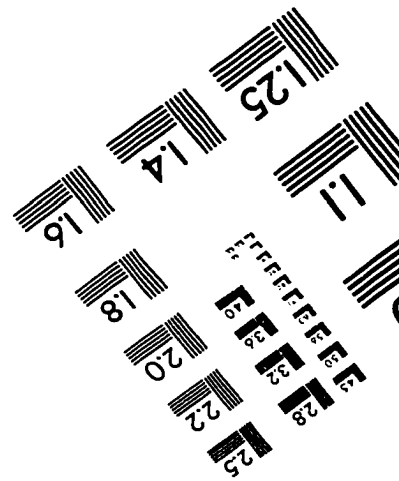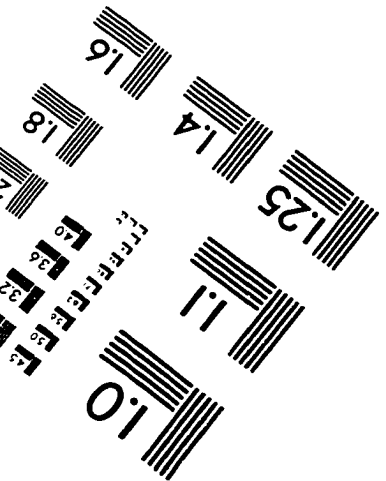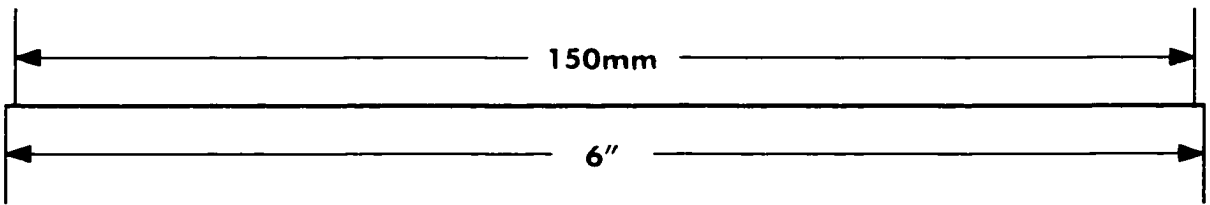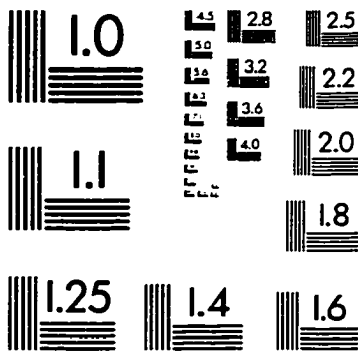Subjected to Wetting/Drying Cycles

Confining Pressure	Deviator Stress	Bulk Stress	Cycles of Wetting/Drying					
			4		8		12	
			Test 1	Test 2	Test 1	Test 2	Test 1	Test 2
kPa	kPa	kPa	Mpa	Mpa	MPa	MPa	MPa	MPa
21	21	83	58.15	58.36	49.61	50.92	51.47	40.61
21	41	103	98.32	106.52	81.72	89.09	79.37	72.12
21	62	124	157.23	177.42	136.28	138.28	118.85	107.08
34	34	138	85.99	72.69	75.03	73.86	79.72	58.88
34	69	172	123.19	130.50	125.40	121.75	111.00	91.98
34	103	207	208.22	233.02	208.84	184.10	179.14	154.17
69	69	276	101.63	185.34	108.04	82.20	135.66	93.36
69	138	345	170.18	336.71	501.87	126.78	163.09	149.28
69	207	414	293.86	420.70	357.04	207.04	264.64	249.87
103	69	379	105.90	155.51	124.36	58.43	107.28	94.88
103	103	414	135.32	198.50	155.37	69.18	142.69	118.80
103	207	517	290.00	435.86	369.24	186.79	266.78	265.94
138	103	517	144.62	255.14	180.17	74.34	137.25	141.69
138	138	552	174.87	255.21	266.44	96.80	150.34	142.24
138	276	690	367.86	510.20	406.58	241.49	334.10	299.66

APPENDIX B   Unit Conversion (from SI to English Unit)

Table B-1.   Conversion Factors (from SI to English Units)

Length	1 m	3.281 ft
	1 cm	3.281×10^{-2} ft
	1 mm	3.281×10^{-3} ft
	1 m	39.37 in.
	1 cm	0.3937 in.
	1 mm	0.03937 in.
Area	1 m^2	10.764 ft^2
	1 cm^2	10.764×10^{-4} ft^2
	1 mm^2	10.764×10^{-6} ft^2
	1 m^2	1550 in.^{2}
	1 cm^2	0.155 in.^{2}
	1 mm^2	0.155×10^{-2} in.^{2}
Volume	1 m^3	35.32 ft^3
	1 cm^3	35.32×10^{-4} ft^3
	1 m^3	61023.4 in.^{3}
	1 cm^3	0.061023 in.^{3}
Force	1 N	0.2248 lb
	1 kN	224.8 lb
	1 kgf	2.2046 lb
	1 kN	0.2248 kip
	1 kN	0.1124 U.S. ton
	1 metric ton	2204.6 lb
	1 N/m	0.0685 lb/ft
Stress	1 N/m^2	20.885×10^{-3} lb/ft^2
	1 kN/m^2	20.885 lb/ft^2
	1 kN/m^2	0.01044 U.S. ton/ft^2
	1 kN/m^2	20.885×10^{-3} kip/ft^2
	1 kN/m^2	0.145 lb/in.^{2}
Unit Weight	1 kN/m^3	6.361 lb/ft^3
	1 kN/m^3	0.003682 lb/in.^{3}

IMAGE EVALUATION
TEST TARGET (QA-3)

150mm

6"